

2010

Tundra Snow Cover Properties from *In-Situ* Observation and Multi-Scale Passive Microwave Remote Sensing

Andrew Rees
Wilfrid Laurier University

Follow this and additional works at: <http://scholars.wlu.ca/etd>



Part of the [Remote Sensing Commons](#)

Recommended Citation

Rees, Andrew, "Tundra Snow Cover Properties from *In-Situ* Observation and Multi-Scale Passive Microwave Remote Sensing" (2010). *Theses and Dissertations (Comprehensive)*. 1105.
<http://scholars.wlu.ca/etd/1105>

This Dissertation is brought to you for free and open access by Scholars Commons @ Laurier. It has been accepted for inclusion in Theses and Dissertations (Comprehensive) by an authorized administrator of Scholars Commons @ Laurier. For more information, please contact scholarscommons@wlu.ca.

NOTE TO USERS

This reproduction is the best copy available.

UMI[®]



Library and Archives
Canada

Published Heritage
Branch

395 Wellington Street
Ottawa ON K1A 0N4
Canada

Bibliothèque et
Archives Canada

Direction du
Patrimoine de l'édition

395, rue Wellington
Ottawa ON K1A 0N4
Canada

Your file *Votre référence*
ISBN: 978-0-494-68754-3
Our file *Notre référence*
ISBN: 978-0-494-68754-3

NOTICE:

The author has granted a non-exclusive license allowing Library and Archives Canada to reproduce, publish, archive, preserve, conserve, communicate to the public by telecommunication or on the Internet, loan, distribute and sell theses worldwide, for commercial or non-commercial purposes, in microform, paper, electronic and/or any other formats.

The author retains copyright ownership and moral rights in this thesis. Neither the thesis nor substantial extracts from it may be printed or otherwise reproduced without the author's permission.

AVIS:

L'auteur a accordé une licence non exclusive permettant à la Bibliothèque et Archives Canada de reproduire, publier, archiver, sauvegarder, conserver, transmettre au public par télécommunication ou par l'Internet, prêter, distribuer et vendre des thèses partout dans le monde, à des fins commerciales ou autres, sur support microforme, papier, électronique et/ou autres formats.

L'auteur conserve la propriété du droit d'auteur et des droits moraux qui protègent cette thèse. Ni la thèse ni des extraits substantiels de celle-ci ne doivent être imprimés ou autrement reproduits sans son autorisation.

In compliance with the Canadian Privacy Act some supporting forms may have been removed from this thesis.

While these forms may be included in the document page count, their removal does not represent any loss of content from the thesis.

Conformément à la loi canadienne sur la protection de la vie privée, quelques formulaires secondaires ont été enlevés de cette thèse.

Bien que ces formulaires aient inclus dans la pagination, il n'y aura aucun contenu manquant.

■+■
Canada

**Tundra snow cover properties from in-situ observation and multi-scale
passive microwave remote sensing**

by

Andrew Rees

**B.Sc. Nipissing University, 2000
M. Sc. University of Calgary, 2003**

DISSERTATION

**Submitted to the Department/Faculty of Geography and Environmental Studies
in partial fulfillment of the requirements for**

Doctor of Philosophy in Geography

**Wilfrid Laurier University
2010**

©Andrew Rees 2010

ABSTRACT

Tundra snow cover is important to monitor as it influences local, regional, and global scale surface water balance, energy fluxes, and ecosystem and permafrost dynamics. Moreover, recent global circulation models (GCM) predict a pronounced shift in high latitude winter precipitation and mean annual air temperature due to the feedback between air temperature and snow extent. At regional and hemispheric scales, the estimation of snow extent, snow depth and, snow water equivalent (SWE) is important because high latitude snow cover both forces and reacts to atmospheric circulation patterns. Moreover, snow cover has implications on soil moisture dynamics, the depth, formation and growth of the permafrost active layer, the vegetation seasonality, and the respiration of CO₂.

In Canada, daily snow depth observations are available from 1955 to present for most meteorological stations. Moreover, despite the abundance and dominance of a northern snow cover, most, if not all, long term snow monitoring sites are located south of 55° N. Stations in high latitudes are extremely sparse and coastally biased. In Arctic regions, it can be logistically difficult and very expensive to acquire both spatially and temporally extensive in-situ snow data. Thus, the possibility of using satellite remote sensing to estimate snow cover properties is appealing for research in remote northern regions.

Remote sensing techniques have been employed to monitor the snow since the 1960s when the visible light channels were used to map snow extent. Since then, satellite remote sensing has expanded to provide information on snow extent, depth, wetness, and SWE. However, the utility of satellite sensors to provide useful, operational tundra snow cover data depends on sensor parameters and data resolution. Passive microwave data are the only currently operational sources for providing estimates of dry snow extent, SWE

and snow depth. Currently, no operational passive microwave algorithms exist for the spatially expansive tundra and high Arctic regions. The heterogeneity of sub-satellite grid tundra snow and terrain are the main limiting factors in using conventional SWE retrieval algorithm techniques. Moreover, there is a lack of in-situ data for algorithm development and testing.

The overall objective of this research is to improve operational capabilities for estimating end of winter, pre-melt tundra SWE in a representative tundra study area using satellite passive microwave data. The study area for the project is located in the Daring-Exeter-Yamba portion of the Upper-Coppermine River Basin in the Northwest Territories. The size, orientation and boundaries of the study area were defined based on the satellite EASE grid (25 x 25 km) centroid located closest to the Tundra Ecosystem Research Station operated by the Government of the Northwest Territories. Data were collected during intensive late winter field campaigns in 2004, 2005, 2006, 2007, 2008, and 2009. During each field campaign, snow depth, density and stratigraphy were recorded at sites throughout the study area. During the 2005 and 2008 seasons, multi-scale airborne passive microwave radiometer data were also acquired. During the 2007 season, ground based passive microwave radiometer data were acquired. For each year, temporally coincident AMSR-E satellite T_b were obtained.

The spatial distribution of snow depth, density and SWE in the study area is controlled by the interaction of blowing snow with terrain and land cover. Despite the spatial heterogeneity of snow cover, several inter-annual consistencies were identified. Tundra snow density is consistent when considered on a site-by-site basis and among different terrain types. A regional average density of 0.294 g/cm^3 was derived from the six years of measurements. When applied to site snow depths, there is little difference in SWE derived from either the site or the regional average density. SWE is more variable from site to site and year to year than density which requires the use of a terrain based

classification to better quantify regional SWE. The variability in SWE was least on lakes and flat tundra, while greater on slopes and plateaus. Despite the variability, the inter-annual ratios of SWE among different terrain types does not change that much. The variability (CV) in among terrain categories was quite similar. The overall weighted mean CV for the study area was 0.40, which is a useful regional generalization. The terrain and landscape based classification scheme was used to generalize and extrapolate tundra SWE. Deriving a weighted mean SWE based on the spatial proportion of landscape and terrain features was shown as a method for generalizing the regional distribution of tundra SWE.

The SWE data from each year were compared to AMSR-E satellite Tb. Within each season and among each of the seasons, there was little difference in 19 GHz Tb. However, there was always a large decrease in 37 GHz Tb from early November through April. The change in ΔTb^{37-19} throughout each season showed that the Tb at 37 GHz is sensitive to parameters which evolve over a winter season. A principal component analysis (PCA) showed that there are differences in ΔTb^{37-19} among different EASE grids and that land cover may have an influence on regional Tb. However, the PCA showed little relationship between end of season ΔTb^{37-19} and lake fraction. A good relationship was found between ΔTb^{37-19} and in-situ SWE. A quadratic function was fitted to explain 89 percent of the variance in SWE from the ΔTb^{37-19} . The quadratic relationship provides a good fit between the data; however, the nature of the relationship is opposite to the expected linear relationship between ΔTb^{37-19} and SWE.

Airborne Tb data were used to examine how different snow, land cover and terrain properties influence microwave emission. In flat tundra, there was a significant relationship between SWE and high resolution ΔTb^{37-19} . On lakes and slopes, no strong relationships were found between SWE and high resolution ΔTb^{37-19} . Due to the complexity of snow and terrain in high resolution footprints, it was a challenge to isolate a relationship between

SWE and Tb. However, as the airborne footprint size increased the amplitude of variability in Tb decrease considerably to the point that Tb in large footprints is not sensitive to local scale variability in SWE. As such, most of the variability evident in the high and mid resolution airborne data will not persist at the EASE grid scale.

Despite the many challenges, algorithm development should be possible at the satellite scale. The AMSR-E ΔT_b^{37-19} changes from year to year in response to differences in snow cover properties. However, the multiple years of in-situ snow data remain the most important contribution in linking Tb with SWE.

ACKNOWLEDGMENTS

This thesis is the culmination of many years of research, field work, and reflection. None of it would be possible without the support of many people and various funding agencies. Most importantly, I am very grateful for the enormous contribution in time, energy, and support from my supervisors Dr. Michael English and Dr. Chris Derksen. From their tireless work in the snow pits of the tundra to the thankless editing of the final document, their enthusiasm has been unparalleled. I am also thankful for the support, advice and contribution to field work from Dr. Richard Kelly and Dr. Claude Duguay, and for the contributions from my other committee members Dr. Steven Roberts, and Dr. Ellsworth LeDrew. Thanks also to Dr. Jim Buttle for providing helpful and thorough comments and serving as the external reviewer. I am also grateful to Anne Walker of Environment Canada for her generous support of the project, especially the various radiometer deployments and the many years of field work at Daring Lake.

Funding support for this research was received from many different agencies. The multiple years of field work and research were supported primarily by the Canadian Foundation for Climate and Atmospheric Sciences (CFCAS). Field work was also supported by the Climate Processes Section of Environment Canada and the CRYSYS program, the Canadian Water Networks, the Polar Continental Shelf Program, and the Northern Scientific Training Program. In-kind support was received from Steven Matthews at the Department of Environment and Natural Resources in the Government of the Northwest Territories, Bob Reid at Indian and Northern Affairs, B.H.P. Ekati Mine, and the Water Survey of Canada. Further support was provided by the Faculty of Graduate Studies and the Department of Geography and Environmental Studies at Wilfrid Laurier University in the form of research assistantships.

The field work at Daring Lake was an integral part of this project and provided many unforgettable moments. It is difficult to summarize the contribution that the

experience from these many trips to the tundra has made on my research and life in general. I have been very fortunate to work with some very dedicated and interesting people in the field. From the beginning in 2004 with the Daring Olympics and lots of money for helicopter travel, the airborne data collection, the collapse of the SBR and the plague in 2005, the skeet practice, snow bowl, and Harleys of 2006, the renewal (and second collapse) of the SBR and SNOWSTAR visit of 2007, the Magna Probe marathon, runaway snowmobile and airborne campaign of 2008, to the low density snow and sampling efficiency of 2009. The tundra has seen many interesting things.

I must express gratitude to those who were there in the field at Daring Lake to help over the years: Chris, Mike, Dave W., Nat, J. R., Kristi, Dave M., Pat, Claude, Alex, Matt, Richard, Alec, Scott, Eric, Andrea, the NRC Twin Otter crew, Ken Asmus for his support on the SBR system, and to Steve Matthews and Robert Mulders of ENR for logistical support in camp. Special mention goes out to Arvids Silis for his endless dedication with the SWE tube, which earned him the name SWE man, and for his work on the airborne data processing in 2005, and also to Peter Toose for his hard work in the field (despite his distaste for chicken) and his helpful contributions to data processing and solving the mysteries of GIS.

Last but not least, I would like to thank my family for their support, enthusiasm and suggestions during the long PhD journey. Special thanks to my wife, Jean, for her patience and understanding as 18 months turned into five years, also to Coco, posthumously for her pleasant company, and most recently, to Harrison for providing entertainment and an extra incentive to actually finish.

TABLE OF CONTENTS

ABSTRACT	ii
ACKNOWLEDGMENTS	vi
LIST OF TABLES	xii
LIST OF FIGURES	xiv
CHAPTER 1: INTRODUCTION	
1.1. Introduction	1
1.2. Research Objectives	3
1.3. Importance of tundra snow cover	4
1.3.1. Introduction	4
1.3.2. Regional and Global Climate	5
1.3.3. Carbon Balance	8
1.3.4. Hydrologic System	9
1.3.5. Permafrost and Active Layer Formation	9
1.3.6. Plants and Animals	10
1.3.7. Potential Environmental Change	11
1.3.7.1. <i>Temperature and Precipitation</i>	12
1.3.7.2. <i>Snow Vegetation Feedbacks</i>	13
1.3.7.3. <i>Human Development</i>	15
1.3.8. Tundra Snow Parameters	16
1.4. Tundra Snow Data	17
1.4.1. Introduction	17
1.4.2. Manual In-situ Snow Data	17
1.4.3. Automated Station Snow Data	19
1.4.4. Canadian Snow Database	20
1.4.5. Modeled Snow Data	21
1.4.6. Snow Data from Remote Sensing	25
1.4.6.1. <i>Visible Spectrum Sensors</i>	26
1.4.6.2. <i>Microwave Sensors</i>	29
1.4.6.2.1. <i>Active Microwave Sensors</i>	29
1.4.6.2.2. <i>Passive Microwave Sensors</i>	31
1.4.6.3. <i>Summary of Remote Sensing Data Sources</i>	31
1.4.7. Trends and Variability in Tundra Snow Cover	32
1.4.8. Summary of Tundra Snow Data Sources	33
CHAPTER 2: MONITORING SNOW COVER WITH SATELLITE PASSIVE MICROWAVE REMOTE SENSING	
2.1. Introduction	35
2.1.1. Passive Microwave Sensors	35
2.1.2. Passive Microwave Data	37
2.2. Passive Microwave Radiometry of Snow	38
2.2.1. Introduction	38
2.2.2. Basis for Passive Microwave Snow Detection	39
2.2.2.1. <i>Dry Snow</i>	39
2.2.2.2. <i>Wet Snow</i>	41

2.3.	Passive Microwave Algorithm Development	42
2.3.1.	Introduction	42
2.3.2.	Hemispheric Algorithm Development	44
2.3.3.	Regional Algorithm Development	45
2.3.3.1.	<i>Open Ground Algorithm Development</i>	46
2.3.3.2.	<i>Boreal Forest Algorithm Development</i>	47
2.3.3.3.	<i>Tundra and High Arctic Algorithm Development</i>	49
2.4.	Factors Contributing to Uncertainty in Estimating Tundra SWE	51
2.4.1.	Introduction	51
2.4.2.	Snow Pack Properties	52
2.4.2.1.	<i>Stratigraphy and Grain Size</i>	52
2.4.2.1.1.	<i>Effect of Depth Hoar</i>	52
2.4.2.1.2.	<i>Effect of Dense Wind Slab</i>	54
2.4.2.1.3.	<i>Effect of Ice Lenses</i>	54
2.4.2.2.	<i>Snow Depth</i>	55
2.4.2.3.	<i>Temporal Evolution of Snow</i>	56
2.4.3.	Terrain and Landscape	58
2.4.3.1.	<i>Soil Condition</i>	58
2.4.3.2.	<i>Vegetation Cover</i>	59
2.4.3.3.	<i>Topography</i>	60
2.4.3.4.	<i>Lake Fraction</i>	62
2.5.	Improving estimates of Tundra SWE	66
2.5.1.	Introduction	66
2.5.2.	Addressing Snow Pack Characteristics	66
2.5.3.	Addressing Snow Distribution Issues	67
2.5.4.	Addressing Lake Fraction	69
2.6.	Summary of Research Protocol and Data Requirements	70
CHAPTER 3: STUDY AREA AND DATA		
3.1.	Introduction	72
3.2.	Study Area	72
3.2.1.	Location	72
3.2.2.	Geology and Soils	73
3.2.3.	Vegetation	74
3.2.4.	Climate	75
3.2.5.	Hydrology	75
3.3.	Data Acquisition	76
3.3.1.	Introduction	76
3.3.2.	Terrain Classification	77
3.3.3.	Landscape Classification	79
3.3.4.	Snow Data	80
3.3.4.1.	<i>Snow Survey Locations</i>	80
3.3.4.2.	<i>Snow Survey Protocol</i>	82
3.3.4.3.	<i>Annual Snow Survey Sample Numbers</i>	83
3.3.5.	Meteorological Data	84
3.3.6.	Ground Based Passive Microwave Radiometer Data	85
3.3.7.	Airborne Passive Microwave Radiometer Data	86
3.3.8.	Satellite Passive Microwave Radiometer Data	88
3.4.	Data Summary	89

CHAPTER 4: DISTRIBUTION AND PROPERTIES OF TUNDRA SNOW COVER

4.1.	Introduction	90
4.2.	Tundra Snow Cover Distribution and Properties.....	91
4.2.1.	Introduction	91
4.2.2.	Snow Cover Properties	92
4.2.2.1.	<i>Snow Density</i>	<i>92</i>
4.2.2.2.	<i>Snow Depth</i>	<i>99</i>
4.2.2.3.	<i>Snow Water Equivalent</i>	<i>102</i>
4.2.2.4.	<i>Snow Stratigraphy</i>	<i>107</i>
4.2.3.	Inter-annual Patterns in SWE	111
4.3.	Variability in Snow Cover	114
4.3.1.	Introduction	114
4.3.2.	Variability Between Survey Years	115
4.3.3.	Variability Within Survey Years Between Terrain Categories	118
4.4.	Snow Cover Classification	125
4.4.1.	Introduction	125
4.4.2.	Terrain Classification	126
4.4.2.1.	<i>Difference of Means</i>	<i>126</i>
4.4.2.2.	<i>Terrain Weighted SWE with all Categories</i>	<i>132</i>
4.4.2.3.	<i>Refining the Number of Terrain Categories</i>	<i>134</i>
4.4.2.4.	<i>Summary of Terrain Weighted SWE</i>	<i>136</i>
4.4.3.	Merging Terrain and Land Cover Information	137
4.5.	Summary of Snow Data	143
4.5.1.	Introduction	143
4.5.2.	Inter-annual Patterns in Tundra Snow Cover	144
4.5.3.	Extrapolation of SWE	145

CHAPTER 5: EVALUATING SATELLITE PASSIVE MICROWAVE DATA

5.1.	Introduction	147
5.2.	The Passive Microwave Satellite Record	149
5.3.	Temporal Analysis of Tb	150
5.3.1.	Introduction	150
5.3.2.	Seasonal Evolution in 19 and 37 GHz Tb.....	151
5.3.3.	Seasonal Evolution in ΔT_b^{37-19}	153
5.4.	Spatial Analysis of Tb	155
5.4.1.	Introduction	155
5.4.2.	Spatial Principal Component Analysis	156
5.4.3.	Spatial PCA on Sub-set of Data	164
5.5.	Comparison of Satellite Tb to in-situ SWE	168
5.5.1.	Introduction	168
5.5.2.	Comparison of In-situ SWE to ΔT_b^{37-19}	169
5.5.3.	Resolving Uncertainty in SWE vs ΔT_b^{37-19}	174

CHAPTER 6: APPLICATION OF MULTI-SCALE PASSIVE MICROWAVE DATA

6.1.	Introduction	178
6.2.	Application of High Resolution Tb Data	179
6.2.1.	Comparing Tb Data to in-situ SWE	179
6.2.2.	Flat Tundra	185
6.2.2.1.	<i>High Resolution Airborne Radiometer Data</i>	<i>185</i>
6.2.2.2.	<i>Ground Based Radiometer Data.....</i>	<i>187</i>
6.2.2.3.	<i>Summary of High Resolution Tb Data over Flat Tundra</i>	<i>189</i>
6.2.3.	Lakes	191
6.2.3.1.	<i>High Resolution Airborne Radiometer Data</i>	<i>191</i>
6.2.3.2.	<i>Transect of Airborne Radiometer Data.....</i>	<i>196</i>
6.2.3.3.	<i>Ground Based Radiometer Data.....</i>	<i>198</i>
6.2.3.4.	<i>Summary of High Resolution Tb Data over Lakes.....</i>	<i>199</i>
6.2.4.	Slopes	200
6.2.5.	Summary of High Resolution Tb vs SWE	204
6.3.	Application of Mid and Low Resolution Airborne Tb	205
6.3.1.	Introduction	205
6.3.2.	High to Low Resolution Tb	206
6.3.3.	Influence of Lake Fraction on Tb	213
6.4.	Summary of the Contribution of Airborne Data	220

CHAPTER 7: IMPROVING PASSIVE MICROWAVE ESTIMATES OF TUNDRA SWE

7.1.	Introduction	222
7.2.	The Quadratic Approach	223
7.3.	Towards and Operational Algorithm	228
7.4.	Summary	230
7.4.1.	Summary of Contributions	230
7.4.1.1.	<i>Summary of Tundra Snow Cover</i>	<i>231</i>
7.4.1.2.	<i>Summary of Satellite Tb Data</i>	<i>232</i>
7.4.1.3.	<i>Summary of Multi-scale Tb Data</i>	<i>233</i>
7.4.2.	Remaining Challenges	235
7.4.2.1.	<i>Terrain and Landscape</i>	<i>235</i>
7.4.2.2.	<i>Snow Cover.....</i>	<i>237</i>

APPENDIX A	239
-------------------------	------------

REFERENCES.....	252
------------------------	------------

LIST OF TABLES

Table 1.1.	The importance of tundra snow cover to natural systems	5
Table 1.2.	Application of snow cover parameters	16
Table 1.3.	Summary of remote sensing sensors for detecting snow cover	32
Table 1.4.	Sources of tundra snow cover data	33
Table 2.1.	Passive microwave sensors	37
Table 2.2.	Factors in the tundra that affect passive microwave brightness temperature	50
Table 2.3.	Snowpack characteristics at spatial and temporal dimensions	66
Table 3.1.	Terrain units and percent of study area	78
Table 3.2.	Landcover classification and percent study area	80
Table 3.3.	Sample n and the percent of total basin area occupied by each terrain category for the survey years	83
Table 3.4.	Summary of SBR instrument characteristics	85
Table 3.5.	Footprint dimensions for SBR radiometers	85
Table 3.6.	Summary of flying heights and radiometer footprint dimensions	86
Table 3.7.	Summary of AMSR-E instrument characteristics	88
Table 3.8.	Summary of field data collected	89
Table 4.1.	Difference of mean density for each survey year.....	95
Table 4.2.	Difference of mean density from each year compared to overall mean density	96
Table 4.3.	The ratio of SWE on flat tundra to SWE on all other terrain categories.....	112
Table 4.4.	Descriptive statistics of yearly SWE (mm) data	117
Table 4.5.	Tundra terrain categories and the factors that control snow cover distribution.....	119
Table 4.6.	The coefficient of variation of SWE for each terrain category in each survey year	122
Table 4.7.	A weighted mean CV of all terrain categories and years surveyed	125
Table 4.8.	Difference of mean SWE (mm) between terrain categories within each survey year, a) 2004, b) 2005, c) 2006, d) 2007, e) 2008, f) 2009	127
Table 4.9.	Summary of post-hoc difference of means tests for	

	a) flat tundra, b) lakes, c) low slopes, and d) high slopes	130
Table 4.10.	Terrain weighted mean SWE compared to arithmetic mean SWE for each survey year.....	133
Table 4.11.	Five category terrain based weighted mean SWE compared to eleven category weighted mean SWE.....	135
Table 4.12.	The coefficient of variation of SWE for the five terrain categories .	136
Table 4.13.	Homogeneity of variance and difference of mean statistics for land cover information	139
Table 4.14.	Statistics of flat tundra SWE categories	141
Table 4.15.	Statistics of lake SWE categories.....	142
Table 4.16.	The percent of the study are occupied by lakes of different sizes .	142
Table 5.1.	Comparison of 19 and 37 GHz Tb for April 1 to April 10 along with in-situ SWE observations	173
Table 6.1.	Relative resolution of aircraft and Tb data	179
Table 6.2.	Summary of the strength of the relationship between SWE and ΔT_{b37-19} over flat tundra	189
Table 6.3.	The linear equations between ΔT_{b37-19} and SWE for the Magna Probe and ground based data	190
Table 6.4.	Descriptive statistics for ΔT_{b37-19} from (F) over land and lakes ...	213
Table 6.5.	Descriptive statistics for 37 GHz Tb at 0 and 100 % lake fraction...	216
Table 6.6.	Descriptive statistics for ΔT_{b37-19} at 0 and 100 % lake fraction	217
Table 6.7.	The sensitivity in SWE for 10 K ΔT_{b37-19}	218
Table 7.1.	Factors in the tundra that affect passive microwave brightness temperature.....	235
Table A.1.	Descriptive statistics of the Churchill Magna Probe experiment....	243
Table A.2.	Difference of mean SWE for the four example footprints in Figure A.6.....	247

LIST OF FIGURES

Figure 1.1.	Canadian daily snow depth network available for analysis	2
Figure 1.2.	The comparison in shortwave energy reflection between a snow surface and bare soil	6
Figure 2.1.	SSM/I scan geometry	37
Figure 2.2.	Penetration depth of microwave emission at different frequencies	40
Figure 2.3.	Using the difference between a longer wavelength emission (19 GHz) and a shorter wavelength emission (37 GHz) to detect the presence of snow grains	41
Figure 2.4.	Penetration depth of microwave emission at 4, 10 and 37 GHz with increasing liquid water content	42
Figure 2.5.	Reversal of modeled TB at 36 GHz	55
Figure 2.6.	Modeled relationship between brightness temperature and ice thickness at different frequencies	64
Figure 2.7.	Observed relationship between TB and ice thickness at 5 GHz	64
Figure 3.1.	Location of the TERS and the study area	73
Figure 3.2.	Approximate shape of the Daring, Exeter, and Yamba Basins manually interpreted from NTS topographic maps	76
Figure 3.3.	Terrain classification of study area	78
Figure 3.4.	ENR 2001 LANDSAT landcover classification	79
Figure 3.5.	Reference grid for survey locations	81
Figure 4.1.	Snow density on lakes, flat tundra, plateaus (a) and slopes both low (b) and high (c), during the 2004 to 2009 snow surveys	92
Figure 4.2.	Frequency histograms of site density	94
Figure 4.3.	Comparison of estimated SWE and measured SWE for each of the survey years	95
Figure 4.4.	Snow depth on lakes and flat tundra during the 2004 to 2009 snow surveys.....	99
Figure 4.5.	Snow depth on slopes of less than 7 degrees.....	100
Figure 4.6.	Snow depth on slopes of greater than 7 degrees	101
Figure 4.7.	The general patterns of snow accumulation on steep and shallow slopes.....	102
Figure 4.8.	ESC 30 SWE compared to Site Average (depth x density) SWE	103
Figure 4.9.	SWE on lakes and flat tundra during the 2004 to 2009 snow surveys .	105
Figure 4.10.	SWE on slopes of less than 7 degrees	105
Figure 4.11.	SWE on slopes of greater than 7 degrees	106

Figure 4.12.	Basic tundra snow stratigraphic and textural attributes	107
Figure 4.13.	Generalized snowpack stratigraphy on different terrain types	109
Figure 4.14.	Frequency histograms of SWE for each of the survey years	116
Figure 4.15.	The North American portion of the global sub-grid SWE depth classification by Liston 2005.....	121
Figure 4.16.	Upland plateau.....	123
Figure 4.17.	Modified terrain based classification	134
Figure 4.18.	The addition of land cover classes to the terrain based snow cover classification	138
Figure 4.19.	Example of a site which contains sparse low shrub vegetation	140
Figure 4.20.	Boulders distributed across the tundra.....	141
Figure 5.1.	Spatial domain of time series EASE grids	149
Figure 5.2.	The seasonal evolution of 19GHz, 37 GHz from November 1 to April 30 for a) 2002/03 to 2004/05 and b) 2005/06 to 2007/08	151
Figure 5.3.	The seasonal evolution of the ΔT_{b37-19} from November 1 to April 30 for 2002/03 to 2007/08	153
Figure 5.4.	The average April 1 – 10 ΔT_{b37-19} from 1979 to 2008	154
Figure 5.5.	The percent variance explained by the first 10 components.....	157
Figure 5.6.	Component loadings for the PCA of April 1 to April 10 ΔT_{b37-19} in 41 EASE grid cells over a 30 year time period.....	158
Figure 5.7.	Component loadings for the PCA of April 1 to April 10 ΔT_{b37-19} and lake cover fraction in 41 EASE grid cells over a 30 year time period	159
Figure 5.8.	The idealized depth of emission at 37 GHz and seasonal evolution of snow and ice in the tundra	160
Figure 5.9.	Maps of the seasons with the highest loading in each PC	162
Figure 5.10.	The ΔT_{b37-19} of 1997-98 (PC 1) and 1978-79 (PC 2) over the NRCan AVHRR land cover classification	163
Figure 5.11.	The inter-annually consistent Canadian SWE band.....	163
Figure 5.12.	The percent variance explained by the first 10 components.....	164
Figure 5.13.	Component loadings for the PCA of April 1 to April 10 ΔT_{b37-19} and lake cover fraction in the subset of 27 EASE grid cells over a 30 year time period	165
Figure 5.14.	Maps of the seasons with the highest loading in each PC	166
Figure 5.15.	The ΔT_{b37-19} of 1999-00 (Subset PC 1) and 2003-04 (Subset PC 2) over the NRCan AVHRR land cover classification	167
Figure 5.16.	In-situ SWE plotted with corresponding April 1 to April 10 mean ΔT_{b37-19}	170

Figure 5.17.	The quadratic function between ΔT_{b37-19} and in-situ SWE plotted with the linear relationship using the Goodison algorithm	171
Figure 5.18.	In-situ SWE plotted with corresponding April 1 to April 10 mean ΔT_{b37-19} considering the 0.40 CV in SWE	172
Figure 5.19.	Calculated brightness temperatures versus SWE for horizontally polarized data at 50° incidence angle	174
Figure 5.20.	Seasonal evolution in 37 GHz from Nov 1 to April 30 in 2003/04 and 2005/06	176
Figure 5.21.	Theoretical depth emission at 37 GHz given different snow cover conditions	177
Figure 6.1.	Contributions to end of winter satellite scale Tb	178
Figure 6.2.	Flight line locations and ground based sites	180
Figure 6.3.	Relating Tb to in-situ snow measurements in the 2005 dataset	180
Figure 6.4.	Relating Tb to SWE measurements using the 2008 Magna Probe dataset	182
Figure 6.5.	High resolution airborne and ground based Tb compared to in-situ SWE	183
Figure 6.6.	Comparison of high resolution airborne and ground based Tb with SWE over flat tundra	186
Figure 6.7.	Ground based radiometer observations of snow removal at two flat tundra sites	188
Figure 6.8.	All Magna Probe and ground based SWE from flat tundra vs ΔT_{b37-19}	190
Figure 6.9.	The distribution of SWE on flat tundra	191
Figure 6.10.	Comparison of high resolution airborne and ground based ΔT_{b37-19} with SWE over lakes	192
Figure 6.11.	Comparison of high resolution airborne ΔT_{b37-19} with Magna Probe SWE over Daring Lake	193
Figure 6.12.	Comparison of high resolution airborne and ground based Tb with SWE over lakes	195
Figure 6.13.	Comparison of high resolution airborne Tb with Magna Probe SWE over Daring Lake	195
Figure 6.14.	Transect in Tb from lake to land for a portion of a 2005 high resolution airborne transect	196
Figure 6.15.	Ground based Tb observations over lakes	198
Figure 6.16.	Comparison of high resolution airborne Tb with SWE over slopes (< 7 degrees)	200
Figure 6.17.	Comparison of high resolution airborne with SWE over slopes (> 7 degrees)	203

Figure 6.18.	Relative location of airborne footprints along flight line	207
Figure 6.19.	Airborne transect across study area EASE grid	207
Figure 6.20.	Tb data for the three resolutions, high (A), mid (B) and low (C), along with AMSR-E Tb	208
Figure 6.21.	ΔT_{b37-19} data for the three resolutions, high (D), mid (E) and low (F), along with AMSR-E ΔT_{b37-19}	211
Figure 6.22.	6.9 GHz Tb vs lake fraction	214
Figure 6.23.	19 GHz Tb vs lake fraction	215
Figure 6.24.	37 GHz Tb vs lake fraction	216
Figure 6.25.	ΔT_{b37-19} vs lake fraction	217
Figure 6.26.	The frequency of lake fraction for the 40 EASE grid cells described in Chapter 5	219
Figure 7.1.	Plot 19, 37, ΔT_{b37-19} and SWE	223
Figure 7.2.	Quadratic function to estimate SWE from ΔT_{b37-19}	225
Figure 7.3.	Selecting the high or low SWE equation from 37 GHz Tb.....	226
Figure 7.4.	Estimates of SWE for the Daring Lake EASE grid from the 30 year satellite time series of ΔT_{b37-19}	227
Figure 7.5.	EC prairie algorithm estimates of tundra SWE.....	228
Figure 7.6.	The seasonal evolution of 19GHz, 37 GHz from November 1 to April 30.....	229
Figure 7.7.	The seasonal evolution of the ΔT_{b37-19} from November 1 to April 30 for 2002/03 to 2007/08	230
Figure A.1.	Plot of SWE \pm 1 STDEV and Tb for flat tundra sites in 2005 and 2008.	240
Figure A.2.	Adjusted mean SWE and original SWE vs ΔT_{b37-19}	241
Figure A.3.	Open fen site, Churchill, Manitoba	242
Figure A.4.	Interpolated surface from 940 probe measurements and location of 30 random measurements	243
Figure A.5.	Residual error between 30 random measurements and predicted surface from interpolation of 940 gridded measurements	244
Figure A.6.	SWE from four example footprints and SWE vs ΔT_{b37-19} for Magna Probe SWE < 120 mm on flat tundra	246
Figure A.7.	The distribution of SWE in two footprints with the lowest and highest ΔT_{b37-19}	248
Figure A.8.	Idealized relationship between surface roughness and snow pack properties.....	250
Figure A.9.	Mean Magna Probe SWE (\pm 1 STDEV) for each land cover class.....	250

CHAPTER 1: INTRODUCTION

1.1. Introduction

Terrestrial snow covers nearly 50 million square kilometers of the Northern Hemisphere each winter (IGOS, 2007). Seasonal snow cover directly affects many aspects of our infrastructure, economy and livelihood. Snow is often viewed as a burden; however, springtime snowmelt provides much needed runoff for agriculture, potable water supply and hydroelectric generation. Furthermore, snow is an essential cryospheric element to understand and monitor as it also has several direct effects on fundamental Earth systems. The high albedo of snow cover reflects incoming solar radiation and perpetuates lower surface temperatures. Moreover, snow is also a good insulator which reduces the depth and extent of ground frost as well as reducing the net heat exchange between ground and the atmosphere. These physical changes affect the atmosphere at its lower boundary, and snow cover is recognized as an important factor which influences the climate on local, regional and global scales (Berry, 1981). Furthermore, the spatial and temporal distribution of snow extent and depth are primary controls on ecosystem carbon exchange. Moreover, recent research suggests that late winter snow depth and spring-thaw timing strongly affect the annual cycling of carbon and nutrients along with other important biogeochemical processes in the Arctic (Larsen et al., 2007). Winter snowfall can comprise a large part of the total annual precipitation, especially in high latitude regions, and the subsequent snowmelt runoff can be the principal component in the annual water balance (Woo, 1998). Likewise, the spatial distribution of snowmelt is important to the ecosystem as it controls the soil moisture dynamics, the depth, formation and growth of the permafrost active layer, and the nature of vegetation productivity (Stow et al., 2004).

The accuracy and dependability of models to predict future changes in climate and snow cover are dependant on their ability to reconstruct past and present conditions (McGinnis and Crane, 1994). However, modeling snow distribution and regional climate for northern latitudes is not a simple task. The primary limitation is that many tundra snow cover data sets are spatially constrained and/or temporally discontinuous (Derksen et. al., 2000). In Canada, daily snow depth observations are available from 1915 to present for selected stations and from 1955 to present for most stations. However, these stations are mostly concentrated in or near populated areas and are only point estimates. Moreover, most, if not all, long term snow monitoring sites are located south of 55° N, despite the abundance and dominance of a northern snow cover (Brown, 1997) (Figure 1.1).

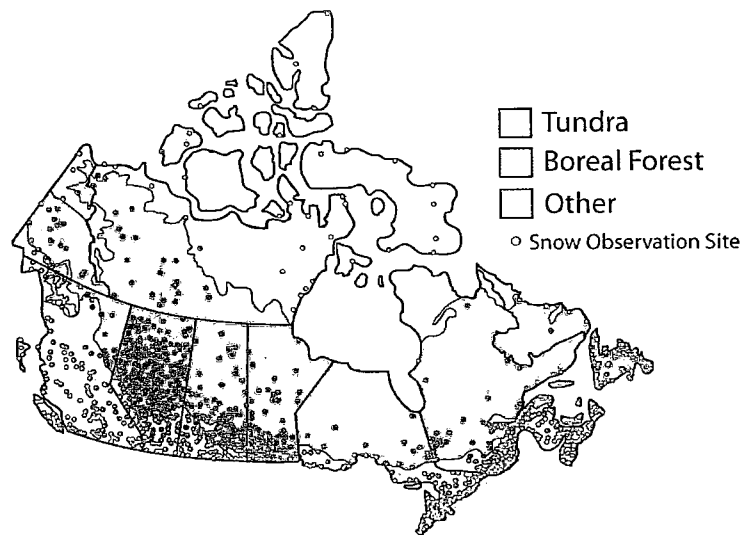


Figure 1.1. Canadian daily snow depth network available for analysis (modified from Brown et al., 2003)

In Arctic regions, it can be logistically difficult and very expensive to acquire spatially extensive in-situ snow data with enough re-visits to compile a useful dataset. Furthermore, deploying and maintaining meteorological stations capable of providing reliable snow data is also difficult and costly. Thus, the possibility of using satellite

remote sensing to estimate snow cover properties is appealing for research in remote northern regions.

1.2. Research Objectives

Given the linkage of tundra snow to many physical systems, the spatial and temporal discontinuity of current data sets, and the lack of operational snow cover monitoring protocol, there is a need for developing an intensive tundra snow cover data set for

- 1) the improvement, development and validation of large scale satellite remote sensing algorithms,
- 2) the extrapolation to large scale process models, and
- 3) the definition of features that cannot currently be easily remotely sensed or modeled (such as snow density and snow on sub-grid scale landscape features).

Snow cover parameters of interest are the spatial and temporal distribution of 1) snow extent, 2) snow depth, and 3) SWE. Snow extent is required for climate, hydrological and ecological research as it defines the percentage of land surface occupied and influenced by a snow cover, required for quantifying land surface albedo and subsequent radiation balance. Snow depth information is an important parameter for studying energy balance, carbon cycling and ecosystem dynamics, while SWE, calculated from snow depth and density, is important for estimating snowmelt runoff, evaluating climate models, and the detection of trends related to snow mass. The seasonal evolution of the snowpack is important; however, estimates of pre-melt tundra snow depth and SWE are most useful for both local and regional scale modeling. Through the review of current snow data acquisition tools in Section 1.3, it is clear that passive microwave sensors provide one of the best opportunities for providing spatially and temporally comprehensive high latitude snow cover data. These sensors have the advantage of being remotely collected with a daily frequency, extremely cost effective,

and immune to atmospheric conditions (cloud cover). Furthermore, a long time series of archived data is available (1978 to present).

The overall objective of this research is to improve operational capabilities for estimating end of winter, pre-melt tundra SWE in a representative study area using satellite passive microwave data. In order to meet this objective a series of steps will be undertaken and detailed in the remaining chapters. They include:

- 1) outlining the importance of tundra snow and sources of snow cover data (Chapter 1),
- 2) reviewing the literature and determining theoretical limitations of passive microwave remote sensing for monitoring tundra snow cover (Chapter 2),
- 3) selecting a representative study area (Chapter 3),
- 4) obtaining in-situ tundra snow cover data sets through multiple years of field surveys (Chapter 3),
- 5) analyzing in-situ data so that a better understanding of the distribution and properties of tundra snow can be achieved (Chapter 4),
- 6) evaluating the performance of current passive microwave algorithms for estimating tundra snow (Chapter 5),
- 7) determining the steps necessary to resolve uncertainty in current methods (Chapter 6),
- 8) summarizing the feasibility of using passive microwave remote sensing to estimate tundra snow cover properties (Chapter 7).

1.3. The Importance of Tundra Snow Cover

1.3.1. Introduction

Tundra environments comprise $7.2 \times 10^6 \text{ km}^2$ or 4.8 % of the entire land surface of the Earth and are characterized by low mean annual temperatures, the absence of a continuous forest cover, long dark winters, continuous permafrost soil, and persistent

snow cover (Ohmura, 2000). Tundra snow cover is an extremely important parameter to understand and monitor as it influences local, regional and global scale surface water balance, atmospheric dynamics, weather and climate patterns, surface energy and biogeochemical fluxes, along with ecosystem and permafrost dynamics (Table 1.1).

Table 1.1. The importance of tundra snow cover to natural systems

	Importance of Snow Cover	Scale
<i>Regional and Global Climate</i>	Snow cover properties control surface thermodynamics and affect atmospheric feedbacks	Regional to Global
<i>Carbon Balance</i>	Timing of melt and accumulation along with mid-winter snow depth influences vegetation respiration and balance between carbon sources and sinks	Regional to Global
<i>Hydrologic System</i>	Snow water equivalent determines potential volume of spring runoff. Timing and duration of melt are important to overall water balance and surface water chemistry	Local to Regional
<i>Permafrost and Active Layer</i>	Snow depth and snow melt timing affect ground thermal regime and active layer formation	Regional to Hemispheric
<i>Plants and Animals</i>	Snow depth insulates vegetation and determines access to food sources. Timing of snowmelt determines nutrient cycles and vegetation dynamics	Micro to Regional

1.3.2. Regional and Global Climate

The climate of the Arctic is characterized by extremes: very cold winter temperatures, highly skewed annual cycle of solar radiation input, dominance of snow cover, and relatively low rates of precipitation, all of which result from its geographic position (Hinzman et al., 2005). Atmospheric dynamics are controlled in part by changes in lower boundaries. As such, snow cover is recognized as a key factor in influencing local, regional and global climates (Berry M. O. 1981, in Gray and Male). Therefore, the spatial and temporal distribution of tundra snow is a key factor in determining the nature of winter climate. Snow has many unique surface properties which influence the surface energy balance. These include 1) a large latent heat of vaporization and fusion

compared to water, 2) a low thermal conductivity, 3) a high albedo compared to soil and vegetation, and 4) a lower surface roughness compared to most land surfaces (Pomeroy and Goodison, 1997). The large scale high albedo surface of seasonal snow, prevalent for several months, significantly influences global circulation patterns. Based on the parameters discussed, Figure 1.2 demonstrates how the energy balance of a snow free soil surface can be compared with that of snow covered land.

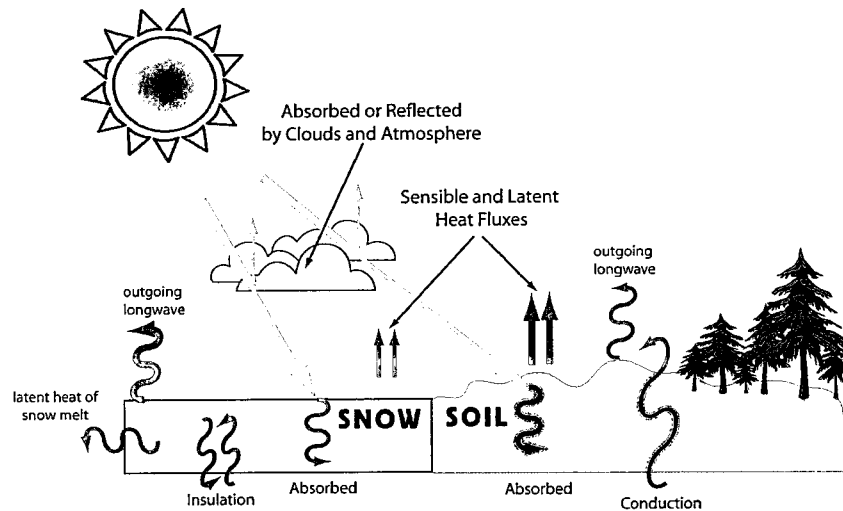


Figure 1.2. The comparison in shortwave energy reflection between a snow surface and bare soil

In Figure 1.2, the incoming and outgoing energy are largely balanced over bare soil; however, there is a large energy deficit produced over the snow covered surface (Cohen, 1994). This deficit exists during winter over large high latitude land areas, which results in significantly lower surface air temperatures. Cold northern snow covered regions act as a source for continental polar air masses which migrate into mid-latitude regions under large-scale circulation (Berry, 1981). These air masses are associated with cold surface temperatures. Snow cover has a large influence on the amount incoming energy lost to the atmosphere. As such, the onset of snow accumulation, the snow depth throughout the winter, the frequency of subsequent snowfall events and the timing of snow melt are key parameters which control snow-climate feedbacks.

The onset of snow accumulation is important as the introduction of even a thin snow cover dramatically increases surface albedo. Newly fallen snow can change the albedo of a surface from 0.25 to above 0.80 in a matter of a few hours (Oke, 1990). However, as a snow pack ages during the winter, the surface albedo drops from around 0.85 for new snow to around 0.70 after 5 days. In mid-latitudes, the albedo can fall to around 0.6 after 20 days due to the accumulation of dirt and debris (Dunne and Leopold, 1978).

As snow depth increases, the thermal gradient from the ground to the atmosphere decreases and the ground surface becomes increasingly insulated and isolated from the atmosphere (Cohen, 1994). Furthermore, as snow depth increases in the tundra, shrub and grass vegetation, which typically range from 0.15 to 1.0 m high, become increasingly covered in snow. Covering protruding vegetation lowers their ability to absorb solar radiation and to provide a boundary heat layer source (Strack et al., 2004). Covering the vegetation completely with snow decreases surface roughness and acts to smooth the land surface.

Before the onset of snow melt the regional climate differences across the tundra are small due to a relatively homogenous layer of snow. However, snow melt is important to climate feedbacks as during the relatively short melt period, the surface albedo can drop from around 0.8 to 0.1 (Ohmura, 2000). As such, the timing of melt onset is as important as is the depth of snow, which partly determines the length of time required to melt the snow pack. At regional and hemispheric scales, the accurate estimation of tundra snow melt extent and duration are important because high latitude snow cover both forces and reacts to atmospheric circulation patterns (Bamzai, 2003, Gong et al., 2003). Furthermore, observations by Ge and Gong (2008) suggest that snow depth, along with the spatial patterns of snow melt may play an important role on potential spring and summer climate.

1.3.3. Carbon Balance

The carbon balance in the tundra is the difference between carbon storage in soils and plants and carbon losses from subsequent decomposition. In high latitude climates, this decomposition is slow and carbon accumulates in the form of thick layers of organic matter (Loya and Grogan, 2004). The net carbon storage in tundra, combined with boreal forests, amounts to an estimated one-third of the global soil carbon sink (Post et al., 1982). As such, snow dominated tundra and boreal landscapes have an important role in the global budgets of atmospheric carbon dioxide (CO₂) and methane (CH₄) (Bonan et al., 1995). Thus, the timing of snow accumulation and snow melt and the spatial extent of snow cover have obvious implications for vegetation seasonality and productivity, and in turn, tundra carbon balance. Recent research has further demonstrated that in arctic ecosystems, once considered dormant during winter, production of CO₂ under snow cover accounts for a significant portion of the annual carbon budget (Brooks et al., 1997, Fahnestock, 1998, Grogan and Jonasson, 2006, Elberling, 2007).

Experiments conducted in tundra ecosystems demonstrate that snow depth has an influence on the extent of CO₂ production. Schimel et al. (2004) show how snow depth increased by a factor of 6 resulted in enhanced respiration and soil nitrogen cycling due to warmer mean winter soil temperatures and reduced temperature fluctuations. Nobrega and Grogan (2007) show how a moderate increase (0.3 m to 1 m) in snow depth affects the total wintertime respiration in the Canadian arctic tundra. The results of the study indicate that under normal snow and summer growing conditions there is an annual net gain in carbon. However, with a moderate increase in snow depth, especially if this prolongs snow melt and delays the growing season, such a tundra environment could switch to being a net source of carbon. Deeper snow also reduces the number of soil freeze-thaw cycles, which can 1) result in high initial pulses of CO₂

production if they involve severe temperature drops, or 2) have little effect on respiration if the temperature fluctuation is minimal. The conclusions of such research suggest that snow depth and snow melt timing are very important in determining biochemical processes and carbon cycling in tundra environments.

1.3.4. Hydrologic System

Seasonal snow cover is present on the tundra for up to 8 months of the year, and snowfall comprises over 50 percent of the total annual precipitation input to high latitude regions (Woo, 1998). Snow-melt water constitutes over 80 percent of the total annual runoff. Accurate estimates of runoff are important in order to quantify the potential melt water available to terrestrial and aquatic systems, for potential water supplies, for flood control, and for hydroelectric power generation.

Local scale snowmelt and runoff processes can occur rapidly over a relatively short period of time and can be difficult to capture and gauge. In the absence of gauge data, snowmelt runoff simulations are used. These models generally consist of a snowmelt energy model that generates melt water from a given snow cover and a hydrologic routing model that moves available melt water to the basin outlet (Pohl et al., 2005). The key input snow cover parameters in both local and regional models are pre-melt snow water equivalent (SWE) and the spatial extent of snow cover (Woo et. al. 1999).

1.3.5. Permafrost and Active Layer Formation

Permafrost soils are prevalent throughout tundra landscapes. The depth and extent of snow have a large control on the wintertime ground thermal regime. Snow-ground interface temperatures can vary significantly within a few hundred metres due to differences in snow thickness (Mackay and Mackay, 1975). The impacts of changes in snow accumulation, extent, melt timing and duration, density, and structure on the ground thermal regime, active layer formation and permafrost have been well

documented (Zhang, 2005, Ling and Zhang, 2007). Furthermore, Hinkel et al. (2006) show how deep drifts generated by the installation of snow fences in Barrow Alaska can strongly modulate ground thermal regimes and raise soil temperature from 2 to 14 degrees Celcius. In addition, these deeper snow drifts persist longer in the spring, which delays soil thaw and active layer formation and limits summer time soil warming.

1.3.6. Plants and Animals

Snow cover is one of the most important variables that control biological activity in arctic ecosystems (Walker et al., 1999). The spatial distribution of snow, as well as the temporal onset of snow accumulation and melt, has an influence on the distribution of plant species, communities, and animal activity (Eugster et al. 2000). A good example of the feedback between snow and vegetation is found in areas where deep snow drifts form. Snow accumulates in depressions, on lee slopes, or in areas of dense vegetation. Plants tend to preferentially occupy such sheltered areas which further enhances the entrapment of drifting snow. During winter, deeper snow provides insulation to the plants, restricting energy loss and reducing desiccation (McKay and Adams, 1981). Deep snow drifts tend to melt more slowly than the thinner snow on the surrounding landscape. The delay in melt slows the warming of the soil and can limit plant growth; however, the slow release of melt water well into the growing season provides beneficial moisture which improves plant productivity. This is one of the main reasons that the spatial distribution of snow during the winter has been highly correlated to summertime vegetation distribution (Bruland et al., 2004). As a whole, the depth of snow in the tundra has been shown to affect species composition, primary production, and biogeochemical cycles (Brooks et al., 1997). More specifically, increased snow depth has been shown to have a large effect on the temporal shift of plant floristics, and patterns of nitrogen cycling (Borner, et al., 2008). The spatial distribution and timing of snowmelt are also important and control 1) soil moisture dynamics, 2) the nature of vegetation productivity, and 3) vegetation phenology as both

the nitrogen availability and carbon-nitrogen ratio are strongly dependant on the number of snow free days (Stow et al., 2004,).

The dynamics of seasonal snow cover also influence the mobility of animals and affect their ability to find adequate shelter and food supplies. Small mammals which occupy the subsurface environment of a snow pack are very sensitive to changes in snow depth and density. They require sufficient depth for insulation, shelter and protection from the weather and predators. Certain species of rodents are quite active in winter due to the benefits of a snow cover. However, if the density becomes too high, it can make it more difficult to forage for food and increase travel on the surface which would increase potential expose to predators (McKay and Adams, 1981). Species which do not live below the surface of the snow are also greatly influenced by snow cover properties. The depth and density also determine the ease with which many species, especially migratory ungulates, move around, forage for food, and evade predators. An extreme example is the development of ice layers in the snow pack from severe wintertime rain-on-snow events. Such ice layers can act as a barrier to ungulate grazing and are linked to large-scale ungulate herd declines via starvation and reduced calf production rates (Grenfell and Putkonen, 2008). The timing of snowmelt is also important as the associated flush of spring growth has a definite influence the grazing patterns of reindeer and woodland caribou, and the feeding of arctic-breeding geese (Van der Wal et al., 2000).

1.3.7. Potential Environmental Change

The dominance of snow and ice makes tundra ecosystems very sensitive to potential environmental change. Recent global circulation models (GCM) predict a significant increase in both winter precipitation and mean annual air temperature (ACIA, 2004 and IPCC, 2007). More pronounced warming is forecast for high latitude regions due to the feedback between air temperature, snow and ice extent, and surface albedo (Lynch et al., 1995). As a corollary, considerable change to the spatial and temporal distribution of snow

cover and vegetation is expected due to the feedback between temperature, precipitation, snow and vegetation. Environmental change is also possible from increasing human activity in the tundra. Over the past decade, there has been a large increase in mineral exploration, mining operations and construction in the tundra. The regional impact of these operations on local and regional snow cover dynamics needs to be considered.

1.3.7.1. Temperature and Precipitation

From the data that are available, the climate of the Arctic appears to have warmed substantially since the end of the Little Ice Age. From the mid-1800s to mid-20th century, the Arctic has warmed to the highest temperatures seen in 400 years (Overpeck et al., 1997). The high sensitivity of snow to fluctuations in temperature and precipitation makes it a key indicator year to year variability. As such, snow is often used to test climate change hypotheses concerning the redistribution and acceleration of the hydrologic cycle (IGOS, 2007). Tundra warming is projected to be greatest in late autumn and winter. Increased winter precipitation is associated with the retreat of snow cover and sea ice (Serreze et al., 2000).

During winter snow cover dominates the terrestrial landscape and unfrozen surface water is rare. As such, a negative annual radiation balance is established and more radiation is lost to space as heat than comes in through solar heating (Hinzman et al., 2005). Several studies have observed a reduction in seasonal high latitude snow extent in recent decades (Brown, 2000, Dye, 2002). The reduction in snow extent is important as it changes the radiation balance through changes in the feedback between snow and bare ground (Qu and Hall, 2006). As snow extent decreases, more energy is absorbed and transferred to the atmosphere which results in increased melt and a positive albedo feedback (Groisman et al., 1994). Through this positive feedback mechanism, changes in snow cover, along with sea ice extent, are expected to contribute to and amplify climate warming (Serreze et al., 2000).

Earlier than normal snowmelt onset, which is forecast for high latitude regions, can further influence the feedback mechanisms between atmospheric circulation and hydrologic processes. The snow melt increases the moisture content of the soil which lowers ground surface albedo and increases the absorption of solar energy. This increases soil temperature, and thus surface evaporation which can be the precursor to drier than normal conditions during summer months. Earlier snowmelt has a much greater impact on the albedo feedback than later snow accumulation in the fall as solar input is much closer to the annual maximum in the spring. A later than normal snow melt period would act in the opposite way, promoting cooler and wetter conditions long after the snow has melted (Cohen, 1994). An increase in the length of the snow-free period or in summer air temperature would also enhance evapotranspiration rates. Unless balanced by an increase in rainfall, the summer water balances for much of the tundra would become increasingly negative which would reduce lake levels and ground water recharge (Rouse et al., 1992).

Evidence suggests that changes in high latitude temperature, precipitation and snow cover may already be occurring. However, quantifying this change is complicated by the high variability of snow cover throughout a large range of spatial and temporal scales (IGOS, 2007). As such, appropriate snow cover data that can define and generalize variable snow covered landscapes are necessary in order to validate models which predict future conditions.

1.3.7.2. Snow Vegetation Feedbacks

The spatial, temporal and functional response of tundra vegetation to changes in snow cover could further influence global climate through direct impacts on radiation and energy balances (Bonan et al., 1995). Both modeling and observational studies have provided evidence of changes to arctic vegetation distribution under increasing air temperatures (Chapin et al., 2005). Most models would agree that warming temperatures would produce a northward expansion of the boreal forest. Observations of Alaskan tundra

show that in the last 50 years, there have been significant in-filling of previously sparse shrub growth, expansion of shrubs into previously shrub-free areas and increasing extent and density of spruce forests at treeline (Sturm et al., 2001a).

In the tundra, shrubs have been shown to modify the distribution, depth and properties of the snow pack. In areas where shrubs are more abundant, there is a greater accumulation of drifted snow, and less snow is lost throughout the winter due to sublimation (Sturm et al., 2001b). Model simulations by Liston et al. (2002) in a tundra basin suggest that enhancing shrub abundance in the domain increased depth by 14%, decreased blowing snow sublimation fluxes by 68%, and increased snow cover thermal resistance by 15%. Furthermore, using blowing snow models and observed data, Pomeroy et al. (1997) show that shrub tundra areas accumulate four to five times more snow than areas of barren tundra. The greater snow depth in shrub areas influences the timing and magnitude of snow melt. Early in the melt season, the deep snow over buried shrubs maintains a higher albedo (Sturm et al., 2001b). However, as the snow melts and vegetation becomes exposed, snowmelt rates under shrub canopies are generally enhanced in comparison with sparsely vegetated tundra (Pomeroy et al., 2006).

The presence of shrubs also enhances sensible heating and evapotranspiration during the snow free period. As such, an expansion of shrubs would result in the positive feedback of air temperature which would augment warming at local to regional scales. The magnitude of vegetation, snow, energy balance feedbacks on potential high-latitude warming is much greater than previously thought (Beringer et al., 2005). For example, a comparison between snow cover and vegetation distribution by Buus-Hinkler et al. (2006) revealed that tundra vegetative vigor in Zackenberg Greenland is primarily controlled by the initiation of the snow-free period rather than air temperature. This is important as it indicates that in such arctic regions an increase in snowfall and snow depth may extend the winter

season and have a greater impact on the ecosystem than projected GCM increases in air temperature or may also act to mitigate the impact of increases in air temperature.

1.3.7.3. Human Development

Large scale human development in high latitude landscapes has typically been focused on resource extraction. Several different mines have operated in the Canadian North since the early 1930s. The discovery of diamonds in the Canadian tundra in the early 1990s sparked a flurry of exploration and, within the last decade, mine development. With three open pit diamond mines currently in operation and much more exploration being done at claim sites throughout the tundra, diamond mining has the potential to have a marked impact on the landscape. Furthermore, there are currently proposals for all-weather road construction spanning from the boreal forests in Yellowknife NWT across the tundra to the Arctic coast at Bathurst Inlet. The impacts of related mineral exploration, mine construction, mining operations, and decommissioning on the landscape are wide ranging and depend largely on the type of mineral being extracted and scale of the operation. Most commonly, the effects of mining on the landscape are most visible surrounding a mine and at a local scale. In an ecosystem considered sensitive to change, the environmental impact of the recent development associated with diamond mining needs to be assessed. Open pit mining has the potential to have a larger environmental impact due to the scale of operations and the amount of dust and rock blasting by-products released into the air. Ammonium nitrate contamination has already been detected in the vicinity of the Ekati Mine near Lac de Gras NWT.

The impact of northern mining operations on vegetation, soil and wildlife has been investigated by many researchers. Airborne dust produced from the Ekati mine and haul roads has been identified as having adverse local effects on vegetation species composition and plant communities (Male and Nol, 2005). However, airborne dust also

has the potential to impact more regional snow melt dynamics. Modeled results by Drake (1981) show how a thin layer of dust on a snow pack can lower surface albedo such that snow melt can be significantly accelerated. These findings are in agreement with observations at Schefferville, Quebec, where snow near active mine sites was observed to be melting up to four days earlier than on the surrounding landscape (Drake, 1981). The extent of dust deposition from active diamond mines and its effect on snow melt has not yet been quantified. However, given the feedbacks between snow melt rates and ecosystem, hydrologic cycle, and permafrost dynamics, dust deposition remains a serious concern, especially as development continues to increase.

1.3.8. Tundra Snow Parameters

The previous section demonstrates the wide range of multi-disciplinary applications for seasonal snow cover data. Several spatial and temporal snow cover parameters have been identified and are summarized in Table 1.2.

Table 1.2. Application of snow cover parameters

Application	Spatial Snow Parameters	Temporal Snow Parameters
<i>Regional and Global Climate</i>	- Snow Extent - Snow Depth - Snow Surface Albedo	- Snow Accumulation - Snow Melt
<i>Carbon Balance</i>	- Snow Extent - Snow Depth	- Snow Accumulation - Snow Melt
<i>Hydrologic System</i>	- Snow Extent - Snow Water Equivalent (SWE)	- Snow Accumulation - Snow Melt
<i>Permafrost and Active Layer</i>	- Snow Extent - Snow Water Equivalent (SWE)	- Snow Accumulation - Snow Melt
<i>Plants and Animals</i>	- Snow Extent - Snow Depth - Snow Water Equivalent (SWE) - Snow Density and Stratigraphy	- Snow Accumulation - Mid-winter melt or rain events - Snow Melt

The onset of snow accumulation, the extent of a snow cover, the depth of snow and the timing of snow melt are the most broadly applicable snow data. However, SWE is the most important factor for hydrological models which determine potential melt water

available to vegetation in the spring, and in validating GCM snow mass outputs. Snow density, surface albedo, along with observations of mid-winter melt and rain-on-snow events, are used in addressing specific research problems, however, they are not as widely applicable.

1.4. Tundra Snow Data

1.4.1. Introduction

Tundra snow cover is a difficult parameter to quantify. Snow accumulation patterns are controlled by differences in regional precipitation and topography, by vegetation distribution and by significant wind redistribution. Furthermore, the rugged terrain and the remoteness of tundra regions make it logistically very difficult to observe regional snow cover parameters with any consistency. However, where they exist, tundra snow cover data are a perfect diagnostic tool for initializing, testing and validating the performance of many different physical models (Barry, 1997). They are also highly sought after for application in many cross-discipline research projects (Table 1). There are several ways in which tundra snow cover data have been and are currently being obtained. The data are

- 1) Measured from in-situ surveys,
- 2) Derived directly from local weather station data,
- 3) Modeled to form distributed data and/or extrapolated from point data, and
- 4) Estimated from remote sensing data.

Each method has its advantages and disadvantages, and the utility of the data is based largely on the required spatial and temporal resolution.

1.4.2. Manual In-situ Snow Data

Manual in-situ measurement of snow depth involves the use of graduated in-ground stakes or the insertion of a ruler or probe into the snow pack. Such data are usually considered to be the most accurate; however, data acquisition requires rigorous

field work, and the data are not guaranteed to be accurate. Error can be accrued using either the stakes or through the manual insertion of rulers and probes. Recording snow depth from fixed stakes requires frequent visits. This is labor intensive and can be problematic during melt when increased traffic changes the snow surface roughness which can accelerate melt. Moreover, snow stakes are spatially constrained, and as such, site selection is important to ensure they are representative of snow cover in a given landscape. Manual snow probe measurements are also labor intensive and usually spatially constrained to easily accessed sites or snow courses. Probe data can misrepresent true snow depth due to ice lenses or very dense snow. In an effort to determine the true base of a snow pack, the probe or ruler may be inserted with too much force causing it to penetrate into the underlying ground vegetation or soil which can introduce an overestimation of snow depth. This is especially problematic in tundra environments as the upper layer of ground vegetation can be thick (usually moss or lichen) and easily penetrated by a snow depth measuring device.

In-situ snow density is typically measured using a calibrated snow tube. The tube is inserted into the snow pack, the depth is recorded, and the sample from within the tube is then weighed in order to calculate density. However, in some snow conditions, it can be difficult to retain a snow sample in the tube. This is especially prevalent in areas of thin snow cover and where there is significant depth hoar at the base of the pack. The inability to retain samples leads to a systematic underestimation of snow density. Snow tube instrument error varies depending on the type of sampler, but ranges between 0 and 10 % mean density error (Goodison et al., 1981). Snow water equivalent is calculated by multiplying depth times density; therefore, it is important to minimize error in both measures.

In-situ measurements, while often the most reliable, are usually confined to small research basins (Woo and Marsh, 1978, Pomeroy et al., 1997, Hirashima, et al., 2004,

Woo and Young, 2004) or are obtained along a defined transect (Sturm and Liston, 2003) or through an annual snow course (Pulliainen, 2006). While all of these data sets have proven to be very useful in defining tundra snow cover characteristics, they are not always sufficiently spatially extensive for direct validation of large scale model results or for algorithm development over large basins and coarse grid resolutions. Furthermore, in the tundra snow depth is quite variable even at the site scale. As such, it can be difficult to assess or quantify variability when using point data.

1.4.3. Automated Station Snow Data

Due to the difficulty in collecting large scale distributed in-situ snow data, few operational in-situ survey sites currently exist in Canada, and the network has been gradually eroding over the past twenty five years (Neumann et al., 2006). The lack of in-situ data has increased the reliance on snowfall and snow depth data collected from automated meteorological stations. Snowfall is defined as the depth of fresh snow which lands on the ground during a given period, while snow depth refers to the amount of snow on the ground at the time of observation (Goodison et al., 1981). Snowfall is captured in a gauge similar to liquid precipitation; however, these gauges are known to produce systematic error caused 1) by loss through evaporation from within the gauge, 2) by the inability to record trace snowfall events (<0.2 mm), and 3) by undercatch during windy conditions (Woo, 1998).

Snow depth is measured using automated sonic ranging snow depth instruments fixed to meteorological stations. Sonic depth sensors emit a downward pulse which can calculate the distance between the sensor and the surface of the snow pack (Gubler, 1981). Errors in measurement can occur during falling and blowing snow events; however, these data can be quality controlled by using hourly trends and snowfall precipitation data when available (Goodison et al., 1988). Sonic sensors, however, do not disturb the snowpack and the snow depth recorded is a spatial average over a

circular area, which may range from 0.2 to 2 m in diameter depending on the height of the instrument. This spatial averaging can compensate for microscale snow surface heterogeneities which are difficult to avoid with typical point measurements (Pomeroy and Gray, 1995).

Snow gauges can provide a long time series of daily snowfall and snow cover information (Brown and Goodison, 1996). However, they can be labor intensive to set up and maintain, as well as costly to purchase and service in remote locations. Furthermore, given that they are posted in a fixed location, the data are even more spatially constrained than in an in-situ survey, remain subject to potential errors, and are not able to quantify the spatial variability in snow depth. Corrections can be applied to overcome systematic gauge error; however, sparse gauge networks, especially in high latitude regions, limit the applicability of the data to large scale modeling (Derksen and LeDrew, 2000).

1.4.4. Canadian Snow Database

Daily snow depth measurements are available from observing stations in the Canadian Arctic from the 1950s and from climate stations from the early 1980s. The current network of data observations is sparse north of 55 degrees and especially sparse in the tundra where sites are biased towards coastal settlements.

The snow depth and SWE data that have been collected are available through the Canadian Daily Snow Depth Database which has been updated to the end of the 2007 snow season (www.ccin.ca). The data contain SWE and snow depth measurements from snow surveys taken by more than twenty agencies at weekly, biweekly or monthly frequencies. The data were subject to rigorous quality procedures following Robinson, 1989, and missing values were filled using a calibrated snow accumulation and melt method driven with daily temperature and snowfall data (Brown and Braaten 1998). The resulting data, mostly reconstructed values prior to 1940 and

predominantly observed values after 1950, with a pronounced peak in the 1976-1985 decade, have been compiled as part of the Canadian National Climate Data Archive. After 1985, the closure of many snow courses combined with the erosion of contacts between the Meteorological Service of Canada and other data collection agencies resulted in a steep decline in the amount of data. However, in the early 1980s, there were over 1700 snow course observations per year in Canada that were compiled in the database (Meteorological Service of Canada, 2000). Brown (2000) identifies a total of 154 stations with more or less complete data coverage from a 1915–93 study period. However, these observations are mainly located in southern Canada south of 55°N, and some of these stations did operate from 1993 to present. The lack of a long time series of high latitude snow cover observations restricts the reconstruction of North American snow cover trends to months when the snow extent dips south of this data limit and severely impacts linkages to large scale circulation models (Brown, 2000).

1.4.5. Modeled Snow Data

The application of snow cover data can be difficult when incompatibilities exist between the scale of the observations and the resolution of computed or modeled outputs. In-situ and gauge measured snow data can be especially problematic as they are collected at one specific site and recorded as point data. Comparing point data from one area to the next and from year to year can be difficult as different sampling personnel, field protocols and/or instruments are often used. As such, most snow cover measurements and long term databases can be prone to inaccuracies stemming from differences in instrumentation, biases in measurement techniques, and the reduction or relocation of gauges or meteorological stations (Bloschl, 1999).

In the absence of spatially extensive observations, models can be applied to extrapolate in-situ or gauge measured snow cover parameters over larger areas. Scaling of snow cover data is becoming increasingly important as there is a need for applying

physically based snow cover parameters in evaluating regional and global circulation models (RCM and GCM) and to basin scale hydrological models (Luce et al., 1999, Bowling et al., 2004). Two main methods have been used to represent point data over larger model grid cells. The first involves using statistical methods to extrapolate point data over larger areas. The second method involves the development of process models which incorporate point snowfall and point meteorological data in order to estimate snow distribution patterns over larger areas.

The evaluation of GCM snow cover simulations is typically limited by a lack of spatially extensive and reliable data. Brasnett (1999) developed a method to provide global, real-time analysis of snow depth data. The method uses observations of snow depth from the synoptic observing network and snowfall estimated from numerical weather prediction (NWP) models. The observed data are incorporated using a method of statistical interpolation called optimum interpolation. The method first involves developing a background field which is interpolated horizontally to observed locations using a bilinear interpolation. The method, described in detail by Brasnett (1999) blends the information from the background with the observed. Corrections to the background are computed at each grid point using a weighted sum equation. The method developed produced realistic snow depth estimates, even in regions with a lower density of observations. However, snow depth estimates were sometimes biased or unrepresentative due to their location in urban areas, in valleys or along coasts. Brown et al. (2003) use the method developed by Brasnett (1999) in order to generate a 0.3° latitude/longitude grid of monthly mean snow depth and corresponding estimated SWE over North America for the evaluation of GCM snow cover products. Modeled historical snow depth data were in good agreement with independent in-situ and satellite observations, and the new gridded dataset was able to capture continental scale variations in SWE and snow extent. Furthermore, the snow depth climatology produced

by Brown et al. (2003) provides an improved continental dataset over the previously accepted Foster and Davy (1988) product, with a notable improvement in early and late season snow line delineation. The data set successfully captured interannual variability in snow extent in SWE during the November – April period, however, it was less successful during the May – October period as the snowline was located over data sparse northern regions.

The paucity of high latitude station data available to Dyer and Mote (2006) for developing trends in observed snow depth, further illustrates how the lack of data across the vast Canadian North severely impacts the accuracy and reliability of continental scale gridded snow depth datasets. Dyer and Mote (2006) interpolate North American snow data to a 1 degree by 1 degree grid. In the tundra, some grid cells do not have a single station within their footprint, while others have only one station to provide data. Furthermore, the few stations that do produce data are not always in the most representative locations, however, they are often relied upon to represent sub-grid average snow conditions. The complexity of the terrain, the snow cover variability between years, and the representativeness of microscale point data for larger spatial domains all need to be considered when extrapolating point station data (Yang and Woo, 1999). The lack of spatially comprehensive in-situ snow observations is not restricted to North America. Several studies lack crucial data for large scale modeling and remote sensing algorithm development. The lack of in-situ data sometimes necessitates the use of climatological global snow depth data like those developed by the USAF/ETAC (Foster and Davy, 1988). While the development of these datasets is certainly robust, it is not a suitable replacement for spatially distributed in-situ measurements. As such, determining a method for accurately extrapolating tundra snow cover data is vital to understanding large-scale tundra snow cover dynamics and improving continental scale snow cover products.

Process snow models are used to estimate snow distributions on a basin scale. For example, various distributed blowing snow models have been developed to calculate mass and energy fluxes of blowing snow and the resulting annual tundra snow accumulation over heterogeneous catchments (Pomeroy et al., 1997). Model landscape elements typically include vegetation, terrain, and exposure and fetch characteristics. Blowing snow models have been employed over larger study areas (Bowling et al., 2004), incorporated with linear windflow models (Essery, 2001), and combined with other land surfaces models (Pomeroy et al., 1998). These models can successfully replicate the relative pattern of snow accumulation in their study basins and are useful for the identification of snow sources, sinks and areas not affected by wind redistribution. However, without measurements of sublimation, available meteorological data, topographic information and frequent in-situ snow surveys, such model results can be difficult to validate.

Liston and Sturm (1998) developed a physically based numerical snow transport model (Snow Tran 3D) which incorporates the effects of vegetation, topography and sublimation and the dynamics of snow transport in order to estimate snow distribution. The model inputs are wind speed and direction, precipitation, air temperature, humidity, solar radiation, topography and vegetation snow holding capacity. The model has been successfully used for reproducing snow distribution in an Alaskan study site (Liston and Sturm, 1998), in a 5.5 km² watershed in eastern Siberia with some modification (Hirashima et al., 2004) and in study areas ranging from 1 km² to 250 km² in Svalbard, Norway, with some changes made to the model (Bruland et al., 2004). These models successfully provide estimates of snow distribution; however, they require meteorological inputs which are not always available nearby, and the modeling methods may not be directly transferable to other study sites.

Physically based models of snow distribution have also been successfully used for hydrological studies in high Arctic catchments. Woo and Young (2004) developed a 1 km grid model for estimating snow distribution and melt using a terrain model, meteorological data and an end of season in-situ snow survey. This modeling, similar to Woo and Marsh (1978) takes into consideration the strong, yet relatively consistent relationship between topography and seasonal snow distribution patterns. In order to lessen data collection requirements, the landscape is broken into classes, and stratified sampling is done based on the distribution and abundance of each class. Random samples of depth and density are taken from a specific class and are used to calculate a class average (Pomeroy and Goodison, 1997). Using this computationally simple technique, weighted average snow distributions can be generated over basins where topographic information is known and end of season snow cover data are available.

1.4.6. Snow Data from Remote Sensing

Remote sensing techniques have been employed to monitor snow since the 1960s when the visible light channels on the National Oceanic and Atmospheric Administration (NOAA) satellites were used to map snow extent (Robinson, 1993). These early snow extent products had their weaknesses and limitations; nevertheless, it became evident that the data were very useful for application to weather model forecasts of surface air temperature (Brasnett, 1999). The long time series of snow data provided by the NOAA satellites remain one of the most valuable tools for examining spatial and temporal variation in snow cover at both a regional and hemispheric scale (Brown and Goodison, 1996, Tait et al., 2000). Since the development of these data sets, satellite remote sensing has expanded to provide information on snow extent, depth, wetness, and SWE with larger spatial swaths, improved spatial resolution and, in some cases, a more rapid revisit frequency. Remote sensing products have the distinct advantage of not being as labour intensive as data collection in the field and are often much less

costly. Once the remote sensing data are parameterized, they can produce near real time operational estimates without corresponding in-situ measurements or meteorological observations. However, the utility of satellite sensors to provide useful, operational tundra snow cover data depends on sensor parameters and the desired resolution of data outputs.

1.4.6.1. Visible Spectrum Sensors

The spatial extent of snow cover over North America has been continuously monitored and mapped on a weekly basis from 1966 to 1997 by NOAA. The snow charts were produced through visible interpretation of 1 km resolution advanced very high resolution (AVHRR) imagery from 1966 to 1997. No digital methods were employed by the data interpreters; instead a binary snow / no-snow classification is used where a grid cell has to contain 50% or more snow cover to be classified as snow (Tait et al., 2000). The charts were produced on an 89 x 89 polar stereographic grid for the Northern Hemisphere, with cell resolution ranging from 126 x 126 km to 200 x 200 km (Robinson et al., 1993).

The weekly snow maps were used primarily for numerical weather modelling. However, large errors in the near surface temperature forecasts were noted due to the temporal infrequency of observations (Ramsay, 1998). One of the main problems was the inability to distinguish the snow / no snow boundary during cloud cover. To address this problem, and improve the spatial and temporal resolution of snow charts, a new interactive multi-sensor snow and ice mapping system was developed (IMS) in 1997. The IMS product integrates passive microwave data in order to provide daily snow maps with a much better spatial resolution (24 km) than the weekly maps (Ramsay, 1998). The new IMS product output was quickly found to be much superior to the weekly maps and integrated into the manual charting of snow and ice in 1999 (Ramsay, 2000). The IMS product was upgraded in 2004 with new system dynamics and input data. The most

notable improvements to the IMS were a shift to a 4 km resolution output, automated snow detection algorithms and expansion to global extent (Helfrich et al., 2007).

There are several factors which compromise the accuracy and reliability of the NOAA snow maps for high latitude environments. Foremost, early snow charts were acquired using only visible spectrum satellite data which are limited to daylight hours and useful only under cloud free conditions. Furthermore, there are also a number of limitations, summarized by Robinson (1993), when manually interpreting snow cover from visible imagery. Tree cover, such as the subarctic boreal forest areas, can mask snow; the low sun angle of high latitude environments reduces the reflectivity and detectability of the snow cover. Moreover, certain types of clouds, such as cirrus, low stratus and small cumulus, are difficult or impossible to visually distinguish from snow covered surfaces (Simic et al., 2004). Wang et al. (2005a) found that the NOAA weekly dataset consistently overestimated high latitude snow cover extent during the spring melt period. Delays in snow melt onset of up to 4 weeks were observed due in part to the frequency of cloud cover and the low frequency of data coverage over high latitudes. Their results suggest that caution should be used when applying these data to studies that rely on snowmelt timing. Brown et al. (2007) found similar results in that the NOAA snow cover duration dataset was not highly correlated with regional spring snow cover duration from surface observations. One of the biggest weaknesses of the NOAA snow maps and IMS products is the lack of snow depth, density or SWE information.

Visible spectrum LANDSAT TM data have also been used for monitoring snow cover. Dozier and Marks (1987) along with Lundberg et al. (2004) utilize the data for snow mapping, while Guneriussen (1997) shows how it can be integrated with other remote sensing techniques, and Hall et al., 2000a, use the data for comparison and validation of other snow extent products. A normalized difference snow index (NDSI) is typically used to discriminate snow cover from bare ground using LANDSAT TM data.

The NDSI uses TM bands 2 (0.56 μm) and 5 (1.65 μm) as follows: $\text{NDSI (LANDSAT TM)} = (\text{Band 2} - \text{Band 5}) / (\text{Band 2} + \text{Band 5})$ (Riggs, 1994). The high resolution of LANDSAT TM data (10 – 30 m) makes them more desirable for monitoring snow extent in smaller basins and in more heterogeneous terrain. However, satellites revisit frequency is limited to 16 days which hinders the ability to monitor rapid changes in snow extent. Furthermore, as a visible wavelength satellite, LANDSAT data are restricted to estimating snow extent during daylight hours and under cloud free conditions.

Data from the moderate resolution imaging spectroradiometer (MODIS) have also been used to map snow extent. MODIS provides data with a 500 m resolution and twice daily overpass times. MODIS snow mapping techniques are fully automated and aim to overcome some of the typical limitations associated with the interpretation of visible imagery and manual mapping of snow cover (Salomonson and Appel, 2004). Snow cover is calculated with a NDSI using reflectance from bands 4 (0.545-0.565 μm) and 6 (1.628-1.652 μm) and is defined as: $\text{NDSI} = (\text{band 4} - \text{band 6}) / (\text{band 4} + \text{band 6})$ (Hall et al., 2002a). Each pixel is classified as snow if the NDSI is ≥ 0.4 and if the reflectance of band 2 is $\geq 11\%$. If the band 4 reflectance exceeds 10%, then the pixel will not be classified as snow. This technique is required as very low reflectance causes the NDSI denominator to be quite low. This prevents very dark target pixels, such as dense coniferous forests, from being classified erroneously as snow cover (Hall et al., 2002b). A thermal mask can also be applied using infrared bands 31 (10.78-11.28 μm) and 32 (11.77-12.27 μm) to differentiate snow from cloud cover (Simic et al., 2004), while a normalized difference vegetation index (NDVI) can be used with the NDSI to avoid the erroneous classification of forested areas and improve the detection of snow in dense forest cover (Klein et al., 1998).

MODIS data are used in combination with NOAA data by Natural Resources Canada and the Canadian Centre for Remote Sensing. The data are used to provide

daily snow and inland ice cover maps over Canada. The maps are produced at a 500 m resolution and a simple binary snow no-snow classification is used (www.nrcan.gc.ca).

1.4.6.2. Microwave Sensors

Spaceborne microwave sensors have proven to be useful for monitoring the cryosphere as they have 24-hour and all weather imaging capabilities, extensive spatial swaths (hundreds of kilometers) at various resolutions and, depending on the sensor, daily revisit possibilities (Sokol, 1999). Microwave sensors are either active or passive. Passive sensors detect and record naturally occurring microwave energy, while active sensors emit microwave energy towards a target and measure the amount reflected back.

1.4.6.2.1. Active Microwave Sensors

The most common type of active microwave sensor used for snow cover research is RADAR. The RADAR sensor sends out a radio signal towards the target and senses the amount of energy that is returned (Holz, 1985). The magnitude of the signal return or backscatter, measured in decibels (dB), is recorded in order to differentiate between different target media. RADAR data are usually obtained using Synthetic Aperture RADAR (SAR) systems which can provide data at spatial resolutions from 10 – 100 m (Ulaby et al., 1982).

The total backscatter produced from a snow pack depends on the dielectric properties of the snow and on the contributions of surface and volume scattering from the air-snow interface, the snow volume and the snow-ground interface (Baghdadi et al., 1999). The dielectric constant of snow is a function of the relative proportion of liquid and ice crystals in the snow. Problems detecting snow cover occur during dry snow conditions as active microwave sensors have difficulty detecting media with a low dielectric constant, and the wavelengths most commonly used (C – Band, 5.3 GHz) are too large to detect snow grains (Rango, 1996). Thus, in dry snow there is negligible

volume scattering, and the microwave energy passes directly through the snow pack. Under these conditions, the dominant controls on backscatter return are the soil dielectric and soil surface roughness properties (Baghdadi et al., 1999).

When a snow pack becomes wet, the snow dielectric increases significantly, and the subsequent scattering and absorption of the microwaves permit the detection of a snow cover (Rott, 1987). The contrast in dielectric between wet snow and dry snow or snow-free conditions is the basis for using SAR data to study changes in snow state. Multi-temporal image subtraction of repeat pass imagery (imaged at the same spatial location with a different time period) is used to detect a wet snow cover (Baghdadi et al., 1997; Caves et al, 1999; Guneriusson et. al. 2001). This image subtraction approach eliminates the effects of topography and macro scale surface roughness problematic to individual SAR scenes (Nagler and Rott, 2000). The estimation of SWE using SAR data has not been successful for the same reason that makes it possible to detect snow wetness. Changes in snow surface dielectric permit detection of wet snow but prevent penetration into the snow pack.

Active microwave data from Ku-band scatterometers (12 to 18 GHz) have also been used to monitor snow cover. Sensors in the Ku-band have similar difficulties to C-band in detecting dry snow cover; however, studies have shown that they are highly sensitive to surface snow melt and largely not affected by vegetation cover (Nghiem and Tsai, 2001). Wang et al. (2005b) use the Seawinds QuikSCAT Ku-band sensor data (13.4 GHz) to produce maps of melt season duration over Canadian Arctic ice caps. Brown et al. (2007) show that the high resolution of QuikSCAT data (5 km) can be effective for monitoring spring snow cover variability at high latitudes.

1.4.6.2.2. Passive Microwave Sensors

Satellite passive microwave data have formed the basis for many snow water equivalent (SWE) and snow depth retrieval algorithms. These methods have been used to successfully monitor snow cover in prairie environments (Goodison and Walker 1995, Derksen et al., 2003), and in boreal forests (Goita et al., 2003; Pulliainen, 2006), but with higher uncertainty at hemispheric scales (Kelly et al., 2003; Biancamaria et al., 2008). Estimates of SWE and snow depth are based on measuring the extent to which naturally emitted microwave energy is absorbed or scattered by the presence of a snow cover. Passive microwave sensors offer promise to provide operational snow cover monitoring for tundra landscapes; however, problems quantifying SWE and snow depth arise when sub-grid scale snow stratigraphy and terrain features complicate the emission, absorption, and scattering properties of the snow pack. The feasibility of passive microwave remote sensing of tundra snow will be discussed in more detail in Chapter 2.

1.4.6.3. Summary of Remote Sensing Data Sources

The previous sections outline how different remote sensing approaches can provide snow data. Each sensor has its own set of strengths and weaknesses. Table 1.3 provides a brief summary of each sensor group and what types of snow cover data they can provide.

Table 1.3. Summary of remote sensing sensors for detecting snow cover

Sensor	Resolution	Revisit Frequency	Detectable Snow Parameters	Limitations
VISIBLE SPECTRUM SENSORS				
AVHRR	1 km	Daily	Snow Extent	<ul style="list-style-type: none">- Cloud Cover- Need Daylight- No SWE or volume data
MODIS	500 m	Daily		
LANDSAT TM	10 m	17 Days		
ACTIVE MICROWAVE SENSORS				
C-Band SAR	10 – 100 m	3 to 35 days	<ul style="list-style-type: none">- Wet Snow Extent- Melt onset/duration	<ul style="list-style-type: none">- Wet snow only- Poor revisit- Difficult to estimate SWE or depth data
Ku-Band	5 – 25 km	Daily		
PASSIVE MICROWAVE SENSORS				
19 and 37 GHz Sensors	12 to 25 km	Twice Daily	<ul style="list-style-type: none">- Dry Snow Extent- SWE- Snow Depth	<ul style="list-style-type: none">- Coarse resolution- Complex sub-grid heterogeneities

The selection of which remote sensing output data are most suitable depends entirely on which snow cover parameters are needed along with the frequency of observation required. For example, snow extent can be mapped using visible sensors, however, not frequently at a high resolution. Wet snow extent can be mapped frequently with Ku-Band sensors; however, the resolution is relatively coarse (multiple kilometers). Passive microwave data are the only current operational option for providing estimates of not only dry snow extent but also SWE and snow depth.

1.4.7. Trends and Variability in Tundra Snow Cover

Many studies have compiled snow data from single sources and from combinations of sources in order to observe large scale spatial and temporal snow cover trends. Most of these long term snow cover records have been developed for comparison with climate models (Brasnett, 1999, Brown et al., 2003, Brown, 2000, Brown, 1997) or for validating remote sensing techniques (Chang et al., 2005, Derksen et al., 2005, Pulliainen, 2006, Biancamaria et al., 2008). This type of research is important because regardless of how robust modeling and remote sensing algorithms are, they must still be tested against

spatially and temporally extensive observed data sets to ensure realistic results (Foster et al., 1996).

Most researchers would agree that, along with a complete spatial coverage, the longer the time series the better. This is especially true when providing snow cover data for use in other disciplines. Spatial and temporal discontinuity is a problem with most current long term northern snow cover datasets, as seen in Dyer and Mote (2006). As a result, without reliable, spatially and temporally complete snow cover data, it is very difficult to validate any large scale model predictions or completely understand tundra snow dynamics.

1.4.8. Summary of Tundra Snow Cover Data Sources

Section 1.3 has described in detail the different sources of tundra snow cover data. Table 1.4 summarizes the different methods and their resolutions, as well as advantages and disadvantages.

Table 1.4. Sources of tundra snow cover data

Method	Resolution		Advantages	Disadvantages
	Temporal	Spatial		
In-situ	- Often limited (bi-weekly at best)	- Depends on survey parameters (generally poor)	- Primary data - Ability to control survey variables and data collection	- Labor intensive - Costly - Could be biased due to human error
Automated Gauge	- Very good, depends on life of gauge	- Poor where there are few stations	- Automatic - Continuous	- Spatially constrained - Instrument maintenance and reliability
Modeled Data	- Can be good once model parameterized - Depend on input data	- Depend on model parameters	- Distribute point data over an area	- Need input data for model runs - Not representative of other areas
Remote Sensing	- Excellent from microwave and coarse resolution visible spectrum	- Good swath coverage - Spatial resolution depends on sensor	- Automatic, continuous, long time series	- Problems depend on spectrum used

In-situ sampling is the only source for primary snow cover data. It is the most reliable data source if the field sampling is properly distributed and collected without bias and with as little human error as possible. The limitations of in-situ data are the costs and labor intensity required to get a good spatial or temporal coverage. The temporal coverage of in-situ data is usually not very good which limits their application to a “snapshot in time” approach. Automatic gauge data provide a good temporal coverage; however, unless there are networks of gauges the data are very spatially constrained. In the case of a single station, in-situ work data need to be collected in order to assess the representativeness of the station data. Modelled snow cover data can be good for distributing point data over larger areas; however, the models need input meteorological data for parameterization and are not always representative of other study areas. Remote sensing platforms have also been used to provide snow cover information. The temporal resolution from coarse resolution visible spectrum and passive microwave sensors is very good (daily). However, the spatial resolution of these sensors limits their application to large scale process studies. The main advantage of remote sensing data is that they are collected automatically and have produced a long time series of data. Specific problems retrieving snow cover parameters depend on the sensor and the wavelength of energy being sensed.

CHAPTER 2: MONITORING SNOW COVER WITH SATELLITE PASSIVE MICROWAVE REMOTE SENSING

2.1. Introduction

All objects emit microwave energy if their temperature is above absolute 0 K. The total amount of microwave energy output depends on the temperature and emissivity of the object. Emissivity, ϵ , can be defined as the microwave brightness of a graybody relative to that of a blackbody at the same temperature (Ulaby et al., 1982). Blackbodies are defined as objects that are perfect absorbers of incoming energy, and in order to remain in thermodynamic equilibrium, are also perfect emitters of that energy. Since objects emit only a fraction of energy relative to a blackbody at the same physical temperature, emissivity can be further defined as

$$\epsilon = T_b / T$$

Where T_b is the brightness temperature of a graybody, detectable with passive microwave remote sensing, and T is the physical temperature of the object (Armstrong et al., 1993).

2.1.1. Passive Microwave Sensors

Passive microwave sensors detect naturally emitted passive microwave energy. Passive microwave sensors have been deployed on operational spaceborne platforms since 1972 with the launch of the Electronic Scanning Multichannel Radiometer (ESMR) aboard the Nimbus satellites. Several researchers discovered that there exists a good correlation between increasing snow depth and decreasing passive microwave emission (Foster et al., 1980). Using data from the ESMR, Foster et al. (1980) found that shorter wavelength (~37 GHz) emission was more sensitive to the structure and condition of the snow, while longer wavelength emission (~19 GHz) was affected by underlying soil condition. However, the resolution of the ESMR sensor (Table 2.1) restricted the application of the data to large areas with very flat uniform terrain (Rango, 1996).

Observations from the ESMR satellites were not extensively analyzed as early understanding of the data was hampered by the coarse spatial resolution (Choudhury, 1989). Following ESMR was the Scanning Multi Channel Microwave Radiometer (SMMR) launched in 1978 aboard the Nimbus 7 and Seasat satellites. The SMMR sensor was a five-frequency, dual polarization radiometer which measured at 6.6, 10.7, 18, 21 and 37 GHz, with a 780 km swath at a constant incidence angle of approximately 50 degrees (Chang et al., 1987). The improved resolution of the SMMR sensor produced more widespread interest and subsequent research initiatives with the sensor data provided the foundation for passive microwave snow research (Chang et al., 1987). The SMMR sensor was replaced by the launch of the Special Sensor Microwave Imager (SSM/I) in 1987 aboard the Defense Meteorological Satellite Program (DMSP) platforms. The SSM/I sensors continue to provide data at 19, 22, 37 and 85 GHz with a 1400 km swath at 53 degrees (Hollinger et al., 1990).

Although neither the SMMR or SSM/I sensors were deployed specifically for monitoring snow cover, they have proven useful for detecting snow cover and for estimating snow depth and SWE (see Section 2.3). Limitations from the coarse resolution of the SMMR and SSM/I sensors were partially overcome by the launch of the Advanced Microwave Sounding Radiometer Earth Observing System (AMSR-E) aboard the Aqua platforms in 2002. The AMSR-E sensors provide data at 6.9, 10.7, 18.7, 23.8, 36.5, and 89GHz, with similar temporal coverage as SSM/I, however, at a finer spatial resolution (Table 2.1) (Kelly et al., 2003).

Table 2.1. Passive microwave sensors

Sensor	Date	Revisit Frequency	Frequency (GHz)	Instrument Field of View (km x km)
ESMR	1972 to 1978	Daily	19 37	33 km
SMMR	1978 to 1987	Every other day	6.6 10.7 19 22 37	148 x 95 91 x 59 55 x 41 46 x 30 27 x 18
SSM/I	1987 to present	Twice daily	19.3 22.23 37.0 85.5	69 x 43 60 x 40 37 x 29 15 x 13
AMSR-E	2002 to present	Twice daily	6.9 10.7 18.7 23.8 36.5 89	76 x 44 49 x 28 28 x 16 31 x 18 14 x 8 15 x 13

2.1.2. Passive Microwave Data

Passive microwave data can be collected on either ground based, airborne or satellite platforms. For consistency, data from each platform are usually collected at a consistent incidence angle of 50 to 53 degrees. The instantaneous field of view (IFOV) of raw data is elliptical in shape and varies in size according to the height above ground and the antenna characteristics (Figure 2.1).

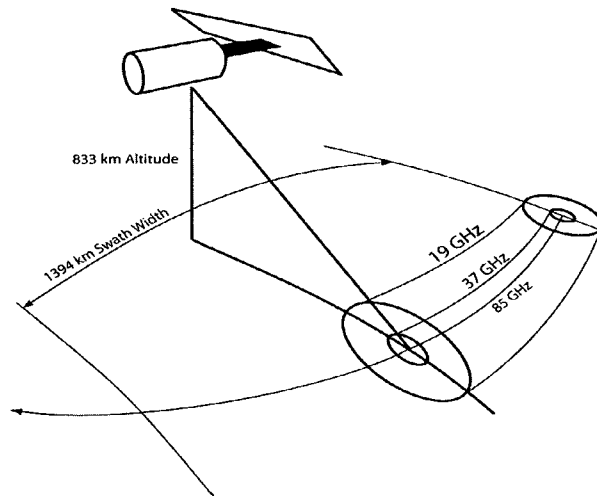


Figure 2.1. SSM/I scan geometry (adapted from Hollinger et al., 1990)

Satellite brightness temperatures (Tb) are collected either as raw, unprocessed swath data or converted to the Equal-Area Scalable Earth Grid (EASE-Grid) format. Swath data have the advantage of retaining the original frequency dependent imaging characteristics. However, for time series observations, changes in orbital location affect the swath level footprint location and necessitate the use of standardized EASE-Grid data (Derksen, 2008).

The Equal-Area Scalable Earth Grid (EASE-Grid) format was developed by the National Snow and Ice Data Center (NSIDC) for the data products generated by the NOAA/NASA Pathfinder Program Special Sensor Microwave Imager (SSM/I) project. These data products included primarily gridded passive microwave Tb derived from the Tb at a relatively coarse 25 km resolution (Armstrong, Brodzik and Varani, 1997). The EASE grid format provides a fixed geographic location for storage and retrieval of satellite passive microwave brightness temperatures. The format is derived using an optimal interpolation binning method of swath data to derive Tb at fixed grid locations. A rectangular grid lattice is produced and superimposed on an equal-area map which most faithfully represents the nominal passive microwave footprint (Brodzik et al., 2002).

2.2. Passive Microwave Radiometry of Snow

2.2.1. Introduction

The total microwave emission from a snow pack is a function of 1) the emission, 2) the dielectric properties, and 3) the physical temperature of the

- Air-snow boundary
- Snow pack volume
- Snow-ground interface
- Underlying soil / regolith

The emission from the snow volume is influenced by many factors, including snow depth, SWE, snow density, liquid water content and snow grain size (Foster et al.,

1980). Within a dry snowpack, when the radii of snow grains approaches a few hundredths of the microwave wavelength, the volume scattering increases enough to produce a detectable decrease in T_b (Chang et al., 1976). However, the absorption capability of dry snow is in the order of 10^5 times less than snow with even a small percentage of liquid water present (Stiles and Ulaby, 1980).

2.2.2. Basis for Passive Microwave Snow Detection

2.2.2.1. *Dry Snow*

In dry snow, the presence of individual snow grains increases the amount of volume scattering and reduces the microwave emission. Thus, the deeper the snow gets, the greater the amount of scattering and loss of emission. Mie scattering, which occurs when particles are just about the same size as the wavelength of the radiation, governs the degree of scattering within a snowpack (Chang et al. 1976). As such, the size of the snow grains and the frequency being used are important in defining the extent of emission from a snowpack.

Low frequency emission (6.9 to 19 GHz) is not affected by dry snow as the wavelengths (4 to 1.5 cm) are much longer than individual snow grains. These lower frequencies are more affected by the properties of the underlying ground and by the snow-ground interface. As the wavelength becomes shorter (0.8 cm, ~ 37 GHz), mie scattering increases, and the emission is affected by the snow pack volume. However, with even shorter wavelengths (0.3 cm, ~ 89 GHz), the penetration depth decreases due to an increase in absorption of the emission by the snow grains. As such, the total emission detectable at these shorter wavelengths is controlled largely by the properties of the snow surface at the air-snow boundary. Figure 2.2, adapted from Ulaby et al., 1986, demonstrates the relationship between grain size, frequency and penetration depth.

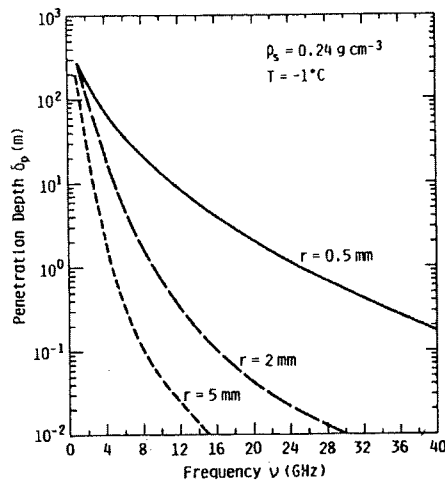


Figure 2.2. Penetration depth of microwave emission at different frequencies (adapted from Ulaby et al., 1986)

Figure 2.2 shows that, at three different snow grain size radii (0.5 to 5 mm), 1) the penetration depth decreases as frequency increases, 2) as the grain size increases the penetration depth for a given frequency decreases, and 3) at the lower frequencies, there is less difference in penetration depth between the different grain sizes.

These relationships have important implications in determining which frequencies would be most useful for dry snow detection. For example, in a snowpack with a grain size of 0.5 mm, the penetration depth is greater than 10 meters below 14 GHz. This means that emissions at these frequencies are not influenced by typical non-alpine snowpacks (0 to 1.0 meters deep). However, at 37 GHz, the penetration depth is much lower, around 35 cm. This indicates that these higher frequencies would be much more sensitive to subtle changes in snowpack depth. The difference in penetration depth between the different frequencies can then be exploited in order to detect a dry snow cover (Figure 2.3).

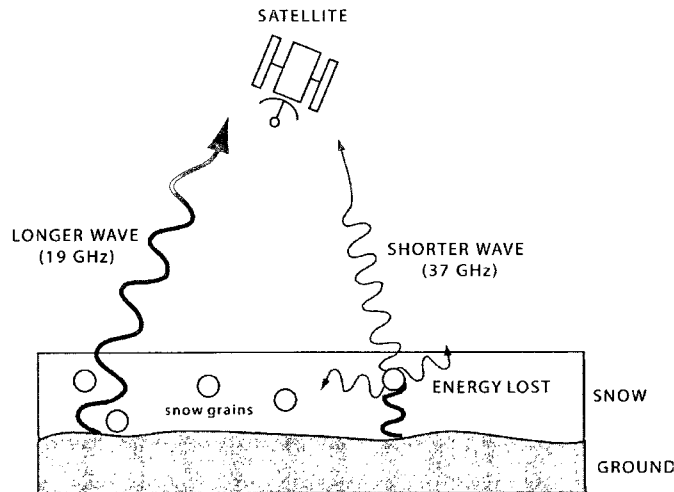


Figure 2.3. Using the difference between a longer wavelength emission (19 GHz) and a shorter wavelength emission (37 GHz) to detect the presence of snow grains.

By using a brightness temperature difference between these two groups of frequencies, both SWE and snow depth can be estimated while the effect of physical temperature is minimized.

2.2.2.2. Wet Snow

The dielectric constant is the measure used in microwave remote sensing to describe an object's electrical character. The dielectric constant for snow is a function of frequency, snow wetness, temperature and density (Henderson, 1998). As the dielectric constant increases, driven mainly by an increase in moisture content, the internal microwave emissivity increases, and in turn, the absorption increases (Matzler, 1996).

The dielectric properties of snow at a given frequency are generally dependent on the relative proportion of liquid and solid water in the snow. At temperatures above freezing, there always exists water in the snow pack as thin films of water tend to bond to the ice crystals. Wet snow completely changes the emissivity within a snowpack. For example, dry or frozen ground has a high emissivity (0.90 -0.95), whereas wet ground has a much lower emissivity (~0.70) with correspondingly lower brightness temperatures (Foster et al., 1980). In a snowpack, as the liquid water content begins to increase, the

snow begins to behave more like a blackbody, absorbing and re-emitting microwave energy. As such, it can be very difficult to detect the presence of a wet snow cover as it resembles snow free ground (Walker and Goodison, 1993).

Even a small amount of liquid water within a snowpack (1-4%) will cause a sharp increase in T_b and decrease in penetration depth (Foster et al., 1980). This is demonstrated in Figure 2.4, adapted from Ulaby et al., 1986.

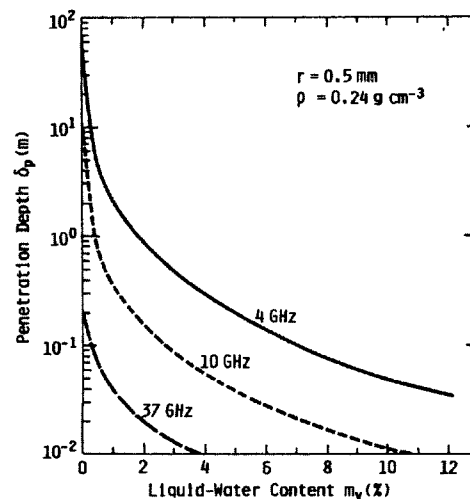


Figure 2.4. Penetration depth of microwave emission at 4, 10 and 37 GHz with increasing liquid water content (adapted from Ulaby et al., 1986)

As the liquid water content increases, the penetration depth drops considerably even at 4 and 10 GHz which have quite high dry snow penetration depth. These relationships show that while detecting wet snow cover may be possible, quantifying snow depth or SWE under wet snow conditions would be very difficult, if not impossible.

2.3. Passive Microwave Algorithm Development

2.3.1. Introduction

There have been many different passive microwave algorithms developed which can provide some estimate of snow cover properties over both hemispheric and regional scales. The common component in most operational algorithms is the use of the difference in emission over snow covered ground between a longer wavelength channel,

usually 18 or 19 GHz and a shorter wavelength channel, 36 or 37 GHz. Algorithms are developed either through radiative transfer modeling or through empirical methods. The general relationship used by both is some form of Equation 1

$$\text{SWE (mm)} = a + b\Delta T_b \quad [1]$$

where a and b are the intercept and slope for the brightness temperature difference (ΔT_b) between a 18 or 19 GHz and a 36 or 37 GHz vertically or horizontally polarized channel. The 19 GHz channel provides a measure of snow free conditions (emission from underlying ground) as the wavelength is long enough (~ 1.5 cm) not to be affected by the snow grains. The 37 GHz wavelength (0.81 cm) channel is, however, influenced by the number of snow grains and records a lower T_b than the 19 GHz channel. The difference between the two allows for the estimation of SWE.

The choice of polarization is not consistent among microwave SWE algorithms. Some utilize horizontally polarized measurements (Chang et al. 1990, and the modified versions of Foster et al. 1997, Kelly et al. 2003), while others are based on vertically polarized measurements (Goodison and Walker 1995, Mognard and Josberger 2002, Goita et al. 2003, Pulliainen 2006). Horizontally polarized channels have been shown to be slightly more sensitive to snow pack stratigraphy, while vertically polarized channels are more sensitive to snow volume (Matzler, 1994).

Algorithms are developed using different parameters which depend on the nature of the snowpack and landscape over which snow cover properties are to be estimated. Algorithms can be grouped into two broad categories, hemispheric or regional scale. The success and operational applicability of individual algorithms depend on the ability to deal with snow pack and local terrain characteristics that adversely affect the normal absorption and scattering properties of the snowpack.

2.3.2. Hemispheric Scale Algorithms

Hemispheric scale snow data are important for both climatological analysis and verification of GCM simulations (Foster et al., 1996). However, hemispheric scale snow cover estimates based on in-situ and automated gauge measurements are typically erroneous due to large spatial gaps and temporal discontinuity (Brown et al., 2003). As such, passive microwave data with their large spatial extent, frequent re-visit times and global standard spatial resolutions have been used to estimate large scale snow cover (Tait, 1998). Hemispheric algorithms using passive microwave data have been produced mainly to monitor snow cover trends over a large spatial extent with a focus on providing a very high temporal resolution. However, at a hemispheric scale, there is the obvious problem of the integration of many different land covers, snow characteristics and terrain types into one single algorithm. Therefore, the trends in T_b that are observed may not necessarily be reflective of changes in snow cover parameters.

Despite these limitations, several researchers have had success monitoring snow cover with passive microwave data at a hemispheric scale. Chang et al., (1987) utilized SMMR data to estimate snow extent and snow depth throughout the northern hemisphere. SMMR snow extent compared favorably to the operational NOAA snow maps and to snow station data. However, due to the penetration of microwaves through shallow snow covers, snow extent was consistently underestimated using the SMMR data. Snow depth estimated by SMMR T_b compared favorably to measured values only in areas of homogenous terrain (Russian Steppe and Canadian Prairies). A hemispheric snow extent and SWE algorithm development by Grody and Basist, (1996) utilized the 85 GHz channel from the SSM/I sensor to estimate Northern Hemisphere snow extent. However, algorithms applicable over entire hemispheres, using a single set of coefficients, have not yet shown to be very accurate or reliable. Foster et al., (1997) attempted to address this issue by improving the methodology used by Chang et al.

(1987). They separated North America and Eurasia based on forest and snow cover effect in an attempt to better estimate snow extent. Tait (1998) further subdivided the northern hemisphere into regions based on forest cover and snow state. However, heavily vegetated environments (sub-Arctic boreal forest), areas with significant depth hoar development (most high latitude environments) and areas that experience significant snow re-distribution (tundra, high Arctic) were identified as problematic to algorithm confidence.

The subdivision of algorithms into different landscape types addresses the spatial heterogeneity of hemispheric snow cover, however, it does not tackle the temporal evolution of a snowpack. Kelly et al. (2003) developed a prototype global algorithm to tackle the issue of temporally static algorithm coefficients. Based on the algorithm employed by Chang et al. (1987) they employ a dynamic approach which integrates the effect of seasonal snow grain growth and the evolution of snow density. The inclusion of these parameters improved the estimates of snow cover; however, more importantly; they represent a significant step forward as they reinforce the need to consider not only spatial differences in snow cover, but the seasonal evolution as well.

2.3.3. Regional Algorithm Development

Regional algorithm development is focused on gaining a better understanding of snow-terrain-microwave emission interaction within specific environments. Regions of study have been typically subdivided based on land cover type. Primary areas of research have included open ground environments (prairies and open plains), sub-Arctic boreal forests and the sub-arctic to arctic tundra. Each region presents a set of unique challenges. The success of each algorithm depends on the ability to account for sub-grid terrain and snow cover heterogeneity. Generally speaking, algorithms have been more successfully employed in simpler, homogenous environments (prairies and open plains).

Algorithms in more complex environments (boreal forest and high arctic) need to consider far more sub-grid landscape features and snow cover parameters.

2.3.3.1. Open Ground Algorithm Development

The first passive microwave algorithms for estimating snow cover were developed over open ground, prairie landscapes. The open plains or prairies are the simplest, most homogenous landscape which receives an annual snow cover. Two important open ground algorithms were developed during the 1980s using SMMR data. The Chang algorithms, developed to estimate SWE (Equation 2) and snow depth (Equation 3) have been used both regionally and hemispherically and still form the basis for some current research and development (Chang et al., 1990). The algorithms utilize the Horizontally Polarized 19 and 37 GHz channels on the SMMR, SSM/I or AMSR-E satellite data.

$$\text{SWE (mm)} = a (\text{Tb19H} - \text{Tb37H}) \quad [2]$$

$$\text{Snow Depth (cm)} = b (\text{Tb19H} - \text{Tb37H}) \quad [3]$$

The coefficients a and b are constants which have been determined for each satellite platform (for example $a = 4.8$ and $b = 1.59$ for SSM/I data). The Chang algorithm has been widely used, modified to incorporate snowpack metamorphism over open ground (Josberger and Mognard, 2002), and incorporated with landcover and topography data for use at global scales (Kelly et al., 2003).

An operational open ground (prairie) SWE algorithm was developed at Environment Canada (EC) during the 1980s for use with SSMR and SSM/I data. EC (formerly Meteorological Service of Canada – MSC) has been using the algorithm operationally to produce weekly prairie SWE maps since 1988; however, the approach has been applied to SMMR data as well in order to develop a longer time series (Derksen et al., 2003). The algorithm was developed for non-vegetated, non-alpine environments and is based on the vertical polarization brightness temperature gradient

from the 19 GHz (18GHz SMMR) and 37 GHz SSM/I Vertically polarized channels (Equation 4) (Goodison and Walker, 1995).

$$\text{SWE (mm)} = -20.7 - 49.27[(\text{Tb}_{37\text{V}} - \text{Tb}_{19\text{V}})/18] \quad [4]$$

The algorithm was developed through an intensive field validation campaign and accurately represents SWE under predominantly dry snow conditions (Goodison and Walker, 1994). The EC algorithm was developed and operationalized for the Canadian prairies but has been applied and tested in other open ground environments and has formed the basis for Canadian boreal forest algorithm development (Goita et al., 2003).

In the prairies, the main limitation of the EC algorithm is the presence of liquid water in the snow pack (increased snow dielectric). This led to the development of the EC wet snow indicator (Walker and Goodison, 1993), which uses both polarizations of the 37 GHz SSM/I data channel and is useful for differentiating between areas of wet snow, dry snow and snow free ground (Derksen et. al. 2000b). However, it remains impossible to quantify SWE under wet conditions (Walker and Goodison, 1993).

The successful estimation of snow extent and SWE using the EC algorithm has led to the development of time series research to examine long term snow cover variability using passive microwave data extending back to 1978. Derksen et al. (2003) found that trends and patterns in passive microwave estimated SWE compare favorably to in-situ data in open and low density forest cover environments. However, in locations where deep snow and/or dense vegetation were present, dataset agreement decreased significantly, and there was little interannual variability in passive microwave SWE retrieval.

2.3.3.2. Boreal Forest Algorithm Development

Boreal forests constitute 15% of the northern hemisphere winter snow covered area and 40% snow covered area in the spring and fall (Foster et al., 1991). The presence of a forest cover significantly complicates the nature of microwave emission

and has a pronounced effect on resulting brightness temperature gradients. Thus, algorithms developed for the boreal forest consider sub-grid forest cover into traditional brightness temperature gradient and provide good context for dealing with other sub-grid heterogeneity.

Foster et al. (1991) found that the inclusion of fractional forest cover improved SMMR SWE estimates in the northern Saskatchewan boreal forest. However, in far more dense boreal forests (northern Ontario and northern Quebec), SWE was significantly underestimated (up to 50 cm less than measured in-situ). Pulliainen and Hallikainen (2001) not only incorporate forest cover fraction but also consider the forest biomass. They derived a forest canopy loss factor for different forest types that is determined by empirical forest canopy transmissivity modeling. These forest cover factors, in combination with considerations of snow grain size, effective soil roughness and atmospheric conditions, were incorporated into the SWE algorithm. The algorithm was most successful at estimating mid-winter SWE, but the accuracy varied from year-to-year depending on annual temperature patterns and related ice layer formation.

Goita et al. (2003) developed a methodology for estimating SWE for Canadian boreal forests by again taking into account the fraction and type of forest cover in each pixel. Forest cover types used were deciduous, coniferous and sparse woodland. The application of slightly different algorithm parameters for each forest type was found to improve SWE estimates; however, there was a consistent overestimation compared to in-situ values. In addition, SWE was not particularly well estimated in the transition zones between forest cover and open areas. Snow cover in these areas is important to monitor as the transition zone between dense forest cover and the tundra is not well defined, can span many kilometers, and extends across the entire landmass of the northern hemisphere (the tree line). Furthermore, the transition between boreal forests and tundra will become increasingly important as it is an environment which will

undoubtedly experience increased vegetation productivity and areal expansion driven by increases in temperature and precipitation (Higgins and Vellinga, 2004). Walker and Silis (2002) examined 10 years of SSM/I estimated SWE data (1988-98) for the Mackenzie River Basin and found that the inclusion of forest type alone may not be sufficient. With the exception of the “sparse forest” algorithm class, there is no accounting for measures of forest density. The inclusion of a forest-density factor, such as stem volume and canopy closure especially in transition zones, may improve algorithm performance for such environments; however, such data are not typically available for northern boreal forests (Derksen et al., 2005).

The traditional 19 and 37 GHz algorithm approach can be limiting in northern boreal forests due to the high correlation between forest cover and 37 GHz brightness temperatures (Derksen, 2008). Furthermore, under deep snow conditions, volume scattering can be evident in the 19 GHz brightness temperature. Derksen (2008) suggests that the 19 – 37 GHz vertically polarized difference be used early in the season when there is a shallow snow cover, while the 19 – 10 GHz difference can be employed under deep snow conditions when scattering becomes evident in the 19 GHz Tb.

2.3.3.3. Tundra and High Arctic Algorithm Development

Passive microwave sensors have often been used to monitor snow cover across tundra landscapes; however, usually the tundra is included in a hemispheric scale algorithm approach (Armstrong and Brodzik, 2002, Kelly et al., 2003, Foster et al., 2005). The accuracy of tundra SWE estimates included in large scale algorithms are not often discussed or have proven difficult to assess due to the lack of validation data. Despite these limitations, passive microwave data have been used to monitor tundra snow cover in several tundra study regions. These areas include 1) northern Manitoba (Boudreau and Rouse, 1994, Pivot et al., 2002, Toose, 2007), 2) northern Quebec (Langlois et al., 2004), 3) across the boreal tundra transition in the Northwest Territories (Derksen et al., 2005), 4) the high

arctic islands (Woo et al., 1995), 5) Alaska (Hall et al., 1991, Sturm et al., 2003, Koenig and Forster, 2004), 6) Siberia (Boone et al., 2006, Grippa et al., 2004), and 6) all sub-arctic and arctic regions throughout the northern hemisphere (Biancamaria et al., 2008).

Each specific region imposes a unique set of challenges and requires a slightly different approach. Moreover, recent research has had the advantage of building on previous successes, failures and recommendations. Despite all the effort, there is no well accepted method for estimating tundra SWE and snow depth. The problem, which is generally agreed upon, is that the conventional algorithm approach using a 19 and 37 GHz Tb difference produces a marked underestimation of ground measured snow (Boudreau and Rouse, 1994, Grippa et al., 2004, Armstrong and Brodzik, 2002, Rees et al., 2005).

The inaccuracies in current snow retrieval algorithms are caused by the inability to properly account for sub-grid heterogeneity in the terrain, landscape and snow cover parameters. The factors that hinder the use of passive microwave radiometry for deriving tundra snow data can be generalized into two categories, 1) snow pack properties and 2) terrain character (Table 2.2). Adding to these challenges is the difficulty in obtaining temporally co-incident and spatially extensive in-situ snow data for comparison with spaceborne Tb.

Table 2.2. Factors in the tundra that affect passive microwave brightness temperature

Factor	Influences on passive microwave emission
Snow pack Properties	<ul style="list-style-type: none"> - Stratigraphy (wind slabs/depth hoar) - Grain Size - Snow Depth - Temporal Evolution
Terrain Features and Landscape	<ul style="list-style-type: none"> - Soil Condition - Vegetation Cover - Topography - Lake Cover Fraction

Each of the factors outlined in Table 2.2 affect Tb at different temporal and spatial scales and contribute to the uncertainty both individually or in combination. These factors will be discussed in more detail in Section 2.4.

2.4. Factors Contributing to Uncertainty in Estimating Tundra SWE

2.4.1. Introduction

Early work in high latitudes utilized the traditional algorithm approach of examining the difference between either the horizontally or the vertically polarized 37 and 19 GHz brightness temperatures. For example, Hall et al. (1991) compared in-situ snow measurements to airborne and spaceborne passive microwave data along a transect from the north coast of Alaska to Fairbanks in central Alaska. Near Fairbanks, an inverse relationship was found between Tb and snow depth; this was similar to results found in the open plains and prairies. Further to the north, in the Brooks Range, there was found to be a noticeable decrease in Tb which corresponded to increasing snow depth and depth hoar. This was expected as areas with the deepest snow and a high percentage of depth hoar should produce the lowest Tb. However, the lowest Tb values were in fact recorded further north in a tundra environment. The low Tb values observed in the tundra were evident in both the airborne and through eight years of spaceborne data. The exact reasons for the drop in Tb were not fully understood at the time. However, the same Tb anomaly was not found to be present in summer data; thus, it was assumed to be a product of the tundra snow pack properties, the ground state or the presence of lake ice in the area. More recent research conducted in different tundra study regions has certainly reinforced the need to investigate the influence of tundra specific snow pack properties, landscape and lake ice on satellite scale Tb (Rees et al., 2006).

2.4.2. Snow Pack Properties

2.4.2.1. *Stratigraphy and Grain Size*

Differences in snowpack structure can complicate the understanding of microwave emission and T_b . Because of these differences, several microwave emission models have been developed to simulate and understand the total emission from multi-layer snowpacks (Weismann and Matzler, 1999). However, these models can be very complex, and some researchers still prefer single-layer models for practicality (Pulliainen et al., 1999). Sturm et al. (1995) indicate that tundra snowpacks typically have between 0 and 6 layers, the fewest number in any snow cover class except ephemeral and prairie snow and consist of basal depth hoar overlain with multiple wind slabs. As such, the parameters which will have the most influence on T_b are a) the development of basal depth hoar (large grain sizes), b) the abundance of dense wind slab ($> 0.400 \text{ g / cm}^3$), and c) the formation of ice crusts and lenses.

2.4.2.1.1. *Effect of Depth Hoar*

The detection of snow cover relies on examining the changes in microwave emission caused by increased scatter from the presence of individual snow grains. Thus, the size of the individual snow grains is an important control on the T_b from a snow pack (Chang et al., 1976). In high latitude environments, the formation of large depth hoar crystals at the base of the snow pack is common. Depth hoar is a product of constructive metamorphism within a snow pack due to the strong temperature gradient between the warmer underlying ground and colder air temperature. The temperature gradients produce associated vapor pressure gradients. Since vapor diffuses from high to low pressure, there is a net transfer of material from warmer (higher vapor pressure) to colder (lower vapor pressure) parts of a snow pack (Langham, 1981). It can be assumed

that depth hoar thickness and grain size will increase throughout a winter season as long as there is a negative temperature gradient (Hall, 1987).

The large grain size of depth hoar increases the scattering of microwave emission as the grain size approaches or exceeds the wavelength being used (Hall et al., 1986). The presence of depth hoar has been shown to be responsible for lower than expected T_b values (Hall, 1987). The reduction in observed T_b at 37 GHz has been observed to be maximized as depth hoar approaches 30 cm in thickness. After 30 cm, no additional scattering loss occurs, and the emission from the snow above the depth hoar begins to dominate the T_b (Sturm et al., 1993). The orientation and shape of the snow crystals have insignificant effects on T_b , and the main factor is the grain size (Foster et al., 1999, Foster et al., 2000). The presence of the large grained depth hoar crystals tends to produce an erroneous overestimation in in-situ SWE as the increased scatter at 37 GHz is not a product of increasing snow depth (Hall et al., 1991).

Koenig and Forster (2004) compare the ability of three different contemporary and one new SSM/I algorithm to estimate SWE over a large spatial domain in Alaska. The new algorithm was empirically developed using regression techniques, specifically for their study area, with both temporally and spatially averaged T_b data and was able to reproduce ground measured SWE with an R^2 of 0.678. However, the algorithm was unable to reliably estimate SWE on a daily basis for individual pixels. Furthermore, there was neither mention of the number of sites sampled within each pixel nor an indication of the within-pixel variability in snow cover. Using a single in-situ SWE value for comparison at a passive microwave pixel scale is not a robust method as the range of sub-grid SWE can be extensive (Rees et al., 2005). Nonetheless, the work done by Koenig and Forster (2004) shows that conventional algorithm approaches can estimate SWE with good consistency in depth hoar-dominated study areas when temporally averaged and considered at multiple-pixel watershed scales.

2.4.2.1.2. Effect of Dense Wind Slab

Dense snow layers, formed by intense, seasonal wind-redistribution, are typical both at the surface and within tundra snow packs. Furthermore, the compaction of snow grains by wind increases the number of grains per unit of depth and should contribute to the saturation of microwave emission similar to deep snow. Unfortunately, the precise effects of dense snow layers on the total T_b are hard to separate from the more pronounced influence from depth hoar which typically forms under dense slab layers (Hall et al., 1986).

2.4.2.1.3. Effect of Ice Lenses

Ice crusts, both within the snow pack and on the surface, have a much different dielectric constant than snow. The presence of ice increases emissivity at high frequencies relative to lower frequencies. This alters the between frequency T_b gradient used in many algorithms to estimate SWE (Derksen et al., 2000b). The sharp contrast in T_b between cold dry versus wet snow has been exploited to detect stages of severe wintertime rain-on-snow events from the initial wetting of the snow to the accumulation of liquid water at the base of the pack and to the post-event refreezing of the snowpack (Grenfell and Putkonen, 2008). Rees et al. (2010), investigate the influence of less intense, short duration melt or rain events, and resulting thin ice lenses, on the ability to quantify SWE and snow depth. Observational data as well as microwave emission models demonstrate that vertically polarized data is not influenced a great deal by the presence of an ice lens. However, horizontally polarized data, even at longer wavelengths are adversely affected by even a thin ice lens. This study has profound implications for the ability of H-pol data to estimate SWE in the presence of ice lenses. Fortunately, in most high latitude environments, mid-winter freeze-thaw or rain events which are responsible for ice crust formation are relatively rare. However, under potential high latitude climate warming, more frequent mid-season melt events and liquid

precipitation could increase the formation and presence of ice layers in the snow pack and complicate algorithm development.

2.4.2.2. Snow Depth

Snow depth exerts a similar control on passive microwave emission than grain size: as the snow depth increases, there are more grains available to scatter and absorb the microwave energy. One difficulty with the traditional T_b inversion algorithm approach is the well documented saturation of microwave energy (Sturm et al. 1993, Kelly et al. 2003, Derksen, 2008). At every frequency, there is a certain threshold at which an increase in SWE or snow depth does not result in lower observed T_b (Durand and Margulis, 2006). In fact, as depth increases beyond the saturation threshold, the snow cover begins to emit its own microwave energy, eventually increasing T_b . This re-emission of microwave energy means that there can be two different possible SWE for a given T_b observation (Figure 2.5) (Matzler et al., 1982, De Seve, 1997).

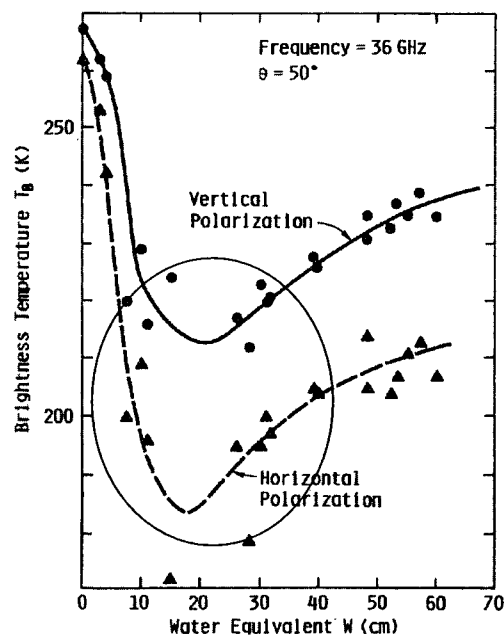


Figure 2.5. Reversal of modeled T_B at 36 GHz (Modified from Ulaby et al., 1986)

The reversal of Tb in a snowpack means that without other methods of inferring snow depth, traditional algorithms are limited to shallow snow cover (less than 150 to 250 mm SWE) (Matzler, 1994, De Seve, 1997, Tait, 1998). Assuming an average tundra snow density of 0.305 g/cm^3 (see Chapter 4), the reversal at 37 GHz would occur at 45 cm of snow depth. The exact snow depth at which the reversal in Tb occurs depends on the frequency being used as well as the properties of the snowpack. Longer wavelength energy (lower frequency) will have a greater penetration depth and a higher saturation point.

The reversal of the Tb creates problems for algorithms developed using linear relationships. Most approaches are not able to compensate for the reversal in slope, and as such, have a certain threshold beyond which they cannot estimate SWE. One solution for detecting SWE in deep snow is to use a difference between two longer wavelength Tb (19 and 10 GHz). Derksen (2008) show how this approach improves the estimation of SWE in boreal forests. Once snow depth increases to the point of saturation at 37 GHz, the algorithm switches to a 19 and 10 GHz Tb difference. The 10 GHz channel is useful as the background as it is unaffected by all but extremely high SWE.

2.4.2.3. Temporal Evolution of Snow

A fundamental property of snow is seasonal metamorphism, which is the change in internal structure without any change in snow depth or water equivalent (Colbeck, 1986). Early passive microwave algorithms exploit the inversion between 37 and 19 GHz emission in order to quantify SWE; however, problems arise using this approach because these temporally static methods cannot deal with changes in Tb associated with the seasonal metamorphism of the snowpack. Rosenfeld and Grody (2000) found that at the beginning of winter, SSM/I snow signatures generally follow a classical pattern. The Tb decreases with increasing snow depth. However, a significant deviation

from this pattern was observed in the middle of winter at which time the Tb approaches a minimum and begins to increase despite constant snow depth.

While success has been achieved using static inversion methods, they rely on spatial and temporal average snow conditions (depth, SWE, density, grain size) to parameterize the algorithms (Kelly et al., 2003). Accurately estimating SWE is possible if static algorithms are always applied in the same spatial location and during the same time of year. However, when temporally heterogeneous snow cover conditions are to be estimated, algorithms need to be parameterized in order to compensate for the dynamic seasonal evolution of snowpack parameters. The midwinter minimum of brightness temperatures and reversal of Tb seen by Rosenfeld and Grody (2000) limits the use of a single regression-type static algorithm to quantify snow depth and SWE throughout an entire season.

There have been several dynamic algorithm approaches which have typically focused on compensating for snowpack metamorphism (change in grain size) throughout a winter season. The goal is to identify areas of snow cover and estimate SWE from early in the accumulation season until the onset of snowmelt. For instance, Kelly et al. (2003) assumed a snow grain diameter evolution scheme and developed nonlinear inversion relationships for use at global scales. Josberger and Mognand, 2002, use a similar premise; however, they examine snow and ground temperature to develop a cumulative index of snowpack temperature gradient which accounts for changes in grain size and improves the estimation of snow depth throughout a winter season. Grippa et al. (2004) combine the static algorithm developed by Chang et al. (1990) with the dynamic approach developed by Josberger and Mognand (2002). They use a dynamic approach in the early through mid-winter portion of the season and employ a static, linear algorithm with varying coefficients later in the season when grain size growth slows. The use of a static algorithms consistently underestimates snow depth,

while a combination of static and dynamic algorithms produces generally a better agreement between the climatological snow depth data provided by USAF/ETAC and SSM/I derived snow depth over seven seasons.

2.4.3. Terrain and Landscape Heterogeneity

2.4.3.1. *Soil Condition*

The condition of the underlying ground surface is important as it is a component of the total microwave emission from a snow covered surface. The most important parameter, similar to the snowpack, is the soil moisture content. Unfrozen, bare, and moist soil has a much different microwave emissivity than frozen bare ground (Matzler, 1994). High soil moisture in warm ground influences microwave emission much like liquid water in the snowpack (Derksen et al., 2000a). However, in most tundra environments, the ground remains completely frozen during the winter season. The presence of this continuous permafrost limits the potential of confounding soil moisture effects. However, complications and uncertainty in microwave emission would certainly occur early in the season, before the active layer is completely frozen and in sub-Arctic tundra where permafrost distribution is discontinuous. Furthermore, soil condition may become increasingly important to understand as potential climate warming stands to change the seasonal evolution and spatial patterns of permafrost soils in high latitude environments (Anisimov and Nelson, 1997).

The formation and presence of ground ice and highly saturated frozen soil at the ground surface could also affect microwave emission at the ground-snow interface similar to ice crusts and layers within the snow pack itself (Matzler, 1994). The sharp contrast in T_b between cold dry snow versus wet snow has been exploited to detect stages of severe wintertime rain-on-snow events and the accumulation ice crusts at base of the pack (Grenfell and Putkonen, 2008).

Boone et al. (2006) build on the work of Grippa et al. (2004) and integrate simulated soil temperature and monthly soil temperature variation into a dynamic algorithm approach. These ancillary data do improve the ability of SSM/I algorithms to replicate SWE which is estimated from land surface schemes. These research methods are important for highlighting the importance of snow evolution and soil temperature in algorithm development. However, it is important to note that algorithms are being developed with simulated soil temperature and are being tested against modeled SWE and not in-situ SWE or snow depth measurements due to a lack of data.

2.4.3.2. Vegetation Cover

The tundra landscape is largely devoid of a continuous closed canopy forest cover. Vegetation cover typically consists of mosses and lichens, sedge grasses, dwarf birch and other shrubs, along with sporadic and stunted coniferous trees. Vegetation has the ability to influence satellite algorithm development indirectly by modifying sub-grid snow cover distribution and directly by contributing to total microwave emission.

In high latitude environments, vegetation patterns alter snow deposition, distribution and metamorphism characteristics. Snow deposited in trees accumulates both in the canopy and on the ground. The snow which is intercepted in the canopy is subject to accelerated sublimation loss due to greater absorption of short wave radiation by the canopy and higher exposure to turbulent exchange forces. Experimentally derived sublimation rates show that mature evergreen forests can return 13 – 40% of the seasonal snowfall to the atmosphere (King et al., 2008). Interception and sublimation of snowfall result in reduced ground snow pack depth when compared to open areas with similar snowfall (Lundberg et al., 2004).

Wind action is the dominant process in open areas. Wind erodes snow from open and sparsely vegetated areas and deposits it in areas of dense vegetation (Essery and Pomeroy, 2004). This action increases snow depth and density on the windward side of

a vegetation stand. Increased deposition, however, does not extend a long distance, which creates a spatially inhomogeneous distribution throughout forest stands. Emergent vegetation of any type traps drifting snow and prevents saltation until it is covered to within 5 cm of its stem tops (Pomeroy, 1997). Once the vegetation becomes buried by snow, there is much less influence, and a more uniform snow surface develops.

In forested areas, the total microwave Tb consists of emission from underlying ground, emission, scattering and absorption from the snow-ground interface, snow pack, snow-air interface, forest cover (trunks, branches and canopy) and snow intercepted by vegetation. As a result, modeling emission and isolating the contribution from the snow pack can be difficult. Algorithms that incorporate within pixel fractional forest cover and forest type seem to provide more reliable estimates of snow cover parameters than those which do not (Foster et al., 1991, Goita et al., 2003, Derksen et al., 2005).

The transition between the boreal forest and tundra clearly illustrates the different challenges associated with each environment. Derksen et al. (2005) show that in-situ SWE can be estimated early in the year if brightness temperatures and forest cover fraction are considered. Later in the season, however, forest fraction is not sufficient to correct algorithms. Furthermore, there was little agreement between estimated and in-situ SWE from the forest into the tundra. More detailed forest information, such as forest transmissivity, which can be derived from MODIS data helps in determining which frequencies are most useful for isolating SWE from forest cover (Derksen, 2008).

2.4.3.3. Topography

The effects of topography on SWE retrieval algorithms are twofold. First, satellite passive microwave sensors operate with a ~ 50 degree incidence angle. As such, in areas of high relief, the sensor is unable to image areas on the lee side of topographic

features. This limits the feasibility of using passive microwave data to gently rolling topography outside of mountainous environments.

The second and more prominent effect is the influence of topography on the wind-redistribution of snow. Snow accumulation patterns throughout most of the tundra are driven primarily by wind redistribution. Drifting snow accumulates in areas of dense vegetation, which are usually topographically controlled, in depressions and on the lee side of topographic features perpendicular to the prevailing wind direction. These uneven snow accumulation patterns create problems for assigning a representative mean snow cover value for coarse resolution grid cells. Furthermore, differences in snow depth would produce a wide range of sub-grid cell emission characteristics. As outlined, there is a limit (~150 mm) to the depth of SWE detectable using most operational T_B inversion algorithms. Drift features on the tundra, in the lee of slopes, can have SWE values well in excess of 150 mm. Therefore, the actual SWE contained in these features is at risk of being significantly underestimated.

Woo et al. (1995) conducted research on the Fosheim Peninsula, Ellesmere Island, Nunavut, to investigate the sub-pixel variability in snow distribution and to compare in-situ snow survey data to 85 GHz SSM/I T_b . The study area was broken down by terrain characteristics, and SWE was measured along transects in each terrain unit. To determine areally weighted SWE for each pixel, the mean SWE for each terrain type was weighted by the area covered by that terrain. In-situ SWE was then compared to 85 GHz T_b . Despite the coarse resolution, spatially variability in the T_b was evident across the study area which may have been related to regional variation in snow cover. Although this was preliminary research and no direct link could be established between the passive microwave data and in-situ SWE, it identified the importance of the distribution and within-pixel variability of snow cover to remote sensing in a tundra environment.

Although these snow and terrain parameters are all important components of a high latitude environment, it is important to prioritize them based on the spatial percentage of the environment they represent. For example, deep snow drifts on leeward slopes in the tundra are a predominant feature as they represent a significant volume of stored water. Snow depths greater than 5 metres can be sampled on drift features just meters from wind-scoured, nearly snow-free plateaus. From a landscape weighted perspective, however, these deep drifts occupy only a small percentage of a pixel area (< 5%) and contribute minimally to overall brightness temperature at the scale of satellite passive microwave observations (Rees et al., 2006).

2.4.3.4. Lake Fraction

Freshwater lakes and wetlands occupy a large fraction, 30 % or more, of the Northern Hemisphere continental surface (Krinner, 2003). As such, lakes have a great potential to influence satellite scale microwave brightness temperature. Research in the Mackenzie River Basin by Derksen et al. (2003) shows that passive microwave SWE estimates remain low throughout the entire winter, and the range of SWE is too narrow. This trend is interannually present, and it is suspected that the inclusion of lakes may be partially responsible as microwave emission from a frozen lake dominates over the scattering signal from snow covered ground. It has been further observed that an increase in within-pixel lake fraction could produce a systematic underestimation of passive microwave SWE (Walker and Silis, 2002). Despite these observations, the microwave emission characteristics from ice and snow on lake ice, and fractional lake ice area are presently not accounted for in any passive microwave snow cover retrieval algorithm.

Microwave emission over lakes is controlled by snow cover, by ice-snow, ice-water interfaces, by ice thickness and by the internal properties of the ice (Hall et al., 1981). Statistics from detailed in-situ snow surveys conducted in northern Manitoba

(Derksen et al., 2005), the Northwest Territories (see Chapter 4) and the Alaskan North Slope (Sturm and Liston, 2003) show that the snowpack on lakes has different properties and is relatively homogenous in comparison to adjacent terrestrial surfaces. The main reason for the homogeneity of snow on lakes is the absence of topographic and vegetative features which control terrestrial snow distribution (scour and drifting) patterns. Variability in snow depth and SWE on lakes is a function of near-shore edge effects and regular, lower magnitude, drifting patterns which depend on wind speeds, direction and fetch.

The difference in snow cover properties from lakes to land does not have as much influence on emission as the ice-snow, the ice water boundaries, and the liquid water under the ice. The sharpest change in T_b occurs during the initial freeze-up, and formation of lake ice as liquid water has a much lower emissivity than ice (Cameron, 1984). As the ice increases in thickness, the effect of the underlying water diminishes proportionally with the penetration depth of microwave energy. As ice thickness increases, there is self emission from the ice, and the T_b becomes more constant. Modeling by Ulaby et al. (1986) demonstrates this relationship. Figure 2.6 illustrates that T_B at 35 GHz increases rapidly as ice thickness increases. However, the relationship begins to level off as ice thickness increases. The T_b begins to approach the physical temperature of the ice as the ice thickness reaches the penetration depth at that wavelength. The same effect is seen at longer wavelengths, however, at greater ice thicknesses.

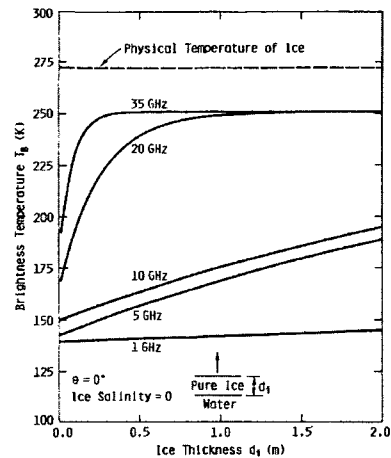


Figure 2.6. Modeled relationship between brightness temperature and ice thickness at different frequencies (Modified from Ulaby et al., 1986)

Snow on the ice surface has a similar effect as ice thickness. As snow depth increases, it acts as a further buffer from the underlying ice-water interface. As such, shorter wavelength frequencies are more sensitive to snow on lakes as well as the initial stages of ice growth, and snow cover contributes more to the observed T_b than the ice does (Hall et al., 1981). Observations with airborne passive radiometers by Hall et al., 1981, show how longer wavelength emission (6.0 cm, 5 GHz) is insensitive to snow and useful for estimating ice thickness (Figure 2.7).

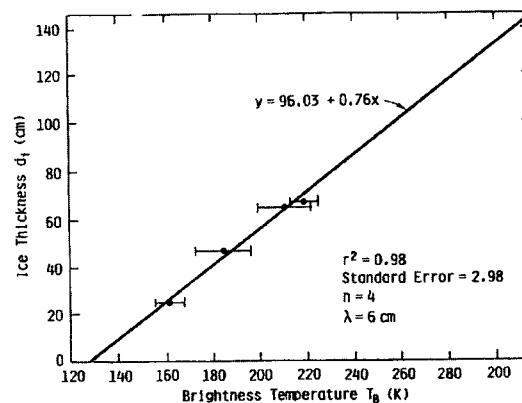


Figure 2.7. Observed relationship between T_b and ice thickness at 5 GHz (modified from Hall et al., 1981)

The properties of the ice can also have an effect on microwave emission. Little research has been done using passive microwave data; however, it has been recognized that ice dielectric, surface roughness, bubble concentration and whether the ice is frozen to bottom can be determined by examining change to active microwave C-Band (5.3 GHz) Synthetic Aperture Radar backscatter (Duguay et al., 2002, Toose, 2007). Different properties of ice across a single lake surface could produce differences in emission that are independent of snow depth and ice thickness (Hall et al., 1981).

The theoretical interaction of microwave emission with snow, ice, and terrestrial surfaces has been well defined (Ulaby et al., 1986, Matzler, 1994). However, further research is required in order to resolve the effect of sub-grid cell lakes in operational satellite scale algorithms. Conventional static T_b inversion SWE retrieval algorithms do not work over lakes because contrary to snow covered land, the T_b over a frozen lake at the 37 GHz channel approaches the brightness temperature at 19 GHz (Hall et al., 1981). Given the nature of the algorithms, when the brightness temperature of the 37 GHz channel approaches or exceeds the 19 GHz measurement, erroneous SWE underestimation (including zero values when 37 GHz > 19 GHz) occurs (Derksen et al., 2005). This occurs in the early season when in grid cells with 100% lake fraction, satellite T_B at 37 GHz can be as much as 20 – 25 K greater than at 19 GHz (Duguay et al., 2005).

Current passive microwave satellite data are too coarse in resolution for determining microwave emission from freshwater ice on all but the very largest of lakes. This underscores the need to develop the capability to consider the influence of sub-grid scale lakes on SWE retrieval algorithms. Derksen et al. (2005) compare fractional grid lake ice percent to SWE retrieval values and found that within-grid lake fraction had a temporally inconsistent influence on SWE estimation. Lake ice seems to have an effect early in the season and becomes increasingly irrelevant towards the end of the season.

2.5. Improving Passive Microwave Estimates of Tundra SWE

2.5.1. Introduction

Currently, no operational passive microwave algorithms exist for the spatially expansive tundra and high Arctic regions due to the complexity in terrain, landscape and snow cover characteristics, along with the lack of in-situ data for development and testing. The heterogeneity of sub-grid tundra snow and terrain are definitely the limiting factors in using conventional SWE retrieval algorithm techniques. However, reliable estimates of SWE in these environments represent the final link to an otherwise nearly complete coverage of northern hemisphere snow cover monitoring and should be a priority.

As mentioned, satellite passive microwave tundra SWE retrieval algorithm development is complicated by a number of factors. From the previous sections, it becomes apparent that the main factors to resolve are the sub-grid variability in 1) snow pack characteristics, 2) distribution of snow cover, and 3) lake ice fraction. The following three sections outline how these issues will be addressed.

2.5.2. Addressing Snow Pack Characteristics

Snow pack characteristics affect microwave emission across both spatial and temporal scales. The spatial distribution of snow cover is more important to consider in the context of static algorithms while the evolution of the snowpack is more important to consider in dynamic algorithm development. The snowpack characteristics which need to be considered are summarized in Table 2.3.

Table 2.3. Snowpack characteristics at spatial and temporal dimensions

Snow Cover Parameters at Spatial Dimensions (static algorithm)	Snow Cover Parameters at Temporal Dimensions (dynamic algorithm)
- Snow depth	- Evolution of snow grain growth
- Snow density	- Change in depth over time
- Snow grain size (depth hoar)	- Change in density over time

At spatial dimensions, the within-grid variability of snow depth, density, and grain size need to be defined. There needs to be an examination of trends in these features over successive years. Somehow the complexity of tundra snow cover needs to be generalized, classified or modeled, so it can be considered at coarse resolutions. The Tb inversion approach of static SWE retrieval algorithms should work in the tundra if properly parameterized. The regression SWE or snow depth on Tb does consider the grain size, density and stratigraphy of the snowpack. However, the snow cover is considered only as within-pixel average conditions which contribute to a given Tb. The challenge, however, is determining if certain snowpack characteristics, such as large depth hoar crystals, will have systematic effects and cause shifts in algorithm retrieval values which are not a product of SWE or snow depth. Furthermore, it is uncertain at this point how integrating snowpack spatial heterogeneity into coarse resolution grid cells will affect simple regression based algorithms.

At temporal dimensions, the evolution of the snowpack must be examined. Static algorithms parameterized for a given “average” snow condition are not expected to perform at different times of year when the snow stratigraphy is much different. Dynamic algorithms are developed to consider the evolution of snow depth, density and snow grain metamorphism. The biggest problem in developing these methods is obtaining temporally and spatially distributed data for algorithm development and testing.

2.5.3. Addressing Snow Distribution Issues

In the context of satellite passive microwave remote sensing, snow cover distribution can be discussed at two scales. Regional scale snow distribution involves characteristic distances of 100 to 1000 km where snow cover is controlled mainly by dynamic meteorological effects, such as standing waves in the atmosphere, lake effects and directional flow around barriers (Pomeroy and Gray, 1995). Snow cover variation at a regional scale does not significantly complicate satellite SWE estimation as regional

differences in snow fall and snow depth and distribution can be discussed for a larger scale than one single pixel. It is the mesoscale or local variations in snow cover parameters that are extremely problematic to SWE retrieval as they occur over linear distances far smaller than the dimension of one spaceborne microwave pixel (< 25 km). The most prominent local scale effects in the tundra are the influences of topography (slope and aspect) and surface cover (vegetation, boulder fields) on the wind-redistribution of a snow cover.

It is not yet known to what extent sub-grid snow distribution will affect satellite scale T_b . Furthermore, there has been little research done to quantify within-grid tundra snow cover variability in the context of coarse resolution algorithms and models.

In order to determine the effect of snow distribution patterns on passive microwave algorithm development, a two tiered approach must be taken.

- 1) A better understanding of the physical processes involved in snow wind re-distribution is required. For example, how do topography and wind direction control snow deposition? Can SWE and snow depth be classified according to topography and land cover? Is there any inter-annual consistency in these patterns?
- 2) Once snow cover distribution areas are classified within a pixel area, airborne and ground based radiometers could be employed to determine the microwave emission characteristics from each feature. This would determine the change in microwave emission across the landscape from flat tundra, through deep snow drifts to blown free ridges.

The first step has been investigated through the development of distributed models described in Section 1.3.5. These models help provide a framework for understanding patterns of tundra snow distribution. However, little research has been done to consider the integrative effect of snow distribution patterns within passive

microwave grid-cells. The key to understanding these relationships is the application of high resolution multi-scale passive microwave data throughout a satellite grid cell.

2.5.4. Addressing Lake Fraction

Snow covered lakes present a significant challenge to algorithm development due to the large contrast in microwave emission from lakes to the land surface. Similar to snow distribution, integrating lake cover fraction into algorithm development involves both a better understanding of within pixel lake cover variability and the effect of different lake characteristics on microwave emission. In tundra environments, within-pixel lake cover varies significantly in terms of total lake cover fraction, individual lake surface area and bathymetry. Lake cover fraction data are available at a 1 km² resolution for all of Canada from the Canadian Center for Remote Sensing (CCRS) and from the International Geosphere–Biosphere Programme (IGBP) land cover classification. The CCRS data are derived through the aggregation of vector maps produced by the Center for Topographic Information of Natural Resources Canada. The vector maps are produced from a combination of air photo and satellite data and are rigorously checked for positional accuracy (Fily et al., 2003). The IGBP global land cover classification is derived from AVHRR and MODIS data and includes other vegetation and land-use classes (Loveland et al. 2000).

Derksen et al. (2005) show that lake cover fraction alone may not be sufficient to explain algorithm imprecision. Part of the problem may be that lake cover fraction provides a value for only the total amount of pixel occupied by lake cover. It lacks more specific information on the size and number of lakes that make up the total fraction. It is possible for two passive microwave pixels with similar fractional water cover to have very different lake characteristics. One pixel may contain a single large lake and almost no smaller ones. However, a second pixel may contain no large lakes but a multitude of smaller lakes whose cumulative surface area is the same as the large lake in pixel one.

Smaller lakes in tundra environments tend to be shallower and are more likely to be frozen to bottom while larger lakes can be very deep and contain a significant volume of water under the ice. This scenario is important to consider in terms of potential differences in microwave emission both spatially and temporally. If there is found to be differences in passive microwave emission between lakes of different characteristics then ancillary data may be needed to classify within-grid lakes beyond simply percent area.

Incorporating lakes into satellite scale algorithms will require the resolution of 1) the difference in microwave emission of snow over lakes versus land, and 2) the difference in snow cover characteristics on lakes versus land. To resolve these issues, there is a need for detailed surveys of snow on lake and land and of lake ice thickness and characteristics, and the deployment of multi-scale radiometers to quantify the nature of microwave emission over tundra lakes.

2.6. Summary of Research Protocol and Data Requirements

The research protocol and data requirements are defined in part by the overall objective of the project. The overall objective, as stated in Section 1.4.5, is to improve operational capabilities for estimating end of winter, pre-melt tundra SWE in a representative study area using satellite passive microwave data.

The key words in this objective are “end of winter, pre-melt snow cover parameters.” Framing the objective in this way eliminates the need to consider the seasonal evolution of the snow pack. The emphasis must be placed first on developing and parameterizing an algorithm which can quantify snow depth and SWE at a given moment in time. Integrating snow metamorphism over the winter to develop a seasonal algorithm approach would require more temporally intensive and costly field work.

Chapter 2 provides a comprehensive review of the current state and challenges of employing passive microwave data to estimate tundra snow cover parameters. The

key data requirements, as discussed in Section 2.5, needed to meet the overall objective are

- 1) Spatially extensive and detailed in-situ snow cover data collected in a representative study area over multiple years, and
- 2) Multi-scale airborne and ground based passive microwave radiometer data to determine microwave emission over homogenous snow and land cover types.

The next step is to define a study area and describe the data sources. These topics will be the focus of Chapter 3.

CHAPTER 3: STUDY AREA AND DATA

3.1. Introduction

The study area for the project is located in the Daring-Exeter-Yamba portion of the Upper-Coppermine River Basin in the Northwest Territories. The region around the study area is ideal for meeting the project objective because the terrain, landscape and snow cover are representative of a large part of the Canadian Shield tundra. Field campaigns were based out of the Government of the Northwest Territories (GNWT) Tundra Ecosystem Research Station (TERS). The station provides a good base for snow surveys as it is free from development and industrial activity. TERS is also the site of 1) the Canadian Tundra Ecosystem Carbon Study (CTECS), aimed at understanding tundra carbon dioxide exchange, 2) Environment Canada's Ecological Monitoring and Assessment Network (EMAN-North), aimed at ecological monitoring to better detect, describe, and report on ecosystem changes, 3) the Canadian Tundra and Taiga Experiment (CANTTEX), which is linked to the International Tundra Experiment (ITEX), which are aimed at monitoring long-term changes in northern terrestrial ecosystems, and 4) GNWT wildlife research projects. All of these projects would benefit to some degree from the intensive spatial and temporal snow cover data sets developed through this project. Monitoring snow cover across this part of the tundra is especially important for evaluating the potential impacts of predicted climate change, mineral exploration and further mine development throughout the region.

3.2. Study Area

3.2.1. Location

The study area is located in the zone of continuous permafrost, above the treeline and is considered a part of Canada's Low Arctic environment (Rouse et al.,

1997). The size, orientation and boundaries of the study area were defined based on the EASE grid (25 x 25 km) centroid located closest to the research station. As outlined in Section 2.1.2, the EASE-Grid is a commonly used projection for satellite passive microwave data. The chosen EASE grid cell centre is located approximately 9 km southwest from the TERS (12 W 472019 7193751) (Figure 3.1).

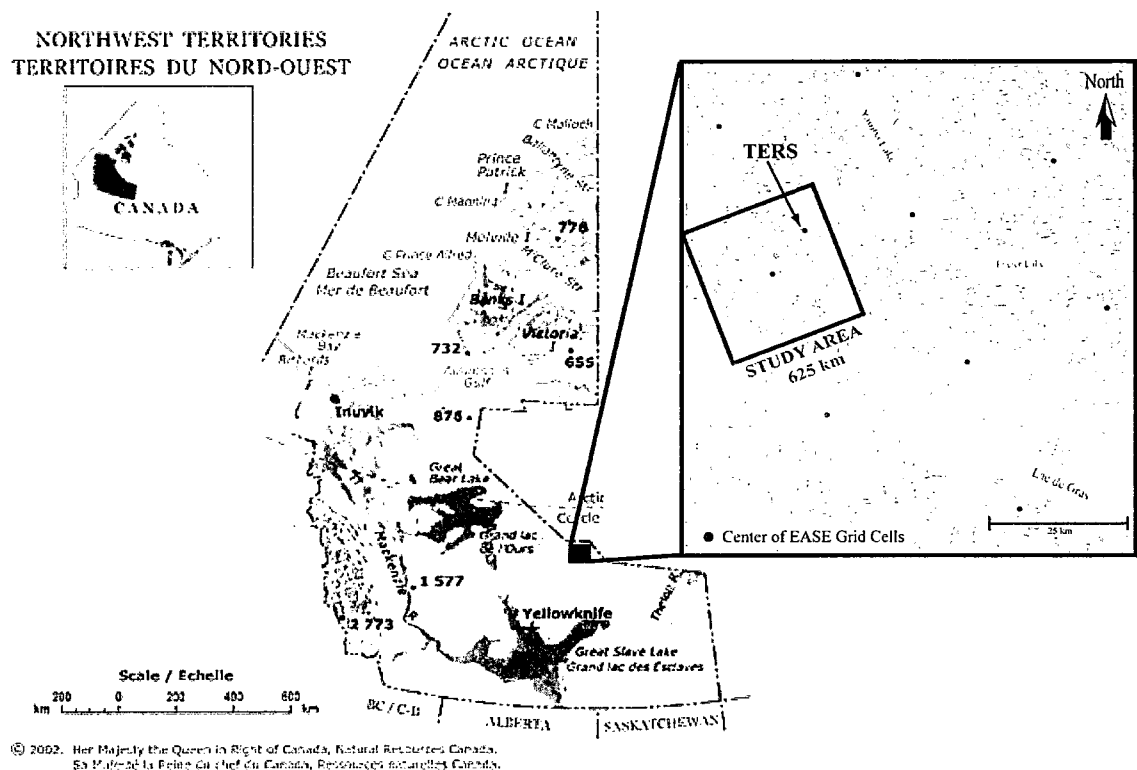


Figure 3.1. Location of the TERS and the study area

3.2.2. Geology and Soils

The study area is situated in the Slave Geologic Province (SGP) of the Canadian Shield. The SGP occupies 213 000 km² and consists of very old granite, gneiss, and metamorphosed sedimentary and volcanic rocks formed during the Precambrian Era (up to 4 billion yrs old). The rocks of the SGP house a variety of mineral deposits and

virtually the entire province is an attractive exploration target for more than one mineral resource (Saxena and Bentz, 1995).

The surficial geology consists of thin sediments and rock fragments which have been reworked considerably during continental glaciation. In general, soil development, though limited, is controlled by climate, topography, biological activity, geochemical weathering of parent material and time. In the study area, parent material is provided largely by the coarse texture sorted sand and silt produced from glacial erosion and deposition. Basin morphometry also plays a role in determining soil moisture conditions. Steeper slopes tend to be better drained while moisture is retained in poorly drained lowland till deposits. Slope aspect is important given the low sun angle at the latitude of the study area. South facing slopes receive significantly more insolation and are typically much drier than north facing slopes. However, climate is the major limiting factor in arctic soil formation as low mean annual temperatures keep the soil frozen as permafrost for most of the year. The short growing season limits biological activity, thus reducing organic matter decomposition which greatly retards soil development. The soil order in the study area is Cryosol with a high degree of variability throughout depth, and the great soil group is classified as a Turbic Cryosol (Oelbermann et al., 2008).

3.2.3. Vegetation

The vegetation in the study area is low arctic shrub tundra which is characterized as largely treeless, dominated by mosses, lichens, low-lying herbs and dwarf shrubs. Vegetation distribution is topographically controlled. Ridge tops are typically rocky with only lichens and herbs present while flatlands are dominated by sedges and mosses. Valleys and localized depressions tend to contain dwarf willow, birch and spruce. Lowland areas are composed of wet sedge meadows with frost features which give a hummocky character to the landscape (Rouse et al., 1997).

3.2.4. Climate

The mean annual daily temperature in the study region is -8.7°C , (-29.8°C in January and 13.9°C in July). The soil remains continuously frozen into early June when the active layer begins to form (Oelbermann et al., 2008). The mean annual precipitation is 260 mm with snow being the dominant input from October until late May. The closest meteorological data are available from an Indian and Northern Affairs (INAC) tower located at the TERS site but the site is unmaintained and measurements are interrupted by lack of power during the winter season. Consistent weather observations (0500 to 1700 local time) are made at the BHP Ekati Mine, located approximately 50 km to the south east of the TERS site.

3.2.5. Hydrology

The study area contains many lakes and rivers which drain into the Exeter-Yamba-Daring portion of the upper Coppermine River. The Coppermine River drains an area of 50 800 km^2 and flows a length of 845 km to its mouth just east of Kugluktuk on the Arctic Ocean. Many parts of the Coppermine basin are undergoing significant land use change due to resource extraction, and concerns have been raised about the cumulative effects of mining and other human development on water quality and on the health of northern aquatic ecosystems (Peramaki and Stone, 2007).

Water quantity is measured continuously at a Water Survey of Canada gauging station (10PA002) located on the Yamba River below Daring Lake (Figure 3.2). The basin area above the gauge is $\sim 3000 \text{ km}^2$ and real time data are available online since the gauge was installed in 1999 (www.wsc.ec.gc.ca).

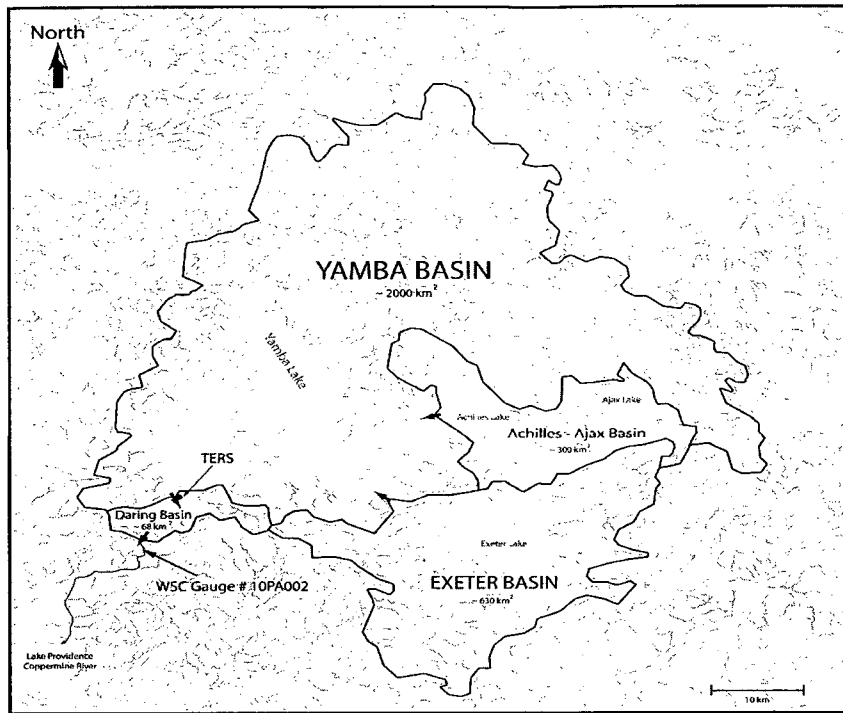


Figure 3.2. Approximate shape of the Daring, Exeter, and Yamba Basins manually interpreted from NTS topographic maps

3.3. Data Acquisition

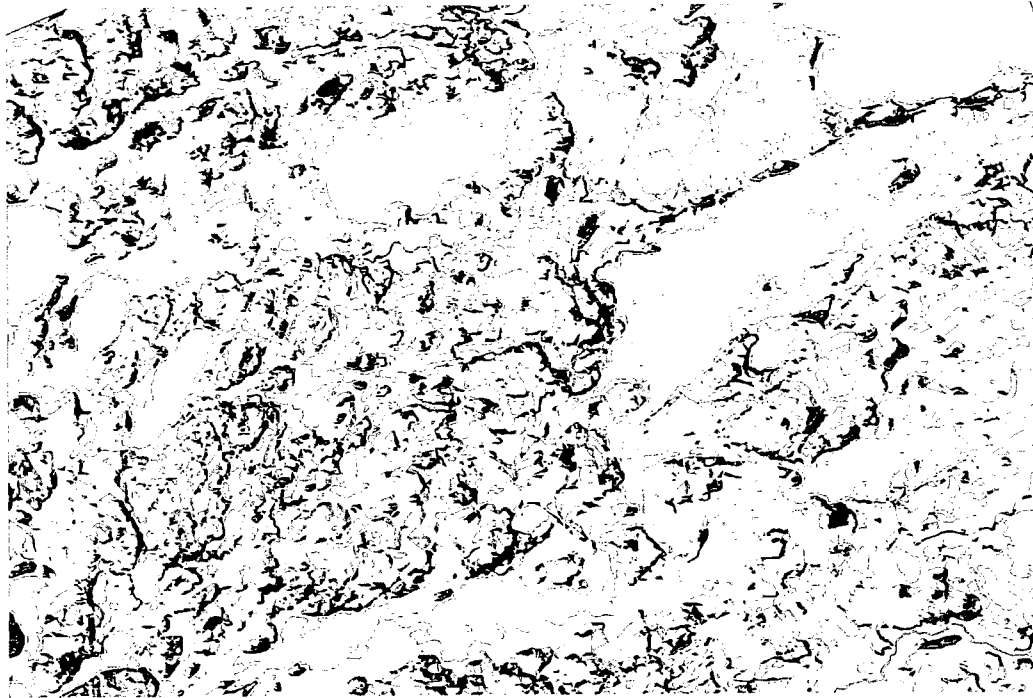
3.3.1. Introduction

Data collected specifically for this research project were obtained during intensive late winter field campaigns in 2004, 2005, 2006, 2007, 2008, and 2009. Data were also available from a preliminary snow survey conducted for another research project during the late winter of 2003. All of the field campaigns were temporally restricted to late winter as it is logistically difficult to monitor snow processes throughout an entire season in a remote tundra location. Furthermore, little melt is observed during mid-winter in tundra environments, and the late winter surveys provide a measure of the total winter snow accumulation. Snow surveys were conducted primarily to quantify pre-melt SWE conditions for comparison to satellite passive microwave data.

Prior to data acquisition, topographic and landscape data of the study area were examined in detail in order to plan the overall sampling strategy. As such, the area was broken down into different strata based on expected heterogeneity in microwave emission and snow cover from different terrain and landscape units, as discussed in Section 2.4. The stratification was based largely on obvious differences in terrain and landscape character.

3.3.2. Terrain Classification

A simple terrain classification was generated using topographic data in order to delineate different terrain and landscape strata in the study area. Unfortunately, limited amounts of topographic data in digital form were readily available for the study area. As such, a large amount of contour data had to be derived through intensive manual digitizing of hard copy National Topographic System (NTS) maps. Ten meter contour data were used to produce a digital elevation model (DEM) for the study area. The DEM was then used to identify and delineate areas of flat tundra and slopes of different angles and aspects. Slope angle is difficult to measure when the ground is covered by a several meter thick snow drift, however, as observed in the field, and summarized by Pomeroy et al. (1997) lee slopes of about 9 degrees promote the formation of drifts with a 5 to 7 degrees slope. As such, snow slopes of 7 degrees were selected as the cut-off between steep depositional slopes and lower slopes. Lake cover data from the NTS maps were then overlain on the DEM to determine the locations and size of lakes in the study area (Figure 3.3).



Terrain Categories	
1	Flat Tundra
2	Lakes
3	Upland Plateaus
4	Low North Slopes
5	Steep North Slopes
6	Low East Slopes
7	Steep East Slopes
8	Low South Slopes
9	Steep South Slopes
10	Low West Slopes
11	Steep West Slopes

Figure 3.3. Terrain classification of study area

The classification of terrain was then used to determine the percent grid area occupied by the different terrain units (Table 3.1).

Table 3.1. Terrain units and percent of study area

	Terrain Unit	Percent Study Area
1	Flat Tundra	36.7
2	Lakes	25.6
3	Upland Plateaus	2.0
4	Low North Slopes	6.0
5	Steep North Slopes	3.1
6	Low East Slopes	4.6
7	Steep East Slopes	2.8
8	Low South Slopes	6.3
9	Steep South Slopes	3.3
10	Low West Slopes	7.4
11	Steep West Slopes	2.5

3.3.3. Landscape Classification

Landcover information was obtained from a GNWT vegetation classification completed in 2001 as part of the West Kitikmeot Slave Study (www.nwtwildlife.com). Landcover types were generated using a supervised classification of vegetation, land cover, ecosystem unit, and habitat compiled by the wildlife division (ENR) of the GNWT. The 2001 classification used eight LANDSAT scenes and covered a total area of about 200,000 km² with a spatial resolution of 30 m. Nineteen classification categories were used: fourteen vegetation units, three un-vegetated and two for water. To generate the classification, ground data were gathered from 300 to 500 sites for each scene to provide information for testing and increasing the accuracy of the computer's classification of the satellite imagery. The accuracy from scene to scene varied from 51% to 82% (www.nwtwildlife.com) (Figure 3.4).

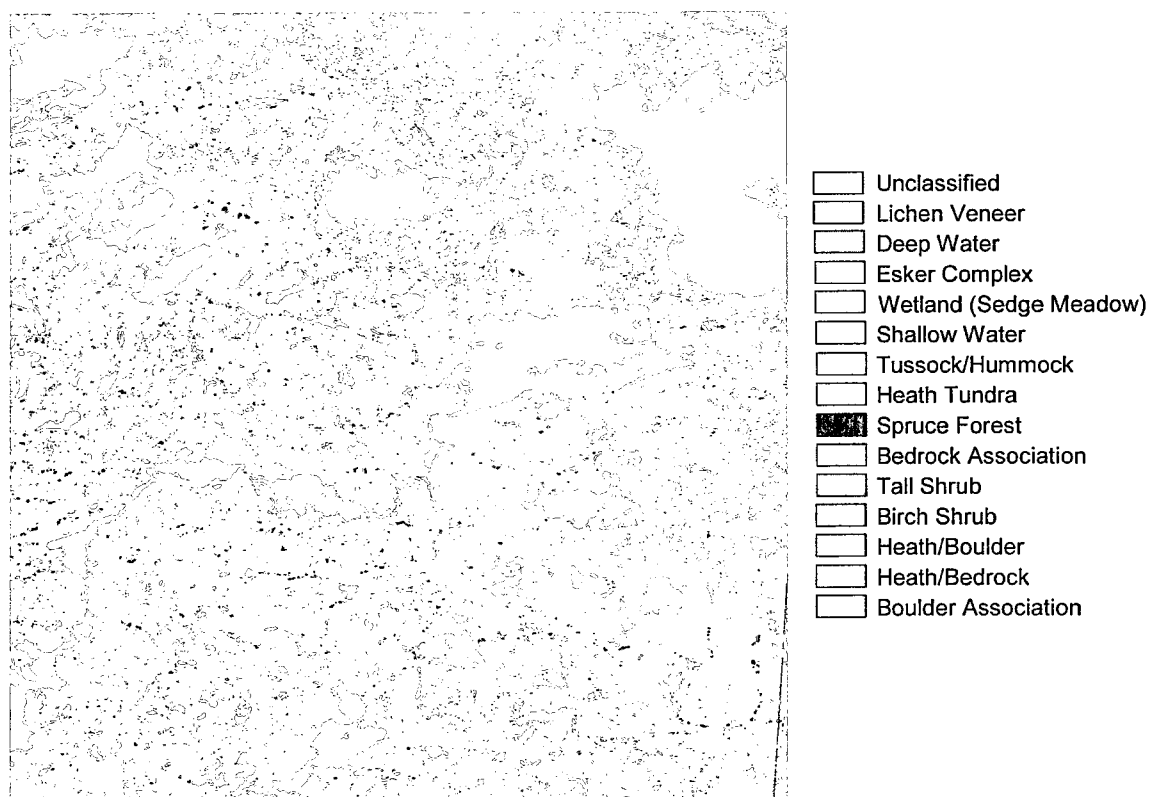


Figure 3.4. ENR 2001 LANDSAT landcover classification

The landscape classification was used to determine the percent grid area occupied by the fifteen different landscape units present in the study area (Table 3.2).

Table 3.2. Landcover classification and percent study area

Grid Code	Landcover Class	Percent Study Area
0	Unclassified	0.10
1	Lichen Veneer	3.62
2	Deep Water	17.94
3	Esker Complex	1.59
4	Wetland (Sedge Meadow)	2.69
5	Shallow Water	10.79
6	Tussock/Hummock	17.88
7	Heath Tundra	24.07
8	Spruce Forest	0.30
10	Bedrock Association	3.90
11	Tall Shrub	0.29
12	Birch Shrub	0.49
13	Heath/Boulder	13.19
14	Heath/Bedrock	2.35
15	Boulder Association	0.92

Another classification was done by ENR for a breeding bird survey in 2004 which used two high resolution IKONOS images (1 m panchromatic, 4 m multispectral) in the immediate vicinity of Daring Lake. The classification was extensively evaluated; however, the data are limited to a small part of the study area to the northeast of Daring Lake.

3.3.4. Snow Data

3.3.4.1. *Snow Survey Locations*

Within the 25 x 25 km study area, a north-south and east-west grid was established using 2.5 km fixed intervals. This grid was used as a reference for snow surveys (see Figure 3.5). Sampling locations were established as follows:

- 1) At the intersection of north-south and east-west grid lines (un-biased, fixed interval sampling),

- 2) At sites along the grid lines where the terrain and snow cover changed significantly and were seen as representative of a given terrain category (biased, stratified transect sampling),
- 3) At other sites of interest throughout the larger Daring-Exeter-Yamba basin (biased site selection, random locations) and,
- 4) At 5 m intervals along selected grid lines (fixed interval, transects, in 2008 and 2009).

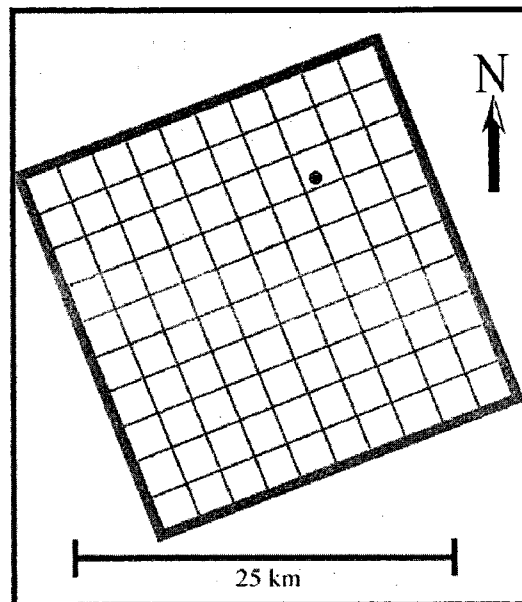


Figure 3.5. Reference grid for survey locations

The primary objective of each annual snow survey was to collect spatially distributed in-situ snow data which could be compared to EASE grid satellite scale brightness temperature (T_b) data. In order to compare data from one year to the next, a secondary objective was to visit the same sites during each field campaign. Most of the sampling was done via snowmobile which determined the proximity to the research station. However, the availability of a helicopter during the 2004 and 2005 campaigns permitted the acquisition of snow data a greater distance from the Daring Lake camp. The acquisition of temporally co-incident airborne radiometer data in 2005 and 2008

necessitated a change in the snow sampling protocol. During these campaigns, more focus was dedicated to sampling along flight lines and less to areas in the grid where the aircraft did not pass overhead. As a result, the distribution of sites surveyed varied somewhat from year to year.

3.3.4.2. Snow Survey Protocol

Site locations based on the pre-determined grid were input into handheld GPS units prior to sampling, and snow survey crews traveled to each site either by snowmobile or helicopter. Upon arrival, the exact sampling locations were chosen to best represent the surrounding terrain and snow cover conditions, however, as close to the pre-determined location as possible. The goal of this decision making was to avoid, whenever possible, extremely localized features, such as small depressions, drifts or rock outcrops. To reduce complexity, these features cannot be considered as separate classes in a generalized classification scheme. These features were noted in the field books; however, since they often occupy a very small spatial extent, and represent an insignificant percentage of the overall landscape they are excluded. Encompassing such features would require an infinitely complex classification system which is not feasible when attempting to generalize snow cover over a 625 km² study area.

At each site, a manual snow probe was used to obtain 30 depth measurements taken in a circular pattern around the site. Five snow cores were taken at random locations using an ESC 30 snow corer. The weight of each core was measured using a hanging Pesola spring scale. The instrument error of these scales is manufactured to be ± 10 g.

Snow density and SWE can be easily calculated from the ESC 30 measurement and the weight of the core as follows:

$$\text{ESC 30 SWE (cm)} = \text{Core Weight (g)} * 30$$

$$\text{ESC 30 Density (g/cm}^3\text{)} = \text{Core Weight (g)} / [30 * \text{Core depth (cm)}]$$

At each grid intersection site, a snow pit was excavated in order to examine snow stratigraphy and grain size and to obtain a snow density profile from the snow-air interface to the ground at 10 cm intervals. The snow density was measured by collecting snow in a 10 cm aluminum wedge cutter and weighing the sample with the Pesola scale.

3.3.4.3. Annual Snow Survey Sample Numbers

The terrain classification developed (see Section 3.3.2) was used to determine the percent area of the basin occupied by each terrain category. For sites not located at pre-defined grid intersections, target sample site numbers for each terrain category were determined based on what percent of the total area the category occupied. The goal was to generate sample numbers for each terrain category as close as possible to the proportion of the study area they occupy. During each year, between 147 and 255 sites were sampled (Table 3.3). In 2008, an automated snow probe (Magnaprobe™ developed by SnowHydro Ltd.) was used to supplement regular sampling. Snow depths were measured using the probe at 2 m fixed intervals along 40 km of transect.

Table 3.3. Sample n and the percent of total basin area occupied by each terrain category for the survey years

Terrain Category	Percent of Total Basin Area	Sample Sites (n) and % of Total n					
		2004	2005	2006	2007	2008	2009
Flat Tundra	35.2	(49) 20%	(55) 32%	(64) 27%	(84) 33%	(47) 32%	(72) 32%
Lakes	27.1	(49) 20%	(31) 18%	(51) 21%	(50) 20%	(32) 22%	(46) 21%
Upland Plateaus	3.5	(41) 17%	(18) 11%	(42) 18%	(36) 14%	(14) 10%	(29) 13%
Low North Slopes	7.1	(13) 5%	(10) 6%	(9) 4%	(18) 7%	(10) 7%	(21) 9%
Steep North Slopes	1.8	(13) 5%	(6) 4%	(10) 4%	(5) 2%	(3) 2%	(5) 2%
Low East Slopes	5.5	(9) 4%	(7) 4%	(11) 5%	(17) 7%	(10) 7%	(14) 5%
Steep East Slopes	1.4	(11) 5%	(9) 5%	(9) 4%	(5) 2%	(4) 3%	(3) 1%
Low South Slopes	7.6	(18) 7%	(7) 4%	(8) 3%	(12) 5%	(9) 6%	(15) 7%
Steep South Slopes	1.9	(12) 5%	(4) 2%	(7) 3%	(6) 2%	(3) 2%	(3) 1%
Low West Slopes	7.8	(13) 5%	(11) 7%	(11) 5%	(11) 4%	(13) 9%	(10) 5%
Steep West Slopes	1.1	(12) 5%	(8) 5%	(10) 4%	(11) 4%	(2) 1%	(4) 2%
TOTAL n		243	170	238	255	147	222

Through the six years of in-situ measurement, this research project has generated a pre-melt snow cover database that is one of the most spatially comprehensive compiled over a Canadian open tundra environment.

3.3.5. Meteorological Data

Meteorological data were obtained from a station located near TERS which is maintained by Mr. Bob Reid of the Department of Indian and Northern Affairs Canada (INAC). Of interest were air temperature, soil temperature, wind speed and direction. The data were used to identify any days where the air temperatures were above zero. As outlined in Chapter 2, any melting of the snow would produce liquid water which would complicate the retrieval of snowpack information with passive microwave data. Similarly, the soil temperature data were used to note whether or not the ground was completely frozen.

During each of the end of winter surveys, the soil temperature was well below zero and often much colder than the air temperature (-10 to -20°C). This is important to note as any difference in observed T_b should not be caused by liquid water in the soil. The air temperature was much more variable and ranged from -35 to +6°C. When the temperature was above zero, radiometer data were no longer collected, and snow sampling with ESC 30 tubes became much more difficult. Fortunately, above zero temperatures did not persist for more than a day or two during any of the field campaigns.

Wind speed and direction were also available and could be used for future comparison with seasonal snow accumulation patterns. However, none of the survey years has continuous wind data due to the INAC station being powered by solar panels. During the early winter, through December to February, there are often significant gaps in the data due to the reduction in daylight hours.

3.3.6. Ground Based Passive Microwave Radiometer Data

Ground based passive microwave brightness temperature data were collected in 2005 and 2007 using Environment Canada's Surface Based Radiometer (SBR) system. The SBR has both vertically and horizontally polarized radiometers at 6.9, 19, 37 and 89 GHz which are mounted at 53 degrees look angle (Asmus and Grant, 1999) (Table 3.4).

Table 3.4. Summary of SBR instrument characteristics

Frequency (GHz)	6.9	19	37	89
Bandwidth [MHz]	500	1000	2000	4000
Sensitivity [K]	0.2	0.04	0.03	0.08
Accuracy [K]	<2	<2	<1	<1
Beam width [°]	9	6	6	6
Look angle [°]	53	53	53	53

The spatial footprint of the radiometers mounted on the SBR is dependent on the instrument beam width and the height mounted above the surface. The footprint of the radiometers is elliptical in shape and outlined in Table 3.5.

Table 3.5. Footprint dimensions for SBR radiometers

	6.9 GHz	19 GHz	37 GHz	89 GHz
Near width (m)	0.48	0.33	0.33	0.33
Far width (m)	0.59	0.37	0.37	0.37
Depth (m)	0.88	0.58	0.58	0.58

Before and after deployment at Daring Lake, the microwave radiometers were calibrated in Yellowknife for conversion of voltage output to brightness temperature (Walker et al., 2002). A two-point calibration technique was used with an ambient temperature microwave absorber as the "warm" reference and liquid nitrogen as the "cold" reference. The liquid nitrogen calibration technique has been described in Solheim (1993). Unfortunately, no post deployment calibration was available during the 2007 deployment; however, drift values were assumed to be similar to those obtained during extensive calibration of the instruments on the aircraft platform during 2005 and 2006.

During these campaigns, instrument drift was observed to be approximately ± 8 K at 6.9 GHz, ± 2 K at 19 GHz, < 1 K at 37 GHz, and ± 4 K at 89 GHz. The instrument drift is considered acceptable for ground based radiometer measurements (Lemmetyinen et al., in press).

3.3.7. Airborne Passive Microwave Radiometer Data

Airborne passive microwave brightness temperature data were obtained from radiometers mounted aboard the National Research Council Twin Otter aircraft (MacPherson et al., 2001). The radiometers mounted to the aircraft are the same units used in the SBR system summarized in Table 3.3. The radiometers are mounted to a special door on the aircraft and acquire data at an incidence angle of 53 degrees.

With the airborne system, the spatial footprint is a function of aircraft altitude. During the 2005 field season, multiple overpass flights were made along all north – south and east – west grid lines in the 25 x 25 km study domain (Figure 3.4). Data were collected with the aircraft at three flying heights of 277, 828 and 2207 m. During the 2008 campaign, flights were conducted along flight lines at two flying heights of 277 m and 2757 m (Table 3.6).

Table 3.6. Summary of flying heights and radiometer footprint dimensions

Aircraft Altitude		Radiometer Footprint			
		6.9 GHz	19 GHz	37 GHz	89 GHz
277 m	Near width (m)	66	45	45	45
	Far width (m)	81	52	52	52
	Depth (m)	121	80	80	80
828 m	Near width (m)	197	135	135	135
	Far width (m)	243	155	155	155
	Depth (m)	363	241	241	241
2207 m	Near width (m)	524	360	360	360
	Far width (m)	646	414	414	414
	Depth (m)	970	642	642	642
2757 m	Near width (m)	655	450	450	450
	Far width (m)	808	517	517	517
	Depth (m)	1211	802	802	802

The data acquisition system in the aircraft collects Tb data with an integration time of approximately one second. The actual footprint size is wider than shown in Table 3.6 because of the distance the aircraft travels in that one second. The aircraft travels at roughly the same speed for each of the data flights so the added footprint width of ~ 45 m is the same for each altitude. As such, the added width is most pronounced in the 277 m and 828 m data and for input into the GIS, these data were adjusted.

Before and after each flight, the radiometers were calibrated at the Yellowknife airport for conversion of voltage output to brightness temperature (Walker et al., 2002). The two point calibration technique described in Section 3.3.5 was also used for the aircraft data. However, one complication with calibrations in Yellowknife was the influence of radio frequency interference (RFI) on the 6.9 GHz instrument. RFI in urban environments is a result of telecommunication towers which transmit signals at frequencies close to 6.9 GHz, and is observed globally (Kidd, 2006). RFI was not observed on flights over the study area; however, it did complicate calibration and would severely limit the use of low frequency radiometers in more populated areas. RFI was not observed during calibrations obtained during an aircraft campaign in Churchill, Manitoba, in 2006, and the instrument was found to have uncertainty of 5 to 7 K in Tb (Toose, 2007). Uncertainty in the high frequency radiometers ranged from +/-2K at 19 GHz, <1K at 37 GHz, and +/-4K at 89 GHz which is consistent with calibrations done in Churchill in 2006 and in previous campaigns summarized by Derksen et al. (2005) and Lemmetyinen et al. (2009). Estimates of error due to within-deployment receiver drift were derived from a comparison of the pre and post calibrations. The error is compensated for by adjusting observed Tb based on the calibration information using a non-linear, multi-iterative process described by Toose (2007).

3.3.8. Satellite Passive Microwave Radiometer Data

Satellite brightness temperatures were obtained from the Advanced Microwave Scanning Radiometer - Earth Observing System (AMSR-E) sensor. Both horizontally and vertically polarized brightness temperatures at 6.9 GHz, 10.7 GHz, 18.7 GHz, 23.8 GHz, 36.5 GHz, and 89.0 GHz were downloaded from the National Snow and Ice Data Center (NSIDC) by Environment Canada. AMSR-E instrument characteristics are summarized in Table 3.7.

Table 3.7. Summary of AMSR-E instrument characteristics

Center Frequency (GHz)	6.925	10.65	18.7	23.8	36.5	89.0
Bandwidth (MHz)	350	100	200	400	1000	3000
Sensitivity (K)	0.3	0.6				1.1
Mean Spatial Resolution (km)	60	38	21	24	12	5.4
IFOV (km)	74 x 43	51 x 30	27 x 16	31 x 18	14 x 8	6 x 4

The swath data were converted to the EASE grid format by the NSIDC, so they could be spatially standardized over the multiple years of the project. Swath data are useful because the original frequency dependent imaging characteristics are retained; however, geolocation errors can occur between satellite overpasses. For example, Poe and Conway (1990) found that for the SSM/I sensor swath geolocation error can be as high as 20 km but can be corrected to around 7 km. The AMSR-E swath location is somewhat more accurate, but geolocation errors do exist between multiple years of data. Hence, EASE grid data are a much better source for the compilation of a Tb time series (Derksen, 2008). AMRS-E data were acquired for the November to April periods during each of the years in which snow cover data were available (2003 to 2009).

3.4. Data Summary

For each year from 2003 to 2009, meteorological observations and AMSR-E satellite Tb were obtained. Data collected in the field varied somewhat from year to year and are summarized in Table 3.8.

Table 3.8 Summary of field data collected

Survey Year	Data Sets
2003	- Preliminary snow survey in sub-basin of Daring Lake
2004	- Snow survey throughout the study area
2005	- Snow survey throughout the study area - Airborne radiometer flights throughout entire study area - Preliminary deployment of ground based radiometers
2006	- Snow survey throughout the study area
2007	- Snow survey throughout the study area - Site surveys and transects with ground based radiometers
2008	- Snow survey throughout the study area - Airborne radiometer flights along 75 km of transect - Over 40 km surveyed with automated snow probe along flight line transects
2009	- Snow survey throughout the study area - Over 15 km surveyed with automated snow probe along transects

The amount of data collected is certainly unprecedented for the Canadian tundra. The scope of this thesis does not allow for a complete analysis of all of the data. However, the data set will provide many opportunities for tangential projects and certainly will prove to be a solid foundation for future research in this area.

CHAPTER 4: Distribution and Properties of Tundra Snow Cover

4.1. Introduction

Snow cover data can be generated for large spatial domains by using distributed models and through remote sensing techniques. However, regardless of how rigorous modeling and remote sensing algorithms may be, they must still be tested against accurate data sets to ensure realistic results (Foster et al., 1996). As such, the validity of model and remote sensing outputs is limited by the reliability of snow cover data. Given the important linkage of snow to physical systems (Section 1.3) and the spatial and temporal discontinuity of current data sets, there exists a need for developing intensive, tundra-specific snow cover data. These data are necessary in order to meet the objectives outlined in Section 1.4 and would be a valuable contribution to many other areas of research. The purpose of this chapter is to establish a more complete understanding of tundra snow cover through the multiple years of late winter, spatially intensive, pre-melt in-situ snow cover measurements introduced in Section 3.3.3. These data will be used in order to provide the following:

- a) A detailed description of tundra snow cover distribution and variability within the 625 km² study area;
- b) A means for extrapolating point observations to EASE grid resolution (25 km) for comparison with satellite passive microwave data (Chapter 5);
- c) A basis for comparison of in-situ snow cover data with multi-scale airborne and ground based passive microwave data (Chapter 6);
- d) A foundation of data to contribute to the development and validation of operational spaceborne passive microwave algorithms (Chapter 7).

4.2. Tundra Snow Cover Distribution and Properties

4.2.1. Introduction

The tundra landscape in the study area can be generally characterized as regionally uniform, devoid of dense forests and significant relief features. However, the gentle undulating hills, intricate post-glacial features, lakes, and rugged rock outcrops produce very complex local snow accumulation patterns. It has been recognized by many researchers that the patterns of tundra snow cover distribution are largely a product of wind re-distribution and complex snow-terrain interaction (Woo and Marsh, 1978, Pomeroy et al., 1997, Woo, 1998, Sturm and Liston, 2003, Hirashima et al., 2004, Essery and Pomeroy, 2004, Woo and Young, 2004). Snow redistributed by varying wind speed and direction interact with micro and macro topography, frozen lake surfaces, emergent vegetation and boulder outcrops to produce highly variable snow cover patterns. During each of the field surveys, the snow cover throughout the study area was found to be generally heterogeneous across the landscape. Thus, assuming a single grid-cell value for any given snow property would not encapsulate the complex snow-terrain accumulation patterns. As such, in order to define complex sub-grid snow cover information, it is necessary to consider the effects of different terrain types on snow accumulation. To meet this objective, a terrain classification, described in Section 3.3.2, was developed to stratify the study area into different terrain categories. This approach should be useful for the compression of large complex data sets and for the inference and extrapolation to areas not directly sampled (Sturm et al., 1995). Furthermore, the terrain categories developed were useful in guiding the snow surveys during each year and form the basis for reporting and discussing snow cover parameters throughout this chapter.

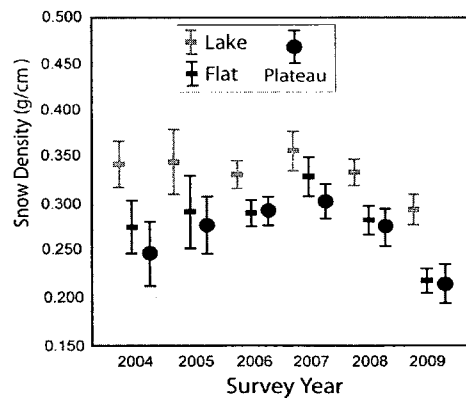
4.2.2. Snow Cover Properties

As outlined in Chapter 1 and 2, the important snow cover parameters to observe are snow density, depth, SWE and general snowpack stratigraphy. Each parameter will be discussed both within and among the multiple years of snow surveys.

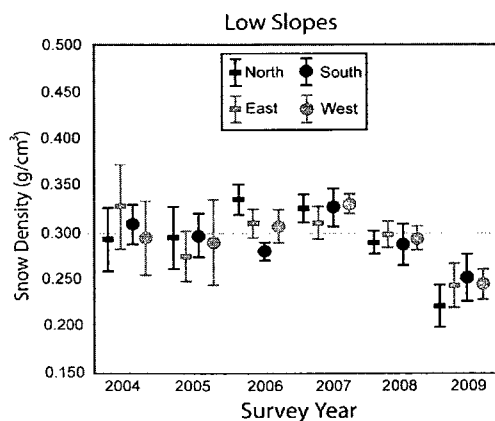
4.2.2.1. Snow Density

As outlined in Section 3.3.3, snow density was measured five times at each site using an ESC snow corer and a hanging balance. The five measurements were used to derive a site mean density. The site means were then binned according to terrain category, and a mean for each category was generated. The terrain category means for each year were then plotted along with one standard deviation (Figure 4.1).

a)



b)



c)

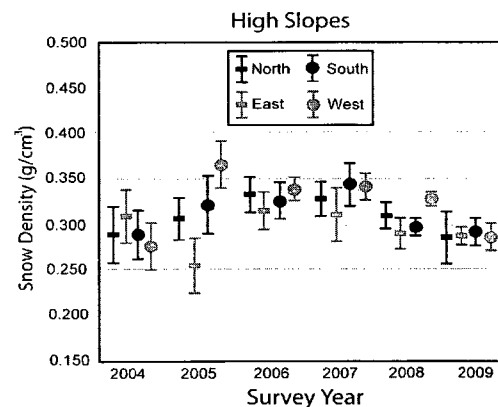


Figure 4.1. Snow density on lakes, flat tundra, plateaus (a) and slopes both low (b) and high (c), during the 2004 to 2009 snow surveys. The heavy center lines and circles represent the mean while the range of values is one standard deviation.

Figure 4.1 shows that snow on lakes had the highest density of all the non-slope areas during each year surveyed. Snow on flat tundra was found to be less dense than lakes but consistently denser than the thin, wind-scoured snow found on upland plateaus. However, the density of snow on slope areas was quite variable among slope aspects in each survey year and when comparing different years. In some cases, the snow on steeper slopes was denser than on shallower slopes; however, this was not a consistent relationship year-to-year. In general, snow on slopes was found to be denser than on flat tundra or upland plateaus.

Based on the data shown, there appears to be increasing density from 2004 to 2007 and towards decreasing density from 2007 to 2009. The mean density of all measurements taken in 2004 was $0.288 \text{ g/cm}^3 (\pm 0.067 \text{ SD})$; in 2005, it was $0.298 \text{ g/cm}^3 (\pm 0.071)$; in 2006, it was $0.311 \text{ g/cm}^3 (\pm 0.033 \text{ SD})$; in 2007, it was $0.322 \text{ g/cm}^3 (\pm 0.038 \text{ SD})$; in 2008, it was $0.295 \text{ g/cm}^3 (\pm 0.042 \text{ SD})$; and in 2009, it was $0.245 \text{ g/cm}^3 (\pm 0.048 \text{ SD})$. It is assumed that annual differences in density are dependent on the magnitude and direction of wind, on the timing of high wind speed events relative to snowfall events, and on the crystal characteristics of falling snow. These relationships, although apparent from anecdotal evidence, are difficult to quantify in remote regions without including detailed weather and blowing snow observations. Unfortunately, meteorological data for the entire winter are not currently available for the study area.

The standard deviation in density appears to decrease from 2004 through 2009. This pattern may be real; however, the decrease in standard deviation from year to year may at least be partially explained by the improvement of field personnel at sampling density. Using snow tubes for sampling can produce error when some of the sample falls out of the bottom of the tube. This significantly reduces the weight of the sample for a given depth, and erroneous densities are recorded. As the proficiency in sampling density increased over the years, there was more attention given to obtaining a complete

sample in the tube. Hence, the variability in density was inadvertently reduced.

Furthermore, the scales used to measure the weight of each core sample were of better quality during the 2006 through 2009 survey years. This allowed for more consistent sampling among different personnel.

Despite these factors, density seemed to be more inter-annually consistent and predictable compared to other snow cover parameters. The only exception was the 2009 season where the density appeared to be and was in fact lower than in previous years. In order to determine if density is consistent from year to year, the difference between the means needs to be tested. For normally distributed data, one-way analysis of variance (ANOVA) tests is typically used for this purpose. The average density for each site was plotted on frequency histograms to demonstrate the normality of the data (Figure 4.2).

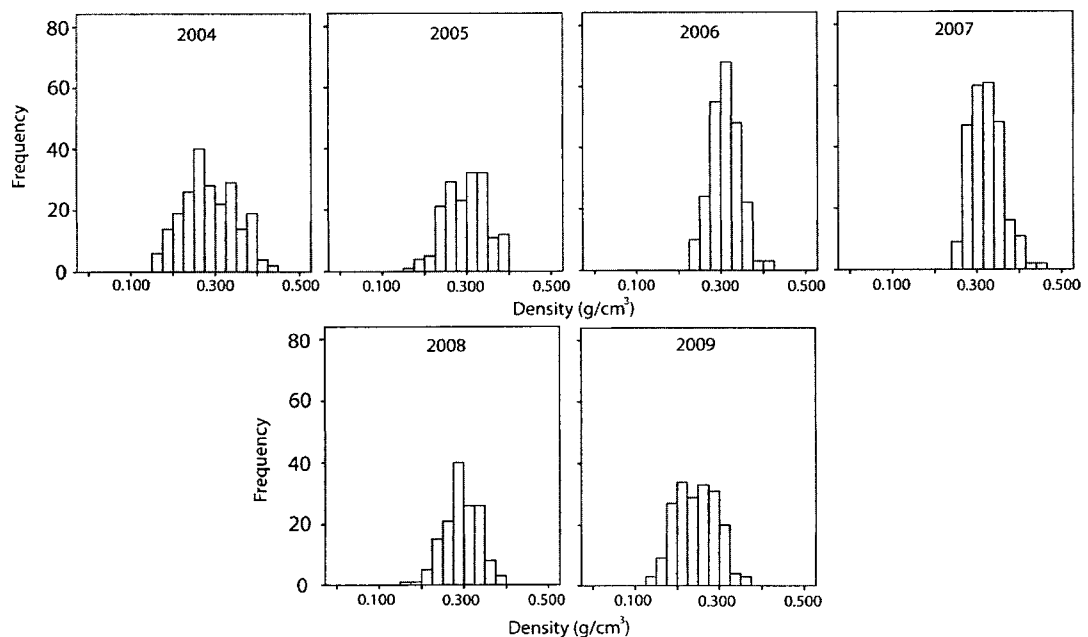


Figure 4.2. Frequency histograms of site density

An ANOVA determines if there are statistically significant differences between groups. However, when there are multiple groups, the ANOVA is not the final step as it does not indicate which groups are different from each other and by how much. For this,

post-hoc tests are used. It is important to note that post-hoc tests are not appropriate if the ANOVA F is not significant, meaning that there are no differences between any of the groups. Determining which post-hoc test is most appropriate depends on the equality of group n as well as the homogeneity of variance between groups. To test for homogeneity of variance the Levene's statistic is used. In snow density dataset, the number of samples are not exactly the same each year, and the Levene's statistic ($p < 0.001$) indicated that the variance in density between years is not equal. As such, a Games-Howell (GH) multiple comparison post-hoc test was chosen to be most appropriate. The GH test was developed specifically for data with both unequal variances and unequal sample numbers (Games et al., 1983). The GH test is preferred over other tests which assume equality of variances and/or equal group sizes. If these assumptions are violated, it can lead to an increased chance of making Type I errors and adding a liberal bias to the significance values (Morgan et al., 2004). The GH was used to perform a pairwise comparison of the mean densities to determine specifically which years were significantly different from each other. The test provides the direction and magnitude of the mean difference in addition to showing groups with significant differences (Table 4.1).

Table 4.1. Difference of mean density for each survey year

Mean Difference						
	2004	2005	2006	2007	2008	2009
2004		-0.011	-0.024	-0.036	-0.008	0.042
2005			-0.013	-0.025	0.003	0.053
2006				-0.012	0.016	0.066
2007					0.028	0.077
2008						0.049
2009						

Indicates the mean difference is significant at 0.05

For most of the years, the mean densities were significantly different. The years not significantly different were 2004-2005, 2004-2008, 2005-2006, and 2005-2008. Of

interest were 2007 and 2009, which were significantly different from all other years. In 2007, the mean density was significantly higher than all other years; while in 2009, the mean density was significantly lower than all others. The next step would be to conduct a more detailed investigation to examine the mean difference between each terrain type within each year. However, this level of analysis will be reserved for SWE as it is calculated using both depth and density.

Despite the significant difference between most of the yearly mean densities shown in Table 4.1, the qualitative perspective from field observations is that there is not that much variability in density from year to year. This can be tested by calculating an overall mean density derived from all measurements taken over the six years of field surveys ($n = 6375$). The mean density from all years is 0.294 g/cm^3 (± 0.053 , CV 18). This regional density of 0.294 g/cm^3 is lower than the 0.380 g/cm^3 from the general snow classification by Sturm et al. (1995) however it compares more favorably to densities of 0.285 g/cm^3 and 0.277 g/cm^3 measure in on northern Alaska tundra by Sturm and Liston (2003).

To quantify the inter-annual consistency in density and the applicability of an overall mean density, a GH test was used to see if the mean of 0.294 g/cm^3 is significantly different from the mean density for each year (Table 4.2).

Table 4.2. Difference of mean density from each year compared to overall mean density

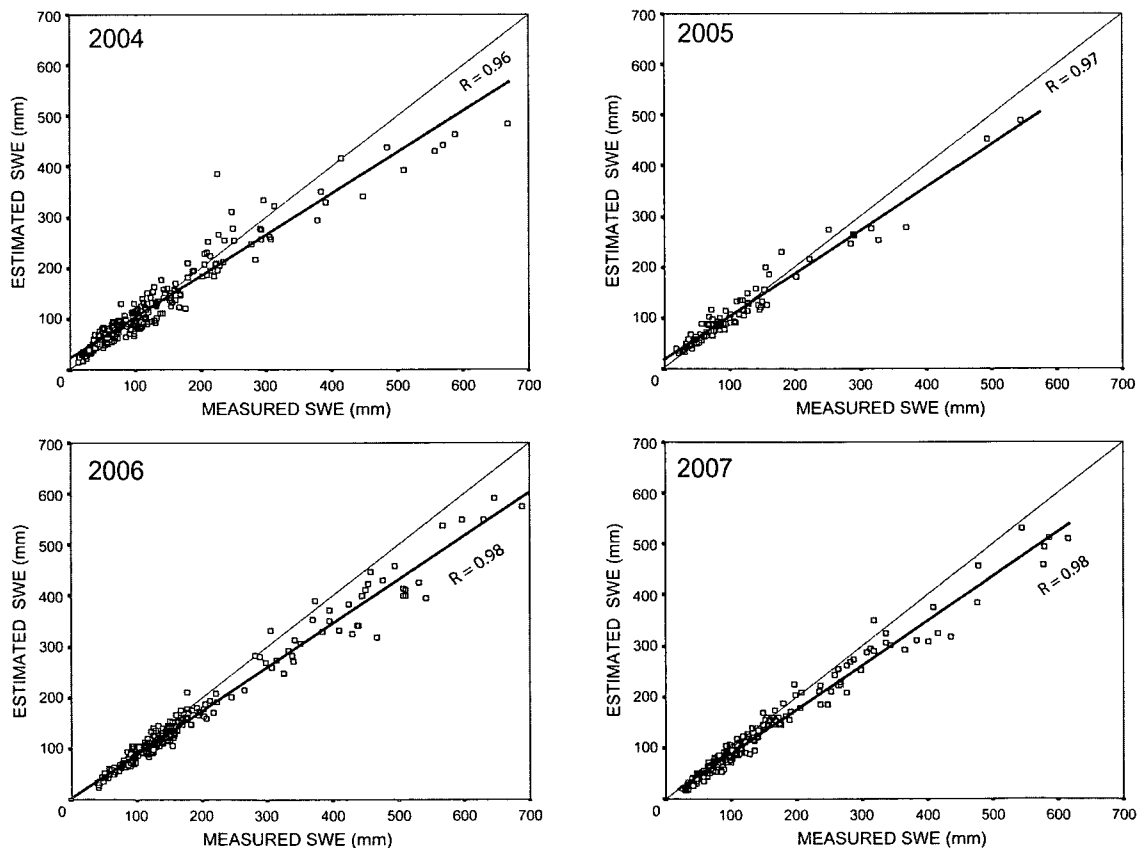
Mean Difference						
	2004	2005	2006	2007	2008	2009
<i>Mean Density 0.294</i>	0.007	-0.004	-0.017	-0.029	0.000	0.049

Indicates the mean difference is significant at 0.05

The overall mean density of 0.294 g/cm^3 was not significantly different than the mean density of measurements taken in 2004, 2005 or 2008. The densities during 2006 and 2007 were significantly higher, while density in 2009 was significantly lower than

0.294 g/cm³. The greatest difference is in the 2009 density which is nearly 0.050 gm/cm³ lower than the overall mean of 0.294 g/cm³. Excluding the 2009 season raises the overall mean to 0.305 g/cm³.

The applicability of an overall mean density of 0.294 g/cm³ was further evaluated by comparing it to measurements made on a site-by-site basis. Estimated SWE were calculated by using the depth measurements of a given site and the overall mean density of 0.294 g/cm³. These estimated SWE were then plotted against measured SWE which was calculated using both depth and density measurements made at a given site. In a sense, by comparing these two values, the validity of the regional average can be determined independent of terrain type on a site-by-site basis (Rees et al., 2005). Estimated SWE were correlated against measured SWE for each of the survey years and plotted on scatterplots (Figure 4.3).



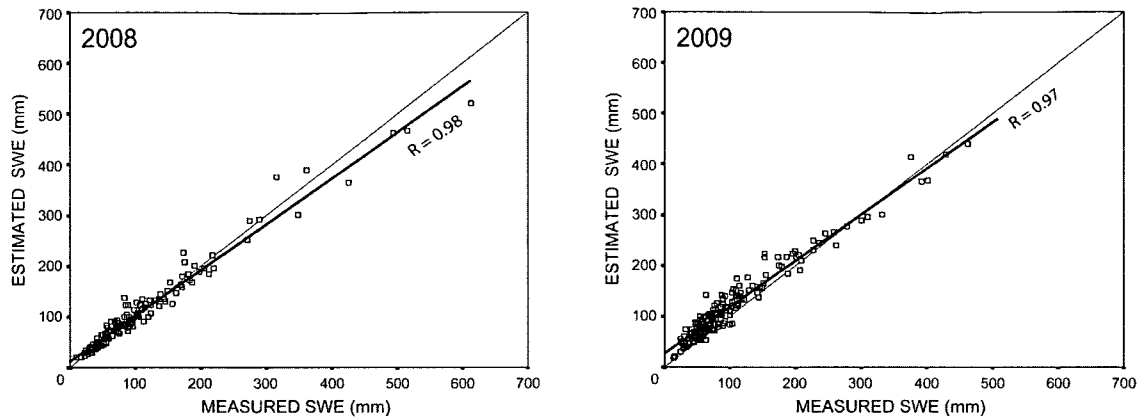


Figure 4.3. Comparison of estimated SWE (calculated using multi-season regional average 0.294 g/cm^3) and measured SWE (calculated from in-situ measurements) for each of the survey years

Figure 4.3 shows that there are very strong and significant ($p > 0.000$) relationships between estimated SWE and measured SWE. This shows that a multi-season overall mean density of 0.294 g/cm^3 produces SWE values which do not deviate very much from the measured SWE calculated at each site. More deviation and a greater uncertainty are noted in the higher measured SWE values of each season. These SWE are always recorded on steep slopes which have a higher bulk density in comparison to snow on flatter terrain. As a result, the measured SWE on slopes is underestimated when a regional density is used. Similarly, lower SWE values, associated with thin or newly deposited snow on upland plateaus or small lakes, have a lower density. In these areas, measured SWE is slightly overestimated using the overall average. The results shown in Figure 4.3 are important because they highlight the fact that tundra snow density is not all that variable when considered on a site-by-site basis between different terrain types and from season to season. As such, the regional average density of 0.294 g/cm^3 can be applied, and on most terrain types, snow depth could be used as a proxy for SWE.

4.2.2.2. Snow Depth

Snow depth was measured at each site as described in Section 3.3.4.2. Mean snow depth was calculated for each site by taking the average of the 30 probe measurements. Site means were then binned according to terrain categories, and a mean for each category was generated. The terrain category means for each year were then plotted along with one standard deviation (Figure 4.4, 4.5 and 4.6).

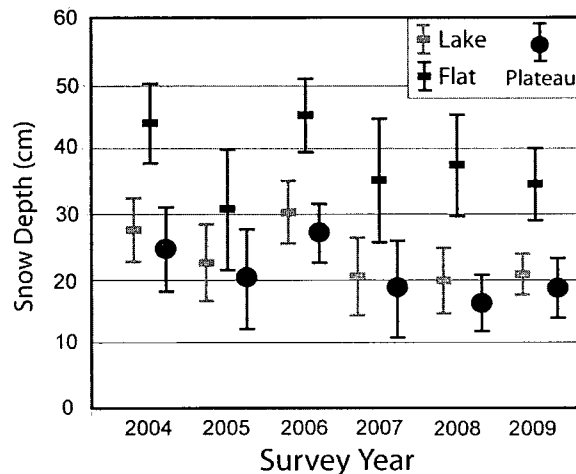


Figure 4.4. Snow depth on lakes and flat tundra during the 2004 to 2009 snow surveys. The heavy center line and circle represent the mean while the range of values is one standard deviation.

Snow depth on flat tundra, lakes and plateaus was found to be greatest in 2004 and 2006 and least in 2005 and 2009. Furthermore, the data show some interesting relationships among the different terrain categories. For example, lake sites appear to be the least variable in terms of standard deviation of snow depth and had consistently less snow compared to flat tundra. The least amount of snow depth was found on upland plateaus during each year due to the removal of snow by wind.

The standard deviation of snow depth on flat tundra and lakes appears to be greater in lower snow depth years of 2005, 2007, and 2008 than in 2004 and 2006. This was also apparent while conducting the snow surveys. The greater variability in low

snow years can be partly explained by the influence of emergent vegetation. Vegetation traps drifting snow and prevents movement (saltation) of snow grains until it is covered to within 5 cm of its stem tops at which point drifting resumes (Pomeroy, 1997). However, in higher snow years, the vegetation becomes completely buried, there is little interaction, and a much more uniform snow surface develops. On lakes, during lower snow depth years there is also more variability. This occurs because without sufficient snowfall, areas of bare ice remain uncovered and are perpetually wind-scoured throughout the season, and snow is continually being moved onto adjacent drifts. The presence of bare ice adjacent to snow drifts at a given site produces a greater range of snow depth and more variability in the mean. An exception to this was the 2009 data which show low snow depths but also relatively low standard deviation which may be due to little wind action preceding the 2009 survey.

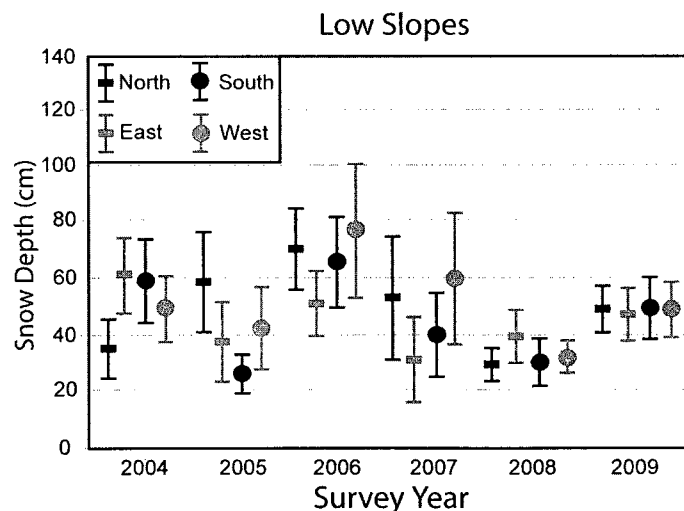


Figure 4.5. Snow depth on slopes of less than 7 degrees. *The heavy center line and circle represent the mean while the range of values is one standard deviation.*

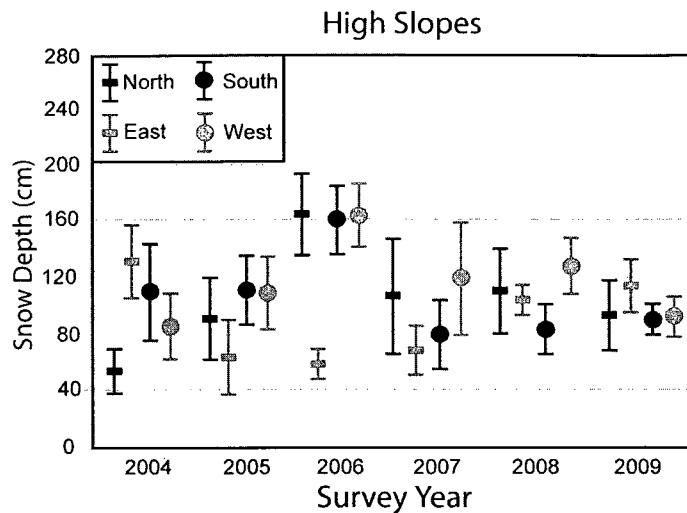


Figure 4.6. Snow depth on slopes of greater than 7 degrees. The heavy center line and circle represent the mean while the range of values is one standard deviation.

Snow on slopes was found to be deeper than on other terrain categories due to the increased accumulation in the lee of topographic features and in areas of dense vegetation often found on slopes. On windward slopes, snow depths were similar to or lower than on flat tundra and lakes. There was more snow accumulation on slopes steeper than 7 degrees, independent of aspect. However, there was no consistent relationship year to year in terms of which slope aspect had the most snow accumulation and highest snow depth. The accumulation of snow on different slope aspects is most likely a function of predominant wind direction during a given season, or during storm events.

Snow depths on slopes were much more variable both from year to year and when compared to other terrain types. Similar observations were made by Woo and Young (2004) in that deep snow drifts on slopes tend to be most variable and have larger standard deviations. This further shows how topography exerts a strong control on snow deposition patterns. Steeper slopes typically have more depth than shallower slopes due to rapid deposition of snow in the lee of a sharp or steep slope break. However, snow on shallow slopes does not accumulate in as short a distance behind the

slope break. This means that snow accumulation is controlled more by sub-surface micro-topography such as boulders and vegetation (Figure 4.7).

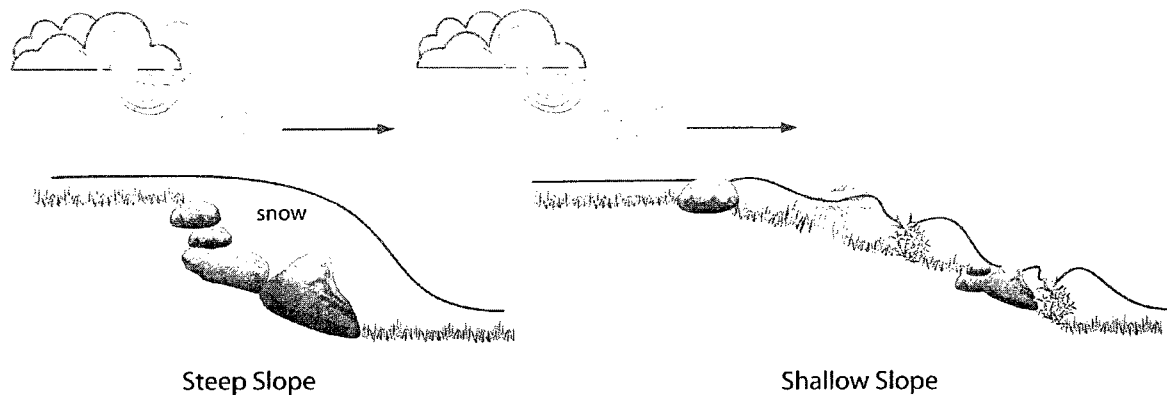


Figure 4.7. The general patterns of snow accumulation on steep and shallow slopes.

Due to the complex relationships between slope angle, aspect and surface roughness throughout a large basin, it is difficult to generalize and anticipate snow accumulation patterns. Therefore, some of the variability in slope snow depth is a product of the broad categories used in the classification. Fortunately, slope areas occupy a relatively small percentage of the total landscape. Employing a more complex classification to encompass all possible iterations of slope properties would be impossible to sample in all but very small study areas.

4.2.2.3. Snow Water Equivalent (SWE)

As outlined in Section 3.3.3, site SWE can be determined in two different ways. The first uses the average of the five ESC 30 measurements directly (weight of the snow cover divided by 30), while the second uses the mean of 5 densities calculated from the ESC snow core multiplied by the mean of the 30 depth probe measurements. A potential issue with the latter method is that uncertainty can accumulate when multiplying a site average depth ($n = 30$) and site average density ($n = 5$). The alternative would be the

first option which uses the average of the five SWE measured directly from the ESC 30. In theory, this might reduce potential uncertainty in the calculation of site SWE. However, using only five core measurements might not capture as much of the variability in snow depth at a given site as do the 30 probe measurements. A plot of SWE calculated using the two methods was generated for comparison. Data from the 2007 season were used as an example because 2007 had the highest number of sites visited (Figure 4.8).

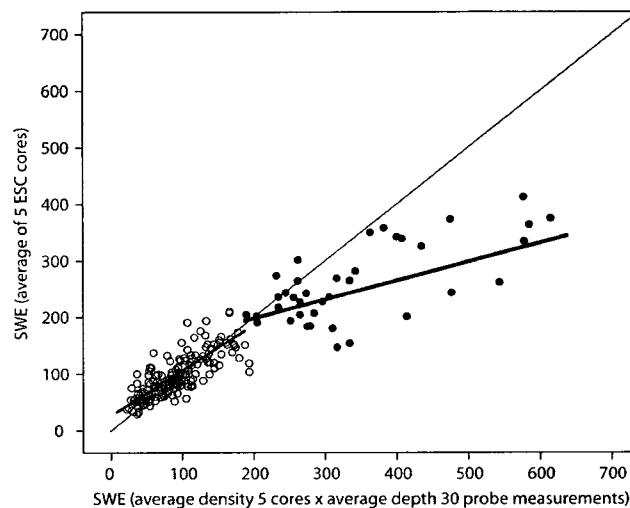


Figure 4.8. ESC 30 SWE compared to site average (depth x density) SWE

Figure 4.8 shows that below 150 mm the relationship between the two methods is quite good (close to 1:1) and fairly well correlated ($r = 0.73$, $p < 0.05$). As the depth of SWE increases (> 150 mm), the correlation remains strong ($r = 0.74$, $p < 0.05$); however, the difference between the two methods becomes greater (further from 1:1). Above 150 mm of SWE, the ESC core-only method begins to underestimate in comparison to the probe depth and mean density SWE method. This occurs because the ESC 30 core tube cannot collect measurements of snow depth beyond 130 cm. As a result, using the ESC 30 alone, site SWE cannot be measured when the snow depth exceeds 130 cm. At sites

with greater than 130 cm depth, cores are taken in areas with less than 130 cm depth and the measurements are assumed to be representative of snowpacks deeper than 130 cm. In some cases at deep snow sites, more than 130 cm can be sampled by stacking two or more core measurements vertically in an excavated snow pit. However, using this technique is difficult and often cores are not retained in the tubes. The snow probes, however, are extendable to beyond 4 m and provide a much better estimate of snow depth.

Using the mean of 30 snow probe measurements along with the five densities from the ESC cores produces a much higher sample size ($n = 35$) than using the cores alone ($n = 5$). Despite the good correlation between the two methods, it is assumed that using the higher n of the probe/density method would provide more statistically significant results and representative site SWE estimates. However, it is interesting to note that using only 5 ESC cores to record SWE on snow packs with less than 150 mm SWE would still provide fairly representative data.

For the rest of the data, site mean snow depths from the 30 probe measurements were combined with site mean snow density from the five ESC 30 cores to derive site SWE. The site mean SWE were then binned according to terrain categories, and a mean for each category was generated. The terrain category means for each year were then plotted along with one standard deviation (Figure 4.9, 4.10 and 4.11). Since SWE is calculated using both depth and density, the standard deviation in SWE is calculated using the following formula:

$$STDEV^{SWE} = (\text{sqrt} (STDEV^{DEPTH} / \text{Mean Depth})^2 + (STDEV^{DENSITY} / \text{Mean Density})^2$$

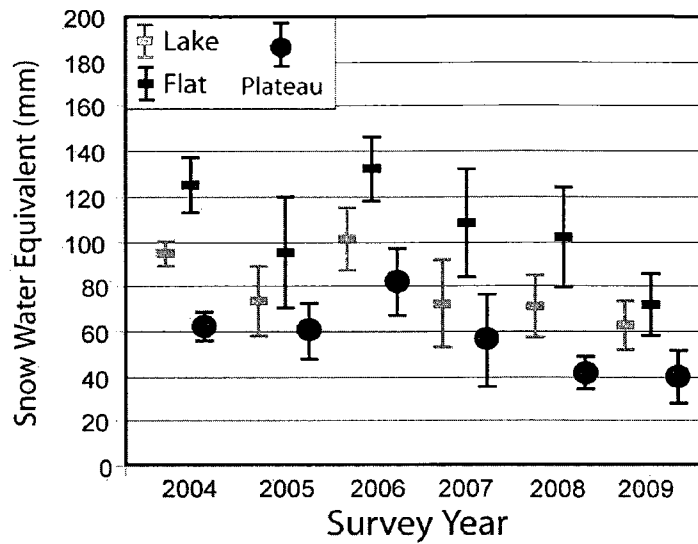


Figure 4.9. SWE on lakes and flat tundra during the 2004 to 2009 snow surveys. *The heavy center line and circle represent the mean while the range of values is one standard deviation.*

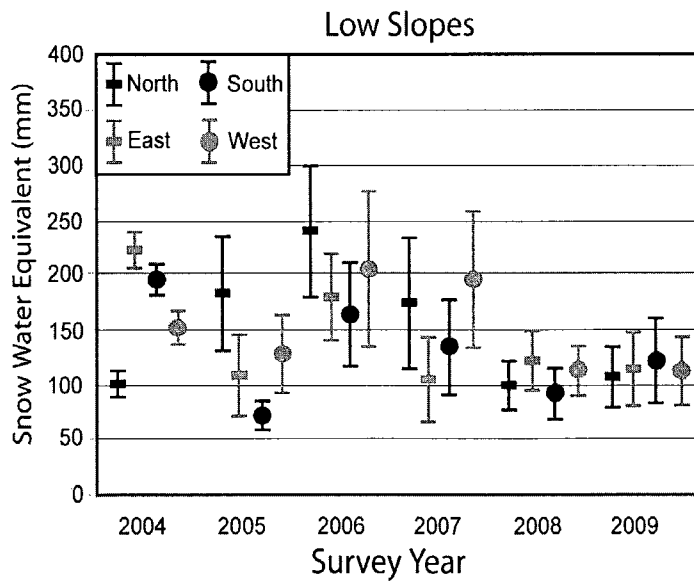


Figure 4.10. SWE on slopes of less than 7 degrees. *The heavy center line and circle represent the mean while the range of values is one standard deviation.*

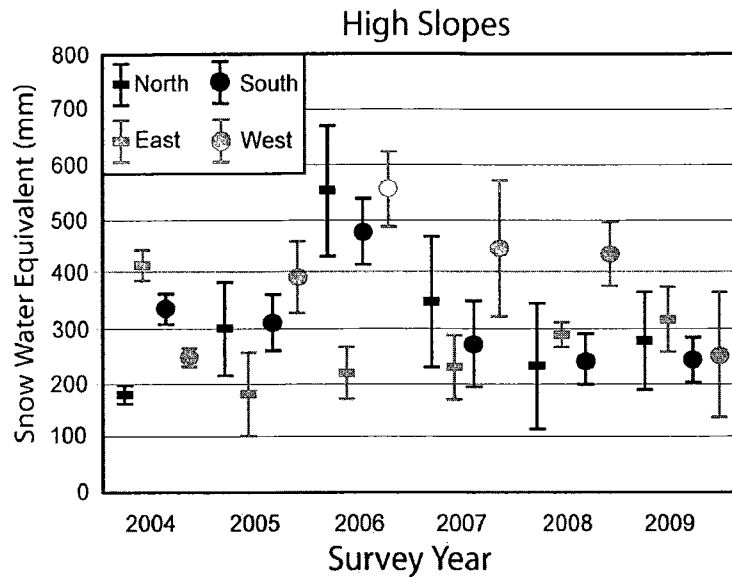


Figure 4.11. SWE on slopes of greater than 7 degrees. *The heavy center line and circle represent the mean while the range of values is one standard deviation.*

Not surprisingly, the patterns of SWE from year to year and among different terrain categories are very similar to those of snow depth. However, certain relationships are more prevalent due to differences or similarities in both density and depth between terrain types. For example, the difference in SWE between lakes and flat tundra becomes less pronounced than when considering snow depth alone. The lower depth of snow on lakes is dampened by the higher density of snow on lakes compared to flat tundra. Similarly, the difference between slopes and non slopes becomes more pronounced as slopes often have both higher depth as well as density.

The discussion of snow cover beyond this section will focus on SWE as it considers both depth and density, is a parameter of interest in many other disciplines, and is estimated through passive microwave remote sensing. The inter-annual patterns in SWE will be discussed in Section 4.2.3, while the variability in SWE will be further investigated in Section 4.3.

4.2.2.4. *Snow Stratigraphy*

Snow stratigraphy refers to the internal vertical structure or layering within a snowpack. This structure is important to consider when using passive microwave remote sensing as the total emission from a snow volume is influenced by many factors, including snow depth, SWE, snow density, liquid water content and snow grain size (Foster et al., 1980). The variability in snowpack structure is often considered as a source of disagreement between surface measurements and passive microwave SWE data (Derksen et al., 2005). Furthermore, end of winter tundra snowpacks can be dominated by large grained depth hoar which can greatly influence passive microwave estimates of SWE (Section 2.4.2.1.1). Thus, in the context of this project, it is necessary to have an understanding of tundra snowpack stratigraphy throughout different terrain categories.

The properties of tundra snow are described in a general snow cover classification by Sturm et al. (1995). Data used to test the classification were derived primarily from northern Alaska. Tundra snowpack stratigraphy is described as being thin, cold, wind-blown snow with a basal layer of depth hoar overlain by multiple wind slabs, and a depth range of 10 – 75 cm (Figure 4.12).

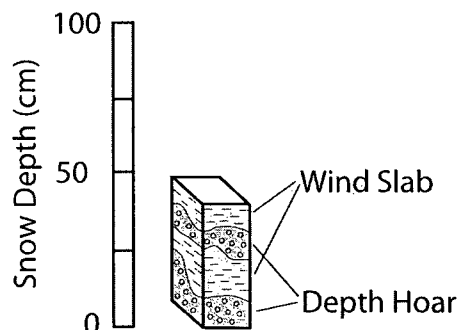


Figure 4.12. Basic tundra snow stratigraphic and textural attributes (adapted from Sturm et al., 1995).

The depth ranges observed in the field (Figures 4.4, 4.5 and 4.6) do not exceed the maximum of 75 cm except on slopes where snow deposition has been enhanced by wind-redistribution. Furthermore, the mean snow depth (± 1 STDEV) did not exceed 75 cm on flat tundra in any of the years surveyed. The general snow stratigraphy outlined in Figure 4.12 is a good general approximation of the snow pack structure observed in the field.

At all sites during each year (with some exceptions), there was a well developed wind slab layer at the top of the pack. The layering below the surface consisted of older, buried wind slabs and intermediate layers in various stages of snow grain metamorphosis. The presence of old wind slabs within the pack acts to impede vapor transport and produce depth hoar like grain growth above the base of the snow pack. These layers, while not traditional depth hoar, have been thought of as a form of suspended depth hoar. The traditional basal depth hoar layer usually occupied a relatively small fraction of the snow pack. This is because depth hoar forms primarily from early season snow deposited between vegetation outcrops or tussocks (Sturm and Benson, 1997).

Subsequent snow and wind events form slabs on top of this early season snow. This effectively caps the development of depth hoar at the bottom of the pack which limits grain growth to the 3 – 6 mm range (Sturm, personal communication). Wind events with concurrent snowfall tend to produce a network of softer snow dunes while wind events without subsequent snowfall produce the dense surface slab layers. Both layers will eventually undergo kinetic growth throughout the season and become somewhat similar to depth hoar. However, the layers which were formerly wind slabs are denser and more cohesive than depth hoar found at the base of the pack. These transformed layers, which were originally wind slabs and are unique to tundra snow, have been termed indurated hoar (Derksen et al., 2009).

Tundra snow stratigraphy exhibits a large degree of site to site heterogeneity due to the complexity in snow deposition, redistribution, and underlying macro and micro topography. Nonetheless, throughout the years, there appear to be some general snow pack properties common to the different terrain types (Figure 4.13).

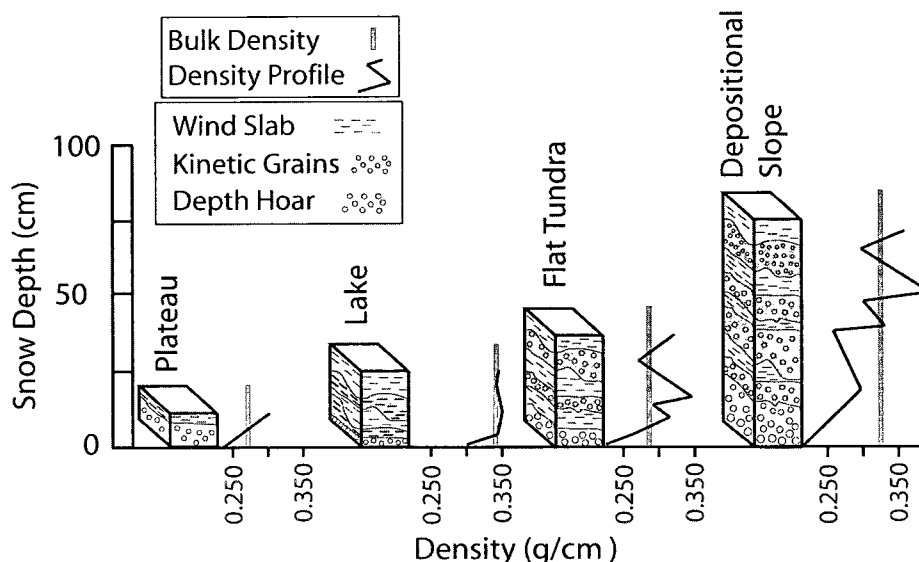


Figure 4.13. Generalized snowpack stratigraphy on different terrain types.

Upland plateaus had the lowest snow depth and also the simplest snow stratigraphy. The vertical structure consisted of low density depth hoar crystals (grain size 2 – 3 mm) overlain by a relatively thin wind slab (grain size 0.5 mm). The depth hoar layer developed in areas sheltered from the wind. This was typically in between micro-topographic features or amongst ground cover present at the site. On vegetated plateaus, the hoar crystals developed in the shelter of grasses, hummocky lichens or dwarf birch shrubs where soil moisture is likely elevated. On rocky plateaus, the depth hoar developed more prominently where sheltered in the lee of boulders or rock outcrops. However, the perpetual removal of snow from upland plateaus clearly limited the development of more complex stratigraphy beyond the sheltered areas.

The snow stratigraphy on lakes was clearly different from that on land. On lakes, there was a much lower percentage of depth hoar, and there was frequently no evidence of any hoar crystal growth. As a result, the density profile of snow on lakes was more uniform, and the density throughout the pack was very similar to the bulk density. Furthermore, frozen lakes are typically more exposed to wind from all directions and have a much lower surface roughness than that of land. As such, lakes typically had a greater proportion of wind slab layers (grain size 0.5 mm). At some sites, there was evidence of kinetic crystal growth in layers between wind slabs. These indurated layers had grain sizes larger than typical wind slabs (from 0.5 to 1 mm). The stratigraphy of lakes was essentially alternating layers of wind slabs with little difference in density from the top to the bottom of the snow pack.

At flat tundra sites, the snow was typically deeper than on plateaus and lakes and the stratigraphy was very similar to that described by Sturm et al. (1995). The nature of the layering in the flat snow packs were determined in part by the type of ground cover present below the snow. If the ground cover was more irregular in terms of hummocks, rocks, or vegetation, then there would be more depth hoar development in amongst these features (grain size 2 – 4 mm). The highest proportion of depth hoar and largest grain sizes were found at sites which had the tallest vegetation, usually dwarf birch shrubs (grain size up to 8 mm). In all cases, the snowpack above the depth hoar consisted of alternating layers of indurated less densely packed kinetic grains (grain size 0.5 to 2 mm) and denser wind slabs (grain size 0.5 mm). On depositional slopes, the snow depth was greatest, and the snowpack had a higher number of alternating layers of kinetic grains and wind slabs. However, the proportion of depth hoar on slopes was still largely driven by the type and height of ground cover.

Despite some differences from site to site and from year to year, the generalization of the characteristics and differences between terrain categories outlined in Figure 4.13 provides a useful summary of tundra snow stratigraphy. These general properties could certainly be extrapolated over large study areas. Furthermore, it is clear that both terrain and ground cover play important roles in the development of snow stratigraphy at each individual site. Moreover, a general classification of these attributes is necessary for application to regional scale models and remote sensing techniques.

4.2.3. Inter-annual Patterns in SWE

Flat tundra is the most spatially expansive and easily defined terrain category throughout the study area. As such, examining the relationship of SWE between flat tundra and other terrain categories would be useful in order to identify any differences or consistencies in the inter-annual tundra patterns of snow distribution on terrain categories. For example, if the ratios of SWE between terrain categories are consistent from year to year, then it would become much easier to extrapolate snow cover patterns over larger areas and into the future. Similarly, data acquired from future in-situ surveys, meteorological stations, or satellite sources could provide an estimate of SWE on flat tundra, and if consistent ratios exist, then SWE could be extrapolated to other terrain categories through the region.

Section 4.2 showed how the depth of SWE observed on the different terrain categories can be quite different from year to year. Nonetheless, there seem to be some general consistencies in the difference in SWE between certain terrain categories. Hence, at first glance, it appears that certain inter-annual similarities in the ratio of SWE between terrain categories do exist. To display this more clearly, the ratio of SWE between the flat tundra categories and SWE on all other terrain categories was plotted in Table 4.3 using the following formula:

$$\text{Ratio} = \text{SWE other terrain unit} / \text{SWE flat tundra}$$

Therefore, ratio values below 1 indicate that, for the given year, SWE in that particular terrain category is less than on flat tundra. Ratio values above 1 indicate that SWE in that terrain category is greater than on flat tundra.

Table 4.3. The ratio of SWE on flat tundra to SWE on all other terrain categories

	2004	2005	2006	2007	2008	2009
Plateau	0.52	0.61	0.60	0.52	0.42	0.52
Flat	1.00	1.00	1.00	1.00	1.00	1.00
Lake	0.79	0.79	0.74	0.65	0.67	0.81
SLOPES						
North - Low	0.82	1.92	1.81	1.40	1.00	1.41
North - High	1.51	3.25	4.11	3.80	2.22	3.74
East - Low	1.85	1.13	1.29	1.04	1.20	1.50
East - High	3.36	1.94	1.61	2.06	2.92	4.04
South - Low	1.61	0.80	1.21	1.22	0.90	1.60
South - High	2.74	3.32	3.44	3.32	2.41	3.31
West - Low	1.24	1.36	1.48	1.58	1.08	1.51
West - High	2.09	4.13	4.04	4.24	4.33	3.30

Table 4.3 shows that despite differences in parameters not measured or compared (annual snowfall and seasonal weather patterns) and in the measured depth of SWE, there are consistent ratios in SWE on flat tundra to other terrain categories. For example, the ratio of SWE on flats to SWE on lakes and upland plateaus was found to be fairly similar among the survey years. SWE on upland plateaus was consistently 39 to 58% less than on flat tundra. This makes sense as plateaus are exposed every year to wind from any direction. As such, they are perennially blown free of snow compared to flat tundra.

SWE on lakes was consistently 19 to 35% less than on flat tundra. Similar results were observed by Sturm and Liston (2003). They found 18%, 25% and 38% less SWE on lakes than on land during three years of observation on lakes of the Arctic Coastal Plain and describe three main factors which contribute to this trend. The first is the loss of early season precipitating snow into unfrozen lakes, second is the accumulation of snow drifts along lake edges, and third, the depletion of snow-depth due to non-

equilibrium blowing-snow fluxes. All of these factors are applicable to the Daring-Exeter-Yamba Basin as it is dominated by many lakes ranging from small ponds to very large lakes (up to 300 km²). The presence of larger lakes, however, diminishes the amount of snow trapped in drifts as there are fewer edges of lakes compared to a basin with many smaller water bodies. Furthermore, larger lakes diminish the non-equilibrium blowing snow conditions and, as such, were found to have deeper and more consistent snow cover than smaller ponds, which are more prone to wind erosion (see Section 4.4.3).

The ratios of SWE on flat tundra to slope areas are less consistent as a result of presumed differences in seasonal wind speed and direction during and following snowfall events. On low slopes, there are between 0.80 and 1.85 times as much snow as on flats. On the dominant depositional slope features (the highest SWE), there are consistently 3 to 4 times more SWE than on flat tundra, yet the aspect associated with the highest depth of SWE relative to flat tundra does vary from year to year. This is most likely a function of differences in wind speed, direction, and snowfall throughout the season. West and south slopes, however, contain consistently more SWE than north and east slopes.

Seasonal wind patterns have a well recognized influence on snow deposition patterns. Wind-redistribution events involve 1) erosion of the snow surface, 2) horizontal transport of snow, 3) snow deposition into drifts, and 4) in-transit snow sublimation (Bowling et al., 2004). Many researchers have investigated and modeled the complex relationships between the tundra landscape, snowfall, and wind velocity (Essery and Pomeroy, 2004, Liston, 2004, Liston and Sturm, 2002, Pomeroy et al., 1997). These models are quite useful for explaining and estimating snow accumulation patterns and loss through sublimation throughout a winter season and would help explain the patterns of SWE on slopes. Unfortunately there is not a continuous record of wind data available

from the meteorological tower at Daring Lake. The tower is solar powered and is not able to record data continuously through the winter months.

If a record of winter meteorological data did exist, there are two assumptions which could be tested to quantify the relationship between seasonal wind patterns and SWE. First, the years with greater average wind speeds should see a higher ratio of snow located in drift features, and second, the dominant wind direction of redistribution events should have an inverse aspect to slopes with the deepest snow drifts. The verification of these assumptions would allow for the improved understanding of the slope ratios in Table 4.3.

4.3. Variability in Snow Cover

4.3.1. Introduction

In many research fields, variability, which characterizes the degree of heterogeneity within a given area, is often more useful to consider than parameters of central tendency alone. This is certainly true in the context of this research project. Section 4.2 showed the general trends in snow cover data among different terrain categories both within and between different years. Furthermore, plotting these data provided a good starting point for enhancing our understanding. However, visually comparing the mean and standard deviation does not quantify variability which would be needed in order to properly extrapolate the data over larger areas.

Of the three parameters outlined in Section 4.2, SWE is of the most interest as it incorporates both depth and density and is the primary parameter estimated by passive microwave remote sensing. Variability in SWE within coarse resolution grid cells is an often overlooked point of discussion. However, it is necessary to examine this in order to properly develop a dataset for algorithm and model development, testing, and validation. As such, the following three aspects of the spatial variability of SWE in the study area need to be determined:

- (a) Variability among different survey years at the study area scale
- (b) Variability within survey years between different terrain categories
- (c) Variability within different terrain categories between sites

Quantifying variability among different years at the study area scale will show how SWE varies without considering differences in terrain. If the variability in SWE is high at the study area scale, then it justifies using a terrain based classification and spatially weighted mean to describe the sub-grid distribution of SWE. Examining the variability within the survey years in different categories will demonstrate how SWE varies with terrain. This will determine the effectiveness of the classification to separate unique snow and terrain categories. Determining the variability within categories will define the heterogeneity in SWE within supposedly uniform terrain categories. This will also test the effectiveness of the classification and determine if the category structure is sufficient. Moreover, the use of a weighted mean SWE will permit the quantitative comparison of year to year snow cover patterns.

4.3.2. Variability between Survey Years

Assessing the variability among survey years is useful to determine whether or not pre-melt tundra SWE is significantly different from year to year. The mean site SWE data from each year were used together, independent of terrain category to create the dataset. The normality and skewness of SWE in each year were assessed through the plotting of frequency histograms (Figure 4.14).

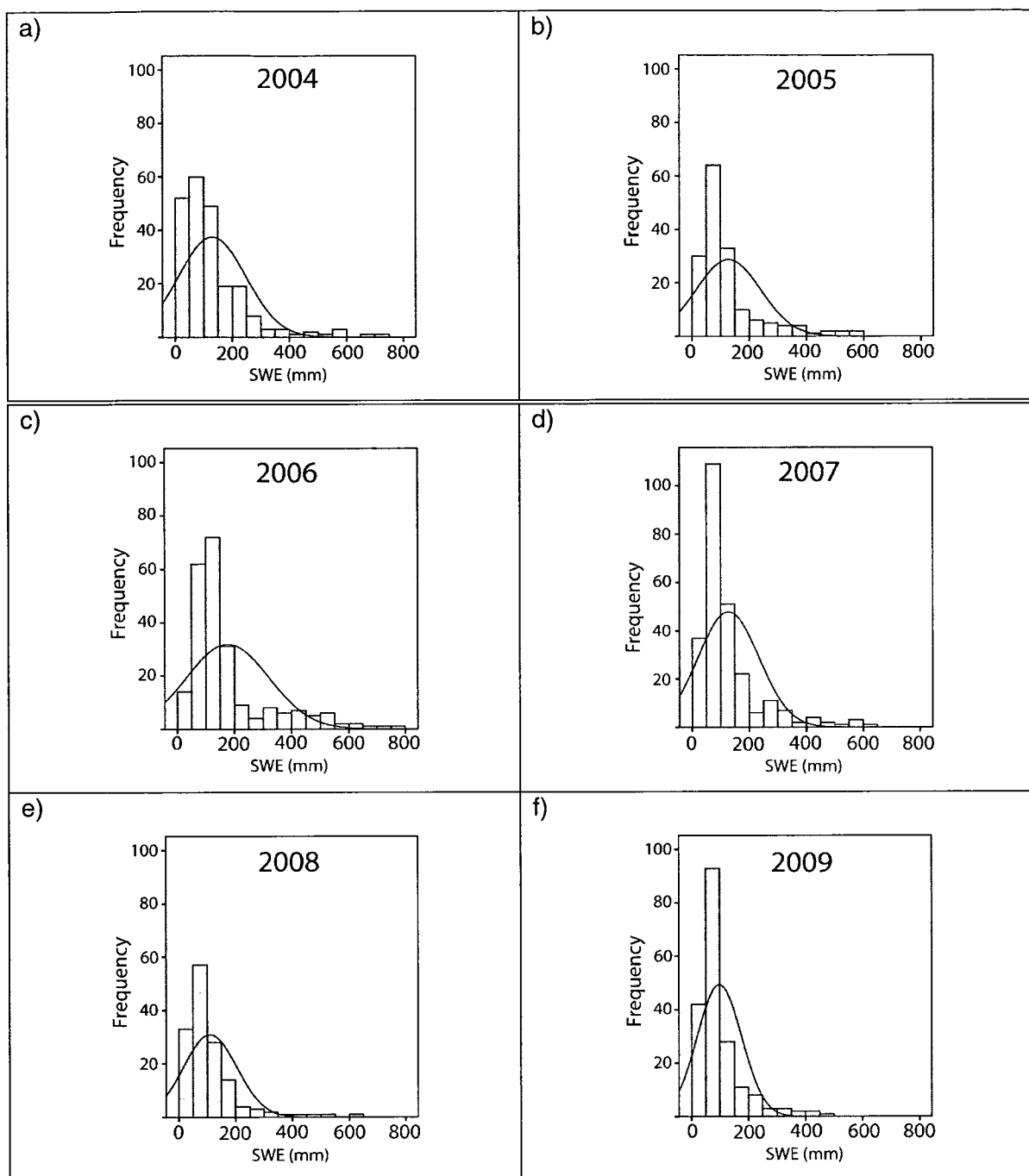


Figure 4.14. Frequency histograms of SWE for each of the survey years

Figure 4.14 shows that the SWE data are uni-modal and skewed in a positive direction towards higher values. This occurs because the higher SWE values, which are a product of deposition on slopes, are not as abundant in the study area. The extent of the skewness in the distributions indicates that the mean SWE for each year may not be representative. This is because a simple arithmetic mean gives too much weight to values which are not that frequent. This presents a problem in assessing variability with measures of standard deviation and coefficient of variation as they assume a normal distribution (Table 4.4).

Table 4.4. Descriptive statistics of yearly SWE (mm) data

Year	n	Min	Max	Mean	Std. Deviation	Coefficient of Variation (CV)
2009	194	12.3	462.7	97.8	77.9	0.79
2008	146	11.0	614.5	110.4	94.3	0.85
2007	256	24.0	934.0	131.0	117.9	0.90
2006	238	37.5	1130.2	182.3	163.5	0.89
2005	169	19.4	567.5	129.2	112.7	0.87
2004	242	6.3	889.2	151.2	152.1	1.00
Valid n (listwise)	146					

The standard deviation and the coefficient of variation (CV) of SWE for each of the years are inflated due to the positive skew in the distributions. The high CV in each year shows that the standard deviation in SWE almost equals the mean when terrain categories are not considered. The skewness of the SWE data makes the mean not necessarily representative and inflates the variability. Hence some type of classification is required to better define sub-grid SWE variability for comparison with modeled or satellite data.

Nonetheless, the distributions in Figure 4.14 show that there seem to be years of relatively higher and lower mean SWE. However, comparing the frequency of a given SWE is somewhat misleading. As described in Section 3.3.4.3, not all survey locations were spatially co-incident from year-to-year. Furthermore, the total number of sites

visited (n) each year was not the same. A direct comparison could only be made if all data were collected from automated stations or recorded at fixed snow stakes which remain in the same location from year to year. The data collected in this study are randomly sampled within each of the terrain category strata. The sampling involved collecting random depth and density measurements within representative terrain categories. The lowest number of sites visited was 146, in 2008, which essentially represents 4380 random depth (probe) and 730 random density (ESC 30 core) measurements at sites within the 11 terrain categories. The SWE shown in Figure 4.14 are derived using all of these measurements in each year. As such, it may be argued that the number of samples is sufficient for a statistical comparison without spatially coincident sampling locations. Moreover, even if site location were consistent from year to year it would be impossible to replicate the placement of the 30 probe and 5 core measurements. Due to differences in micro-topography and in seasonal drifting patterns, quite a bit of variability should be expected within sites let alone between sites and from year to year. Therefore, to examine the variability of SWE, the data need to be broken down into different terrain categories within each of the years

4.3.3. Variability Within Survey Years Between Terrain Categories

Variability in SWE across the tundra is a function of the interaction of wind-redistributed snow with the terrain and landscape. In theory, the amount of variability in each terrain category would depend on the extent of this interaction. Figure 4.14 shows that there can be differences in the distribution of SWE from year to year. Thus, there are expected to be different weather patterns (snowfall and wind) between different years. However, landscape (vegetation) and terrain (topographic) properties do not change much on an annual or even decadal scale. As such, variability in SWE should be similar in a given terrain category from year to year. The lowest variability should be seen in categories whose patterns of seasonal snow accumulation are least affected by

wind re-distributed snow. Variability should be greater in categories with terrain or landscape features which would interact with blowing snow and highest in terrain categories which preferentially accumulate snow under certain wind speed, wind direction, and snowfall conditions. Essentially, the terrain category with the least number of factors which interact with blowing snow should have the lowest variability, and those with the greatest number of factors should have the highest (Table 4.5).

Table 4.5. Tundra terrain categories and the factors that control snow cover distribution


Terrain Category	Factors that control the interaction with blowing snow	Expected Variability
Lake	<ul style="list-style-type: none"> - Lake Size and Orientation - Surrounding Topography - Fetch 	<p>LEAST</p>  <p>MOST</p>
Flat Tundra	<ul style="list-style-type: none"> - Surrounding Topography - Fetch - Surface cover: vegetation, boulders - Micro topography 	
Upland Plateaus	<ul style="list-style-type: none"> - Surrounding Topography - Fetch - Surface cover: vegetation, boulders - Micro topography - Size of plateau 	
Shallow Slopes	<ul style="list-style-type: none"> - Surrounding Topography - Fetch - Surface cover: vegetation, boulders - Micro topography - Slope Length - Slope angle - Slope aspect 	
Steep Slopes	<ul style="list-style-type: none"> - Surrounding Topography - Fetch - Surface cover: vegetation, boulders - Micro topography - Slope Length - Slope angle - Slope aspect - Nature of Slope break 	

Table 4.6 shows that lakes should have the least variability in SWE as they are relatively simple landscapes. Flat tundra is also fairly simple but has different surface covers which would influence snow accumulation. Plateaus are similar to flat tundra but are more exposed to wind. Slope areas are expected to produce the most variability in

SWE as there are more potential factors to interact with blowing snow. In order to verify if the assumptions of Table 4.6 are correct, two questions need to be addressed. They are 1) does variability in SWE change based on the number of factors which interact with blowing snow, and 2) is the variability in SWE among different terrain categories similar from year to year because the terrain does not change?

Variability in SWE can be most easily described using standard deviation, which is a measure of the spread of data about the mean in the same units as the original data. Standard deviation was used in Section 4.2.2 to visually show the general differences in variability among different terrain categories. However, because standard deviation is a measure of the spread about the mean, it is difficult to compare variability from one year to the next independent of differences in the mean. The amount of SWE in any terrain category is determined primarily by the amount of snowfall and the degree of wind redistribution throughout a given season. In order to isolate variability from the differences in the mean SWE, and to provide a normalized measure of dispersion, the coefficient of variation (CV) is used. The CV is expressed as the ratio of the standard deviation to the mean. As such, the CV allows for a unitless comparison of the variability in SWE between similar terrain categories throughout different years. A lower CV indicates that there is less variability about the mean. If the CV is multiplied by 100, it can be thought of as a percentage of variability in a given terrain category.

The CV of SWE and snow depth are often used in snow cover models in order to describe variability within large scale grid cells. Liston (2004) describes how different snow distribution categories, defined based on seasonal air temperature, wind speed and topographic variability, can have inter-annually similar CV values. Table 4.6 shows how variability should differ based on a number of factors. Hence, it can be assumed that the variability (CV) should not change from year to year in a terrain category because the factors that influence the pattern of snow accumulation and distribution are

generally the same (Sturm et al. 1995, Liston, 1999). Based on these assumptions, a global sub-grid SWE depth classification was developed by Liston (2005) (Figure 4.15).

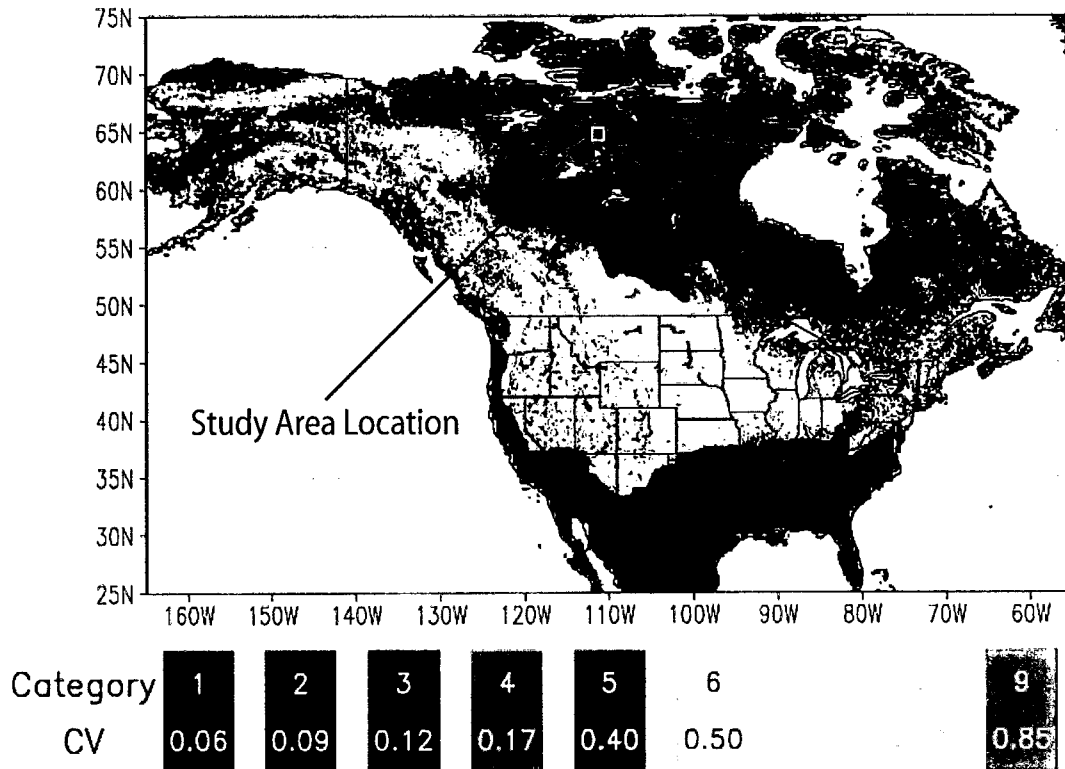


Figure 4.15. The North American portion of the global sub-grid SWE depth classification by Liston 2005

Figure 4.15 shows that the study area is located in Category 5, the arctic tundra, which has a mean CV of 0.40. In order to compare this value to the SWE data from the study area and provide a measure of variability, the CV in SWE was calculated for each site for each of the survey years. To summarize the data, the mean and STDEV of the CV were also calculated for each terrain category during each year. The mean and STDEV were also ranked from highest to lowest within each year to facilitate the comparison between terrain categories within each year (Table 4.6).

Table 4.6. The coefficient of variation of SWE for each terrain category in each survey year

	2004				2005				2006				2007				2008				2009				ALL			
	mean CV	rnk	STDEV CV	rnk	mean CV	rnk	STDEV CV	rnk	mean CV	rnk	STDEV CV	rnk	mean CV	rnk	STDEV CV	rnk	mean CV	rnk	STDEV CV	rnk	mean CV	rnk	STDEV CV	rnk	mean CV	rnk	STDEV CV	rnk
Lakes	0.37	10	0.14	8	0.35	9	0.11	9	0.29	10	0.09	7	0.43	9	0.20	3	0.39	7	0.15	4	0.30	10	0.13	7	0.36	11	0.05	10
Flat	0.37	10	0.14	8	0.47	5	0.18	2	0.33	8	0.07	8	0.35	11	0.10	10	0.35	10	0.10	10	0.35	7	0.10	9	0.37	10	0.05	10
Plateau	0.71	1	0.29	1	0.61	1	0.18	2	0.46	1	0.14	1	0.64	1	0.16	7	0.62	1	0.14	5	0.56	1	0.15	2	0.60	1	0.08	6
Slopes < 8 degrees (LOW)																												
North	0.62	5	0.21	4	0.37	8	0.14	8	0.35	5	0.13	4	0.64	1	0.16	7	0.45	5	0.17	2	0.49	2	0.14	3	0.49	2	0.12	4
East	0.58	8	0.19	6	0.47	5	0.15	7	0.38	4	0.11	5	0.56	3	0.25	1	0.43	6	0.19	1	0.45	4	0.16	1	0.48	3	0.08	6
West	0.59	6	0.14	8	0.48	4	0.18	2	0.33	6	0.07	8	0.48	4	0.20	3	0.47	3	0.15	4	0.49	2	0.14	3	0.47	5	0.08	6
South	0.59	6	0.23	3	0.50	3	0.18	2	0.46	1	0.14	1	0.44	7	0.09	11	0.47	3	0.16	3	0.40	6	0.14	3	0.48	3	0.06	9
Slopes > 8 degrees (HIGH)																												
North	0.70	3	0.21	5	0.35	9	0.07	10	0.27	11	0.07	8	0.44	7	0.21	2	0.37	9	0.12	6	0.45	4	0.07	10	0.43	8	0.15	2
East	0.50	9	0.23	3	0.59	2	0.21	1	0.34	8	0.10	6	0.47	5	0.17	5	0.49	2	0.12	6	0.32	9	0.06	11	0.45	6	0.10	5
West	0.64	4	0.18	7	0.33	11	0.17	6	0.31	9	0.05	11	0.41	10	0.12	9	0.35	10	0.11	7	0.35	7	0.12	8	0.40	9	0.13	3
South	0.71	1	0.24	2	0.41	7	0.08	11	0.46	1	0.14	1	0.47	5	0.17	5	0.38	8	0.11	7	0.20	11	0.14	3	0.44	7	0.17	1

Table 4.6 shows that there is a range in the mean CV for different terrain categories both within and between different years. According to Table 4.5, the terrain categories with fewer factors influencing snow distribution should have a consistently lower CV. Lakes and flat tundra, which have the least number of influencing factors, had consistently less variability than other terrain categories. This is evident when looking at the rank (rnk) of mean CV. Out of 11 categories, the lakes are shown to be consistently ranked as 7th to 10th least variable from year to year and 11th least variable in the mean of ALL CV. Flat tundra had a very similar CV to that of lakes in all years, and these surfaces were only separated by 0.01 in the mean of ALL CV.

Plateaus were expected to have the next lowest CV and especially lower than for slopes. However, plateaus had the highest CV of all terrain categories in each of the years. This is most likely due to the exposure to wind events from all directions which would exaggerate the effect of surface roughness and micro-topography on snow accumulation. The low SWE, or no SWE measured from wind scoured areas also has the effect of inflating the CV. Small changes in low SWE values have a greater influence on the CV than do similar changes at greater SWE. Nonetheless, the variability on plateaus was high due to the contrast between wind scoured areas and adjacent small drifts in the lee of rocks or vegetation (Figure 4.16).



Figure 4.16. Upland plateau

Low slopes had a higher CV than flats or lakes in almost all cases. This follows what was estimated in Table 4.5 based on the effect of blowing snow events on slope SWE. However, contrary to Table 4.5, steeper slopes often had a lower CV than on shallower slopes or on some flats or lakes. Despite the higher number of factors on steep slopes, especially the pronounced effect of steep slope angles on snow accumulation, it would seem as though SWE on steep slopes is more uniform than expected. Variability on steep slopes is lower as they are often either consistently depositional with deep drifts or consistently wind scoured. Furthermore, in the lee of steep slopes, it does not take long before drifts accumulate enough depth to cover and negate the effect of the underlying ground cover.

It is possible, however, that the lower CV on steep slopes may have more to do with the low number of sites visited (Table 3.3). Moreover, there is also possible bias in SWE sampling on steep slopes because on deep drifts it is difficult to establish the precise start and end of the slope under the snow. As such, high slope areas are identified and sampled based on the pronounced deposition of snow (deep drifts) and

not on the underlying topography. This makes it difficult to establish a consistent sampling scheme from slope to slope and, in some cases can lead inadvertently towards a bias in measuring only areas of high SWE.

The ALL column in Table 4.6 shows the mean and STDEV in CV of all of the years surveyed. The relatively low STDEV of lakes and flats means that the CV was quite consistent from year to year and ranked 11th and 10th most variable respectively. Similarly, the mean CV of plateaus was always higher than all other terrain categories and ranked 1st as most variable in all years. The mean CV of low slopes was quite similar from year to year but greater and with a higher STDEV than flats and lakes. Steep slopes had similar mean CV values to low slopes but had the highest STDEV. Table 4.3 demonstrated that the ratio of SWE on high slopes changed from year to year presumably based on different seasonal wind patterns. As a result, the large STDEV in ALL high slope CV from year to year was not surprising.

Table 4.6 is very useful in answering the two questions posed at the beginning of this section. The ranking of variability in SWE in different terrain categories, described in Table 4.5 is, with the exception of some steep slopes, more or less correct. Furthermore, the variability (CV) in each terrain category is quite consistent and ranked in similar order from year to year. This shows that despite the difference in mean SWE from year to year, variability (CV) in a given terrain category is quite similar.

A final step is to derive a mean CV for the study area as a whole for comparison with the CV of 0.40 from Liston (2005) shown in Figure 4.15. To derive a study area CV, the mean CV for each terrain category from the ALL column of Table 4.6 was used. A spatially weighted mean CV was calculated, as opposed to an arithmetic mean, because it takes into consideration the proportion of each terrain category in the study area (Table 4.7).

Table 4.7. A weighted mean CV of all terrain categories and years surveyed

	ALL mean CV	Percent Study Area	Weighted Mean CV
Lakes	0.36	36.7	0.13
Flat	0.37	25.6	0.09
Plateau	0.60	2	0.01
Slopes < 8 degrees (LOW)			
North	0.49	6	0.03
East	0.48	4.6	0.02
West	0.47	7.4	0.04
South	0.48	6.3	0.03
Slopes > 8 degrees (HIGH)			
North	0.43	3.1	0.01
East	0.45	2.8	0.01
West	0.40	2.5	0.01
South	0.44	3.3	0.01
			0.40

Table 4.7 shows that the overall weighted mean CV for the study area is 0.40. This CV is exactly the same as the CV proposed for the arctic tundra by Liston 2005. The remarkable agreement of the six years of data collected for this study with previously published data is quite encouraging. However, it is important to remember that within the study area, there have been large differences in CV among terrain categories and from year to year. Nonetheless, the derivation of a study area weighted mean is very applicable and useful for studies done at the scale of satellite passive microwave data.

4.4. Snow Cover Classification

4.4.1. Introduction

The terrain based snow cover classification was developed as a first order stratification of the study area to aid in field sampling and in providing a context for defining sub-grid snow cover distribution. The different classes were developed based on expected differences in snow distribution. As shown in Sections 4.2 and 4.3, breaking down the snow cover according to terrain does seem to make sense. There do appear to be differences in the depth of SWE and in variability among the different terrain categories chosen. However, to this point little has been done to statistically test the rigorousness of the classification scheme. The following section will evaluate the

differences and similarities among the terrain based categories, determine an optimum number of categories, and investigate whether or not the inclusion of landcover information would improve the classification.

4.4.2. Terrain Classification

The terrain classification was conceived and generated prior to data collection in the field. Hence, the 11 classes were chosen based on the expected patterns of snow accumulation in the study area. As discussed in Section 4.3.2, the study area needs to be broken down into different categories in order to better define the spatial distribution of both depth of and variability in SWE. However, up to this point, there has been no analysis to show how many categories are needed, or more specifically, whether the 11 pre-selected categories are appropriate to best define sub-grid SWE. In order to determine the most efficient number of terrain categories in the classification, both difference of means and equality of variance tests will be used.

4.4.2.1. *Difference of Means*

The difference among terrain category mean SWE was tested. The ANOVA F for each year was significant as was the Levene's statistic. This indicates that during each of the years there are differences among the categories, and there are unequal variances between the categories. Furthermore, from Table 3.3, the sample numbers in each terrain category are not the same. As such, a GH post-hoc test was used to indicate where the category SWE is significantly different from each other. The GH test produced a pairwise comparison of the category mean SWE and determined the magnitude and direction of any difference between the means. Because of the conservative nature of the GH test, significant differences at 0.05 as well as 0.10 are shown (Table 4.8).

Table 4.8. Difference of mean SWE (mm) between terrain categories within each survey year, a) 2004, b) 2005, c) 2006, d) 2007, e) 2008, and f) 2009

a)


Mean Difference SWE (mm) 2004				SLOPES							
	Flat	Lake	Plateau	N-Low	N-High	E-Low	E-High	S-Low	S-High	W-Low	W-High
Flat		64.6	106.0	60.5	-30.5	-61.8	-212.7	-52.5	-167.6	19.2	-101.7
Lake			41.4	-4.1	-95.1	-126.4	-277.3	-117.1	-232.2	-45.4	-166.3
Plateau				-45.5	-136.5	-167.8	-318.7	-158.5	-273.6	-86.8	-207.7
North Low					-91.0	-122.3	-273.2	-113.0	-228.1	-41.3	-162.2
North High						-31.3	-182.2	-22.0	-137.1	49.8	-71.2
East Low							-150.9	9.3	-105.8	81.0	-39.9
East High								160.2	45.1	232.0	111.0
South Low									-115.1	71.7	-49.2
South High										186.8	65.9
West Low											-120.9
West High											

Indicates the mean difference is significant at 0.05

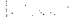
Indicates the mean difference is significant at 0.10

b)

Mean Difference SWE (mm) 2005				SLOPES							
	Flat	Lake	Plateau	N-Low	N-High	E-Low	E-High	S-Low	S-High	W-Low	W-High
Flat		16.7	36.8	-88.7	-260.4	-10.6	-89.9	17.7	-220.8	-35.0	-298.5
Lake			20.1	-105.4	-277.1	-27.3	-106.6	1.0	-237.5	-51.8	-315.2
Plateau				-125.5	-297.2	-47.4	-126.7	-19.1	-257.6	-71.9	-335.3
North Low					-171.7	78.1	-1.2	106.4	-132.1	53.6	-209.8
North High						249.8	170.5	278.1	39.6	225.3	-38.1
East Low							-79.3	28.3	-210.2	-24.4	-287.9
East High								107.6	-130.9	54.9	-208.6
South Low									-238.5	-52.7	-316.2
South High										185.8	-77.7
West Low											-263.5
West High											




Indicates the mean difference is significant at 0.05




Indicates the mean difference is significant at 0.10

c)

Mean Difference SWE (mm) 2006				SLOPES							
	Flat	Lake	Plateau	N-Low	N-High	E-Low	E-High	S-Low	S-High	W-Low	W-High
Flat		34.6	62.1	-111.1	-425.9	-40.6	-83.0	-46.5	-375.0	-108.0	-417.4
Lake			27.5	-145.7	-460.6	-75.2	-117.6	-81.1	-409.6	-142.6	-452.0
Plateau				-173.2	-488.0	-102.6	-145.1	-108.6	-437.1	-170.0	-479.5
North Low					-314.9	70.5	28.1	64.6	-263.9	3.1	-306.3
North High						385.4	343.0	379.5	51.0	318.0	8.6
East Low							-42.4	-5.9	-334.4	-67.4	-376.8
East High								36.5	-292.0	-25.0	-334.4
South Low									-328.5	-61.5	-370.9
South High										267.0	-42.4
West Low											-309.4
West High											



Indicates the mean difference is significant at 0.05



Indicates the mean difference is significant at 0.10

d)

Mean Difference SWE (mm) 2007				SLOPES							
	Flat	Lake	Plateau	N-Low	N-High	E-Low	E-High	S-Low	S-High	W-Low	W-High
Flat		38.7	51.9	-43.0	-305.4	-4.2	-114.8	-23.4	-252.6	-63.2	-352.8
Lake			13.2	-81.7	-344.1	-42.9	-153.5	-62.1	-291.3	-101.9	-391.5
Plateau				-94.9	-357.3	-56.2	-166.7	-75.3	-304.5	-115.1	-404.7
North Low					-262.4	38.8	-71.8	19.6	-209.6	-20.2	-309.8
North High						301.1	190.6	282.0	52.8	242.2	-47.4
East Low							-110.6	-19.2	-248.3	-59.0	-348.5
East High								91.4	-137.8	51.6	-238.0
South Low									-229.2	-39.8	-329.4
South High										189.4	-100.2
West Low											-289.6
West High											

Indicates the mean difference is significant at 0.05

Indicates the mean difference is significant at 0.10

e)

Mean Difference SWE (mm) 2008				SLOPES							
	Flat	Lake	Plateau	N-Low	N-High	E-Low	E-High	S-Low	S-High	W-Low	W-High
Flat		33.1	57.8	0.2	-267.8	-20.6	-193.0	10.4	-140.9	-8.0	-333.6
Lake			24.8	-32.8	-300.8	-53.6	-226.1	-22.7	-174.0	-41.1	-366.7
Plateau				-57.6	-325.6	-78.4	-250.8	-47.5	-198.8	-65.8	-391.4
North Low					-268.0	-20.8	-193.2	10.1	-141.2	-8.2	-333.8
North High						247.2	74.8	278.1	126.9	259.8	-65.8
East Low							-172.5	30.9	-120.4	12.6	-313.1
East High								203.4	52.1	185.0	-140.6
South Low									-151.3	-18.4	-344.0
South High										132.9	-192.7
West Low											-325.6
West High											

Indicates the mean difference is significant at 0.05

Indicates the mean difference is significant at 0.10

f)

Mean Difference SWE (mm) 2009				SLOPES							
	Flat	Lake	Plateau	N-Low	N-High	E-Low	E-High	S-Low	S-High	W-Low	W-High
Flat		14.4	36.5	-31.3	-209.9	-38.7	-232.7	-45.7	-177.2	-39.4	-175.9
Lake			22.1	-45.7	-224.2	-53.0	-247.0	-60.1	-191.5	-53.8	-190.2
Plateau				-67.8	-246.4	-75.2	-269.2	-82.2	-213.7	-75.9	-212.4
North Low					-178.6	-7.4	-201.4	-14.5	-145.9	-8.2	-144.6
North High						171.2	-22.8	164.1	32.7	170.4	34.0
East Low							-194.0	-7.1	-138.5	-0.8	-137.2
East High								186.9	55.5	193.2	56.8
South Low									-131.4	6.3	-130.1
South High										137.7	1.3
West Low											-136.4
West High											

Indicates the mean difference is significant at 0.05

Indicates the mean difference is significant at 0.10

Table 4.8 shows that the SWE in certain categories are always significantly different from each other while others are sometimes or never significantly different. The only inter-annually consistent difference seems to be between plateau and flat, which are significantly different in each year survey. Plateau and lake are significantly different in each year except 2005 and 2007. Lakes and flat are significantly different in three of the six years, 2006, 2007, and 2008. The results of the slope categories are somewhat

surprising in that there are relatively few significant differences, especially in 2005, 2008 and 2009. The 2006 survey exhibits differences which would be expected in most years. High slopes are significantly different from flat, plateau, lake, low slopes, and often other high slopes. However, in years other than 2006, there is a lack of significant difference between slopes and all other categories.

The GH test is used because it is the most robust test when the categories have unequal sample n and heterogeneity in variance (Toothaker, 1999). However, the results are not altogether expected. The lack of significant differences between slopes and other categories could easily be a product of low sample n in some high slope categories and the conservative nature of the GH test. Traditionally in statistics, a researcher aims to meet the assumptions of a given test. However, in this case, the relevant question is not whether ANOVA and related post-hoc test assumptions are exactly satisfied. The concern is whether or not possible violations of these assumptions have consequences for the validity of the results (Glass et al., 1972). As indicated, the GH test is used because of the heterogeneity of variance and unequal sample sizes. However, the Levene's test, which is used to determine homogeneity of variance, is not performed in a pair-wise fashion. As such, there is a single Levene statistic and significance for each year instead of for each category within each year. As a result, certain categories within the years may in fact have equal variance. If the equality of variance is not known, it is best to assume inequality and use the GH test. However, for comparative purposes, the more liberal Tukey-Kramer Honestly Significant Difference (HSD) post-test was also used. The Tukey-Kramer HSD (TK) test is applied when there are unequal sample sizes; however, it is not as robust when uncertainty about homogeneity variance exists (Toothaker, 1999). Table 4.9 shows the results of both the TK and GH post hoc difference of means tests.

**Table 4.9. Summary of post-hoc difference of means tests for
a) flat tundra, b) lakes, c) low slopes, and d) high slopes**

a)

FLAT						
	2004	2005	2006	2007	2008	2009
Lake						
Plateau						
North Low						
North High						
East Low						
East High						
South Low						
South High						
West Low						
West High						

Significant at 0.05 using both Tukey and GH
 Significant at 0.05 using Tukey
 Significant at 0.05 using GH

b)

LAKES						
	2004	2005	2006	2007	2008	2009
Flat						
Plateau						
North Low						
North High						
East Low						
East High						
South Low						
South High						
West Low						
West High						

Significant at 0.05 using both Tukey and GH
 Significant at 0.05 using Tukey
 Significant at 0.05 using GH




c)

NORTH LOW SLOPE						
	2004	2005	2006	2007	2008	2009
East High						
South High						
West High						
EAST LOW SLOPE						
	2004	2005	2006	2007	2008	2009
North High						
South High						
West High						
SOUTH LOW SLOPE						
	2004	2005	2006	2007	2008	2009
North High						
East High						
West High						
WEST LOW SLOPE						
	2004	2005	2006	2007	2008	2009
North High						
East High						
South High						

Significant at 0.05 using both Tukey and GH
 Significant at 0.05 using Tukey
 Significant at 0.05 using GH

d)

NORTH HIGH SLOPE						
	2004	2005	2006	2007	2008	2009
East High						
South High						
West High						
EAST HIGH SLOPE						
	2004	2005	2006	2007	2008	2009
North High						
South High						
West High						
SOUTH HIGH SLOPE						
	2004	2005	2006	2007	2008	2009
North High						
East High						
West High						
WEST HIGH SLOPE						
	2004	2005	2006	2007	2008	2009
North High						
East High						
South High						

 Significant at 0.05 using both Tukey and GH
 Significant at 0.05 using Tukey
 Significant at 0.05 using GH

The TK test does show some significant differences among categories where the GH does not. For example, using the TK test, flats are never significantly different from lakes, however, they are often significantly different from both high and low slopes. Both tests seem to concur that flats are significantly different from plateaus. Similarly, using the TK test, lakes are also more often significantly different from slopes, especially in 2009. Table 4.10c shows an interesting result in that neither the GH or TK test indicate any significant difference between low slopes in any of the years. For high slopes, the TK test does show more significant differences than the GH in some years, especially between east high slopes and all others. Neither the TK nor the GH tests indicate very many significant differences between north, south, and west high slopes.

Using two difference of means test does offer some reassurance but also some concerns as some of the results vary. It is important to note that the GH test results are more statistically robust, and any conclusion from this analysis should not be based solely on the TK test results. Nonetheless, both post-hoc tests have shown some interesting inter-annual relationships between the categories. To summarize, the most interesting findings are:

- (a) SWE on low slopes on north, east, south, and west aspects were never found to be different from each other.
- (b) SWE on low slopes were never different from SWE on flats using the GH test and only different in three cases using the TK test.
- (c) SWE on flats and plateaus were found to be significantly different in every year using the GH test and four of six years using the TK test.
- (d) SWE on flats and lakes were significantly different in only three of the six years using the GH test and never different using the TK test.
- (e) SWE on north, south, and west high slopes were only different from each other in three cases using the TK test.

It can be concluded from these summary points that it is not necessary to include all eleven categories in the terrain classification. The implications of combining different categories will be investigated in the next section.

4.4.2.2. *Terrain Weighted SWE with all Categories*

The main goal of a terrain based classification is to better define how SWE is distributed throughout the study area. The end goal is to create a terrain weighted SWE value which would take into consideration the proportion of features in the study area and weight the depth of SWE appropriately. A terrain weighted mean SWE was calculated first, using all eleven categories, and the following equation:

$$\text{Weighted mean SWE} = \sum \partial_1 x_1 + \partial_2 x_2 \dots \partial_n x_n$$

where ∂ represents the percent of each terrain category and x represents the mean SWE for each terrain category. For comparison, an arithmetic mean SWE was generated using the following equation:

$$\text{Arithmetic mean SWE} = \frac{\sum x_1 + x_2 \dots x_n}{N}$$

where x represents the mean SWE for each terrain category and N represents the total number of categories. The weighted mean SWE are compared to the arithmetic mean SWE for each year in Table 4.10.

Table 4.10. Terrain weighted mean SWE compared to arithmetic mean SWE for each survey year

	% Study Area	2004		2005		2006		2007		2008		2009	
		A	W	A	W	A	W	A	W	A	W	A	W
Flat Tundra	36.7	123	45.1	95	34.9	137	50.3	109	40	100	36.7	77	28.3
Lakes	25.6	97	24.8	75	19.2	102	26.1	73	18.7	67	17.2	62	15.9
Upland Plateaus	2.0	64	1.28	58	1.16	89	1.78	57	1.14	42	0.84	40	0.8
Low North Slopes	6.0	101	6.06	182	10.9	248	14.9	175	10.5	100	6	108	6.48
Steep North Slopes	3.1	186	5.77	309	9.58	563	17.5	364	11.3	223	6.91	286	8.87
Low East Slopes	4.6	228	10.5	107	4.92	177	8.14	106	4.88	121	5.57	115	5.29
Steep East Slopes	2.8	413	11.6	184	5.15	220	6.16	223	6.24	293	8.2	309	8.65
Low South Slopes	6.3	198	12.5	76	4.79	166	10.5	136	8.57	90	5.67	122	7.69
Steep South Slopes	3.3	337	11.1	315	10.4	471	15.5	288	9.5	241	7.95	253	8.35
Low West Slopes	7.4	153	11.3	129	9.55	203	15	197	14.6	108	7.99	116	8.58
Steep West Slopes	2.5	257	6.43	392	9.8	554	13.9	447	11.2	434	10.9	252	6.3
MEAN SWE		196	146	175	120	266	180	198	137	165	114	158	105
<i>Difference (A - W)</i>		50		55		86		61		52		53	

A represents the Arithmetic mean SWE

W represents the weighted mean SWE

It is clear from Table 4.10 that using a weighted mean, which takes into consideration the proportion of different terrain categories in the study area, produces much lower mean SWE than using the arithmetic mean. However, the weighted mean is more realistic as it diminishes the relative influence of the terrain categories which are spatially constrained. This is most prominent in steep slopes, which do not occupy much of the study area but have much higher SWE than other categories.

It is important to note the difference in the values of arithmetic mean SWE between Table 4.10 and mean SWE shown in the descriptive statistics of Table 4.4. The mean SWE values in Table 4.4 are lower due to the fact that they are derived using a different approach. In Table 4.4, the mean SWE are calculated summing all SWE measurements taken during that survey year and dividing by the number of measurements. This method derives an arithmetic mean but is affected by differences in

the number of samples taken in each category from year to year. In Table 4.10, the mean SWE for each terrain category are used instead of each individual site SWE. This eliminates the effect of a difference in sample numbers and site location from year to year. However, this method assumes that sites chosen are representative, and the terrain category mean is a good approximation of SWE within that specific category anywhere in the study area.

4.4.2.3. Refining the Number of Terrain Categories

In Section 4.4.2.1, several difference of means tests were conducted. The results shown in Table 4.9 demonstrate that the SWE in several categories are not necessarily significantly different from each other. Based on these analyses the terrain classification can be modified, and several classes can be combined (Figure 4.17).

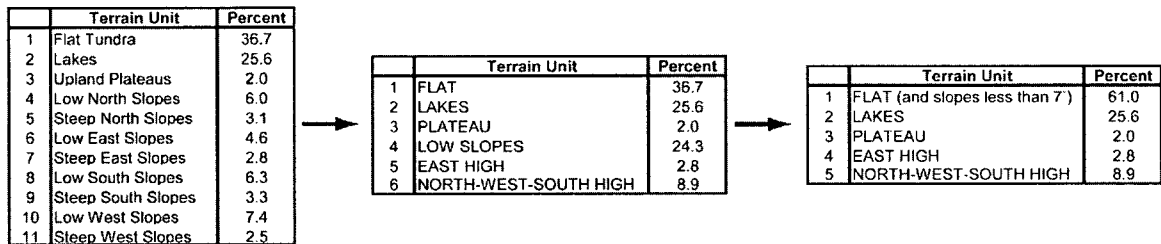


Figure 4.17. Modified terrain based classification

The original eleven categories were initially reduced to six based on the most significant and obvious results. East high slopes were kept separate from north, west, and south high slopes as there were more cases where they were significantly different. However, a further step was taken to reduce the number of categories to five. This was justified as there were no cases where low slopes were significantly different from flats using the GH test and only three instances where low slopes were significantly different from flats using the TK test. The terrain weighted mean SWE values were then re-calculated using the five new categories and compared to the weighted SWE using the original 11 categories (Table 4.11).

Table 4.11. Five category terrain based weighted mean SWE compared to eleven category weighted mean SWE

	% Study Area	2004		2005		2006		2007		2008		2009	
		A	W	A	W	A	W	A	W	A	W	A	W
Flat Tundra (less than 7°)	61.0	168	103	108	66	160	98	122.1	75	103	63	94	57
Lakes	25.6	97	25	75	19	102	26	73	19	67	17	62	16
Upland Plateaus	2.0	64	1	58	1	89	2	57	1	42	1	40	1
Steep East Slopes	2.8	413	12	184	5	220	6	223	6	293	8	309	9
Steep N-W-S Slopes	8.9	269	24	347	31	518	46	424	38	331	29	261	23
NEW FIVE CATEGORY MEAN SWE		202	164	154	117	218	171	180	138	167	119	153	106
<i>Difference (A - W)</i>		38		37		47		42		48		47	

ELEVEN CATEGORY MEAN SWE (TABLE 4.10)	196	146	175	120	266	180	198	137	165	114	158	105
<i>Difference NEW (5) - OLD (11)</i>	6	18	-20	-3	-49	-9	-18	1	2	5	-5	1

A represents the Arithmetic mean SWE

W represents the weighted mean SWE

The weighted mean using five categories produces a lower value than the arithmetic mean SWE similar to using all eleven categories. Using five categories instead of 11 does produce a much lower arithmetic SWE in some years (2005, 2006, 2007), while in other years, it is quite similar (2004, 2008, 2009). The five category weighted SWE is quite similar to the 11 category weighted SWE in all years. The greatest differences are 18 mm lower in 2004 and 9 mm higher in 2006. Otherwise, the difference between the two approaches is quite small. This would imply that using five categories would not produce values radically different from using the original eleven categories.

A potential problem with using the five category classification is that it may not provide the same level of information about snow cover variability as the eleven category version. As outlined in Section 4.3.3, the coefficient of variation (CV) is very useful for comparing variability between different categories. The CV was calculated for the five categories for comparison with the CV for the eleven categories (Table 4.12).

Table 4.12. The coefficient of variation of SWE for the five terrain categories

	% Study Area	2004		2005		2006		2007		2008		2009		Weighted Mean CV
		CV	W-CV	CV	W-CV	CV	W-CV	CV	W-CV	CV	W-CV	CV	W-CV	
Flat Tundra (less than 7°)	61.0	0.82	0.50	0.61	0.37	0.51	0.31	0.49	0.30	0.45	0.28	0.55	0.33	0.349
Lakes	25.6	0.37	0.09	0.35	0.09	0.29	0.07	0.43	0.11	0.39	0.10	0.30	0.08	0.091
Upland Plateaus	2.0	0.71	0.01	0.61	0.01	0.46	0.01	0.64	0.01	0.62	0.01	0.56	0.01	0.012
Steep East Slopes	2.8	0.50	0.01	0.59	0.02	0.34	0.01	0.47	0.01	0.49	0.01	0.32	0.01	0.013
Steep N-W-S Slopes	8.9	0.85	0.08	0.41	0.04	0.41	0.04	0.40	0.04	0.50	0.04	0.44	0.04	0.045
Five Category Weighted Mean CV			0.70		0.53		0.44		0.47		0.45		0.47	0.51

The CV for the new flat tundra category is higher in all cases than the former flat category in the eleven category classification, especially in 2004. This is due to the amalgamation of the four low slope categories with the flat category. However, the amalgamation of the three steep slopes (north, west and south) did not change the CV very much, except in 2004. It is clear that while the classes may not be significantly different, the combination of multiple categories does increase the variability in measured SWE. This is further demonstrated in the overall weighted mean CV. In Table 4.12, the weighted mean CV for all years and categories is 0.51. This is an increase from the overall weighted mean CV of 0.40 in Table 4.7. However, the CV for flat and steep n-w-s categories is much higher in 2004 than in other years. If the 2004 season is ignored, the overall weighted mean CV using five classes drops to 0.46, which is much closer to the 0.40 of Table 4.7.

4.4.2.4. Summary of Terrain Weighted SWE

The use of five categories instead of eleven does not produce much difference in annual weighted mean SWE. However, there is an increase in the CV when the categories are collapsed from eleven to five. In terms of extrapolating snow cover to the scale of the study area and beyond, the use of five categories is likely sufficient to maintain a CV of around 0.40 to 0.50. Due to the small differences between the classifications, the weighted SWE values using the five category approach will be used for comparison with satellite data in Chapter 5.

4.4.3. Merging Terrain and Land Cover Information

In high latitude tundra in regions with no shrubs or other tall vegetation, snow distribution is driven largely by terrain (Bruland et al., 2001, Hirashima et al., 2004). However, the region around Daring Lake is considered to be low arctic shrub tundra. In this type of tundra, terrain is not the only variable which can influence the distribution of snow. Many researchers have recognized the role of vegetation on the pattern of snow accumulation (Pomeroy et al., 1997, Essery et al., 1999, Sturm et al., 2001b). In Section 3.3, the study area was delineated using a satellite derived land cover classification. The utility of including this information in a snow cover classification must be investigated.

Despite the recognized influence of vegetation on snow accumulation, the determination of land cover over large areas is not a simple process during winter field campaigns. This is because most of the ground cover is not easily delineated under a blanket of snow. As such, recording land cover was not always a priority during data collection in the field. Moreover, relying on the satellite classification is not ideal without in-situ land cover observations for validation.

The 2007 field season was the largest in terms of personnel and time spent in the field. This translated into the most sites visited during all surveys and the collection of land cover information on flat tundra, lakes and plateaus. The data collected in 2007 provide an opportunity to evaluate the addition of land cover information to the terrain based consideration of snow cover. From the data collected in 2007, the flat, plateau and lake categories were expanded (Figure 4.18).

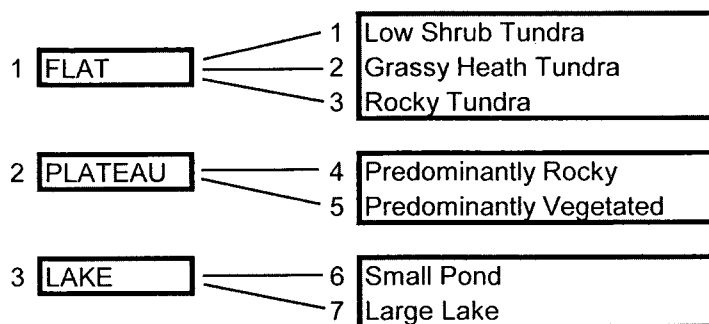


Figure 4.18. The addition of land cover classes to the terrain based snow cover classification

The inclusion of land cover information does make some sense intuitively as areas with emergent vegetation should see greater and more variable depth of SWE compared with areas with no vegetation or buried vegetation (see Section 4.2.2). Furthermore, the complex surface roughness associated with rock outcrops and boulder deposits could increase the variability of the snow cover, especially density. While technically not land cover information, it was observed in the field that small ponds (less than 60 000 m²) were typically more affected by wind scour and had more areas of bare ice. On lakes larger than 60 000 m², the depth of SWE seemed to be more consistent. To assess the utility of adding land cover information two questions will be addressed:

1. Are the seven sub-groups identified in Figure 4.18 significantly different from each other?
2. Do the inclusion of land cover data and the use of seven instead of three categories decrease the variability in SWE (CV) in the overall classification?

To address whether or not the sub-classes of land cover are significantly different from each other, an ANOVA was used along with the Levene's statistic. The GH multiple difference post-hoc test was applied to flats because there were more than two groups. The results are summarized in Table 4.13.

Table 4.13. Homogeneity of variance and difference of mean statistics for land cover information

Flat		Plateau		Lake	
Leveens	0.02	Leveens	0.705	Leveens	0.46
ANOVA	0.00	ANOVA	0.816	ANOVA	0.00

Mean Difference SWE (mm)					
	Shrub	Grass	Rock		
Shrub		51	18		
Grass			-33		
Rock					

	Veg	Rocky		
Veg		-2		
Rocky				

	Small	Large	
Small		-39	
Large			

Indicates the difference is significant at 0.05

Table 4.13 shows that in the flat tundra category, there is a significant difference between shrub and grass and between rocky areas and grass, however, there is no difference between low shrub and rock. The low shrub land cover had the highest SWE while the grass had the lowest. The Leveens statistic is significant, meaning there is heterogeneity in variance between the three groups. This would suggest that separating flat tundra into at least two sub-groups may improve the classification. The two categories would be flat tundra grass and flat tundra shrub-rock.

However, a potential problem with this approach is the separation of these flat tundra classes throughout large scale study areas. Land cover and SWE data are recorded in the field as point data. Moreover, the LANDSAT land cover classification described in Section 3.3.3 provides only broad classes which are assumed to be homogenous in a 30 m pixel area. Another issue is the matching of LANDSAT classes, derived from a summer image, with land cover observed in winter. For example, the LANDSAT tall shrub classes comprise a very small part of the study area (Tall Shrub 0.29 %, and Birch Shrub 0.49 %). However, in the field, it is evident that there are large areas with low shrubs ranging from sporadic to quite dense (Figure 4.19).

Figure 4.19. Example of a site which contains sparse low shrub vegetation



Table 4.13 shows how these shrub areas have the highest SWE. The problem is that the LANDSAT classification does not have a distinct low shrub class. This is due primarily to the difficulty in quantifying the abundance of shrubs within a 30 m pixel. The rocky flat tundra category proposed in Figure 4.18 could be subject to the same problem. The LANDSAT boulder association class is very small, while the heath/boulder class is somewhat larger at 13 %. Certain parts of the study area are dominated by boulders and rock outcrops, and it may again be difficult to quantify the degree of boulders within a 30 m pixel (Figure 4.20). The only hope would be to distinguish between the heath/boulder (12%) and the heath tundra grassy class (24% of the study area). This, however, would not address the delineation of low shrubs and hamper the use of the shrub-rock category.

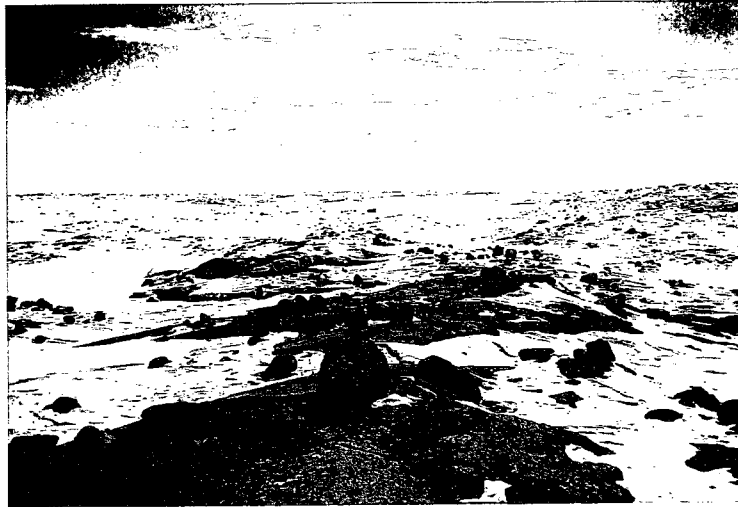


Figure 4.20. Boulders distributed across the tundra

The utility of sub-dividing flat tundra into two classes is further examined by looking at the change in the CV of SWE moving from one to two groups (Table 4.14).

Table 4.14. Statistics of flat tundra SWE categories

	Mean SWE	STDEV	CV	n
Flat	109	45	0.41	84
Shrub-Rock	125	44	0.35	56
Grass	78	27	0.34	28

Table 4.14 shows that the CV in SWE decreases from 0.41 to 0.35 when flat tundra is separated into two categories. These results suggest that in the future, flat tundra should be separated into either grass heath tundra or low shrub–rock tundra. However, the extrapolation of these sub-categories beyond the site scale would be very difficult using the existing remote sensing land cover classification.

Similar to flat tundra, the plateau category was separated into either vegetated or rocky (Figure 4.18). Table 4.13 shows that while the two categories had homogenous variance (Leveens statistic $p = 0.705$), there was no significant difference (ANOVA

0.816). These results suggest that the two categories need not be created, and a single category for upland plateaus can be used.

The lake category was also separated into two categories based on lake area. The Levene's statistic was not significant which indicates that the two groups have homogeneity of variance. However, the ANOVA was significant (0.000), which indicates that the SWE in the two lake categories was significantly different. There was significantly less snow on smaller lakes as compared to larger lakes. Furthermore, the separation of lakes into two categories does change the CV of SWE (Table 4.15).

Table 4.15. Statistics of lake SWE categories

	Mean SWE	STDEV	CV	n
Lake	71	28	0.40	50
Large Lake	89	17	0.20	27
Small Lake	50	24	0.48	23

It was suggested in Section 4.3.3 that lakes have the least variability in SWE. Table 4.15 shows that the variability in SWE is much lower on large lakes. A greater relative fraction of small lakes are influenced by wind scour, and as a result, have much higher variability and lower SWE. As such, separating lakes into two categories would be beneficial in improving the classification.

The need for separating lakes is further demonstrated by examining the proportion of large and small lakes in the study area. In the study area, small lakes occupy a very small part of the total landscape area (Table 4.16).

Table 4.16. The percent of the study area occupied by lakes of different sizes

		Percent Study Area
Study Area	625000000 m ²	
Total Lake Area	159762876 m ²	26%
Area small lakes (< 60000 m ²)	9787207 m ²	1.57%

Table 4.16 shows that small lakes comprise only 1.57 % while large lakes comprise 24.4 % of the total study area. Hence, small lakes should have little influence in a study area weighted mean SWE. However, when the measurements are lumped with large lakes into a single lake class, they have a greater influence on the lake category SWE. Essentially, small lakes have a disproportionate spatial influence on mean SWE as well as variability in SWE within the existing lake category. In the future, it will be necessary to separate lakes into at least these two categories in order to improve the weighted mean classification of SWE. Unlike classes which rely on remote sensing land cover information, the separation of lakes into two classes is easily done within a GIS.

4.5. Summary of Snow Data

4.5.1. Introduction

The purpose of this chapter was to establish a more complete understanding of tundra snow cover properties and variability through the multiple years of late winter, spatially intensive, pre-melt in-situ snow cover measurements. The data from the six years of field surveys reinforce several of the assumptions outlined in Chapters 1 and 2 and in Section 4.2.1. First and foremost, the spatial distribution of snow depth, density and SWE was dominantly controlled by the interaction of blowing snow with different terrain and land cover types. Furthermore, the snow cover data collected confirmed that spatially constrained measurements of any kind are not sufficient to understand snow distribution and properties in the tundra. However, despite the heterogeneity of the snow cover distribution, several inter-annual consistencies were identified. Moreover, the use of a terrain and landscape classification system was explored and proved to be useful for the generalization of snow cover properties throughout large study areas.

4.5.2. Inter-annual Patterns in Tundra Snow Cover

The results shown in Section 4.2.2.1 are very noteworthy because they highlight the fact that tundra snow density is not all that variable when considered on a site-by-site basis, between different terrain types and from season to season. A regional average density of 0.294 g/cm^3 was derived from the six years of measurements and is comparable with those proposed by other researchers, especially if the low densities observed in 2009 are excluded.

The ratios of SWE derived in Section 4.2.3 are also quite interesting. Despite potential differences in seasonal weather patterns, there were many consistent ratios in the depth of SWE on flat tundra to the depth SWE in other terrain categories. This further reinforces the data from Woo (1998) who suggested that, despite differences in seasonal snowfall, the inter-annual patterns of snow cover deposition do not change very much. Furthermore, Hirashima et al. (2004) indicated that the depth of snow drifts remains similar, and it is the areal extent of deposition which changes from year to year. In this study, Table 4.3 and Figure 4.11 demonstrate that the depth of SWE in drifts does change from year to year, as does the slope aspect containing the most SWE. The areal extent of snow accumulation in drifts was not quantified; however, anecdotal observations suggest that in this study area the extent of snow drift deposition does increase as SWE depth increases. The ratios calculated in Table 4.3 represent a contribution for the planning of future field campaigns or placement of automated gauges. Future patterns of SWE on different terrain types throughout the study area could be approximated from measurements taken only in areas of flat tundra.

Quantifying variability among different years at the study area scale was useful in showing how SWE varied without considering differences among terrain categories. The high variability in SWE between years shown in Section 4.3.2 reinforced the need to use a terrain based classification to better understand snow cover distribution. Table 4.6

showed how variability (CV) in SWE was relatively consistent based on the assumptions of snow re-distribution with terrain categories outlined in Table 4.6. Perhaps the most interesting result is that shown in Table 4.7 where the overall weighted mean CV for the study area was shown to be 0.40, which is identical to that proposed for tundra snow by Liston (2005). The analysis of variability did show that between terrain types and survey years there were large differences in the CV of SWE. However, the weighted mean CV in SWE of 0.40 is a very useful generalization for studies done using coarse resolution grids and at a regional scale.

4.5.3. Extrapolation of SWE

At local scales, tundra snow cover is heterogeneous due to the interaction of blowing snow with terrain and landscape features. However, at a regional scale, the seasonal distribution and variability of snow cover follow predictable patterns. These patterns need to be exploited as, no matter how intensive, ground data collected through in-situ field observation or by automated gauges are spatially constrained. Hence, for application to remote sensing and other grid based modelling, snow cover data need to be generalized and extrapolated over larger areas to be of any use. Moreover, coarse resolution passive microwave remote sensing data attempt to provide single estimates of SWE over 625 km² EASE grid cells. These estimates are essentially useless unless they can be related to sub-grid snow cover properties.

The issues of generalizing, extrapolating and downscaling snow cover information are addressed through the use of a terrain and landscape based classification scheme. In this way, sub-grid snow cover can be explained by working up from point data or down from EASE grid data. Deriving a weighted mean SWE based on the proportion of landscape and terrain features was shown as the best method for providing regional snow cover information (Table 4.10). The optimum number of

categories for the study area was reduced from eleven to five due to indifferences in SWE between certain categories (Figure 4.17).

The use of a terrain classification and weighted mean approach is not without limitations. For example, the quantification of the percent area for each category is in itself difficult to validate. The use of GIS and topographic information from digital sources means that the classification is inherently a gross oversimplification of the true landscape. Certain features are smoothed out considerably just by virtue of the contour interval (10m) and classification grid resolution (10m). Moreover, the modelled boundaries between categories are not as discrete as the GIS would suggest. However, the use of an areally weighted mean SWE and a terrain classification is the best solution given the size of the study area and the objectives of the project. The extrapolated snow cover will be used for comparison with satellite based passive microwave data in Chapter 5 while the point data collected will be compared to spatially coincident multi-scale ground based and airborne passive microwave data in Chapter 6.

CHAPTER 5: EVALUATING SATELLITE PASSIVE MICROWAVE DATA

5.1. Introduction

Passive microwave sensors aboard spaceborne platforms have been operational since 1972 with the launch of the Electronic Scanning Multichannel Radiometer (ESMR). The development of the Scanning Multi Channel Microwave Radiometer (SMMR) in 1978, with improved resolution, resulted in interest in using passive microwave data in snow research (Chang et al., 1987). The SMMR sensor was followed by the Special Sensor Microwave Imager (SSM/I) in 1987 aboard the Defense Meteorological Satellite Program (DMSP) platforms. The SSM/I sensors are still in orbit and continue to provide passive microwave data. Application of SMMR and SSM/I data were restricted to large areas due to coarse spatial resolution. The Advanced Microwave Sounding Radiometer Earth Observing System (AMSRE) sensors aboard the Aqua platforms in 2002 provide a finer spatial resolution and data at similar frequencies to those previously collected. Hence, the AMSRE data often replace the still operational SSM/I data in current research efforts.

The time series of data provided since the launch of SMMR is of great interest for its potential to provide over 30 plus years of spatially extensive snow cover information. Several researchers have exploited all or part of the available time series for application to hydrologic processes or evaluation of climate models (Derksen et al, 2000c, and 2003, Wulder et al., 2007, Biancamaria et al., 2008). Furthermore, the time series of passive microwave estimates can be merged with conventional data records dating from the early 1900s to produce an even longer time series of snow cover information (Derksen et al., 2004).

As outlined in Chapter 2, passive microwave sensors have a proven record of estimating SWE over different landscapes. However, there still is no well accepted method for estimating tundra SWE. The common problem is that the conventional

algorithm approach using a 19 and 37 GHz Tb difference produces an underestimation of ground measured SWE (Boudreau and Rouse, 1994, Grippa et al., 2004, Armstrong and Brodzik, 2002, Rees et al., 2005). As such, there has been little work done to exploit the existing multi-sensor time series over the tundra.

The theoretical challenges hampering tundra SWE algorithm development were outlined in Section 2.4. Essentially the biggest challenge is addressing the potential influence of sub-grid terrain and land cover properties on satellite Tb. However, before sub-grid heterogeneity can be resolved, there needs to be a comparison of satellite scale data with the in-situ SWE data described in Chapter 4. This is, in part, to confirm the underestimation of SWE using the conventional 37 – 19 GHz approach and to examine the behavior of each frequency with differing SWE. When the conventional 37 – 19 GHz approach is used, there are several basic assumptions made:

- 1- Satellite Tb at 37 GHz changes throughout a winter season
- 2- Satellite Tb at 19 GHz does not change very much throughout a winter season
- 3- The Tb at 19 and 37 GHz are not systematically influenced by landscape or terrain
- 4- The difference between 19 and 37 GHz can be used to estimate SWE

These assumptions need to be investigated in order to better understand why SWE is not well estimated in the tundra. The first two assumptions are important to examine because if violated, then the 37 – 19 approach would be totally ineffectual at estimating SWE. Similarly, the third assumption is critical because a systematic influence would mean that Tb data are being perpetually affected by confounding factors and are not sensitive, or less sensitive to changes in SWE. Finally, the fourth assumption indicates that if there is in fact a difference between Tb at 19 and 37 GHz, then it can be related to SWE. In order to evaluate the first three assumptions, a spatial and temporal analysis was performed using the time series of currently available satellite

passive microwave data (1979-2008). To evaluate the final assumption, in-situ snow survey data from Chapter 4 were compared to spatially and temporally coincident satellite passive microwave Tb.

5.2. The Passive Microwave Satellite Record

Satellite data for the study region are available from the SMMR, SSM/I and AMSR-E platforms. The SMMR data were collected every second day, beginning with the fall/winter of 1978/79. The SSM/I data were collected daily beginning in the 1988/89 season. AMSR-E data were also collected daily, starting in the 2001/02 season. The final season available at the time of analysis was 2007/08. All data were acquired in the EASE grid format from the National Snow and Ice Data Center (NSIDC). To investigate spatial patterns in Tb, an arbitrary domain of 40 EASE grid pixels was selected around the study area pixel. The domain was selected to be predominantly outside of the boreal forest and with varying lake fraction (Figure 5.1).

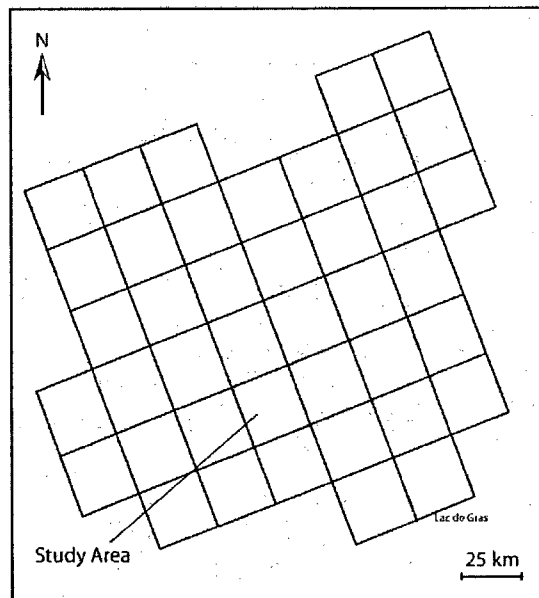


Figure 5.1. Spatial domain of time series EASE grids

Brightness temperatures at 19 and 37 GHz were acquired at the vertical polarization. Vertically polarized data were used as horizontally polarized data can be influenced by ice layers which alter Tb independently of SWE (Rees et al., 2010). To capture end of winter pre-melt SWE and minimize daily variability, an average Tb was taken over a ten day period from April 1 to April 10. This time period was chosen as it most likely represents maximum SWE for each season and minimizes the likelihood of any melt events. Tb data from the morning, or cold overpass were used to further minimize the likelihood of wet snow from any diurnal melt events (Derksen et al., 2000b). To examine temporal and spatial patterns in the data, the average April 1 to April 10 Tb difference from 37 and 19 GHz vertically polarized data (ΔTb^{37-19}) were analyzed along with individual frequencies where appropriate. The ΔTb^{37-19} was used as it forms the basis for algorithm development and theoretically minimizes the influence of differences in physical air temperature between different years.

5.3. Temporal Analysis of Tb

5.3.1. Introduction

The following section will address the first two assumptions noted in Section 5.1.

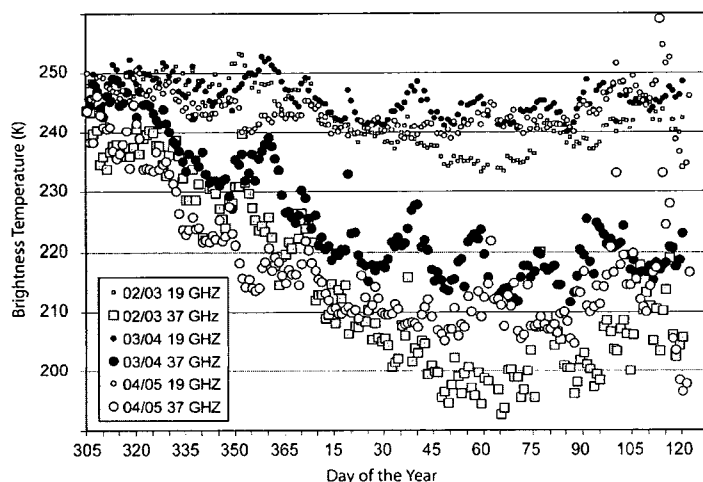
- 1- Satellite Tb at 37 GHz changes throughout a winter season
- 2- Satellite Tb at 19 GHz does not change very much throughout a winter season

The testing of these two assumptions is important to determine if there are in fact changes in Tb throughout a single season and from year to year. Chapter 4 showed that the mean SWE measured in the study area can reach a maximum of 171 mm at the end of the season and that mean SWE was different from year to year. If the 37 GHz Tb does not change throughout a season (from November to April) and if there are no differences in the end of season Tb from year to year, then there will obviously be serious problems in estimating SWE using passive microwave data.

5.3.2. Seasonal Evolution in 19 and 37 GHz Tb

To examine the seasonal evolution of Tb within a single season the 37 GHz and 19 GHz time series were plotted from November 1 to April 30 for the study area EASE grid pixel for each of the years with in-situ SWE data (Figure 5.2).

a)



b)

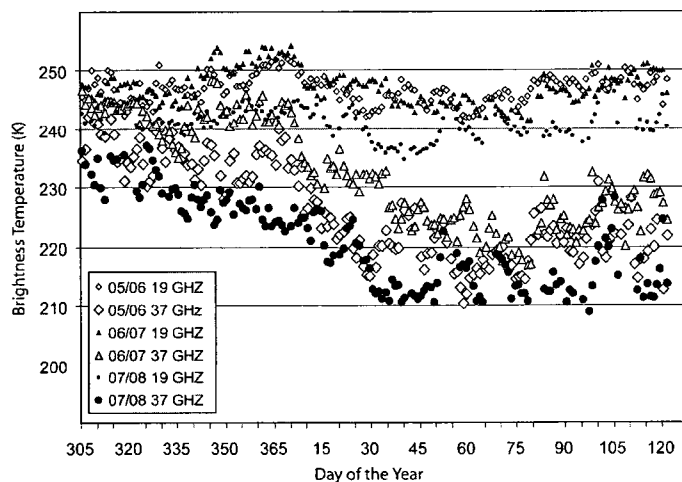


Figure 5.2. The seasonal evolution of 19GHz, 37 GHz from November 1 to April 30 for a) 2002/03 to 2004/05 and b) 2005/06 to 2007/08

During each of the seasons plotted in Figure 5.2, the 19 GHz Tb values start somewhere between 245 and 250 K each season, dip to a minimum value of 235 to 245 K around day 30 to 60 and return close to their starting point at the end of the winter. At 19 GHz, the mid-winter decrease in Tb is likely a response to a decrease in air,

underlying ice and ground temperatures. However, the changes in 19 GHz Tb throughout the season are not smooth. There are many jumps in Tb and, in some cases, over a relatively short period of time (for example 2003/04 from day 30 to 45). The jumps in data could be due to daily or weekly changes in temperature, however, ground and lake ice tend to have more stable seasonal temperatures than air. As such, the fluctuations in 19 GHz Tb are likely a product of variation in the geolocation of the satellite overpasses used in the resampling necessary to produce EASE grid data (Kelly, personal communication; Armstrong and Brodzik, 1995). Swath data collected by the AMSR-E sensors have a spatial resolution of 28 x 16 km in an elliptical shape at 19GHz (Figure 2.1). When swath data get re-gridded to the EASE grid projection, there will be differences in how many swath footprints are integrated and where those are located. To minimize the jumps in Tb, swath data may be more appropriate for seasonal timescales. However, swath footprints do not cover the same location from orbit to orbit and so some processing of Tb data would still be required.

The 37 GHz does not follow the same seasonal pattern as 19 GHz. The 37 GHz Tb starts off roughly equal to 19 GHz but decreases throughout the season, reaching a minimum value at around day 60 to 75. After this point, there is often little change or a slight increase in Tb towards the end of the season. This increase may be due to the recognized reversal of 37 GHz Tb when snow depth reaches a certain point (Section 2.4.2.2). However, determining the cause of change in 37 GHz Tb can be only speculative in the absence of seasonal snow cover information. Nonetheless, jumps and fluctuations in 37 GHz Tb, similar to 19 GHz, are seen throughout each season. This may also be attributed to EASE grid and swath geolocation issues. However, emission at 37 GHz is influenced by the properties of the snow volume and by snow surface temperatures, which make it more sensitive to changes in air temperature.

5.3.3. Seasonal Evolution in ΔT_b^{37-19}

Figure 5.2 does help validate the two assumptions outlined at the beginning of this section. During each of the plotted seasons, the 19 GHz channel does not change very much from its original value, and there is a decrease in the 37 GHz Tb over time. This would imply that the use of a brightness temperature difference between the two frequencies should be possible. The ΔT_b^{37-19} was plotted for November 1 to April 30 from the study area EASE grid for each of the years with in-situ SWE data (Figure 5.3).

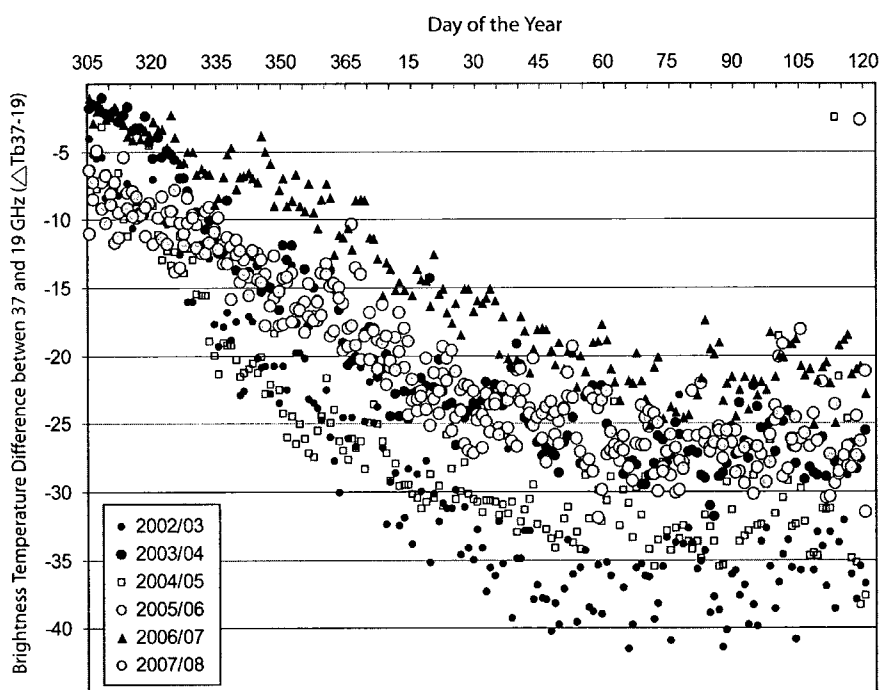


Figure 5.3. The seasonal evolution of the ΔT_b^{37-19} from November 1 to April 30 for 2002/03 to 2007/08

Figure 5.3 clearly shows that the ΔT_b^{37-19} changes from near zero in early November (Day 305) to a maximum value of -20 to -42 at around days 75 to 90. This change in ΔT_b^{37-19} throughout each season shows some sensitivity to parameters that evolve over a winter season. In the tundra, from November to April, there are several cryospheric elements which evolve: 1) changes in air temperature, 2) freezing of active layer, 3) lake ice thickness, 4) snow depth, 5) snow density, and 6) snow stratigraphy.

The challenge is isolating which of these elements is influencing the change in ΔT_b^{37-19} . Figure 5.3 also shows that there are different end points in ΔT_b^{37-19} between different seasons. This is important because we would expect differences in cryospheric elements between different seasons and, as mentioned, the in-situ measured SWE is significantly different between these seasons.

The end of winter (April 1 to April 10) ΔT_b^{37-19} were plotted for the entire 1979 to 2008 time series using the study area EASE grid pixel to see if there was any variability or noticeable trends over time (Figure 5.4).

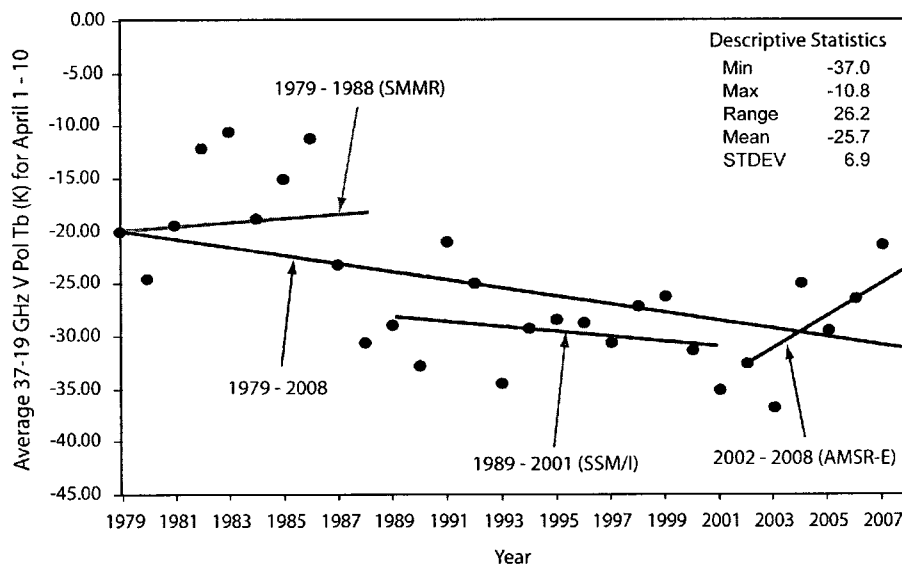


Figure 5.4. The average April 1 – 10 ΔT_b^{37-19} from 1979 to 2008

The mean end of winter ΔT_b^{37-19} for the 1979 to 2008 time series is -25.5 with a standard deviation of 6.4 K, a coefficient of variation of 0.25 and a large range of 27.3 K. Figure 5.4 shows that there are definitely differences in end of winter ΔT_b^{37-19} from 1979 to 2008 and that the points are not entirely randomly distributed. In order to provide a visual impression of changes throughout the time series, lines of best fit were added using a sum of least squares method. The 1979 – 2008 line shows a significant ($p = 0.05$) decreasing trend towards a greater ΔT_b^{37-19} over the years. However, the time series displays heteroscedasticity as the first half has a much larger dispersion than the

second half. Each sensor period was examined separately. The 1979 – 1988 SMMR line shows a slightly increasing trend; however, the slope of the line is not significantly different than 0 ($p > 0.05$). The 1989 – 2001 SSM/I line shows a decreasing trend similar to the overall time series trend. The slope of the SSM/I is also not significantly different from 0 ($p > 0.05$) while the 2002-2008 AMSR-E line shows a steep increase in ΔT_b^{37-19} ($p = 0.02$).

The trends in ΔT_b^{37-19} time series are interesting but not that applicable at this point because they cannot yet be related to SWE. It is also interesting to note that there are some differences between sensors which should be investigated if the time series is to be applied to further research. The three separate lines do show, however, that discussing any trend in ΔT_b^{37-19} really depends on which years are chosen as a start and end point. What is most important is that there is in fact variation in ΔT_b^{37-19} over the 30 year time series. If there was little change in ΔT_b^{37-19} over the years, then it would clearly not be sensitive to the annual differences observed in the in-situ SWE. Before the ΔT_b^{37-19} is compared to in-situ SWE, the third assumption must be addressed to determine if seasonal differences in ΔT_b^{37-19} are influenced by landscape or terrain. The most likely example of this is a potential systematic influence on Tb from lake ice (Rees et al., 2006). The spatial extent of lakes does not change from year to year; however, as ice grows from the beginning of a season to the end, there could be a corresponding change in Tb. If lake ice growth is the dominant influence, then there should be a good correlation between ΔT_b^{37-19} and the spatial distribution of lakes.

5.4. Spatial Analysis of Tb

5.4.1 Introduction

The following section addresses the third assumption:

- 3- The Tb at 19 and 37 GHz are not systematically influenced by landscape or terrain.

Different spatial patterns in SWE from year to year are expected. Snow fall amounts can be different throughout the region due to seasonal weather patterns, and snow depths can vary due to spatial differences in wind speed and direction. On the other hand, there could be spatial patterns of SWE which seem to re-occur from year to year. For example, when comparing 18 seasons of data across the prairies and boreal forest, locations where deep snow and/or dense vegetation were present, Derksen et al. (2003) found that the agreement between in-situ SWE and Tb decreased significantly, and there was little inter-annual variability in SWE retrieval. This precipitated the development of new algorithm approaches for estimating SWE in these areas. Moreover, Derksen and Mackay (2006) investigated the dominance of an inter-annually consistent band of high SWE between the boreal forest and tundra. The third assumption outlined at the beginning of this chapter is directed towards addressing these issues throughout the study region. With the absence of boreal type forests and mountainous topography, the assumption made in Chapter 2, as pointed out by Derksen et al. (2003), hypothesized by Rees et al. (2006) and further discussed by Derksen et al. (2009), is that lake cover is the most likely candidate to have a systematic influence on seasonal ΔT_b^{37-19} .

5.4.2. Spatial Principal Component Analysis

To look for dominant spatial patterns in the ΔT_b^{37-19} data, a principal components analysis (PCA) was used. PCA is a statistical technique which mathematically transforms large amounts of data into a set of uncorrelated components to summarize the majority of original information (Shaw, 2003). Moreover, PCA is a common method used in snow climatology to isolate spatially or temporally coherent regions of snow cover extent, SWE or snow cover duration (Leathers and Luff, 1997, Frei et al., 1999, Frei and Robinson, 1999, Derksen et al., 2000d, Pivot et al., 2002).

The average April 1 to April 10 ΔT_b^{37-19} for the 40 regional EASE grid cells over the 1979 to 2008 time series were subjected to a rotated principal component analysis in order to identify the dominant spatial patterns. The varimax rotation method was chosen as it has the advantage of maximizing variance between each component and the original time series (Horel, 1981). This helps to increase the discrimination among the component loadings, making them easier to interpret (Richman, 1986). A standardized PCA (correlation matrix) was used as opposed to an unstandardized PCA (covariance matrix) because it is commonly preferred for climate and snow cover applications (Derksen et al., 2000d). Moreover, covariance is sensitive to the unit and scale of measurement while correlation is standardized to scale by dividing the covariance by standard deviation (Field, 2005).

Eigenvalues are an output from the PCA with give precise information on the relative importance of each axis. The first component always has the highest eigenvalue followed by the second. Eigenvalues for each PC are created and often used as a threshold for determining which are most useful for interpreting the data (Shaw, 2003). By graphing eigenvalues for each factor (scree plot), the relative importance of each factor can be determined. Moreover, eigenvalues were converted into percent total variance explained and plotted to assist in determining how many factors should be considered (Figure 5.5).

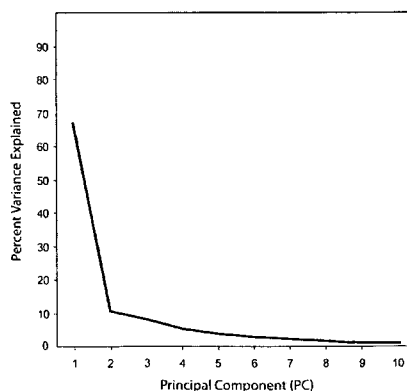


Figure 5.5. The percent variance explained by the first 10 components

Figure 5.5 shows that the first component (PC 1) explains 66 % of the total variance in ΔT_b^{37-19} over the 30 year time series, while the second component (PC 2) explains only 10 %. The variance explained diminished after the second component. Plotting eigenvalues or variance explained is useful but not the only step in selecting the number of factors. Kaiser (1960) suggests retaining all factors with eigenvalues over 1. Although this criterion is sometimes considered too strict, the PCA of ΔT_b^{37-19} produced four components whose eigenvalues are over 1. These four components explain 88 % of the total variance in the spatial patterns of ΔT_b^{37-19} over the entire time series.

This high percent explained by PC 1 suggests that there could be a dominant spatial pattern in the ΔT_b^{37-19} from season to season. To investigate the relationship between the components and the original data, the component loadings can be examined. A high positive loading indicates that the spatial pattern of ΔT_b^{37-19} in the original data is similar to that being summarized by the component. A negative loading indicates an inverse spatial pattern between the original data and the component. Loadings near zero mean there is little similarity between the original data and the component (Field 2005). The component loadings were plotted for the first four components (Figure 5.6)

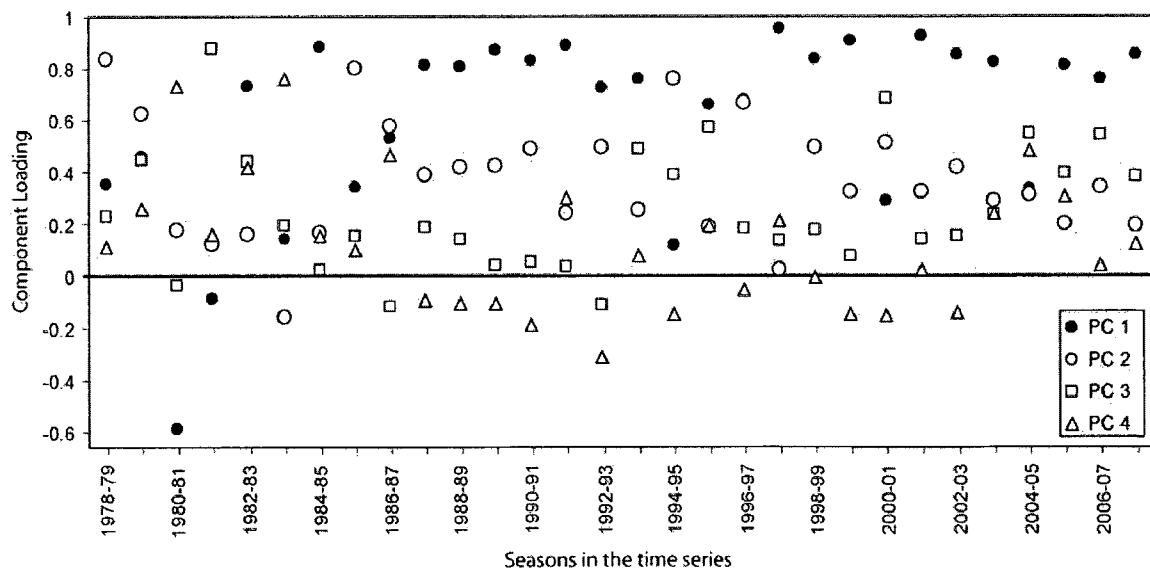


Figure 5.6. Component loadings for the PCA of April 1 to April 10 ΔT_b^{37-19} in 41 EASE grid cells over a 30 year time period

The component loading patterns in Figure 5.6 further suggest that PC 1 is summarizing a dominant spatial pattern in the time series. PC 1 loads most heavily into most seasons after 1987-88. The only years not loaded dominantly into PC1 after 1988 are 1994-95 (PC 2), 1996-97 (PC 1 and PC 2), 2000-01 (PC 3), and 2004-05 (PC 3). The dominant loading into PC 1 suggests there is little spatial variability in ΔT_b^{37-19} between different EASE grid cells, especially after 1988. This suggests that the spatial pattern of ΔT_b^{37-19} is linked to spatially consistent features such as lakes or land cover.

To determine if lakes have a systematic spatial influence, a PCA was run using EASE grid lake fraction determined from 1:250 000 scale NTS topographic maps. The analysis produced similar results as the first, however, included five PCs with eigenvalues over 1. PC 1 still explained most of the variance at 63% while PC 2 explained 11 %. The component loadings were plotted for the first five components (Figure 5.7).

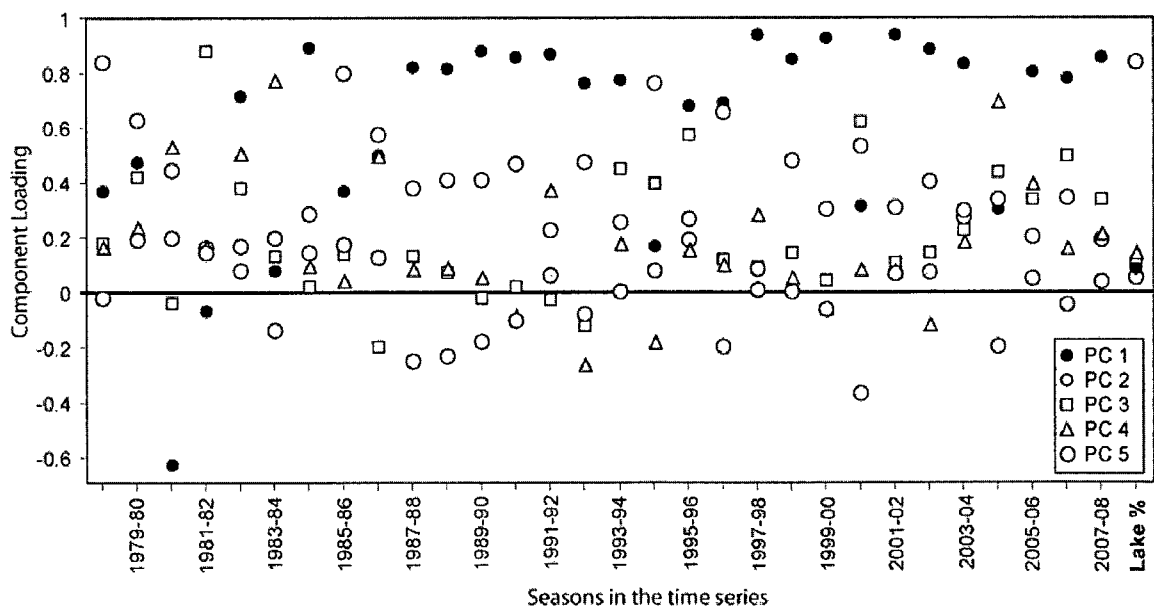


Figure 5.7. Component loadings for the PCA of April 1 to April 10 ΔT_b^{37-19} and lake cover fraction in 41 EASE grid cells over a 30 year time period

The loading pattern remains the same as in Figure 5.6 except the final point on the x-axis shows the loadings of the EASE grid lake fraction (Lake %). Interestingly, lake fraction does not have a high component loading in PC 1. This suggests that the spatial distribution of EASE grid lake fraction is not well correlated to the dominant spatial pattern of ΔT_b^{37-19} summarized by PC 1. However, lake fraction has a high component loading in PC 5, which is not related to any of the ΔT_b^{37-19} . This again shows that in most cases, lake fraction is not well spatially correlated to ΔT_b^{37-19} . If lake fraction was systematically influencing end of season ΔT_b^{37-19} , we would expect it to be more positively loaded into the components, especially PC 1.

Although the PCA suggests that lake fraction does not have an influence on end of season ΔT_b^{37-19} in these 41 EASE grid cells, it does not imply this influence is temporally static. Derksen et al. (2009) show how the influence of lakes on 19 and 37 GHz changes throughout a winter season. This makes sense given the penetration depth at the frequencies being used. At 37 GHz, the depth of emission can range from 8 to 80 cm in dry snow (Chang and Foster, 1992). Assuming a maximum 80 cm, it is likely that over the course of a season as both snow and ice accumulate, the dominant source of 37 GHz emission changes (Figure 5.8).

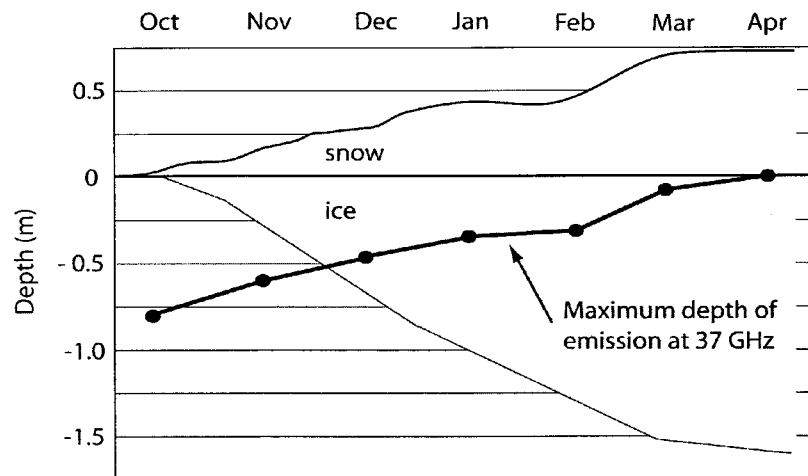
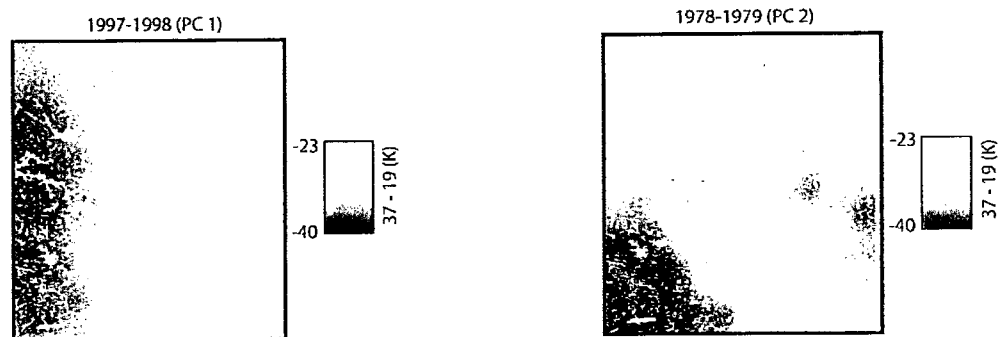


Figure 5.8. The idealized depth of emission at 37 GHz and seasonal evolution of snow and ice in the tundra

Figure 5.8 shows how the depth of emission can change throughout a season due to seasonal variability in snow and ice cover properties. As such, at the end of the season, lake ice is not contributing much to emission at 37 GHz. The implications of the theoretical depth of emission at 37 GHz will be discussed further in Section 5.5.

The PCA was useful for generalizing patterns in ΔT_b^{37-19} throughout the time series; however, component loadings are not useful for visualizing the spatial patterns. It is clear that PC 1 is the dominant spatial trend; therefore, the year that loads highest into that component would be representative of the spatial pattern being summarized. In order to visualize the difference between components, the years which had the highest loadings were mapped. EASE grid data can be displayed as a grid of 25 x 25 km cells with a single value for each cell. However, for simplicity of display and comparison, a smoothed surface was generated using inverse distance weighting (IDW) interpolation of the EASE grid centroid values (Figure 5.9).



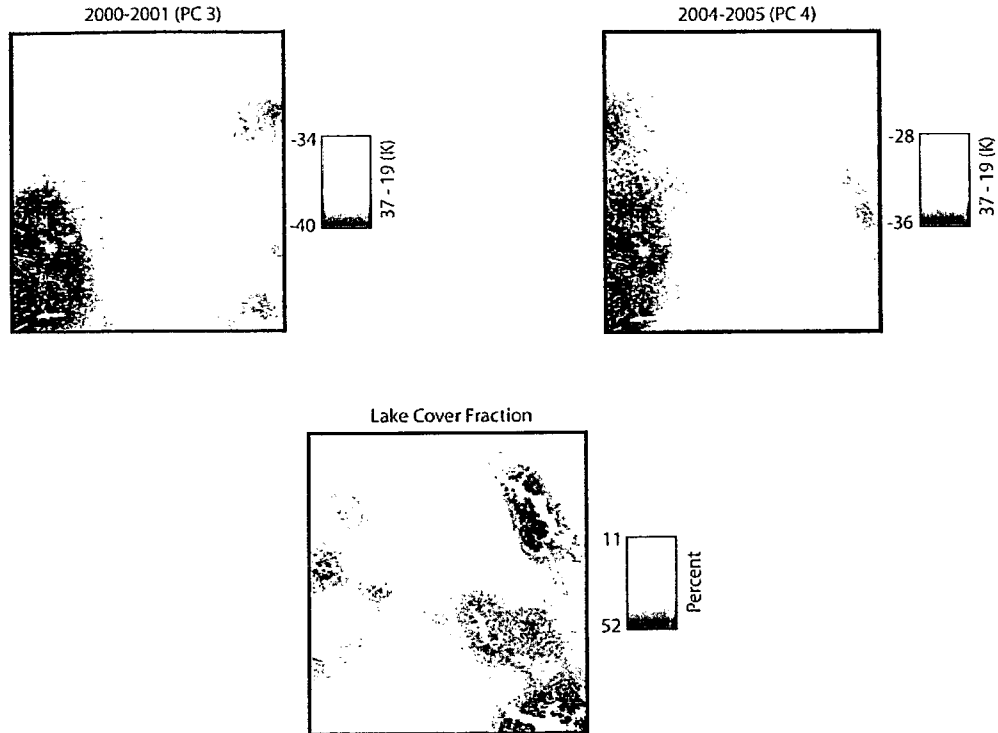


Figure 5.9. Maps of the seasons with the highest loading in each PC

The spatial pattern of ΔT_b^{37-19} is clearly unique between the different components. The map of PC 1 (1997/98) shows a very distinct west to east longitudinal gradient in ΔT_b^{37-19} . The lowest values ($-39 \Delta T_b^{37-19}$) are located to the west, and there is a longitudinal gradient eastward to higher values ($-23 \Delta T_b^{37-19}$) in the east. This pattern is somewhat different than the other PCs shown in Figure 5.9 and very different than the lake cover fraction. However, consistent to PC 1, PC 2, and PC 3 is that the lowest ΔT_b^{37-19} is located in the southwest corner of the domain. These spatial patterns and the longitudinal gradient in PC 1 suggest that there is an inter-annually consistent systematic influence on ΔT_b^{37-19} . If the pattern is not related to lake fraction then it could be related to land cover or to differences in snow accumulation. To investigate a possible relationship between ΔT_b^{37-19} and land cover, the Natural Resources Canada (NRCan) AVHRR 5 km land cover classification for the eastern NWT was mapped along with PC 1 and PC 2 (Figure 5.10).

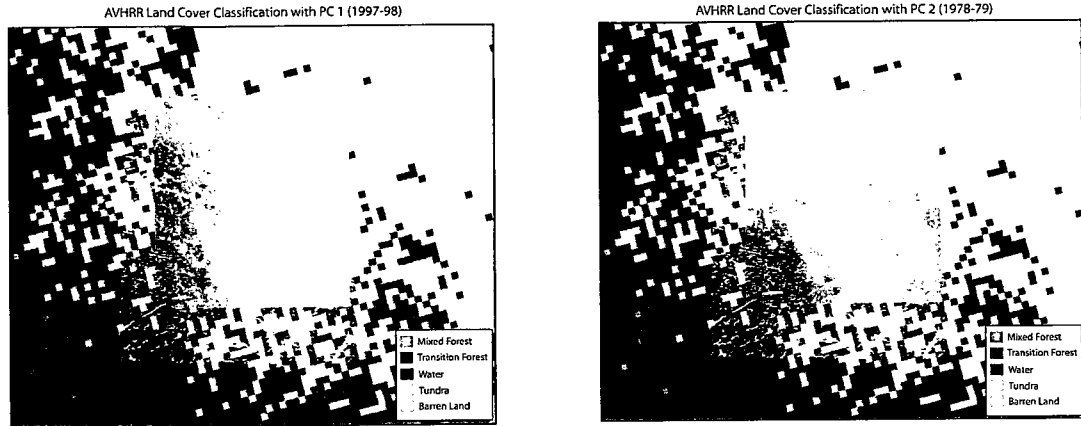
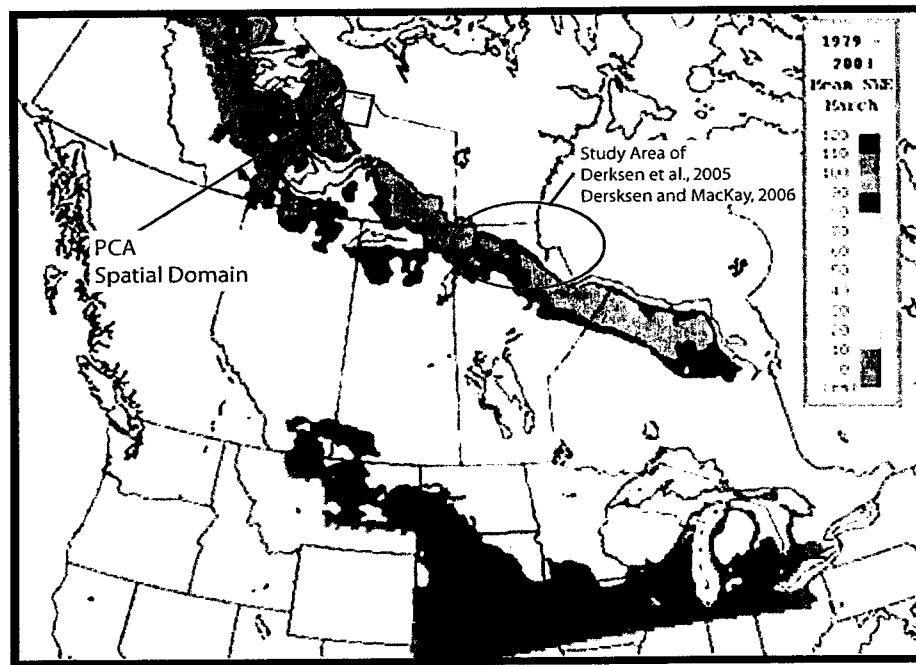


Figure 5.10. The ΔT_b^{37-19} of 1997-98 (PC 1) and 1978-79 (PC 2) over the NRCan AVHRR land cover classification

Figure 5.10 suggests that the spatial pattern summarized by PC 1 could in fact be a product of the change in land cover from transitional forest to tundra. The lower values to the west correspond roughly with the edge of the transitional forest class. This pattern matches with similar inter-annually consistent spatial pattern of SWE seen in the boreal to tundra transition of northern Manitoba (Derksen et al., 2005). The spatial domain of Figure 5.10 is highlighted with this SWE band (Figure 5.11).



**Figure 5.11. The inter-annually consistent Canadian SWE band
Adapted from Derksen and Mackay 2006**

Derksen and MacKay, 2006, characterize the SWE band primarily by satellite passive microwave retrievals, but they describe how it is also evident in an independent reanalysis of surface observations combined with a simple snowpack model by Brown et al., 2003. What is not clear, however, is whether or not the pattern in ΔT_b^{37-19} shown in the PC 1 is due to the change in land cover or to changes in snow cover as a result of differences in land cover. Hence, the transition in ΔT_b^{37-19} cannot be confirmed without other sources of data.

5.4.3. Spatial PCA on Sub-set of Data

The domain for the spatial analysis was reduced to include only 27 EASE grid cells with predominantly tundra or barren land cover. The objective was to run a PCA analysis again on a sub-set of data to minimize the influence of this land cover transition. For this analysis, lake fraction was again included. Longitude was also added to see if there are similar east-west trends in the second PCA. The percent variance explained by the first 10 components was plotted (Figure 5.12).

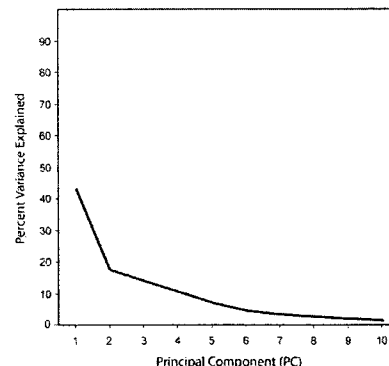


Figure 5.12. The percent variance explained by the first 10 components

The variance explained by the first component was 42%, which is much less than the over 60% explained by the first component in the original PCA (Figure 5.5). This suggests that the first component in the new PCA may not be as dominant throughout

the time series. To compare the components with the original data, the loadings for the first six components were plotted (Figure 5.13).

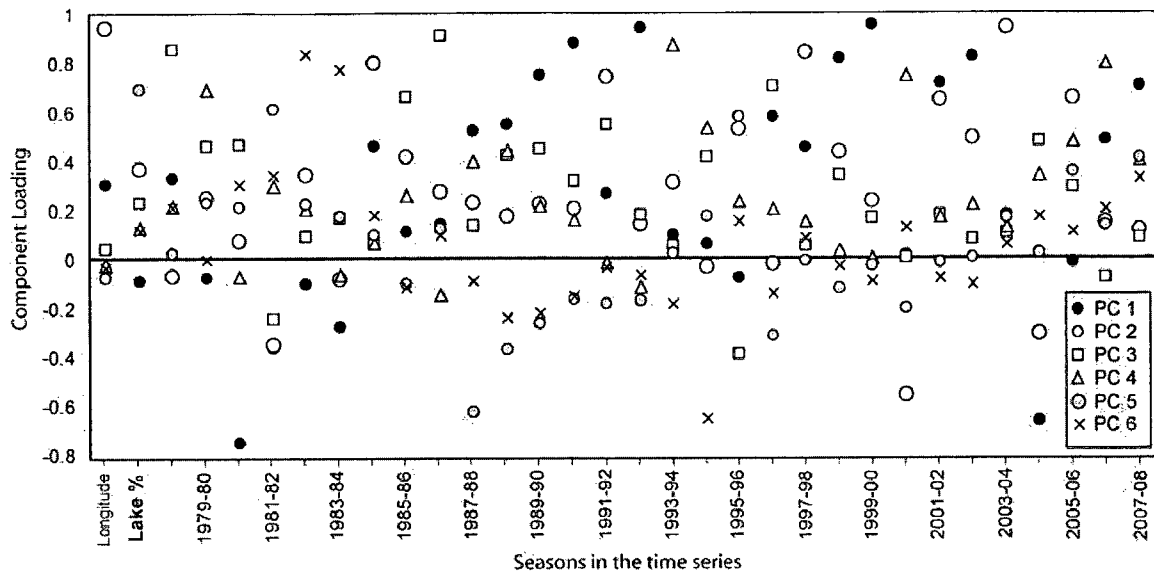


Figure 5.13. Component loadings for the PCA of April 1 to April 10 ΔT_b^{37-19} and lake cover fraction in the subset of 27 EASE grid cells over a 30 year time period

The first principal component loads heavily into far fewer seasons than in the original PCA and is not well correlated to longitude or lake fraction. However, longitude is loaded heavily into the second component. This suggests that there may be systematic patterns in ΔT_b^{37-19} , correlated to longitude, in any year loaded heavily into PC 2. The fifth component again reflects the pattern of lake fraction, however, there are only two years which are predominantly loaded positively into PC 5 (1981-82 and 1995-96). Component six is interesting in that it reflects a spatial pattern of ΔT_b^{37-19} seen in only two seasons (1982-83 and 1983-84). It is evident from Figure 5.13 that changing the spatial domain from 41 EASE grid cells across different land cover types to a subset of 27 with predominantly tundra land cover has changed the distribution of component loadings. In order to visualize the difference between the components, the seasons which had the highest loadings for the first four components were mapped (Figure 5.14).

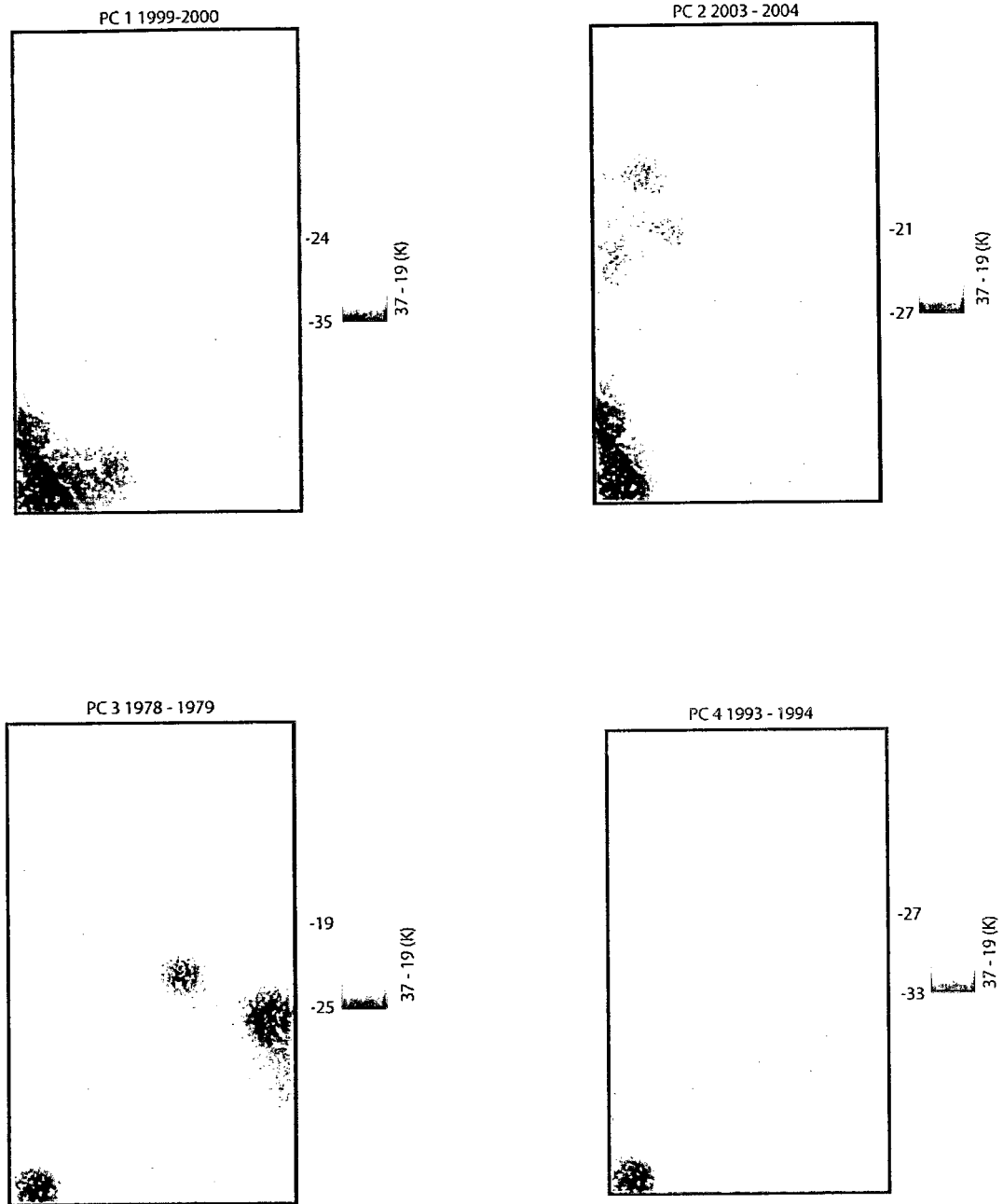


Figure 5.14. Maps of the seasons with the highest loading in each PC

The longitudinal trend in ΔT_b^{37-19} seen in the original PC 1 (Figure 5.9) is no longer present in any of the first four PCs using the sub-set of EASE grids. However, the southwest corner of the new domain has a consistently lower ΔT_b^{37-19} than any other area. This is the dominant spatial pattern in all of the first four PCs shown in Figure 5.14.

PC 1 shows the greatest range in ΔT_b^{37-19} within the image, from -24 to -35, while the other three images show a range of only 6 K. However, by taking the subset of EASE grids, the range in ΔT_b^{37-19} is much less than in the original PCA. The lowest ΔT_b^{37-19} seen in the southwest corner of the new domain could still be a product of a change in land cover. The AVHRR landcover classification was plotted with the first two components of the subset PCA (Figure 5.15).

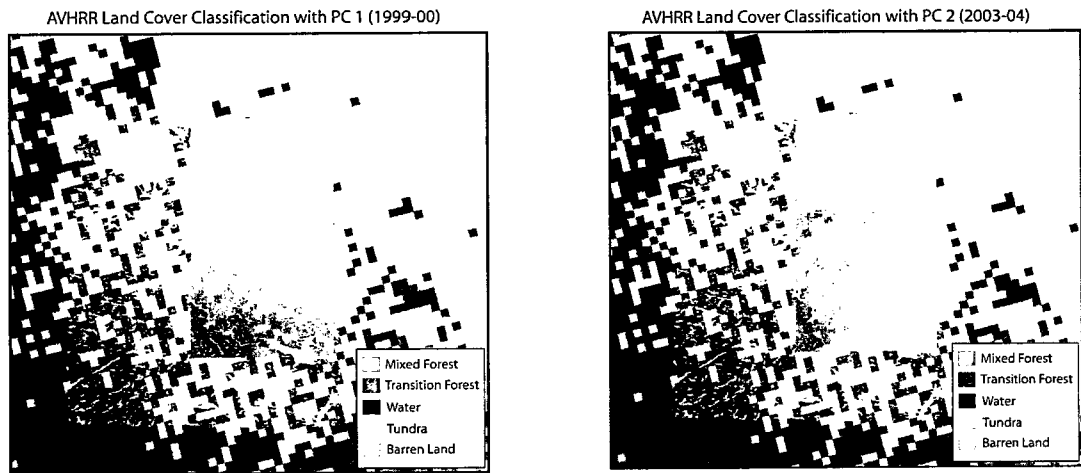


Figure 5.15. The ΔT_b^{37-19} of 1999-00 (Subset PC 1) and 2003-04 (Subset PC 2) over the NRCAN AVHRR land cover classification

Figure 5.15 suggests that even in the subset of EASE grids, there could still be a relationship between ΔT_b^{37-19} and variability in land cover. However, little transition to forest was observed in this area during various flights in and out of the Daring Lake Camp. Despite the apparent influence of land cover in the south-west corner, the subset of ΔT_b^{37-19} data exhibit more spatial variability from year to year than the original dataset. This is evident in the factor loadings as well as in the percent variance explained plots which show much less variance explained for PC 1 in the subset of data. It is important to note that neither the original nor the subset PCA suggest that lake fraction is strongly spatially correlated to the end of winter ΔT_b^{37-19} . Furthermore, without snow cover data, the gradient in ΔT_b^{37-19} across the study domain cannot be linked entirely to differences in land cover. Since snow data for this study were collected only in one EASE grid cell, it

is also difficult to compare regional ΔT_b^{37-19} to snow cover. However, a trans-continental transect from Fairbanks Alaska to Baker Lake NWT (SNOWSTAR) was conducted in 2007 as described in Derksen et al. (2009). Although not entirely coincident with the domain used in this study, snow surveys taken along this transect do not show differences in SWE to help explain the observed differences in ΔT_b^{37-19} seen in PC 1. However, the transect was conducted in the 2006-07 season which has the highest component loading in PC 4. Figure 5.14 shows that in PC 4 there was little difference in ΔT_b^{37-19} except in the southwest corner which was not on the transect route. Unfortunately, no similar datasets exist for other seasons.

It is clear from both the spatial and temporal analysis that there are changes in ΔT_b^{37-19} within and between different seasons. Moreover, lake fraction does not seem to have a systematic influence on ΔT_b^{37-19} ; however, land cover may have a profound influence in the transition from forest to tundra.

5.5. Comparison of Satellite Tb to in-situ SWE

5.5.1. Introduction

The following section addresses the fourth assumption:

4- The difference between 19 and 37 GHz can be used to estimate SWE

Several research projects have exploited the good correlation between increasing snow depth and decreasing microwave emission due to snowpack volume scatter. As summarized in Chapter 2, early work showed that shorter wavelength (~37 GHz) emission was more sensitive to the structure and condition of the snow, while longer wavelength emission (~19 GHz) was affected more by underlying soil condition (Foster et al., 1980). The first operational and widespread algorithms developed to estimate SWE from satellite passive microwave data were those of Chang et al. (1990) and Goodison and Walker (1995).

The algorithm described by Goodison and Walker (1995) was developed by Environment Canada (EC) for non-forested, prairie environments and utilizes the 19 and 37 GHz vertically polarized channels:

$$\text{SWE (mm)} = -20.7 - 49.27[(\text{Tb}37\text{V} - \text{Tb}19\text{V})/18]$$

The Chang algorithms for SWE and snow depth have been applied hemispherically and utilize the 19 and 37 GHz horizontally polarized channels:

$$\text{SWE (mm)} = 4.8 (\text{Tb}19\text{H} - \text{Tb}37\text{H})$$

$$\text{Snow Depth (cm)} = 1.59 (\text{Tb}19\text{H} - \text{Tb}37\text{H})$$

The structure of the algorithms is very similar in that they were developed using the difference between lower frequency 19 and higher frequency 37 GHz data. The EC algorithm describes an empirically derived linear relationship between SWE and ΔTb^{37-19} while the Chang algorithm was derived using theoretical relationships between ΔTb^{37-19} and SWE. The Chang algorithm assumes a snow density of 0.300 g/cm^3 and is intended for snow depths under one metre.

Neither the Chang or EC algorithms were derived for nor have been properly parameterized for tundra environments. However, the use of ΔTb^{37-19} began with these algorithm approaches and has been embraced in countless other studies. Hence, comparing in-situ observations to ΔTb^{37-19} is an obvious place to start.

5.5.2. Comparison of in-situ SWE to ΔTb^{37-19}

The mean ΔTb^{37-19} from April 1 to April 10 from the AMSR-E sensor were compared to the six years of in-situ SWE data described in Chapter 4 as well as the SWE data from the preliminary survey conducted in 2003 (described in Chapter 3). Vertically polarized 19 and 37 GHz data were used to minimize the effect of any surface ice lenses which may be present (Rees et al., 2010). The ΔTb^{37-19} were plotted against the seven years of in-situ SWE (Figure 5.16).

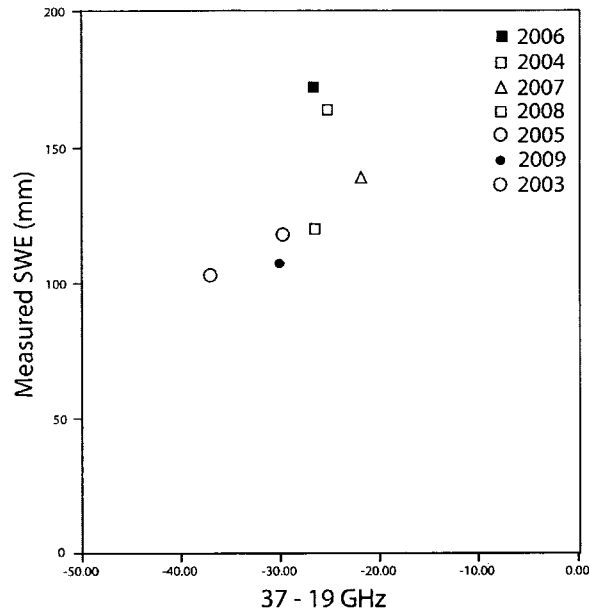


Figure 5.16. In-situ SWE plotted against corresponding April 1 to April 10 mean ΔTb^{37-19}

The plot of ΔTb^{37-19} and in-situ SWE shows some interesting patterns. Below 140 mm, the points show a positive linear relationship. As the ΔTb^{37-19} increases so does the in-situ SWE. Above 140 mm, the relationship is linear but in the opposite direction (although there are only three points in the plot). The inflection about 140 mm is interesting because it corresponds with the theoretical and observed reversal in 37 GHz with increasing SWE (see Section 2.4.2.2). Below and above 140 mm, the scatter of points is quite linear, but together the points resemble a quadratic curve. A curve estimation regression analysis was performed using SPSS, and the resulting coefficient of determination (r^2) was found to be 0.89. This means that a quadratic function can be fitted to the points and explains 89 percent of the variability in the data ($p < 0.05$). The function is as follows:

$$SWE = \frac{-2.02 \pm \sqrt{4.08 - (-0.028(-169.08 - Tb_{37-19}))}}{-0.014}$$

It is interesting that the observed SWE vs. ΔT_b^{37-19} can be described by the curve; however, the shape of the curve does not compare favorably to the expected linear relationship between ΔT_b^{37-19} as developed by EC and Chang. The quadratic function was plotted along with the linear relationships of SWE estimated using the EC algorithm (Figure 5.17).

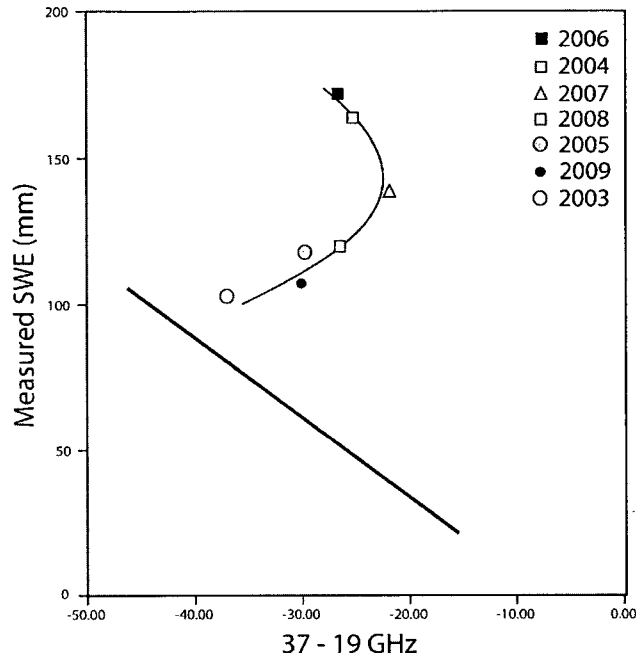


Figure 5.17. The quadratic function between ΔT_b^{37-19} and in-situ SWE plotted with the linear relationship using the Goodison algorithm

Figure 5.17 clearly shows the difference between the quadratic function derived and the EC linear relationship. The main concern is not that the points do not fit directly on the EC line, but that below 140 mm SWE they show a completely opposite relationship. The linear EC relationship suggests that as the SWE increases, the difference between 19 and 37 GHz should get larger (a lower ΔT_b^{37-19}). The quadratic shows that below 140 mm SWE, as the SWE increases, the difference between 19 and 37 GHz decreases. Beyond 140 mm SWE, the quadratic shows a relationship in the same direction as the EC line.

The inverse relationship between the expected EC linear and in-situ SWE derived quadratic is quite pronounced. It is possible that the difference between the relationships is a product of how satellite scale in-situ SWE is being defined. A single value does not account for any variability in sub-grid SWE. However, even when the variability in SWE described in Chapter 4 is considered, it is difficult to fit the data to a slope similar to the EC algorithm. From Chapter 4, a coefficient of variation (CV) of 0.40 was considered and plotted with each mean in-situ SWE against ΔT_b^{37-19} (Figure 5.18).

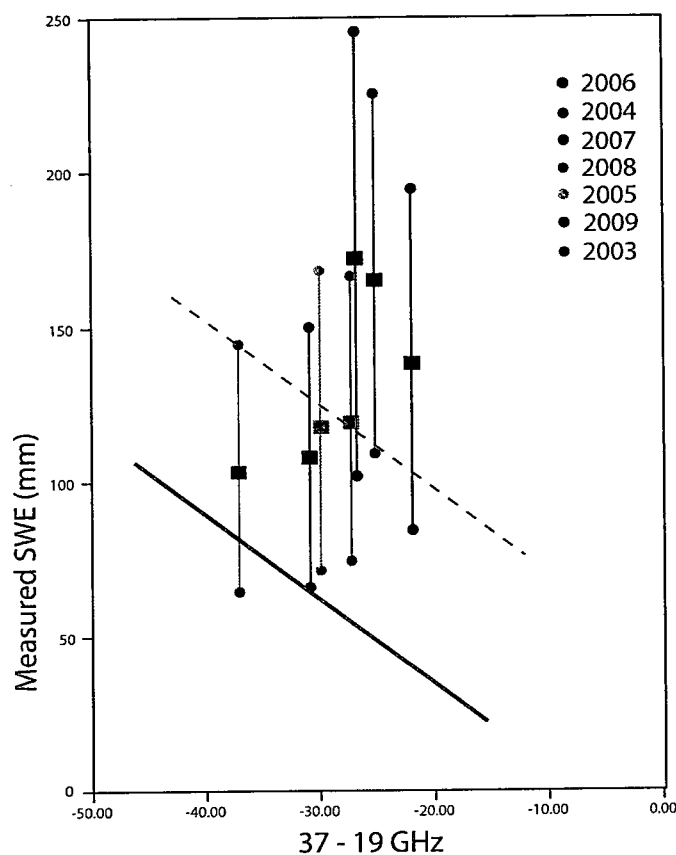


Figure 5.18. In-situ SWE plotted with corresponding April 1 to April 10 mean ΔT_b^{37-19} considering the 0.40 CV in SWE

The dashed line in Figure 5.18 shows that a slope similar to the EC is possible if the variability in SWE is considered. However, given the way in which the spatially weighted mean SWE are calculated, it is not likely that the dashed line represents the true relationship between SWE and ΔT_b^{37-19} . Figure 5.18 does raise an interesting point

about how grid cell SWE is defined based on sub-grid measurements. Moreover, it also raises the issue of what proportional effect sub-grid snow and terrain have on EASE grid scale Tb. The SWE used in Figure 5.18 is calculated using a spatially weighted mean. This method weights EASE grid SWE based on the spatial proportion of sub-grid SWE in defined terrain categories. On the other hand, EASE grid Tb is assumed to be an equal product of emission from all snow cover, terrain and landscape features. However, this may not be the case as certain features may have a disproportionate influence on EASE grid Tb. These issues will be investigated in more detail in Chapter 6.

The relationship between ΔT_b^{37-19} and in-situ SWE can be investigated further by looking at the behavior of the individual 37 GHz and 19 GHz frequencies. To produce a linear relationship similar to the EC line, we would expect the 19 GHz Tb to be generally similar between years and 37 GHz Tb to be lower for the years with higher SWE. The seasonal evolution in 19 and 37 GHz for the 2003 to 2008 was plotted in Figure 5.2 and shows that each year there is relatively little change in the 19 GHz compared to a large drop in 37 GHz Tb. However, the end point (April 1 to April 10) of 37 GHz Tb is not the same from year to year. The differences in Tb between seasons and in-situ SWE observations are compared in Table 5.1.

Table 5.1. Comparison of 19 and 37 GHz Tb for April 1 to April 10 along with in-situ SWE observations

	2002/03	2003/04	2004/05	2005/06	2006/07	2007/08	2008/09	Min	Max	Range
19 GHZ	240	246	246	248	246	240	242	240	248	8
37 GHZ	203	222	216	222	224	214	212	203	224	21
ΔT_b^{37-19}	-37.0	-25.2	-29.6	-26.7	-21.7	-26.7	-30.0	-37.0	-21.7	15.3
SWE	102	164	117	171	138	119	106	102	171	69.0

Table 5.1 shows that the years with the greatest amount of SWE (2003/04 and 2005/06) have the lowest ΔT_b^{37-19} . In these years, the 19 GHz Tb is quite similar to other years; however, the 37 GHz Tb is much higher. The years with the lowest SWE (2002/03, 2004/05 and 2008/09) had the lowest 37 GHz emission and the lowest ΔT_b^{37-19} .

5.5.3. Resolving Uncertainty in SWE vs ΔT_b^{37-19}

It is clear from Figure 5.2 and Table 5.1 that the expected relationship of lower 37 GHz for greater SWE, is not present in this dataset. It would seem from the data that the greater the SWE the higher the 37 GHz T_b . As outlined in Chapter 2, microwave emission measured by spaceborne sensors comes from the snow volume and from the underlying ground. As such, T_b at 37 GHz will decrease with increasing snow grains because more ground and snow emission is scattered away from the sensor. However, at a certain threshold of SWE depth there is saturation of the scattering and self emission from the snowpack. This can occur in certain snowpacks at as low as 30 cm in snow depth given certain grain size conditions (Sturm et al., 1993). Usually T_b will decrease with snow grain size as larger grains are more effective at scattering and absorbing emitted energy (Chang et al., 1997). Hence, grain size can have a strong influence on T_b independently of SWE. The theoretical extent to which grain size influences T_b at 18 and 37 GHz is shown in Figure 5.19.

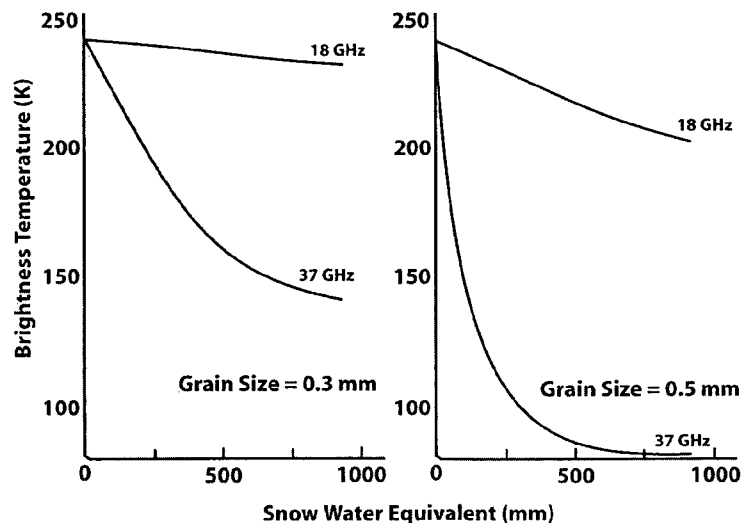


Figure 5.19. Calculated brightness temperatures versus SWE for horizontally polarized data at 50° incidence angle (modified from Chang et al., 1987)

The influence of grain size shown in Figure 5.19 is quite profound. For the depth of SWE observed in the study area, a grain size shift from 0.3 mm to 0.5 mm would result in a difference of ~ 65 K at 37GHz. It is important to note that Figure 5.19 from Chang (1987) does not consider the threshold at which 37 GHz Tb reverses due to saturation and self emission. Field observations show that the dominant grain size in the snowpack from year to year is 0.5 mm. There is increasing grain size in indurated layers and up to 1 cm grain size in basal depth hoar. However, as described in Chapter 4, the traditional basal depth hoar layer usually occupies a relatively small fraction of the snow pack in each season and develops mainly between vegetation outcrops or tussocks. Consequently, there were not large differences in grain size observed between years. However, with site to site differences and the qualitative nature of grain size descriptions, it is difficult to infer any statistically significant difference in grain size from high snow to low snow years. The biggest difference between years seems to be in the depth of SWE rather than in stratigraphy.

Lower ΔT_b^{37-19} for the high snow years may be due to the reversal in 37 GHz described in Section 2.4.2.2. The reversal in 37 GHz Tb, shown in Figure 2.5, suggests that Tb follows a decreasing curve up to about 150 mm then begins to increase. If this were the situation occurring in 2003/04 and 2005/06, we would expect the seasonal evolution of 37 GHz Tb to follow a similar pattern. The 37 GHz Tb for 2003/04 and 2005/06 were plotted in order to examine their evolution throughout the season (Figure 5.20).

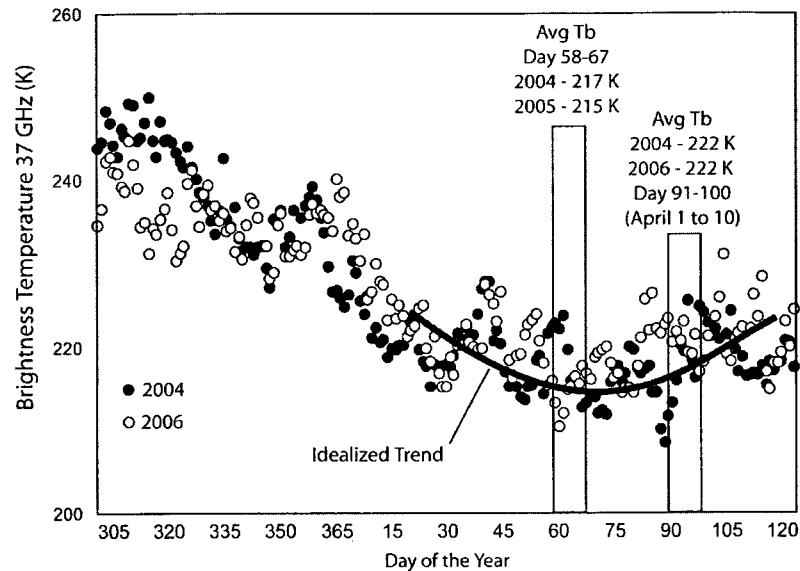


Figure 5.20. Seasonal evolution in 37 GHz from Nov 1 to April 30 in 2003/04 and 2005/06

Figure 5.20 does show a slight reversal in 37 GHz Tb in both the 2003/04 and 2005/06 seasons. A minimum Tb is observed around days 58 to 67 rather than the days 91 to 100 used to compare with in-situ SWE in Figure 5.16. However, re-computing the ΔT_b^{37-19} using the day 58 to 67 Tb results in only a slight decrease from -25 to -26 K in 2004 and from -27 to -28 in 2006. Although the observed reversal in 37 GHz may impact eventual algorithm development, it does not help to explain why other seasons with lower SWE have much lower minimum Tb at 37 GHz and larger ΔT_b^{37-19} .

Perhaps the explanation lies somewhere in understanding how the emission from the underlying ground changes from years with high SWE to years with low SWE. The theoretical maximum depth of emission at 37 GHz is shown in Figure 5.8. As the snow depth increases, the emission from the ground and lake ice is muted by the overlying snow grains. As such, in thin snow years, the emission at 37 GHz should have a greater contribution from the underlying surfaces. Moreover, in shallower snow years, there is less overlying snow to mask the comparatively large grained basal depth hoar and to cover bare ground (Figure 5.21).

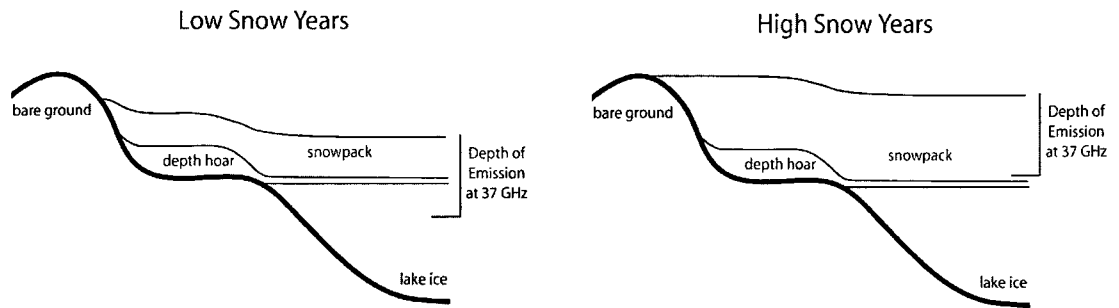


Figure 5.21. Theoretical depth emission at 37 GHz given different snow cover conditions

Figure 5.21 suggests that emission at 37 GHz should change with increasing snow depth. This moves the maximum depth of emission further away from the underlying ground and depth hoar. Hence, the low snow years would see lower T_b at 37 GHz if lake ice, depth hoar, and bare ground had the effect of decreasing emission. Moreover, higher snow years would see higher T_b at 37 GHz if decreasing lake ice, depth hoar, and bare ground had the effect of increasing emission. Verifying these relationships and their effect on ΔT_b^{37-19} is not possible using satellite scale data. To investigate these issues further, the multi-scale T_b data from airborne and ground based sensors described in Chapter 3 will be used.

CHAPTER 6: APPLICATION OF MULTI-SCALE PASSIVE MICROWAVE DATA

6.1. Introduction

Defining a relationship between in-situ SWE and satellite Tb data is a necessary step for operational algorithm development. However, as shown in Chapter 5, the relationship between measured tundra SWE and AMSR-E Tb does not follow expected patterns. Traditional techniques rely both on a decrease in 37 GHz Tb as SWE increases from the start of a winter season to the end of the season and on little change in 19 GHz Tb throughout the winter. These patterns of satellite Tb were evident for the study area data; however, the end of season ΔTb^{37-19} values relate to SWE differently than expected. Normally, a greater ΔTb^{37-19} relates to higher SWE, while a lower ΔTb^{37-19} relates to lower SWE. For the data analyzed in Chapter 5, the relationship between ΔTb^{37-19} and SWE was the opposite. Furthermore, Chapter 4 showed that there is considerable variability in sub-grid SWE across different types of terrain. The spatially weighted mean provides a generalized SWE value for comparison with Tb. However, there is little understanding of how microwave emission from sub-grid terrain and snow cover aggregate into EASE grid Tb.

These issues are difficult to resolve using coarse resolution satellite data as Tb is a function of more than just SWE. Within a single EASE grid, there are other snow and underlying ground parameters, outlined in Chapter 2, which contribute to Tb (Figure 6.1).

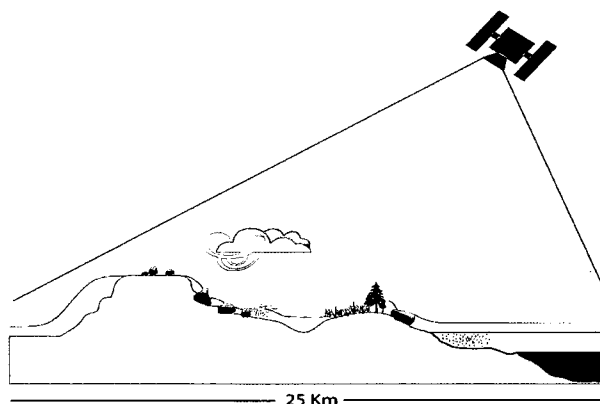


Figure 6.1. Contributions to end of winter satellite scale Tb

In order to improve the confidence in satellite SWE retrievals it is necessary to investigate the contribution of Tb from sub-EASE-grid scale features. The focus of this chapter is to address these issues through the use of Tb measurements acquired from ground based and airborne radiometers. To simplify the discussion, only vertically polarized data are used, and the airborne Tb data are categorized into either high, mid or low resolution based on aircraft altitude (Table 6.1).

Table 6.1. Relative resolution of aircraft and Tb data

Aircraft Altitude	Year	Resolution		Radiometer Footprint (m)		
				6.9 GHz	19 GHz	37 GHz
277 m	2005	High	Near width	66	45	45
	2008		Far width	81	52	52
			Depth	121	80	80
828 m	2005	Mid	Near width	197	135	135
			Far width	243	155	155
			Depth	363	241	241
2207 m	2005	Low	Near width	524	360	360
			Far width	646	414	414
			Depth	970	642	642
2757 m	2008	Low	Near width	655	450	450
			Far width	808	517	517
			Depth	1211	802	802

6.2. Application of High Resolution Tb Data

6.2.1. Comparing Tb Data to in-situ SWE

As outlined in Chapter 3, airborne Tb data were collected along east–west and north-south flight lines in both 2005 and 2008. In-situ snow depth, density and SWE measurements were recorded at sites along these lines. Ground based radiometer sites were situated in close proximity to the Daring Lake Camp (Figure 6.2).

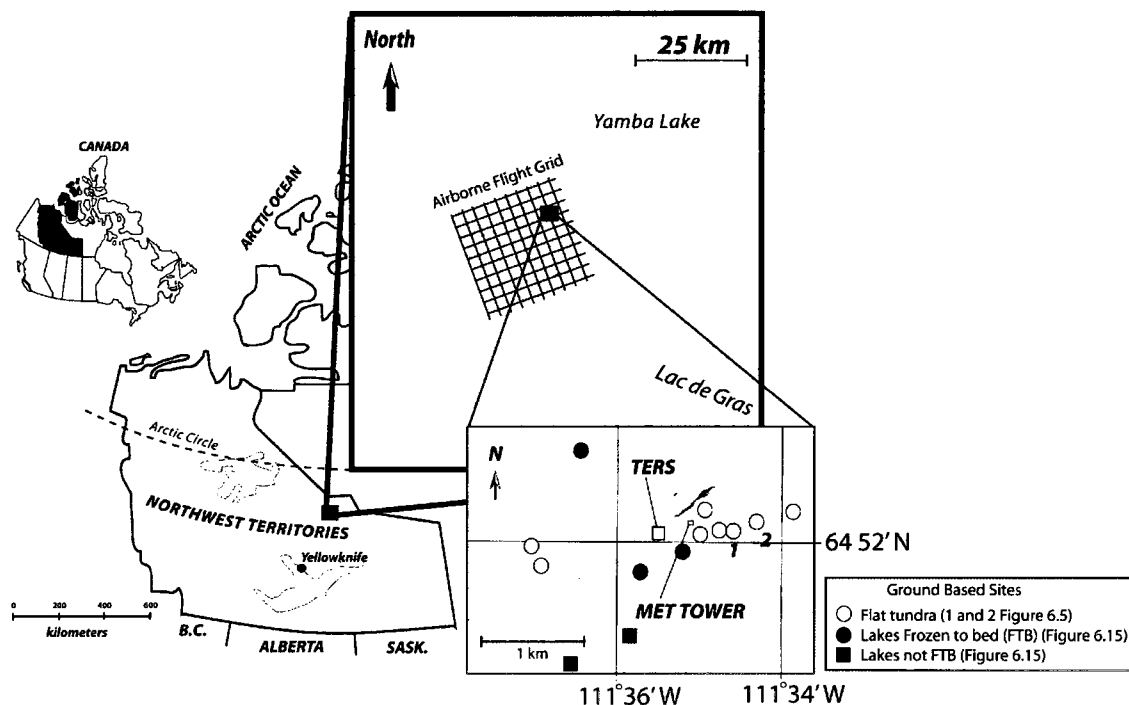


Figure 6.2. Flight line locations and ground based sites

A GIS database was created to link airborne radiometer data with spatially coincident in-situ snow measurements. For the 2005 and 2008 datasets, Tb data were related to in-situ sites which fell within an airborne footprint (Figure 6.3).

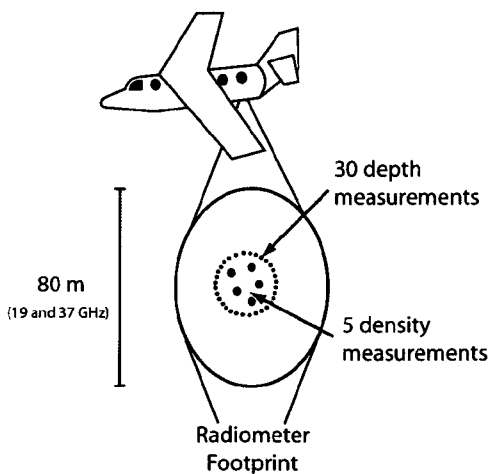


Figure 6.3. Relating Tb to in-situ snow measurements in the 2005 dataset

When an in-situ site was located outside of footprint areas, Tb was assigned from the closest footprint. However, this was done only when in-situ sites were less than 80 m from a footprint location and in areas of relatively homogenous terrain. At all sites, SWE were derived from the average of the 30 depth and the five density measurements. The STDEV and CV of SWE were also calculated for each site from the depth and density data. For the 2008 dataset, a similar approach was taken.

In 2008, there were also data collected in transects along the flight lines using an automated Magna Probe snow depth recorder. The Magna Probe facilitated the efficient collection of snow depths along flight transects. Depth data were collected at 5 m intervals with location information automatically recorded by the probe. Snow cores for density were measured on each transect at 100 m intervals in homogenous terrain and at shorter intervals when the terrain varied. Densities were derived from these snow cores and applied to the nearest snow depth measurement, in a similar terrain category to estimate SWE.

The comparison of Tb to SWE measurements was different using the Magna Probe data collected in 2008. Since the Magna Probe data were acquired along flight lines, multiple points were available within each airborne footprint. However, due to the in-flight motion, not all Tb footprints were aligned with pre-determined flight lines. In order to make the best comparison to Tb, only probe measurements which fell at least 10 m within an airborne footprint were used. Furthermore, only airborne footprints with at least 10 magna probe measurements were used (Figure 6.4).

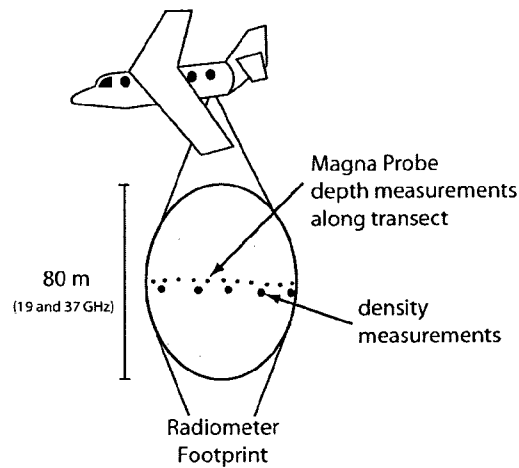
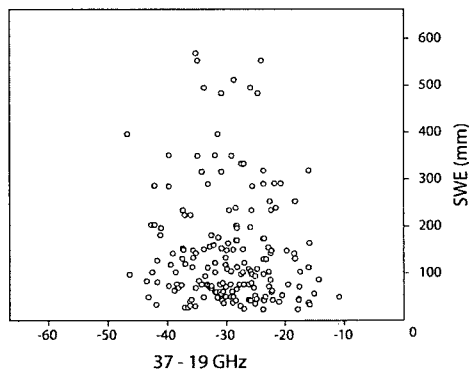


Figure 6.4. Relating Tb to SWE measurements using the 2008 Magna Probe dataset

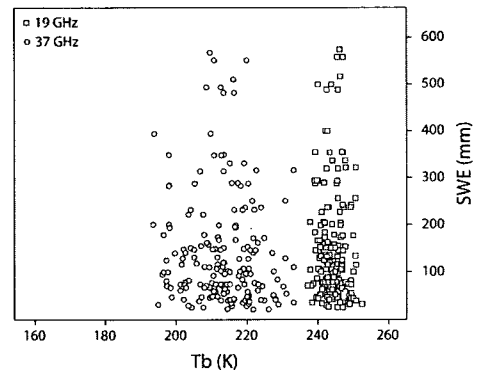
From the probe measurements, the average SWE was calculated for comparison with Tb. The STDEV and CV in SWE were also calculated for each footprint location.

For the ground based radiometer measurements, SWE was measured multiple times within the radiometer footprint. The average SWE was used for comparison with Tb. The Tb from high resolution aircraft and ground based data were plotted against SWE (Figure 6.5).

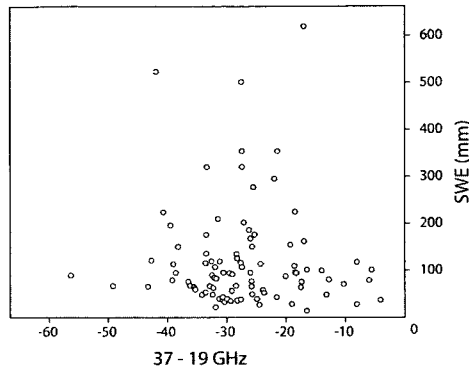
a) 2005 in-situ site SWE vs. ΔT_b^{37-19}



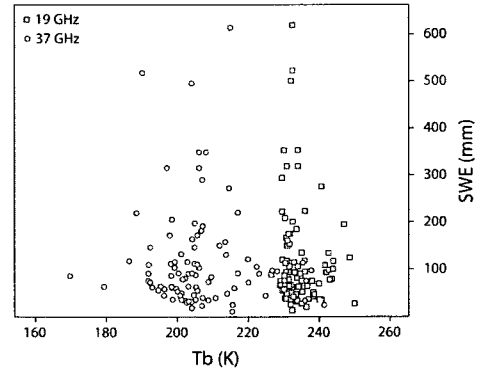
b) 2005 in-situ site SWE vs. 37 and 19 GHz Tb



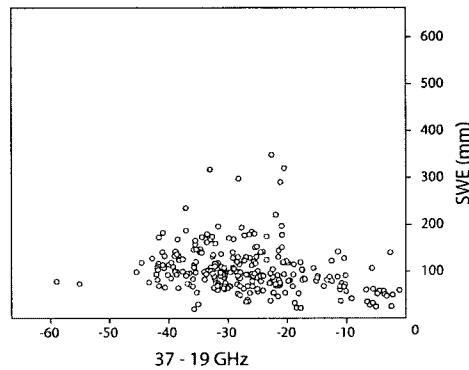
c) 2008 in-situ site SWE vs. ΔT_b^{37-19}



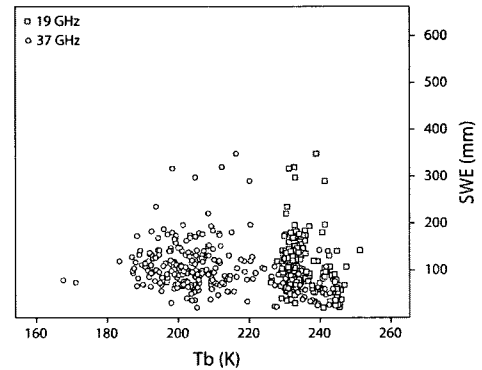
d) 2008 in-situ site SWE vs. 37 and 19 GHz Tb



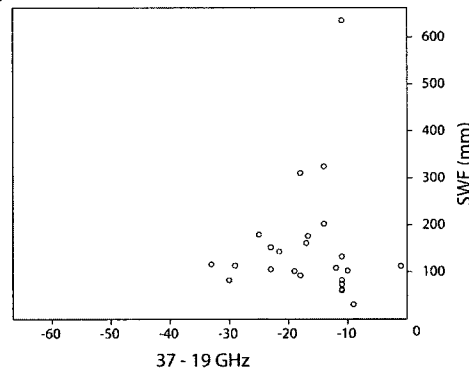
e) 2008 Magma Probe SWE vs. ΔT_b^{37-19}



f) 2008 Magma Probe SWE vs 37 and 19 GHz Tb



g) 2007 in-situ site SWE vs. ground based ΔT_b^{37-19}



h) 2008 in-situ site SWE vs. ground based 37 and 19 GHz Tb

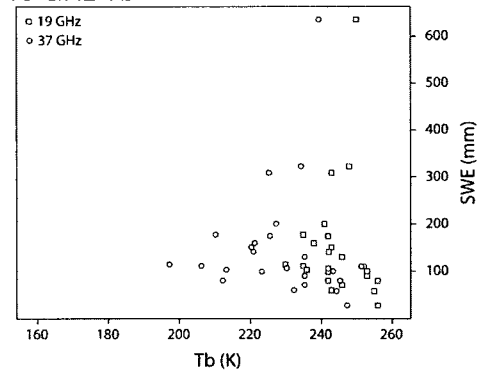


Figure 6.5. High resolution airborne and ground based Tb compared to in-situ SWE

Figure 6.5 shows no clear relationship between either 37-19 GHz or the individual 37 and 19 GHz Tb and SWE. The lack of relationship suggests either that there is little relationship between tundra SWE and Tb as a whole or that there are other

influences on Tb not being considered. Nonetheless, the Tb at 19 GHz SWE was consistently higher and had a lower range than the 37 GHz Tb. The 37 GHz Tb is more influenced by differences in snow cover properties and should be more variable. However, the 37 GHz Tb is clearly not linked to SWE as a large range of Tb were measured for a given SWE. No relationship at 37 GHz is obviously a primary reason that there are no strong relationships with ΔT_b^{37-19} . Figure 6.5e (2008 Magna Probe data) shows the most promising relationship between ΔT_b^{37-19} and SWE. There is a very weak negative relationship indicating that as SWE increases the ΔT_b^{37-19} decreases. However, this relationship may be more evident in these data because the Magna Probe is limited to snow depths of < 120 cm. Hence, there are very few Magna Probe SWE data above 200 mm to produce the scatter shown in 6.5a and 6.5c.

The data plotted in Figure 6.5 suggest that there are indeed factors in the tundra other than SWE which are influencing Tb, especially at 37 GHz. As such, the next step is to identify as many of these confounding factors as possible. The Tb and SWE data need to be examined over specific terrain and landscape areas individually instead of being plotted together. For flat tundra and lakes, it is relatively easy to delineate homogenous footprints in the high resolution airborne data. For slopes, it is more difficult because slope and aspect characteristics are rarely homogeneous even within a 50 m scale measurement. For instance, most slopes are adjacent to wind scoured plateaus, and even high resolution airborne footprints are often a combination of both terrain types. With the ground based radiometers, it is easy to define which terrain type the data are being collected in; however, the instrument was not used on slopes due to platform stability in uneven terrain. Due to the complexity of defining slope terrain in footprint areas, slopes of all aspect and angle were grouped together into a single class.

Because of the reversal in 37 GHz Tb with increasing SWE, described in Sections 2.4.2.2 and 5.5.2, the Tb data were grouped into high or low SWE categories. An initial threshold of 120 mm was chosen for the point of inflection; however, the reversal in Tb for non-tundra snowpacks has been documented as being between 120 and 180 mm (De Seve et al., 1997; Matzler et al., 1982; Matzler, 1994).

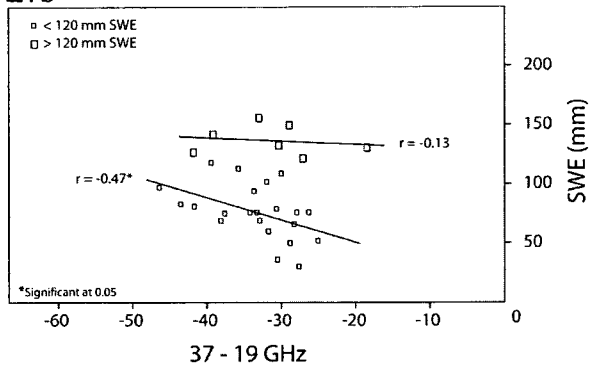
For the 2005 and 2008 sites, terrain categories were determined in the field during in-situ data collection. The site data were plotted in a GIS and field observations of terrain were compared with the terrain classification described in Section 3.3.2. Sites were used for comparison with Tb if the terrain was homogenous within the footprint. With the Magna Probe data, there were no in-situ observations of terrain. As such, the DEM classification was used to select footprint terrain. This process was straightforward for lakes, flat tundra, and low slopes, however, it posed problems for steep slopes and plateaus. There were only two footprints with only steep slope terrain and one footprint composed entirely of a plateau. As such, plateaus were not used, and steep slope footprints were also selected if they overlapped with steep slope categories. Although not ideal, this should give some sense of how Tb compares to SWE in and around steep slopes.

6.2.2. Flat Tundra

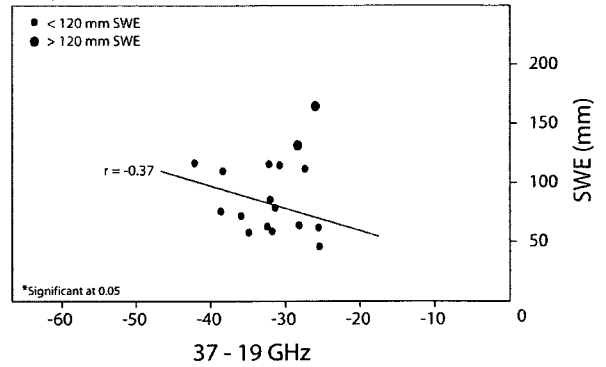
6.2.2.1. *High Resolution Airborne Radiometer Data*

As outlined in Chapter 3, flat tundra comprises approximately 35 % of the study area. Areas of flat tundra were relatively simple to identify in the field and in the terrain classification from the DEM. Spatially coincident in-situ and magna probe SWE from homogenous flat tundra sites were compared to Tb from the 2005 and 2008 high resolution airborne data and from the 2007 ground based data (Figure 6.6).

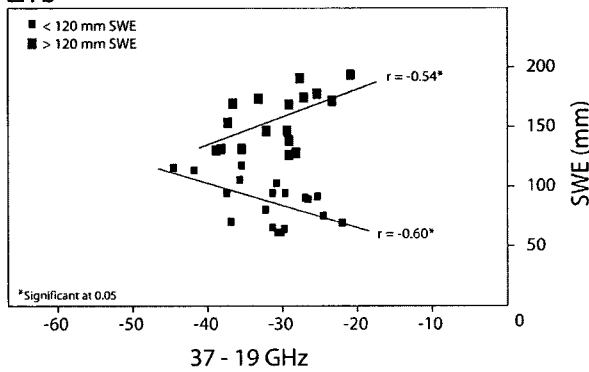
a) 2005 in-situ site SWE from Flat Tundra vs. ΔT_b^{37-19}



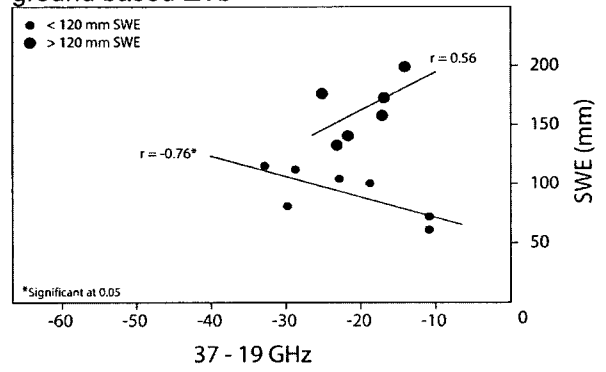
b) 2008 in-situ site SWE from Flat Tundra vs. ΔT_b^{37-19}



c) 2008 Magna Probe SWE from Flat Tundra vs. ΔT_b^{37-19}



d) 2007 in-situ site SWE from Flat Tundra vs. ground based ΔT_b^{37-19}



e) All SWE from Flat Tundra vs. ΔT_b^{37-19}

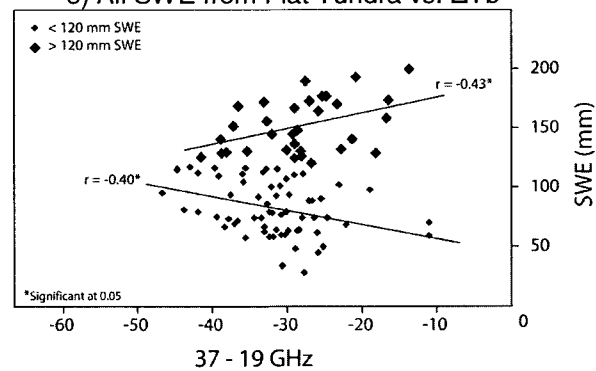


Figure 6.6. Comparison of high resolution airborne and ground based T_b with SWE over flat tundra

Figure 6.6 shows that there is a much better relationship between ΔT_b^{37-19} and SWE over areas of homogenous flat tundra than there is when considering the whole dataset as shown in Figure 6.5. It is also evident that reversal in the slope appears to occur

around 120 mm of SWE. Least squares regression was used to find the breakpoint of SWE, where the reversal occurs, which explains most of the overall variance.

Segmented regression uses an iterative approach where the breakpoint location is changed until the overall r^2 is maximized. The overall r^2 between Flat Tundra SWE and ΔT_b^{37-19} was maximized when the breakpoint in SWE was between 115 and 118 mm. However, placing the breakpoint between 115 and 118 mm instead of 120 mm explains 1% more variance (r^2 from 0.17 to 0.18). Due to the scatter in Figure 6.6e, the overall r^2 values are not very high. A breakpoint between 110 and 130 mm yields a very similar r^2 , and 120 mm is a good approximation.

Using the regional density derived in Chapter 4 of 0.294 g/cm^3 , 120 mm of SWE corresponds to 35 cm of snow depth. This depth threshold is very similar to the determination of Sturm et al. (1993) (using ground based radiometer measurements) that volume scatter produces a decrease in 37 GHz T_b due to volume scatter to a critical snow depth of 31 cm. At depths above this threshold, emission from the snowpack drives an increase in T_b .

6.2.2.2. Ground Based Radiometer Data

Ground based radiometer data were collected in 2007. At each site, the T_b of the undisturbed snow pack was measured with the radiometer system. Measurements with a 1 second integration time were averaged over a 15 minute observational period. At some sites, snow layers were carefully removed, and the T_b was again measured. A summary of the 15 minute averaged T_b measurements was used to compare with snowpit observations. Because their layers are very distinct, it was easy to remove each layer while preventing any significant disturbances to the snow surface roughness between the two sets of observations. No modifications were made to the position or orientation of the radiometers, and measured snow depth and SWE were noted with the

removal of each layer. The change in SWE and Tb as the snow layers were removed was plotted at two flat tundra sites (Figure 6.7).

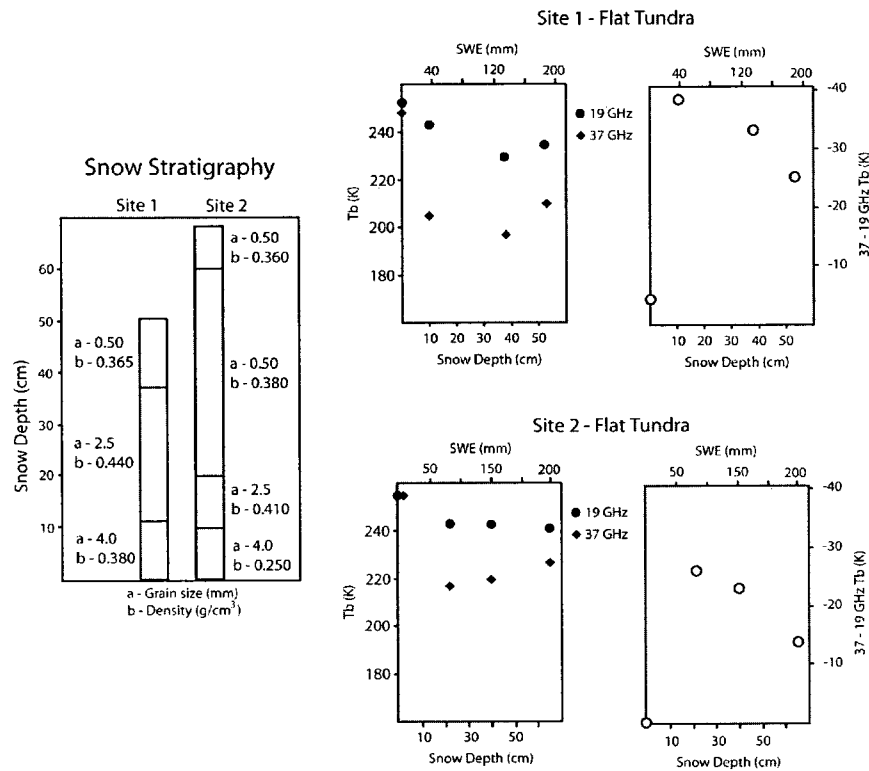


Figure 6.7. Ground based radiometer observations of snow removal at two flat tundra sites

Figure 6.7 shows that there is a definite reversal in the Tb at 37 GHz at both sites. Site 1 also shows a drop of almost 10 K in 19 GHz Tb which is normally thought of as being insensitive to snow cover. The left panel of Figure 6.5 shows that Site 1 has a fairly large grain size (~2.5 mm) and dense (0.440 g/cm³) slab layer in the middle of the snow pack in addition to a dense depth hoar layer at the base of the pack. Together, these layers could be enough to cause scattering (lower Tb) at 19 GHz. The snow pack at Site 2 has a mid-pack layer with much smaller grain size and a lower density than at Site 1. Consequently, the Tb at 19 GHz for Site 2 is more stable as the layers were removed.

Both sites do not pin-point the exact reversal in 37 GHz as snow layers were removed in irregular intervals. However, the data suggest that the reversal in 37 GHz would occur between 40 and 120 mm SWE at Site 1 and between 90 and 150 mm SWE at Site 2. These observations help to suggest that the reversal at 37 GHz occurs somewhere at or below 120 mm of SWE.

6.2.2.3. Summary of High Resolution Tb Data over Flat Tundra

When the high resolution airborne and ground based Tb with SWE over flat tundra were plotted (Figure 6.6), the slope of the line below 120 mm of SWE is in a similar direction to other algorithms which use the ΔT_b^{37-19} approach. This suggests that a linear relationship could be applied to estimate SWE (< 120 mm) over flat tundra. However, the strength of the relationship varied among the different data sets. The correlation coefficients for each dataset are summarized in Table 6.2.

Table 6.2. Summary of the strength of the relationship between SWE and ΔT_b^{37-19} over flat tundra

		2005 Site Data	2008 Site Data	Magna Probe	Ground Based	All Data
<120 mm SWE	Pearson's r	0.47*	0.37	0.60*	0.76*	0.40*
>120 mm SWE	Pearson's r	0.13	N/A	0.54*	0.54	0.43*

*denotes that the relationship is significant at 0.05

The Magna Probe and ground based radiometer data show the strongest relationship between SWE and ΔT_b^{37-19} both above and below 120 mm SWE. If a linear relationship exists between Tb and SWE it should be evident in the Magna Probe data because a transect of measurements provides the best representation of within-footprint SWE. Furthermore, ground based radiometer data should provide a good opportunity to examine the relationship between SWE and Tb with little mixing of terrain and land cover. The relationship between SWE and ΔT_b^{37-19} was plotted using only the Magna Probe and ground based radiometer data (Figure 6.8).

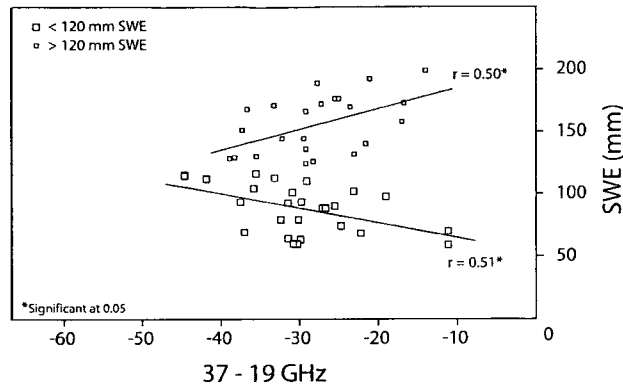


Figure 6.8. All Magma Probe and ground based SWE from flat tundra vs ΔT_b^{37-19}

By using only the Magma Probe and ground based data, the r improves to 0.50 ($p < 0.05$) for SWE above 120 mm and an r of -0.51 ($p < 0.05$) for SWE below 120 mm. The linear equations derived from least squared regression of these relationships are shown in Table 6.3.

Table 6.3. The linear equations between ΔT_b^{37-19} and SWE for the Magma Probe and ground based data

	Regression Equation	r	R^2	SEE (mm)
<120 mm SWE	$SWE = 53 - 1.19(\Delta T_b^{37-19})$	0.51	0.26	16.9
>120 mm SWE	$SWE = 203 + 1.16(\Delta T_b^{37-19})$	0.50	0.25	20.5

*Slope and intercept significant at 0.05 for both models

Because of the reversal in 37 GHz Tb around 120 mm, the slopes of the two equations are in opposite directions. Hence, the challenge is in knowing which relationship applies given a certain Tb. For example, if a ΔT_b^{37-19} of -30 K were recorded by a sensor for flat tundra, using these equations, two values of SWE would be estimated (94 mm and 154 mm).

As such, it would be helpful to know the proportion of the flat tundra in the study area with a SWE above and below 120 mm. However, if the study area had both areas above and below 120 mm, then both equations would need to be used. If the flat tundra was mostly below 120 mm SWE, then a single equation could be applied. Given the variability in SWE, it is likely that there are no large areas with SWE consistently above or below 120 mm. Even within high resolution airborne footprints, there would be areas

with SWE above and below 120 mm. The distributions of SWE within flat tundra were plotted for each survey year (Figure 6.9).

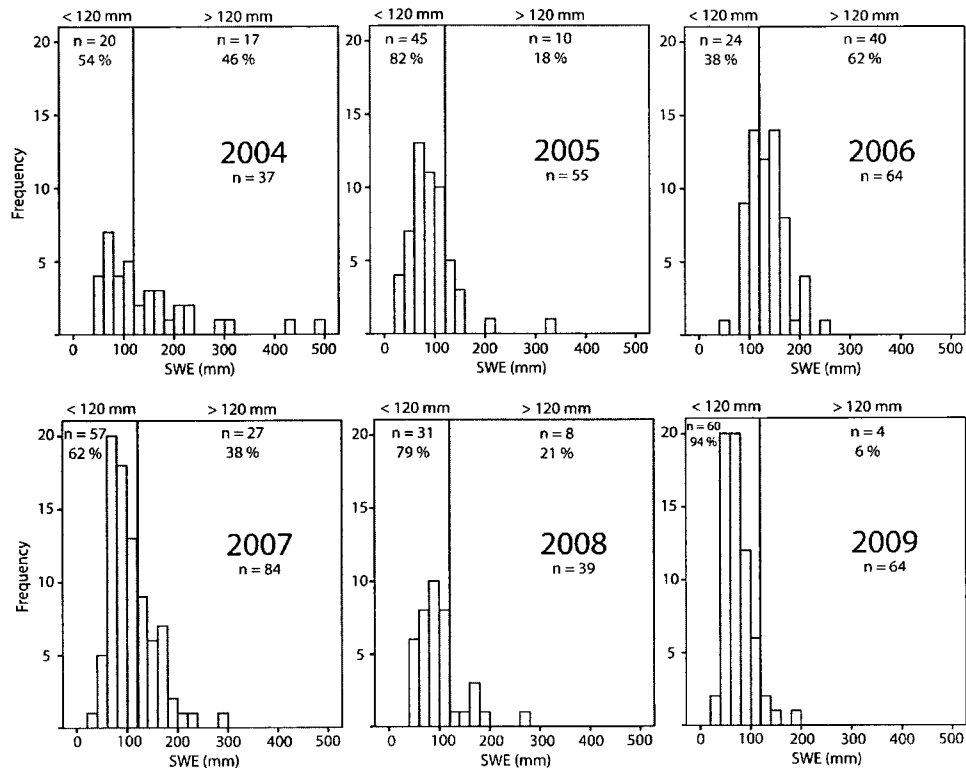


Figure 6.9. The distribution of SWE on flat tundra

During most of the survey years, a higher percentage of flat tundra sites had less than 120 mm of SWE. In 2005 and 2009, more than 80 % of the site SWE were below 120 mm., while in 2008 79 % of the site SWE were below 120 mm. However, in years with greater snow accumulation, the site SWE can be equally above and below 120 mm (2004) or predominantly above 120 mm (2006). Figure 6.9 shows that a single equation for relating Tb to SWE may not apply and that prior knowledge would be needed to know which equation is appropriate.

6.2.3. Lakes

6.2.3.1. High Resolution Airborne Radiometer Data

Lakes comprise approximately 26 % of the study area and are the easiest to delineate in the field and from the terrain classification. Spatially coincident in-situ and Magna Probe

SWE from lakes were compared to Tb from the 2005, 2008 high resolution airborne data and from the 2007 ground based data (Figure 6.10).

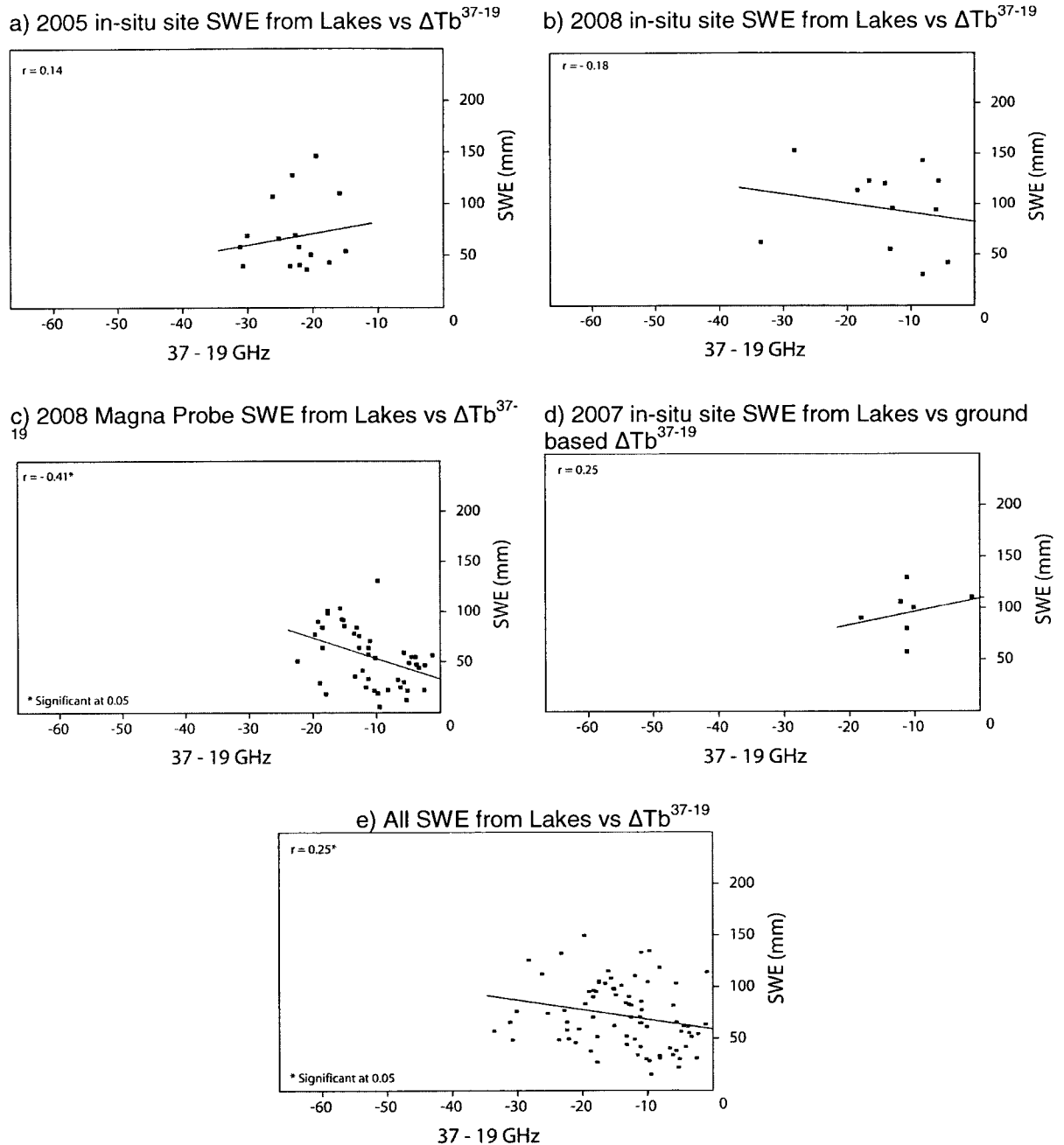


Figure 6.10. Comparison of high resolution airborne and ground based ΔT_b^{37-19} with SWE over lakes

Figure 6.10 shows that the relationships between SWE and ΔT_b^{37-19} are not as strong over lakes as they are over flat tundra. However, the 2008 Magna Probe SWE does have a moderate negative relationship with ΔT_b^{37-19} ($r = -0.41$, $p < 0.05$). The

strength of the relationship is similar to that on flat tundra; however, the scatter of points is quite large. The other data sets do not show any significant relationship between ΔT_b^{37-19} and SWE. All lake sites were compiled in Figure 6.10 e. There is a weak negative correlation of -0.24 ($p < 0.05$) between SWE and ΔT_b^{37-19} and there is a high range of possible SWE for a given ΔT_b^{37-19} . For example, between -10 and -20 ΔT_b^{37-19} , the SWE ranges from below 50 mm to around 150 mm. As a result, at most lake sites, similar to flat tundra, there are factors other than SWE which are influencing Tb.

The Magna Probe SWE (Figure 6.10 c) show the strongest relationship between ΔT_b^{37-19} and SWE. The Magna Probe data were from transects on small number of lakes across the entire width or length of a lake. In contrast, the site data were collected in a localized area with often only one site per lake. As such, the site data are compared to single footprints from different lakes. The Magna Probe footprints plotted ($n = 45$) come from only five different lakes. Approximately half of the footprints ($n = 23$) were taken from a 1.8 km transect on a single lake (Daring Lake). Each footprint had between 10 and 14 SWE measurements. The 23 Daring Lake footprints were plotted separately as ice and bathymetric conditions across the transect are similar relative to other lakes (Figure 6.11).

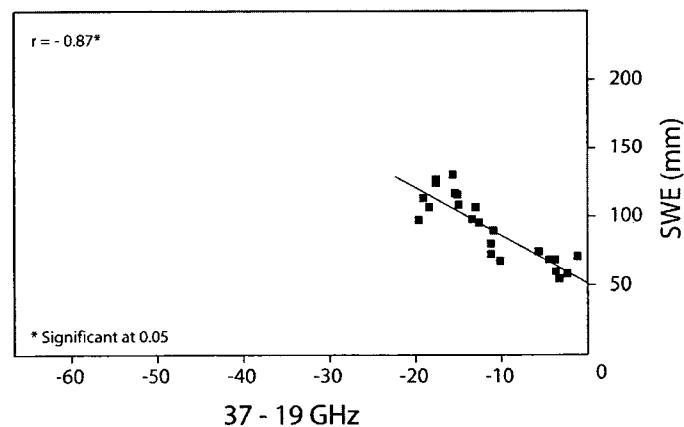
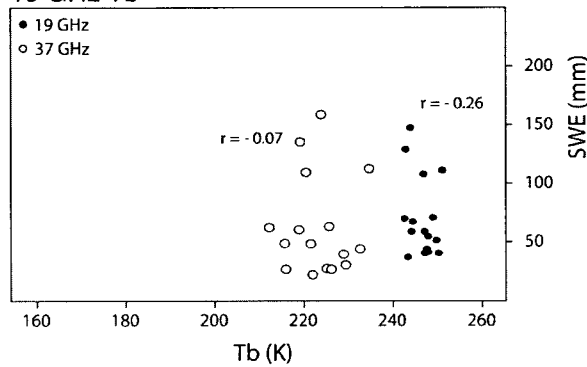


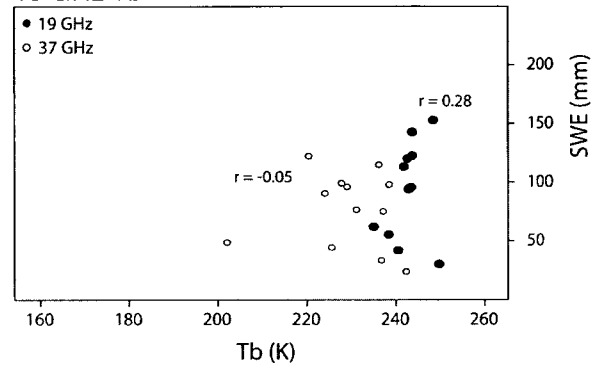
Figure 6.11. Comparison of high resolution airborne ΔT_b^{37-19} with Magna Probe SWE over Daring Lake

The relationship between ΔT_b^{37-19} and SWE on Daring Lake is very strong ($r = -0.87$, $p < 0.05$). This suggests that T_b is being influenced by SWE on a single lake. The lack of a similar relationship when plotting all lakes together reinforces the theory that the relationship between T_b and SWE is different depending on lake and ice properties. To see where the uncertainty in ΔT_b^{37-19} comes from, the 19 and 37 GHz T_b over lakes were plotted (Figure 6.12).

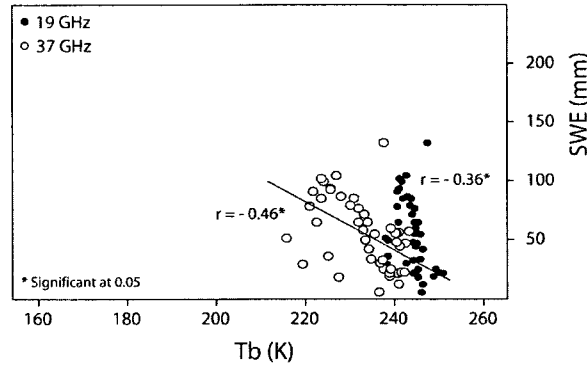
a) 2005 in-situ site SWE from Lakes vs. 37 and 19 GHz T_b



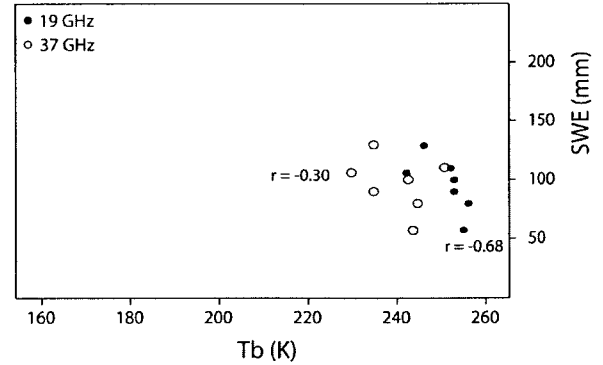
b) 2008 in-situ site SWE from Lakes vs. 37 and 19 GHz T_b



c) 2008 Magna Probe SWE from Lakes vs. 37 and 19 GHz T_b



d) 2007 in-situ site SWE from Lakes vs. 37 and 19 GHz T_b



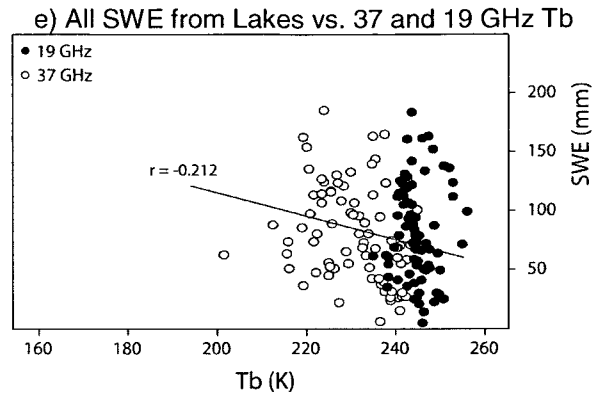


Figure 6.12. Comparison of high resolution airborne and ground based Tb with SWE over lakes

Figure 6.12 shows that there is scatter in both 19 and 37 GHz Tb for a given SWE. However, there is more variability in 37 GHz Tb than in the 19 GHz Tb. Moreover, as with ΔT_b^{37-19} , the Magna Probe data (Figure 6.12c) provide the strongest relationship with 37 GHz Tb. The Daring Lake Magna Probe footprint 37 and 19 GHz Tb were plotted (Figure 6.13).

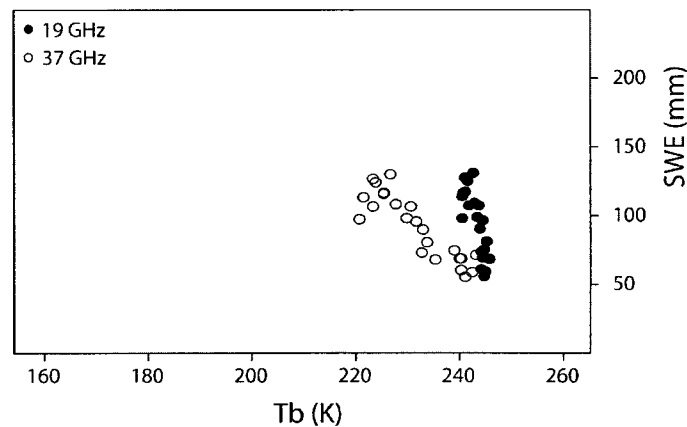


Figure 6.13. Comparison of high resolution airborne Tb with Magna Probe SWE over Daring Lake

The Daring Lake data show that there is a clear relationship between Tb at 37 GHz and SWE with little change in 19 GHz Tb. When plotted together with the rest of the lake footprints (Figure 6.12e), there is a much higher variability in both 37 and 19 GHz for a given SWE than in the Daring Lake footprints. Lake ice conditions (ice thickness,

ice type, air bubble properties) have been shown to have an effect on active microwave backscatter (Duguay et al., 2002) and more recently on the ability to simulate Tb, especially at 19 GHz (Gunn et al., in review). Due to the complexities in simulating emission from ice and snow, estimating SWE on a given lake remains a challenge.

6.2.3.2. Transect of Airborne Radiometer Data

Airborne data were collected in overlapping footprints along flight line transects (Section 3.3.7). Hence, the nearly continuous Tb data can be plotted to see the variability along lakes and how the Tb changes in the transition from lake to land. The 6.9 GHz Tb data were plotted along with 19 and 37 GHz Tb (Figure 6.14).

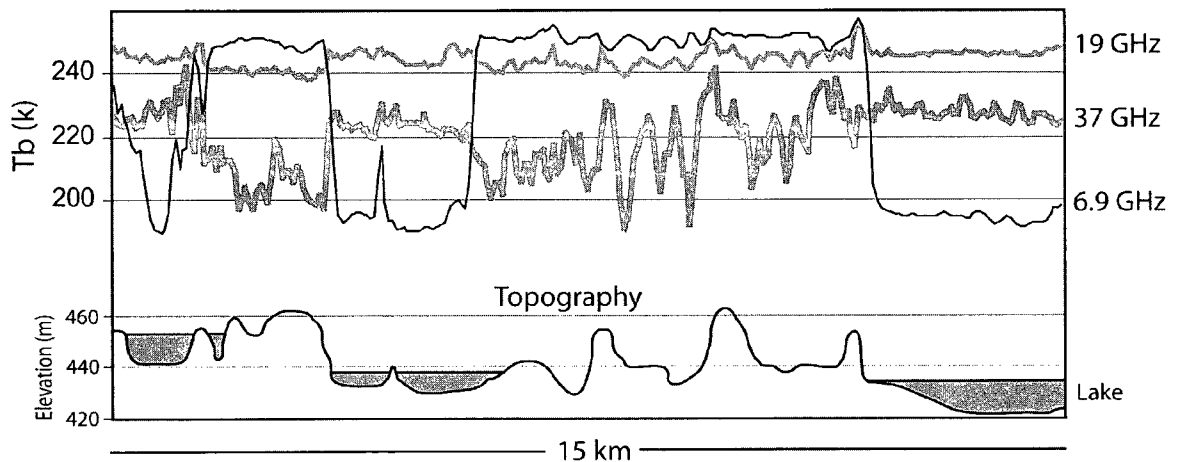


Figure 6.14. Transect in Tb from lake to land for a portion of a 2005 high resolution airborne transect

The Tb at 6.9 GHz drops dramatically over lakes. The depth of emission at 6.9 GHz is great enough to be influenced by the water below lake ice. The presence of water produces the sharp drop in Tb over lakes compared to land. The transition in Tb is fairly sharp for the lakes on the left, in the middle and to the right of the figure. However, the drop in Tb is more gradual near the edges of lake to the left as more ice is frozen to the bottom of the lake which does not produce the same drop in Tb.

The Tb at 19 GHz does not change as dramatically in the transition from lakes to land. Moreover, Tb does not decrease and is slightly higher over lakes than it is over land. Over lakes, there is less variability in Tb, especially on the lake to the right of the Figure 6.14. This suggests that 19 GHz Tb is not affected by the underlying water in the same way as at 6.9 GHz. The Tb is not dramatically lower over lakes, and there is little sensitivity to differences in SWE. The transect confirms that the depth of emission at 19 GHz (approximately 2 m from Derksen et al., 2009) is above the water and below the base of the snow pack. The slightly higher 19 GHz Tb over lakes could be due to the difference in the physical temperature between lakes and land. The water under the ice provides a heat source, more prominently in early winter. On land, the heat from unfrozen soil in the active layer is depleted by mid winter. As a result, the snow ground interface temperature drops throughout the winter (Olsson, et al., 2003). This maintains a snow-ice interface temperatures several degrees warmer than the land snow-ground interface temperatures throughout most of the winter (Sturm and Liston, 2003).

Over the land surface, the 37 GHz Tb varies the most of the three frequencies. However, the variability in 37 GHz is much higher over land than over lakes. The 37 GHz Tb is consistently lower than the 19 GHz Tb. This results in a negative ΔT_b^{37-19} over both lakes and land. The relative homogeneity in Tb at 37 GHz on lakes is due to the consistency of the snow and ice surface compared to the complexity of snow depth and stratigraphy on the land surface. Similar to 19 GHz, the 37 GHz Tb is also higher over lakes than surrounding land. In Figure 6.14, there appear to be some differences in the Tb at 37 GHz between the three different lakes surveyed on the transect. Unfortunately, no supplemental data are available to quantify where these differences in Tb exist. There are many potential lake parameters such as ice thickness, bubble concentration, type (white or black), and lake depth, and whether or not the ice is frozen to bottom which could influence microwave emission.

6.2.3.3. Ground Based Radiometer Data

The ground based data collected in 2007 provide an initial examination of the differences in Tb on lakes with different ice properties. Three sites were examined on lakes where the ice was frozen to the bottom (FTB). Two sites were examined over deep lakes (depth > 10 m). At each site, layers of snow were removed, and the Tb of bare ice recorded (Figure 6.15).

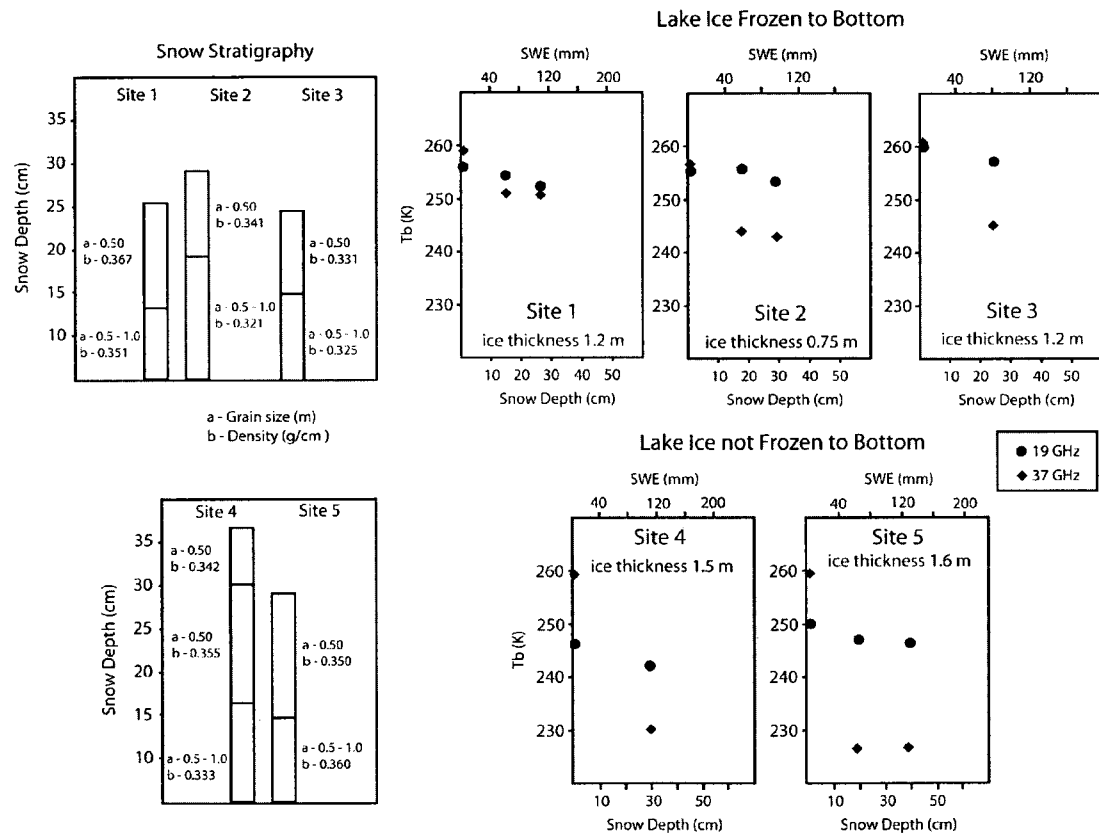


Figure 6.15. Ground based Tb observations over lakes

The 37 GHz Tb for bare ice is very similar (~ 260 K) at all lake sites. However, there is less change in 37 GHz Tb from snow covered to bare ice on lakes FTB. On lakes not FTB, the 37 GHz Tb increases by over 30 K and exceeds the 19 GHz Tb with the removal of the snow pack. The 19 GHz Tb is lower on lakes not FTB, perhaps due to

the ice temperature or other physical properties. All lake sites do not show much change in 19 GHz Tb from snow covered to bare ice. However, the 37 GHz Tb is quite sensitive to SWE on lakes. At each site there is a drop in Tb with the removal of the snow cover. This reinforces the relationship between airborne 37 GHz Tb and Magna Probe SWE in Figure 6.13. The data in Figure 6.15 provide a glimpse of how the differences in Tb may be explained from different lake sites. However, the data are not sufficient to provide a systematic analysis of how lake parameters influence Tb. This is an area which should definitely receive attention in the future.

6.2.3.4. Summary of High Resolution Tb Data over Lakes

Microwave emission models are often used to simulate Tb under different snow conditions (Rees et al., 2010). Models can also be applied to examine the effect of different lake ice properties on both observed and simulated Tb (Kontu et al., 2008, Gunn et al., in review). However, in the tundra, there are several lake ice questions which still need to be addressed. Primarily, it should be determined why there seem to be a range of Tb from a single lake and very different Tb observed over multiple lakes. Emission models could be useful in order to run a Tb sensitivity analysis using different lake and ice parameters. Possible variables include lake depth, ice type, ice thickness, ice and snow ice interface temperatures, and the surface roughness. A model parameterized for these variables would be useful for explaining the range of possible Tb over tundra lakes. The results from model simulations would also help determine which lake parameters need to be known in order to accurately estimate SWE over lakes. Moreover, models may help to explain why there is a strong linear relationship in some cases (Figure 6.11, 6.13), while not in others. Resolving these issues is certainly important in understanding the contribution of sub-grid lakes on satellite scale Tb.

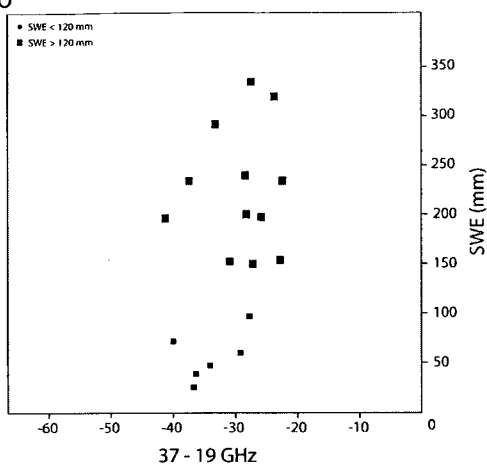
6.2.4. Slopes

Slopes in the study area were classified according to slope and aspect. Low slopes ($<7^{\circ}$) of all aspects comprise approximately 24 % of the study area, while steep slopes ($>7^{\circ}$) make up only 11 %. Chapter 4 showed that snow on steep slopes is usually significantly deeper than on low slopes. However, slopes of less than 7° did not have significantly different SWE than that on flat tundra. As such, a similar relationship between Tb and SWE as shown on flat tundra should exist on low slopes. Because SWE almost always exceeds 120 mm on steep slopes, it may not be possible to establish a similar relationship with Tb.

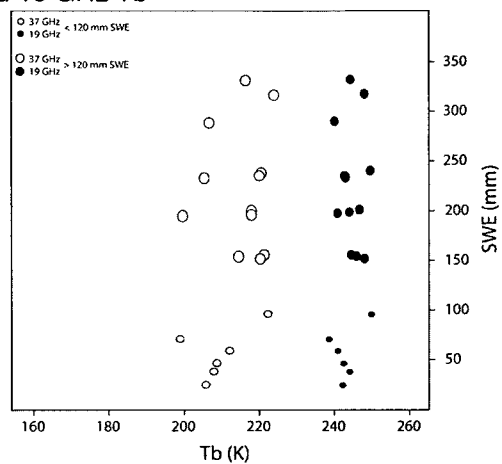
Classifying (generalizing) steep slopes in the field is a complicated task. The terrain classification delineates slopes into general classes from 10 m digital topographic data. However, in the field, slopes are much more complex. Slope angles, aspect, curvature and land cover can all vary, and no two slopes are truly similar. Moreover, it is very difficult to assess and quantify the land surface characteristics of steep slopes in the field as they are covered by deep snow drifts. The topographic classification of slopes is an over simplification of a complex environment. Considerable variability in SWE exists on slopes, and similar variability should be expected in Tb.

As mentioned in Section 6.2.1, a relationship between Tb and SWE may be hard to establish for slopes as, unlike lakes or flat tundra it is difficult to find completely homogenous footprints. The airborne data should help investigate the behavior of Tb in these complex areas. To simplify the initial analysis, slope aspects were grouped together, and slopes were broken down into either high or low slope classes. In-situ site and Magna Probe SWE from low slopes were compared to Tb from the 2005 and 2008 high resolution airborne data (Figure 6.16).

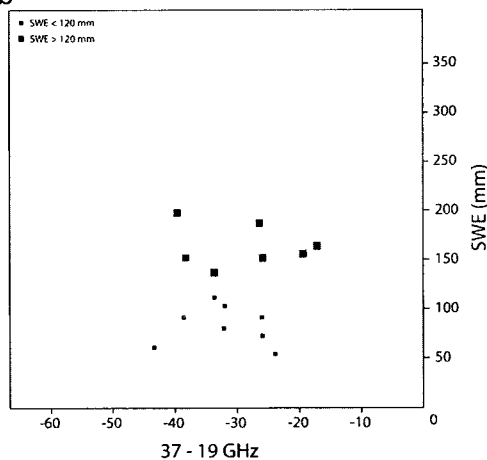
a) 2005 in-situ site SWE from low slopes vs ΔT_b^{37-19}



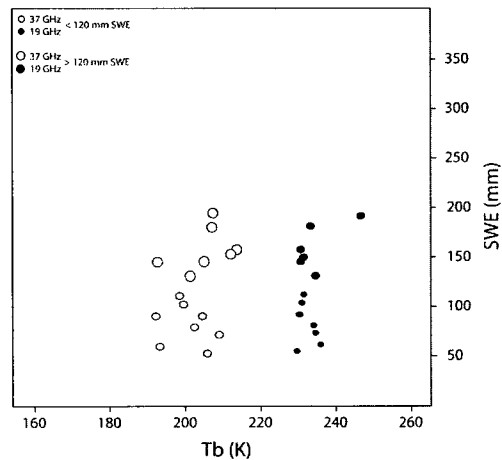
b) 2005 in-situ site SWE from low slopes vs 37 and 19 GHz Tb



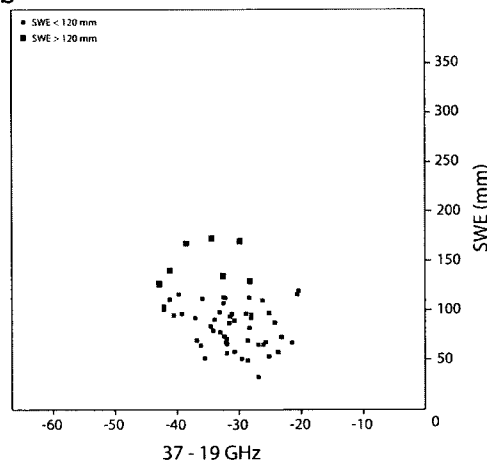
c) 2008 in-situ site SWE from low slopes vs ΔT_b^{37-19}



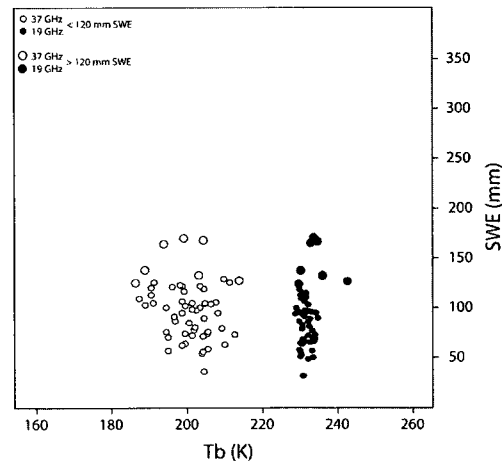
d) 2008 in-situ site SWE from low slopes vs 37 and 19 GHz Tb



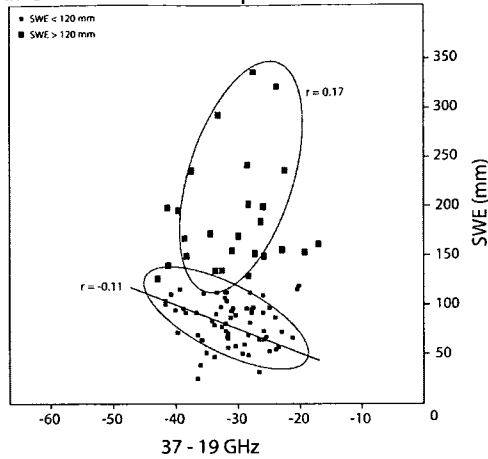
e) 2008 Magna Probe SWE from low slopes vs ΔT_b^{37-19}



f) 2008 Magna Probe SWE from low slopes vs 37 and 19 GHz Tb



g) All SWE from low slopes vs ΔT_b^{37-19}



h) All SWE from low slopes vs 37 and 19 GHz Tb

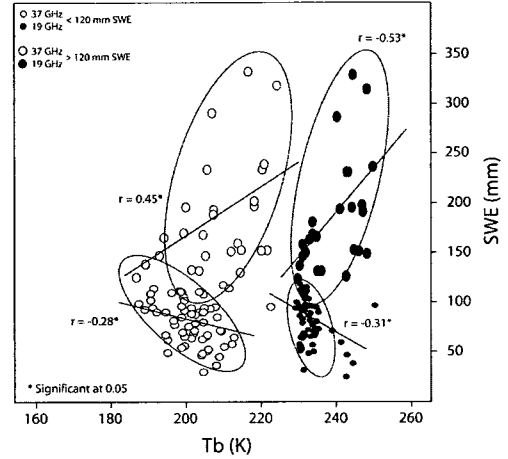


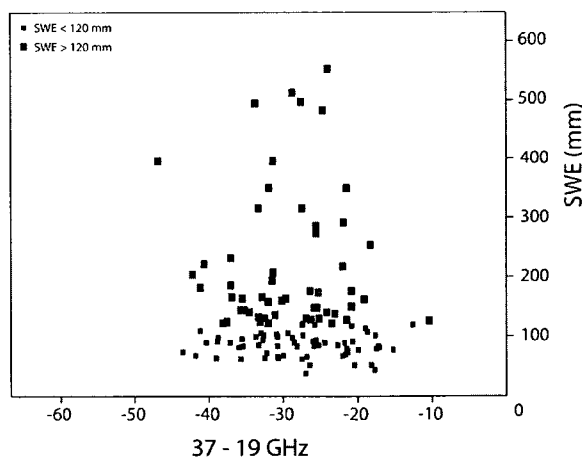
Figure 6.16. Comparison of high resolution airborne Tb with SWE over slopes (< 7 degrees)

There are no strong relationships between ΔT_b^{37-19} and SWE on slopes of < 7 degrees. However, there are significant relationships between 37 and 19 GHz Tb and SWE. The problem is that in every data set, there is a high range in SWE for a given Tb or ΔT_b^{37-19} . This variability is most evident in the 2005 data (Figure 6.16 a) and b)). Moreover, there is also a high range of Tb values for a given SWE. This is most evident in the 2008 site data (Figure 6.16 c and d). The Magna Probe data do not show a full range of SWE depths because the probe is limited to 120 cm of snow depth. When all low slope data were plotted (Figure 6.16 g and h), some general trends were noted. The ellipses show a possible general trend in ΔT_b^{37-19} and 19 and 37 GHz Tb. A threshold around 120 mm of SWE may in fact yield a reversal in the general relationship in ΔT_b^{37-19} , 37 GHz and perhaps even 19 GHz Tb. However, the scatter in the data produces low correlation coefficients, and no significant relationships are present with ΔT_b^{37-19} . The lack of a strong relationship limits the ability to estimate SWE from Tb for low slope areas. This is most evident if SWE were to be estimated for a ΔT_b^{37-19} of -30 K. The range of SWE for footprints with -30 ΔT_b^{37-19} is nearly 300 mm, from a low of 50 mm to a high of close to 350 mm. Even if the reversal in ΔT_b^{37-19} at 120 mm SWE were

considered, the best estimate of SWE would still be ± 50 mm. On low slopes, it would be difficult, if not impossible, to relate SWE to Tb in an airborne footprint because the values of SWE are not an accurate reflection of footprint SWE, or there are other factors which influence Tb on low slopes. For example, the geometry of slopes may have an influence on Tb. The airborne data are collected at a fixed radiometer incidence angle of 53 degrees. Along a flight line, there is a variety of different slope angles and aspects. Slopes facing the radiometer would be in effect foreshortened while slopes facing away from the radiometer would be elongated. The precise influence of slope geometry on Tb is not clear; however, it would have the greatest effect in high resolution footprints.

Steep slopes ($> 7^\circ$) are even more problematic when comparing Tb and SWE. They are the most spatially constrained and variable terrain feature. Leeward slopes can have up to 4x the amount of snow as flat areas. Furthermore, as outlined in Section 6.2.1, the geo-location of slopes with footprint SWE is very difficult. Footprints with any overlap to steep slopes were used for comparison with Tb (Figure 6.17).

a) All SWE from high slopes vs ΔT_b^{37-19}



b) All SWE from high slopes vs 37 and 19 GHz Tb

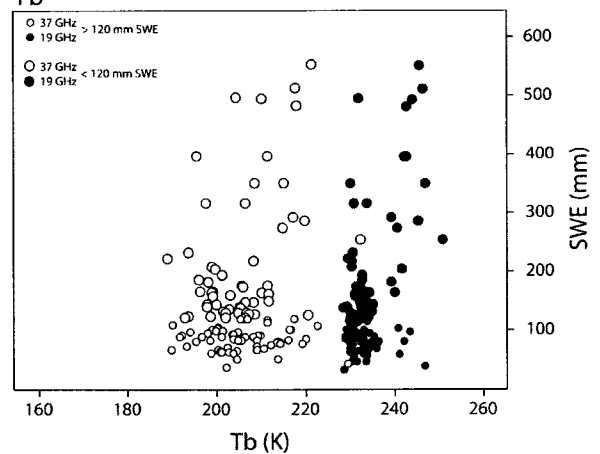


Figure 6.17. Comparison of high resolution airborne with SWE over slopes (> 7 degrees)

Similar to low slopes, there is a large range in Tb for a given SWE and also a large range in SWE for a given Tb. There is also a larger range of 19 GHz Tb for a given SWE than in any other terrain. This could be due to areas of deep snow; however, the

range in 19 GHz is towards warmer Tb which may suggest that bare ground from plateaus is a component of the footprints. Given the variability in Tb and SWE, it is clear that it is nearly impossible to estimate SWE on steep slopes with high resolution airborne data. However, steep slopes comprise a very small percentage of the landscape at the satellite scale (Section 3.3.2). Hence, it is hypothesized that they contribute little to satellite scale Tb.

6.2.5. Summary of High Resolution Tb vs. SWE

The previous sections showed that there are relationships between SWE and Tb on flat tundra and at some lake sites. However, a strong relationship is certainly not evident when all high resolution radiometer data are combined. On slopes, the lack of a relationship is at least partially a result of the challenges in geolocating in-situ snow measurements with small footprint airborne Tb. High resolution data are certainly important in resolving satellite scale uncertainty; however, two challenges persist:

- 1- Providing an accurate estimate of within footprint SWE;
- 2- Finding homogenous terrain and land cover footprints in which to isolate the effect of SWE on Tb given all other possible influences on microwave emission.

The first challenge is a product of the natural variability in tundra SWE. The single SWE value used for comparison with Tb is an average of all measurements taken within each footprint. However, at most, there are 30 points measured in a footprint. The variability among these 30 measurements can be considerable, and little has been done to define the spatial variability beyond the measurement locations. Hence, the lack of relationship with Tb could easily stem from an improper quantification of within-footprint SWE. The nature of SWE in high resolution footprints is further discussed in Appendix A.

The second challenge is somewhat unexpected in that tundra terrain and land cover are generally thought to be somewhat less complex than other environments. High resolution airborne data are not sufficient to explain why different terrain and land cover

would produce a range of T_b , independent of SWE. Furthermore, lakes should offer the most homogenous footprint in terms of surface roughness and snow cover. However, different lakes have very different T_b characteristics due to the heat from underlying water. This suggests that over lakes, like flat tundra, there are factors other than SWE which influence T_b .

The resolution to this challenge is better defining how the combination of land surface and snow cover influences microwave emission. The T_b recorded from a footprint is the integration of all features within that area. Essentially what needs to be addressed is the proportional contribution of both snow and land features to T_b . Ground based data offer the only real opportunity to study end members of T_b and SWE for different terrain and land cover. Attempting to isolate homogenous terrain and land cover is helpful; however, at operational scales, there will always be a mixture of terrain, land and snow cover properties. As such, the comparison of multiple resolutions of T_b data will be addressed in Section 6.3 in order to work towards resolving satellite scale uncertainty.

6.3. Application of Mid and Low Resolution Airborne T_b

6.3.1. Introduction

High resolution radiometer data are useful for examining the relationship between SWE and T_b in a given terrain category. However, as Section 6.2 showed, the variability in SWE limits the ability to interpret a relationship with T_b . Hence, at even high resolutions, airborne data have terrain, land cover and SWE mixing issues similar to satellite data. Ground based sensors do not have the same problems with spatial mixing of terrain and land cover; however, T_b are not directly related to SWE without knowing the contribution from snow density, grain size, stratigraphy, and underlying ground surface.

High resolution data are hampered by small scale variability in snow, terrain and land cover. Resolving issues at these scales may not contribute to resolving uncertainty in satellite data. However, coarse resolution airborne data integrate much of the high frequency variability seen in high resolution data. The mid and low resolution data can be used to address whether or not there are systematic trends in T_b which are not related to SWE. Chapter 5 showed that at the satellite scale, land cover can have an inter-seasonal influence on T_b where lake fraction does not. Moreover, in the satellite data, there was little difference in T_b across multiple EASE grid pixels during a single season. Working from high to low resolution, airborne T_b data may help explain what contributes to satellite scale T_b and help identify any issues in relating T_b to SWE.

6.3.2. High to Low Resolution T_b

At the satellite scale, passive microwave sensors integrate every type of terrain, land cover and snow surface into a single T_b . Hence, the challenge is to understand how these sub-grid features collectively influence satellite scale T_b . The high resolution ground based and airborne data were useful for investigating fundamental relationships between SWE and T_b . However, at these resolutions, the relationships are hard to define due to the considerable variability in land cover and SWE within footprints. However, moving from high to low resolution of data should provide some insight into what features have most influence on T_b . The 2005 airborne data were used to examine the relationship in T_b as three altitudes were flown, giving three resolutions of data along identical flight transects.

The increase in aircraft altitude provides coarser footprints with a very similar along track sampling frequency. However, since the aircraft flew over the same line for each successive flight, the footprint centroids for the different resolutions are offset and do not overlap (Figure 6.18).

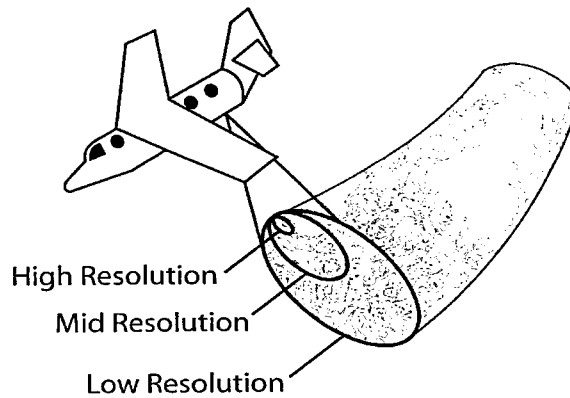


Figure 6.18. Relative location of airborne footprints along flight line

As a result, some difference in T_b can be anticipated due to this shift in footprint location. However, more pronounced differences in T_b can be expected as the resolution increases because many more features are integrated into each footprint. The radiometer integration time was not changed from flight to flight; however, as flight altitude increased so did the ground speed of the aircraft. As such, the lowest altitude, highest resolution data have more along-track observations than the two successively higher flights. This makes it difficult to precisely co-locate features in terms of T_b ; however, general changes in T_b along the line should be apparent in all resolutions. Several flight lines were flown throughout the study area EASE grid. A representative transect, across various terrain and land cover, was chosen for a multi-resolution comparison of T_b (Figure 6.19).



Figure 6.19. Airborne transect across study area EASE grid

The Tb data were plotted for each flying height along with ground topography, lake cover and temporally co-incident daily AMSR-E satellite Tb (Figure 6.20).

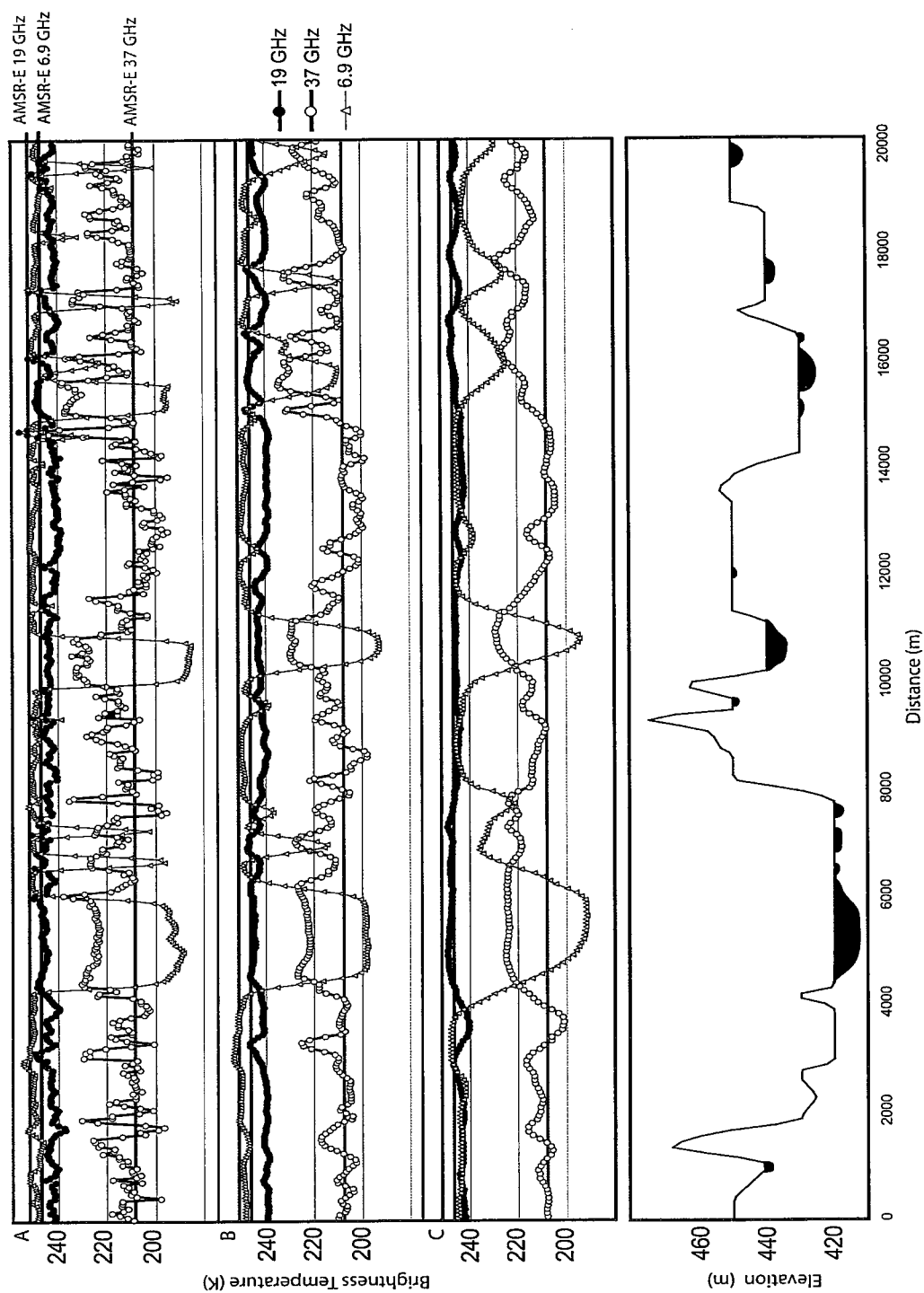


Figure 6.20. Tb data for the three resolutions, high (A), mid (B) and low (C), along with AMSR-E Tb

At the highest resolution (A), there is much more variability in Tb at all frequencies. The variability is evident at 37 GHz which shows its sensitivity to the different land cover, terrain and snowpack properties. The variability in 37 GHz is much larger over land than lakes due to the wide range of possible land, snow cover, and topography combinations. Over lakes, the snow and ice properties which contribute to Tb at 37 GHz are more consistent. The Tb over lakes is higher most likely due to the consistently smaller basal snow grain size. The 19 GHz (A) shows comparatively little variability in Tb. Values predominantly range from 240 to 245 K, with a sharp spike noted in both 19 and 37 GHz at 14 500 m. The land cover in this area is classified as heath tundra, and it is between a small pond and another lake. Unfortunately, no ground snow cover observations were taken at this location, and this spike reinforces the difficulty in relating variability in Tb to SWE at this resolution without ancillary data. The 6.9 GHz in (A) has relatively low variability across land; however, the Tb drops sharply over lakes (as noted in Figure 6.15). The Tb at 6.9 GHz drops to below 200 K over large deep lakes, however, it does not seem to be sensitive to some of the smaller lakes which are classified as shallow and likely frozen to bed.

In the mid-resolution data (B), there is lower amplitude in the variability of Tb. At this resolution, the footprint size is over seven times larger than in (A). As such, there are many more features integrated into a single footprint. This integration has the effect of smoothing the transition in Tb between different features. Moreover, due to the footprint offset (Figure 6.18), there are features, such as lakes, which appear in the mid and low resolution footprints but do not appear in (A). As in (A), the 6.9 GHz Tb shows almost no variability across land. There is a sharp decrease in 6.9 GHz Tb over deep lakes which is coincident with the decreases in the high resolution transect (A). At 19 GHz, there is also less variability in Tb than in (A). Some similar patterns are evident; however, much of the small amplitude variability in (A) is not present in (B). The Tb at 37

GHz shows the most variability, particularly over land; however, the range is not as high as in (A). Over lakes, the 37 GHz Tb is higher and more consistent, similar to (A). Lake Tb values in (B) are very similar to (A).

At the lowest resolution (C), the amplitude of variability in Tb is a great deal lower than in (A) and (B). At 19 GHz, the Tb is very consistent with a small range. Similar to (A) and (B), the 19 GHz Tb are lower than the AMSR-E Tb. This could be due to instrument differences or calibration uncertainty which makes it difficult to compare absolute Tb from airborne to satellite platforms. The 6.9 GHz Tb show very little change over land, similar to (B), however, they still drop over lakes. The transition from lake to land is much more gradual in (C) due to the footprint size being over six times larger than in (B). In (C), due to the larger footprint size, there is more integration of terrain, and only larger lakes impact 6.9 GHz Tb. Interestingly the AMSR-E Tb corresponds quite well to the 6.9 GHz over land. At 37 GHz, there is much less variability in Tb than in (A) or (B). Over land, the amplitude of variability is far smaller than in (B), and only gradual differences are observed. The large footprints integrate almost all of the high frequency variation in (A) and (B). At the scale of (C), it appears as though the main differences in Tb are between lakes and land. The one exception is a rise in 37 GHz Tb at around 12 500 m. This rise is evident in (B) but not in (A) due to the footprint offset and the effect of larger footprints. At 12 500 m, the footprints of (B) and (C) are located over a lake, while in (A) the footprints are located over adjacent land. At the coarsest resolution, the biggest differences in Tb at 37 GHz are between lakes and land. The AMSR-E 37 GHz Tb coincides with the airborne data over land areas but, not over lakes. As mentioned, however, the absolute Tb between platforms is not expected to be exactly the same.

The ΔT_b^{37-19} was plotted for the three resolutions of data (Figure 6.21).

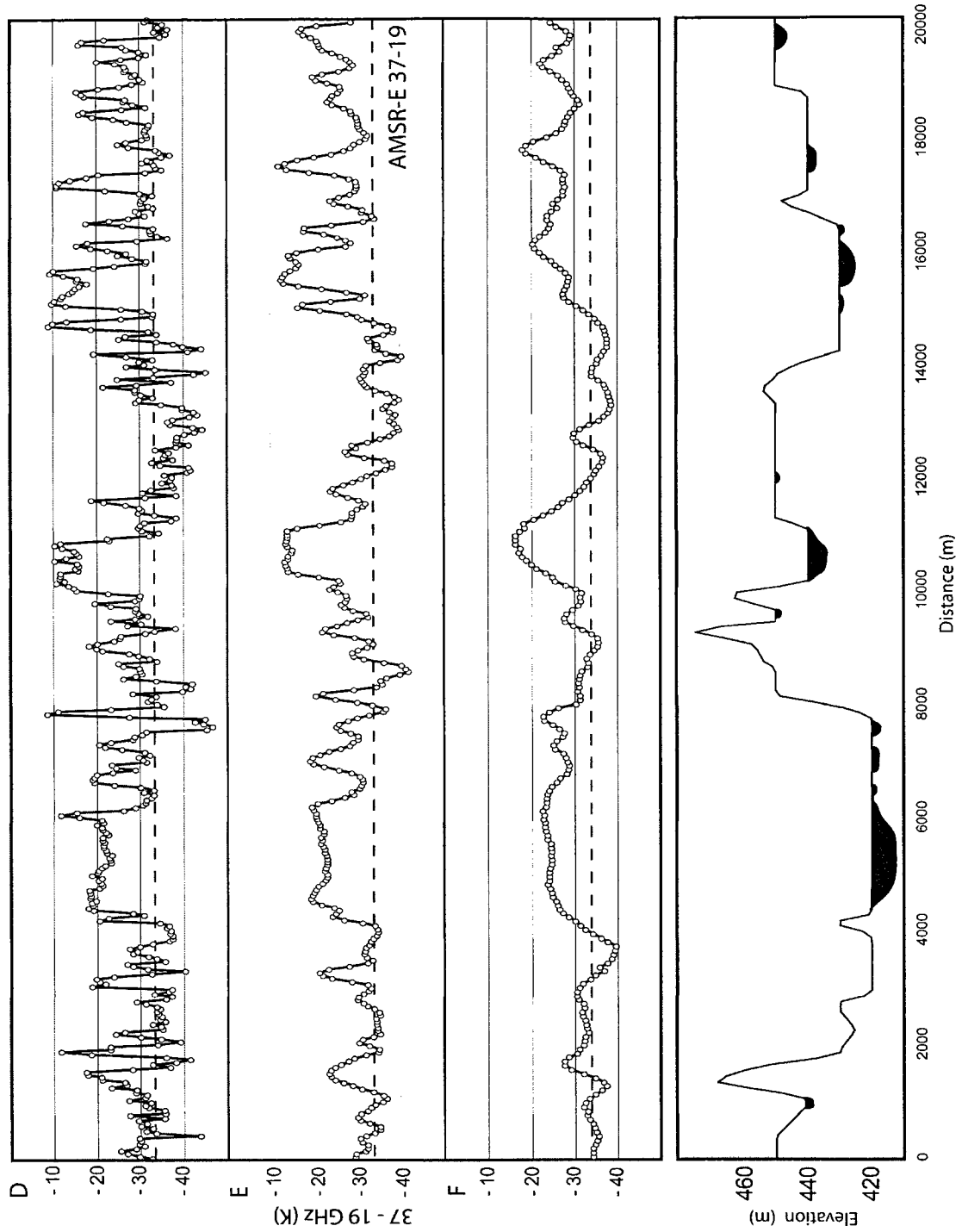


Figure 6.21. ΔT_b^{37-19} data for the three resolutions, high (D), mid (E) and low (F), along with AMSR-E ΔT_b^{37-19}

Similar patterns in variability are expected in Figure 6.21 as ΔT_b^{37-19} is driven primarily by change in 37 GHz Tb. Moreover, it is clear that the footprint size has a large influence on the spatial variability of ΔT_b^{37-19} . Plotting ΔT_b^{37-19} in addition to Tb data is useful as it is the technique often used for estimating SWE with satellite scale data. If a model were developed to estimate SWE using the ΔT_b^{37-19} in (D), it would have to account for a large amount of variability. The lower resolution of data in (E) and to (F) would make this task much easier. For example, for footprints in (F) with no lake component, there is little change in ΔT_b^{37-19} . Over lakes, however, the ΔT_b^{37-19} shifts to a higher value and remains consistent, especially over deep lakes. The transition from land to lakes is much more gradual as the footprint size increases. This occurs because the increased size of the footprint has a wider reach, and footprints not centered over lakes can still have a large lake fraction. Along the flight line, as the footprints approach lakes, the lake fraction gradually increases and ΔT_b^{37-19} gradually increases.

In Section 6.2, it was difficult to establish a clear relationship between ΔT_b^{37-19} and SWE over all terrain types. One of the main problems was the difficulty in co-locating ΔT_b^{37-19} over homogenous terrain with a representative estimate of footprint SWE. As the footprint size increases there is more generalization and much less noise in the Tb. At the coarsest resolution, the main difference in Tb is over lakes and land. Moving to a coarser resolution, (F) is a must because it is a more realistic approximation of satellite scale Tb.

The ΔT_b^{37-19} was summarized for low resolution (F) homogenous footprints over both lakes and land (Table 6.4). Land footprints were classified as having up to 5% percent lake fraction while lakes footprints were restricted to those with 100% lake fraction.

Table 6.4. Descriptive statistics for ΔT_b^{37-19} from (F) over land and lakes

LAKE	N	200	MIN	-38	STDEV	5
	MEAN	-28	MAX	-16	CV	0.18
LAND	N	177	MIN	-40	STDEV	4
	MEAN	-33	MAX	-18	CV	0.12

*note: mean ΔT_b^{37-19} significantly different ($p < 0.05$)

The mean ΔT_b^{37-19} over lakes is higher than over land by 5 K. The difference between the two groups does not seem large; however, it is significant ($p < 0.01$). The significant difference is in part due to the low variability about the mean in both groups (low CV). These data indicate that at the coarsest resolution, ΔT_b^{37-19} over lakes is different than over land, yet the variability within the two groups is relatively small.

Based on the different snow and land surface properties, the ΔT_b^{37-19} should be different between land and lakes. Moreover, as the footprint resolution increases, it is not surprising that the variability within these groups diminishes. The end points of 0 and 100 % lake fraction show a significant difference in ΔT_b^{37-19} ; however, most footprints, and EASE grids have lake fraction between 0 and 100%. Resolving the influence of lake fraction on ΔT_b^{37-19} requires an examination of the proportional influence of lake fraction on Tb from land to lake and back again.

6.3.3. Influence of Lake Fraction on Tb

In Chapter 5, no relationship was found between lake fraction and Tb at the EASE grid scale. However, in Section 6.3.2, the Tb at 37 GHz and the ΔT_b^{37-19} over lakes was shown to be higher than over land in all three resolutions of airborne data. The Tb data for the three resolutions from all airborne transects in the 2005 dataset were plotted against lake fraction from 1 to 99 % (Figure 6.22, 6.23, 6.24).

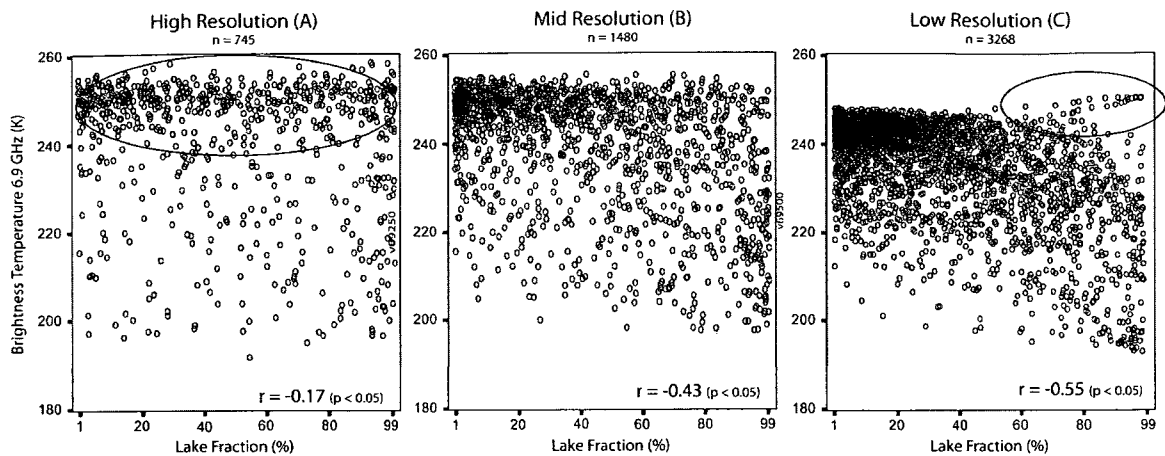


Figure 6.22. 6.9 GHz Tb vs. lake fraction

The relationship between 6.9 GHz Tb and lakes is apparent in Figure 6.22.

Despite the large amount of noise in the data, the general pattern is towards a decrease in Tb for increasing lake fraction. However, the correlation between Tb and lake fraction is stronger in the low resolution data. It ranges from $r = -0.17$ in (A), $r = -0.43$ in (B), and $r = -0.55$ in (C). The points highlighted with an ellipse in (A) shows a range of lakes with high Tb, meaning they are likely frozen to bottom. Moreover, in the high resolution data, there is a greater chance of footprints being completely within smaller lakes which typically freeze to bottom. The variability near 0 percent decreases considerably in the mid and low resolution data. This suggests that at these resolutions, smaller land features which produce low Tb in (A) are not as visible. Moreover, most footprints in (C) near 99% lake fraction have lower Tb. This is because the lakes completely within low resolution footprints are large and typically do not freeze to bottom. The footprints highlighted in (C) have higher Tb with high lake fraction. These footprints are most likely over a larger lake which does not freeze to bottom. At all three resolutions, the difference in mean 6.9 GHz Tb from 0 to 100 % lake fraction is 43 K. Although 6.9 GHz Tb is not considered in current SWE algorithms, these relationships are useful for demonstrating the strong relationships between long wavelength emission at 6.9 GHz and tundra lake

fraction. Moreover, lake fraction and the general properties of lakes within footprints can be assessed from the relationship with 6.9 GHz Tb.

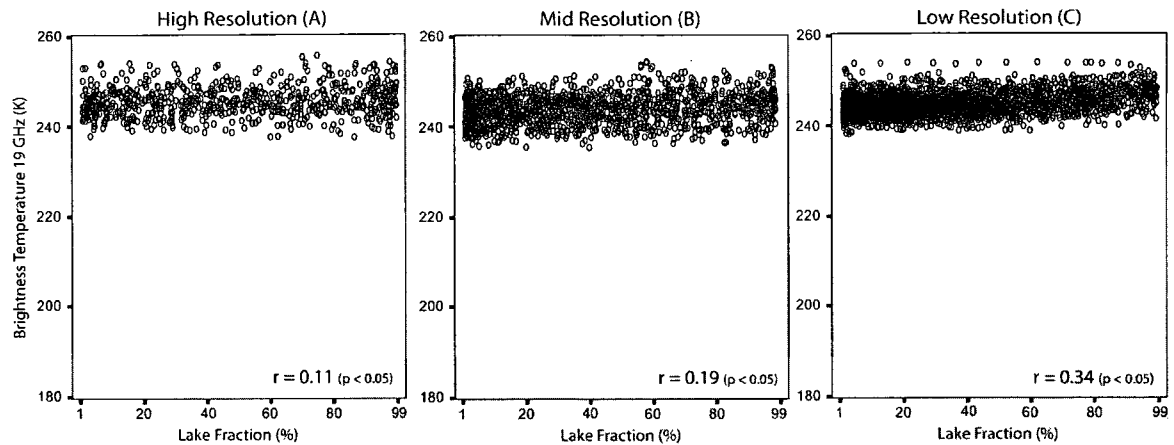


Figure 6.23. 19 GHz Tb vs lake fraction

The relationships between 19 GHz Tb and lake fraction are not as strong as at 6.9 GHz. The correlation coefficients are weak at 0.11 in (A), 0.19 in (B), and 0.34 in (C). The variability in Tb at both 1 and 99% is largest in the high resolution data. As the resolution gets lower, 19 GHz shows less variability. The rate of change (slope) in Tb in relation to lake fraction is quite small. The cloud of points indicates an increase in Tb towards increasing lake fraction. The change in mean Tb from near 0 to 100% lake fraction is 3 K in the high resolution, 5 K in the mid resolution and 5 K in the low resolution data. These shifts in Tb are not as large as in the 6.9 GHz Tb because the latter is influenced by the water under the ice. At 19 GHz, due to the shorter penetration depths, the water does not have the same effect.

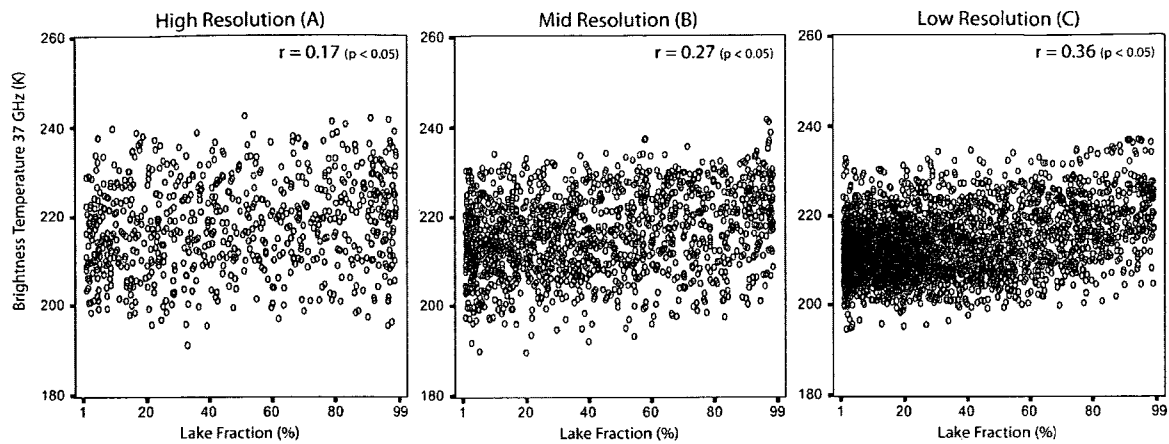


Figure 6.24. 37 GHz Tb vs lake fraction

The relationships between 37 GHz Tb and lake fraction are much more evident than at 19 GHz. The most variability is present in the high resolution data (A) due to the sensitivity to smaller scale terrain, land and snow cover change. Similar to Section 6.3.2, the Tb at 37 GHz increases with increasing lake fraction. In addition to the plots, the descriptive statistics for 0 and 100% lake fraction at each resolution were generated (Table 6.5).

Table 6.5. Descriptive statistics for 37 GHz Tb at 0 and 100 % lake fraction

Lake Fraction	High Resolution Tb (K)				Mid Resolution Tb (K)				Low Resolution Tb (K)			
	Mean	SD	CV	Diff	Mean	SD	CV	Diff	Mean	SD	CV	Diff
0 %	212	9	0.04	14	211	7	0.03	15	210	5	0.02	15
100 %	226	7	0.03		226	6	0.02		224	4	0.01	

The variability in Tb is very similar at 0 and 100 % lake fraction. However, the mean Tb from 0 to 100 % lake fraction is quite different. In the high resolution data, it increased by 14 K, and increased by 15 K in the mid and low resolution data. This shift is not as great as at 6.9 GHz but is 10 K greater than the shift in 19 GHz Tb. The shift in Tb at 6.9 GHz is due to sharp contrast in emission from water under ice. However, at 37 GHz, the Tb is not influenced by water under the ice and only slightly influenced by ice temperature. The Tb is higher on lakes primarily because of the difference in snowpack properties from those on land.

To determine the sensitivity of lakes to potential SWE algorithm development, the relationship between ΔT_b^{37-19} and lake fraction was plotted (Figure 6.25).

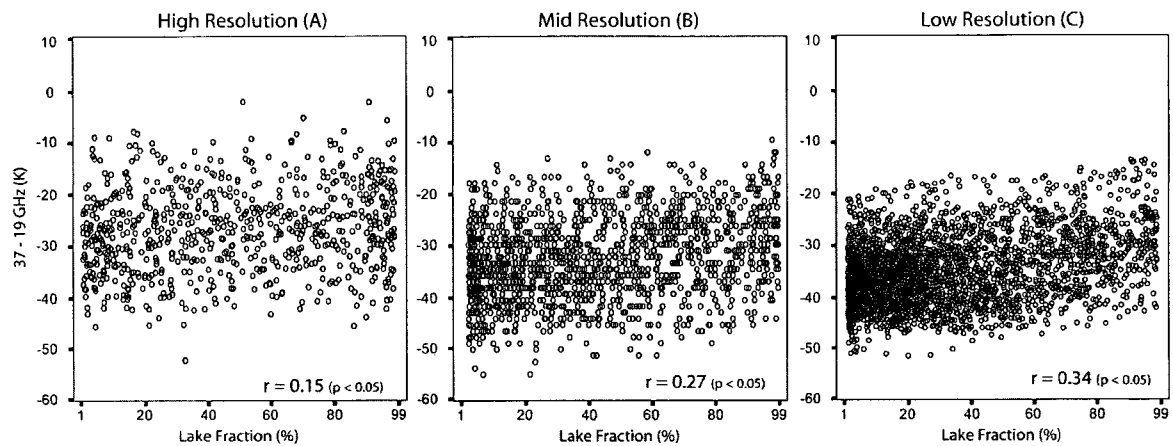


Figure 6.25. ΔT_b^{37-19} vs lake fraction

Due to the insensitivity of 19 GHz to lake fraction, the patterns in ΔT_b^{37-19} are nearly identical to those for 37 GHz T_b . Table 6.5 showed that for a single flight line the mean ΔT_b^{37-19} over lakes was higher than over land by 5 K. In Figure 6.25, which considers all flight line data, the difference in ΔT_b^{37-19} from 1 to 99% lake fraction appears to be greater than 5K. In addition to the plots, the descriptive statistics of ΔT_b^{37-19} for 0 and 100% lake fraction at each resolution were generated (Table 6.6).

Table 6.6. Descriptive statistics for ΔT_b^{37-19} at 0 and 100 % lake fraction

Lake Fraction	High Resolution ΔT_b^{37-19}				Mid Resolution ΔT_b^{37-19}				Low Resolution ΔT_b^{37-19}			
	Mean	SD	CV	Diff	Mean	SD	CV	Diff	Mean	SD	CV	Diff
0%	-31	8	0.26	10	-31	6	0.19	11	-33	4	0.12	10
100%	-21	6	0.28		-20	5	0.25		-23	3	0.13	

Similar to the 37 GHz T_b , the variability in ΔT_b^{37-19} decreases as resolution gets lower. However, the mean ΔT_b^{37-19} at each resolution is very similar at 0 and 100 % lake fraction. This suggests that the integration of more features with coarser resolution does not change the mean ΔT_b^{37-19} for land or lakes. The difference in mean ΔT_b^{37-19} between 0 and 100 % lake fraction is 10 K for the high resolution, 11 K for the mid and 10 K for the low resolution data.

A difference of 10 K in ΔT_b^{37-19} from lakes to land could have a large impact on the ability to estimate SWE, especially considering that in some snow survey years (Section 4.4), the depth of SWE on land was not significantly different from that on lakes. Three separate SWE retrieval equations were used to demonstrate the sensitivity in SWE for a difference of 10 K in ΔT_b^{37-19} . The EC open ground algorithm, described in Section 2.3.3.1, was used along with the strongest relationships between SWE and ΔT_b^{37-19} over flat tundra shown in Table 6.2. Although none of these linear algorithms are properly parameterized for absolute SWE in the tundra, they provide a good example of possible uncertainty associated with the shift in 37 GHz Tb and ΔT_b^{37-19} due to lake fraction. The sensitivity in SWE (mm) was generated for each equation (Table 6.7).

Table 6.7. The sensitivity in SWE for 10 K ΔT_b^{37-19}

Estimate of SWE	Equation	Sensitivity in SWE for 10 K ΔT_b^{37-19}
Table 6.2 <120 mm SWE	$SWE = 53 - 1.19(\Delta T_b^{37-19})$	12 mm
Table 6.2 >120 mm SWE	$SWE = 203 + 1.16(\Delta T_b^{37-19})$	12 mm
EC Open Ground (Section 2.3.3.1)	$SWE \text{ (mm)} = -20.7 - 49.27[(\Delta T_b^{37-19})/18]$	27 mm

A shift of 10 K in ΔT_b^{37-19} would result in a change of 12 mm using the two equations from Table 6.2. However, using the EC algorithm, 10 K produces a difference of 27 mm. This shows that if lake fraction was not considered, in the most extreme case there would be an error of 27 mm in SWE.

At the satellite scale, Chapter 5 demonstrated that there was no clear relationship between lake fraction and ΔT_b^{37-19} . The correlation between AMSR-E 37 GHz Tb and lake fraction for the 30 year satellite time series ranges from a high of $r = 0.27$ to a low of $r = 0.00$ with a mean of $r = 0.14$. However, the relationship between ΔT_b^{37-19} may not be as apparent at the satellite scale due to the range of lake fraction found in the EASE grid cells examined. The range of lake fraction for the 40 EASE grid cells was plotted on a frequency histogram (Figure 6.26).

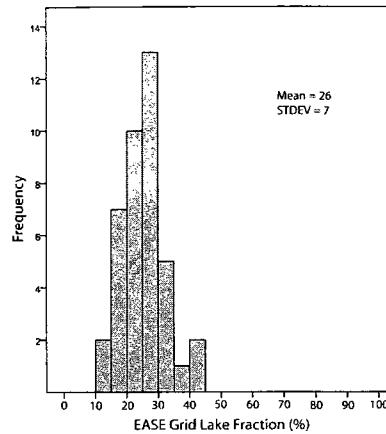


Figure 6.26. The frequency of lake fraction for the 40 EASE grid cells described in Chapter 5

The range of lake fraction for the EASE grid cells is much more constrained than in the airborne data. There were no grid cells with less than 10 % lake fraction and none with more than 50 % lake fraction. This could explain why the relationships seen using airborne data are not as apparent in the EASE grid data. For the range of lake fraction at the EASE grid scale (10 – 45%), there is little change in ΔT_b^{37-19} . Most of the slope (change in ΔT_b^{37-19}) is evident below 20 % and above 80 % lake fraction. Hence, a relationship between ΔT_b^{37-19} and lake fraction may not be apparent at the satellite scale because no EASE grid cells with < 20 or > 80 % lake fraction were examined.

A linear relationship could be used to correct for the influence of lake fraction on ΔT_b^{37-19} . However, this assumes that there is no significant difference in SWE on lakes and land. The linear relationships would be simpler as the equation could be applied to a given ΔT_b^{37-19} based on the lake fraction. However, unless EASE grid cells, which have < 20 or > 80 % lake fraction, are considered, the correction does not appear to be necessary. It is important to note that the difference in ΔT_b^{37-19} is not due to the presence of lakes themselves. It is because the snow pack properties on lakes are different than on land, mainly due to smaller basal grain size, and because ice has very

different emission characteristics than the land surface. Nonetheless, lake fraction does have a systematic influence on Tb at 6.9, 37 GHz and on the ΔT_b^{37-19} .

6.4. Summary of the Contribution of Airborne Data

Section 6.2 showed that for some terrain and land cover combinations there is a significant relationship between SWE and ΔT_b^{37-19} . However, airborne data, especially at a high resolution, present many challenges in isolating a relationship between Tb and SWE. A further complication was the definition of within-footprint SWE. The three resolutions of airborne data show that as footprint size increased the amplitude of variability in Tb decrease considerably. Explaining the variability in Tb in the high or mid resolution data would be very difficult and require a multi-factor mixing model. It is unlikely the snow, terrain, and land cover data could be collected to build such a model. Moreover, such an effort would be next to useless as airborne data are not available to provide operational estimates of SWE. Luckily, much of the variability in Tb at high and mid resolutions was not present in the low resolution data.

It can be assumed that most of the variability seen in the high and mid resolution airborne data is not going to be evident at the EASE grid scale. In the low resolution data, the variability of Tb is not sufficient to explain the natural variability in SWE at any one location. Hence, Tb data are reflective of only general differences. In the low resolution data, the only differences were in 37 GHz Tb and between land and lakes. However, in some years, the SWE on lakes was not significantly different from on land. If the SWE were not significantly different, a correction could be applied to compensate for the influence of lake fraction on Tb. However, the effect of lake fraction on Tb is most pronounced below 20 % and above 80 % lake fraction.

Given the generalization of Tb in the low resolution airborne data, it is not likely that slopes or other spatially constrained terrain features have a major influence on EASE grid ΔT_b^{37-19} . Moreover, at a given moment in time, with the possible exception of

lakes and land, there is little difference in ΔT_b^{37-19} across the tundra. Thus, it is essentially impossible to generate a satellite scale algorithm from airborne data. Moreover, satellite scale ΔT_b^{37-19} should not be expected to show much regional variability. However, differences in ΔT_b^{37-19} between seasons should be indicative of relative changes in snow cover properties.

CHAPTER 7: IMPROVING PASSIVE MICROWAVE ESTIMATES OF SWE

7.1. Introduction

Satellite passive microwave data have been used in the prairies and boreal forests to provide operational estimates of SWE. Operational algorithms rely on a linear relationship between ΔT_b^{37-19} and SWE. As SWE increases, there is greater scattering and absorption of emission at 37 GHz which results in a lower T_b . The complexity of tundra snow cover and landscape properties has limited the production of reliable estimates of SWE. Linking T_b change to SWE in the tundra is challenged by considerable heterogeneity in terrain, snowpack properties, land cover and surface water bodies. Multi-scale airborne passive microwave data show the extent to which T_b can vary at a sub-EASE grid satellite scale. However, using high resolution airborne data over flat tundra, a good relationship exists between SWE and ΔT_b^{37-19} . In general, as SWE increases, the ΔT_b^{37-19} decreases. This occurs up to a threshold of ~ 120 mm where the slope of the relationship reverses.

In other terrain categories, there are no strong relationships between ΔT_b^{37-19} and SWE. Over slopes and lakes, it is difficult to isolate the effect of SWE on T_b because of the influence of other snow, land cover, and lake ice properties on microwave emission. However, with decreasing resolution (larger footprint size), there is a greater mixing of terrain and snow cover properties. As a result, the variability in T_b diminishes; however, defining within footprint SWE becomes more difficult. Unfortunately, producing an algorithm to estimate SWE from airborne T_b data is not possible because, for flight data obtained in a short time period, there is little relative difference in snow pack properties and T_b . Ground based data may be able to provide the end-members necessary to understand how different snow cover properties influence T_b . However, the extremely small ground based footprints help understand the effect of mixing different terrain and land cover on T_b . Moreover, airborne and ground

based data are both spatially and temporally constrained. As such, satellite data are the only option for operational algorithm development as they are collected at regular intervals over large spatial extents.

7.2. The Quadratic Approach

A relationship between observed differences in tundra SWE and Tb is evident in satellite data presented in Chapter 5. However, the nature of the relationship does not follow expected trends. Normally, a greater ΔT_b^{37-19} relates to higher SWE, while a smaller ΔT_b^{37-19} relates to lower SWE. For the quadratic function presented in Chapter 5, the relationship between ΔT_b^{37-19} and SWE was positive for $SWE > \sim 150$ mm and in the opposite direction for $SWE < \sim 150$ mm. The quadratic function explains a large amount of the variance in in-situ SWE with ΔT_b^{37-19} . This suggests that on an empirical basis, the ΔT_b^{37-19} is sensitive to relative changes in SWE among the different seasons. The troubling part is that a greater ΔT_b^{37-19} should indicate higher SWE, not lower SWE. To investigate the difference in Tb from year to year, the 19 and 37 GHz Tb were plotted along with SWE, snow depth and ΔT_b^{37-19} (Figure 7.1).

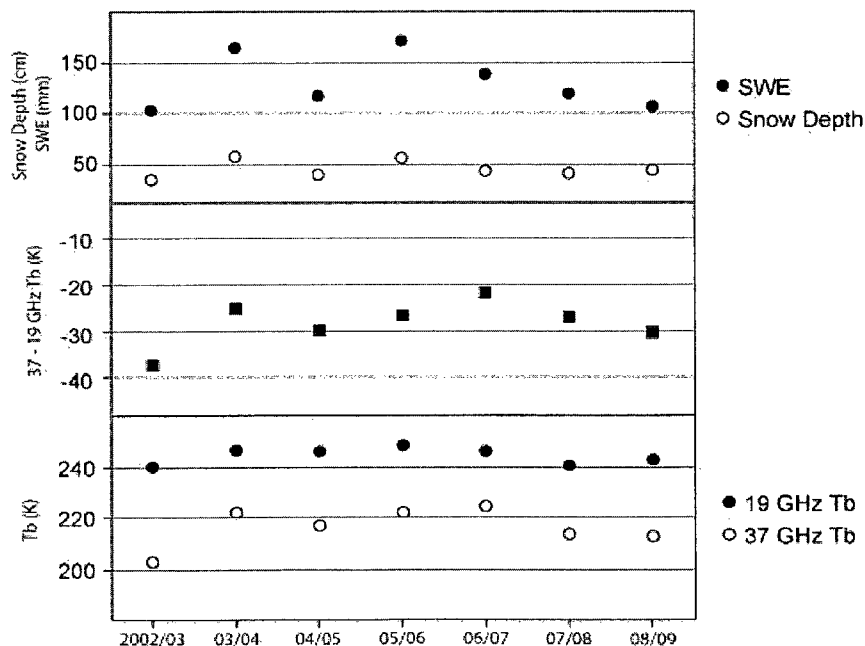


Figure 7.1. Plot 19, 37, ΔT_b^{37-19} and SWE

The difference in snow cover among years is most evident in the SWE. The snow depth does not vary as much as SWE. However, the years with higher snow depth also have higher SWE. This occurs because when the snow depth is greater, dense wind slab layers are thicker, and represent a higher proportion of the snow pack. In low snow years, the wind slab is thinner, and more of total depth is low density depth hoar.

In Figure 7.1, when SWE is greater, the ΔT_b^{37-19} is higher which, indicates less difference between 37 and 19 GHz Tb. The difference between the two frequencies is lower because the 37 GHz Tb is higher with greater SWE. As mentioned, in conventional algorithms the 37 GHz Tb should decrease with increasing SWE (below 120 mm SWE). In the years plotted, the lowest SWE (2003) also has the lowest 37 GHz Tb.

To explain the relationships in Figure 7.1, differences in snow stratigraphy must also be considered. Basal depth hoar has a large influence on 37 GHz Tb because the grain size often approaches the wavelength of emission. Depth hoar has the effect of lowering 37 GHz Tb disproportionately relative to the depth of SWE. For example, in the ground based data shown in Figure 6.7, the biggest shift in 37 GHz Tb occurred in the lower 20 cm of the snow pack, which was predominantly basal depth hoar. Above 20 cm depth, there was much less of a change in 37 GHz Tb. This is because at a certain point, the fine grained wind slab begins to self-emit which balances loss and can even raise the Tb.

If grain size has a stronger influence on Tb than SWE, then the years with larger snow grain sizes should also have lower Tb at 37 GHz. However, field observations show that the basal grain size and wind slab grain sizes do not vary much from year to year. Moreover, the thickness of the depth hoar depends on land surface properties and for a given location is relatively similar from year to year. However, the thickness and density of the wind slab layer over the depth hoar does change.

The years with higher snow depth also have a thicker wind slab. The thick slab masks the influence of underlying depth hoar on Tb by self-emission or by raising the depth of emission above the basal depth hoar layer. As a result, for years with thicker wind slab layers, the Tb at 37 GHz is higher. In low snow years, the depth hoar is absorbing more of the emission, and there is little wind slab to either raise the depth of emission or self emit. If these scenarios are plausible, then the inverse relationship between 37 GHz and SWE can be accounted for, and it can be inferred that satellite Tb is more sensitive to grain size and stratigraphy than SWE. However, the quadratic function fits observed SWE well. This can be explained because the differences in SWE are directly related to differences in snow stratigraphy. The quadratic function which defines the relationship between in-situ SWE and ΔTb^{37-19} is as follows:

$$SWE = \frac{-2.02 \pm \sqrt{4.08 - (-0.028(-169.08 - Tb_{37-19}))}}{-0.014}$$

Because the function describes a quadratic curve, there are two possible SWE for each ΔTb^{37-19} (Figure 7.2).

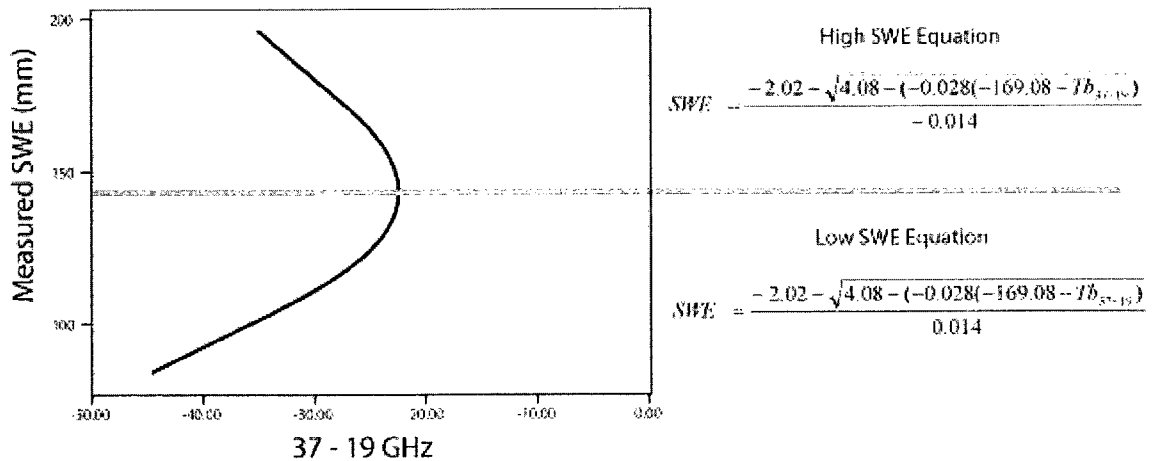


Figure 7.2. Quadratic function to estimate SWE from ΔTb^{37-19}

If the quadratic function is to be applied to years without field observation, then a method must be derived to decide which of the two SWE equations is appropriate.

Because of its sensitivity to grain size and stratigraphy, the 37 GHz Tb can be used to

determine if years fit better to the high or low SWE equation. If the 37 GHz Tb is low, it is likely because the wind slab is thin and the depth hoar is the predominant influence. In higher snow years, the influence of the depth hoar is diminished by the thicker wind slab, and higher 37 GHz Tb is produced. An initial threshold of 220 K was selected based on the available data. If the 37 GHz Tb is < 220 K, then the low SWE equation is used, and if the Tb is > 220 K, the high SWE equation is used. Using this simple logic, the fit of in-situ SWE and ΔT_b^{37-19} can be replicated (Figure 7.3).

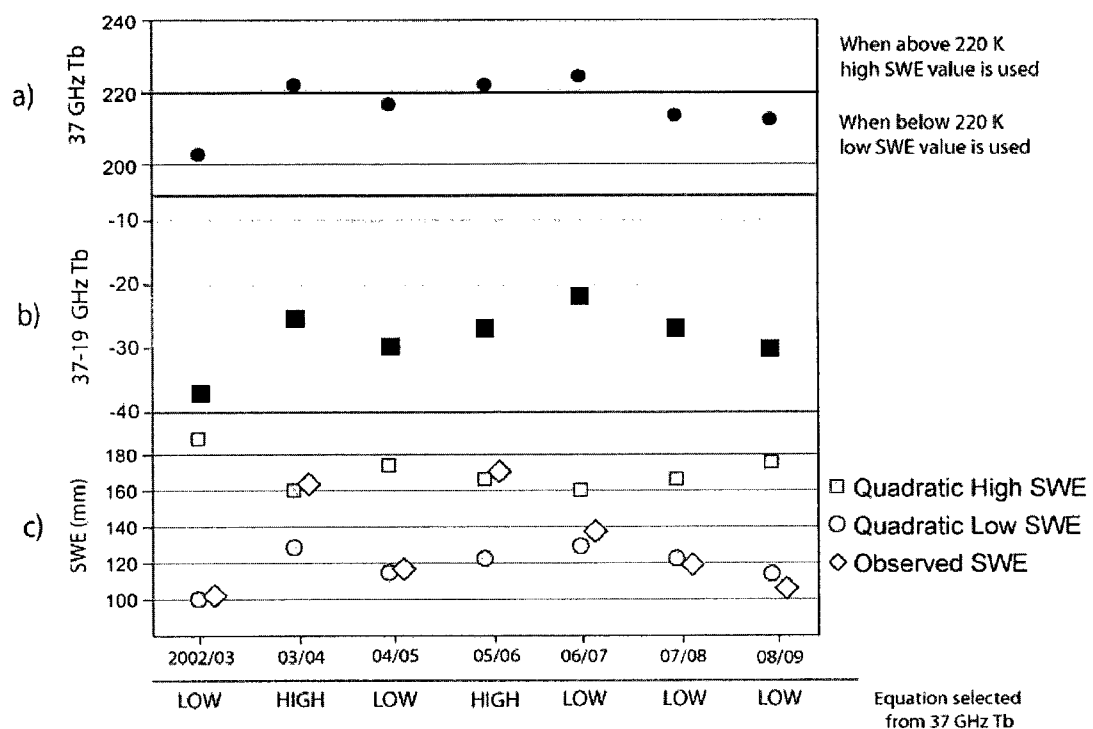


Figure 7.3. Selecting the high or low SWE equation from 37 GHz Tb

Figure 7.3 shows how the 37 GHz Tb can be used to select the appropriate equation for the best fit with observed SWE. This relationship is an important step towards understanding how Tb may be linked to changes in snow cover. However, without additional field data, there is little to suggest whether the relationship applies to past data or will be applicable in the future. Despite the inherent uncertainty, the satellite time series data were plotted using the quadratic function and high/low SWE indicator (Figure 7.4).

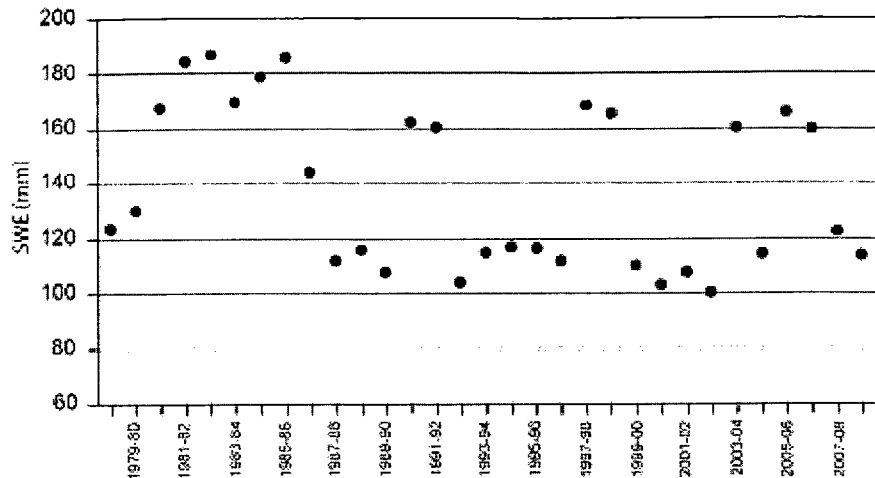


Figure 7.4. Estimates of SWE for the Daring Lake EASE grid from the 30 year satellite time series of ΔT_b^{37-19}

The quadratic function is an interesting empirical relationship derived from seven years of field data. However, beyond the years with in-situ data, it is not possible to determine the accuracy of the SWE estimates. Over the satellite time series (Figure 7.4), there are more SWE using the low SWE equation than the high SWE equation. However, in the SMMR data (1978 to 1988), the high SWE equation is used more often. This sensor specific pattern is unlikely a natural trend in SWE. It is likely that the 37 GHz threshold for the selecting the proper equation is not appropriate, especially for the SMMR data. Since the inception of the SSM/I sensor (1988), there have been only seven years that use high SWE equation. Three of the years (03/04, 05/06, and 06/07) have in-situ data to suggest that the higher SWE equation is appropriate. In the years using the low SWE equation, there is little difference in estimated SWE. Most years range from 100 to 120 mm SWE. One interesting pattern is that there are few estimates between 120 and 160 mm SWE. While these step changes are not likely a natural trend, the function provides some perspective on the relative changes in ΔT_b^{37-19} and how that may relate to tundra SWE.

The quadratic function to estimate SWE from ΔT_b^{37-19} performs well using the data in-situ collected for the study area. However, there is little to determine how well it would perform in other study areas or how well it is estimating past conditions. The quadratic shows that in the tundra the traditional relationships between ΔT_b^{37-19} and SWE may not necessarily apply. Moreover, it also shows that there are snowpack properties other than SWE which may be influencing satellite Tb.

7.3. Towards an operational algorithm

An operational algorithm for estimating tundra SWE has not yet been developed as the relationships with Tb are different than for other landscapes. Moreover, algorithms developed in other environments often perform poorly when compared to observed tundra SWE. For example, the EC open ground algorithm developed for the prairies (Goodison and Walker, 1995) consistently underestimates tundra SWE (Figure 7.5).

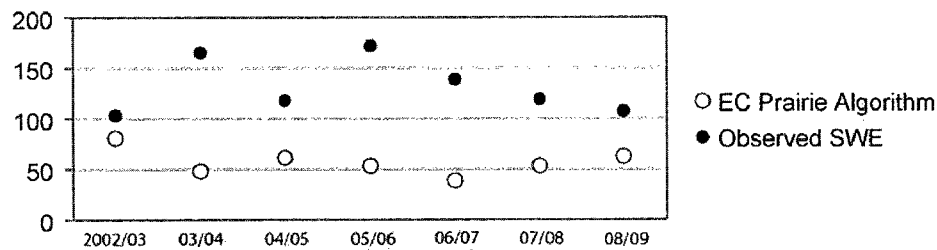


Figure 7.5. EC prairie algorithm estimates of tundra SWE

The prairie EC algorithm is based on a linear relationship between ΔT_b^{37-19} and SWE and was not parameterized for tundra snow packs. Furthermore, it is not intended for use when SWE exceeds 120 mm because it does not compensate for the reversal in 37 GHz Tb. Nonetheless, it is sensitive to the relative changes in SWE from year to year. However, the change in ΔT_b^{37-19} is inverse to observed SWE.

More recent algorithms perform somewhat better in the tundra. Derksen et al. (in press) developed a new approach using only 37 GHz Tb to estimate SWE. Airborne and satellite measurements were coupled with intensive tundra snow surveys to develop the

tundra-specific SWE algorithm. By using a single frequency, the influence of sub-grid lake fraction and the slope reversal in 37 GHz Tb with self-emission can be taken into account. Any change in Tb from January through April is thought to be largely due to an increase in SWE deposition. During low snow years, the Tb will decrease, and the threshold for the reversal in 37 GHz Tb may not be reached. However, in high snow years, the 37 GHz will begin to increase when the threshold of reversal is reached. By looking at the cumulative change in Tb, SWE can continue to be estimated through self-emission. A greater cumulative change in 37 GHz Tb from January through April should indicate higher end-of-season SWE.

This approach should yield reasonable results as the 37 GHz Tb does decrease from the start of the season to the end of the season in each year studied (Figure 7.6).

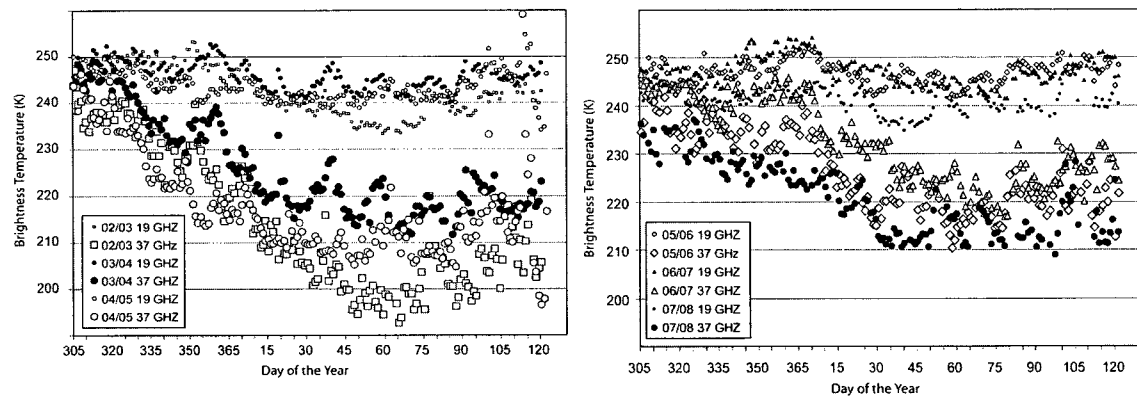


Figure 7.6. The seasonal evolution of 19GHz, 37 GHz from November 1 to April 30 (From Figure 5.2)

However, from Figure 7.6, it appears as though the years with higher SWE (03/04, 05/06) do not have the lowest 37 GHz Tb. Moreover, the years with lowest SWE (02/03, 04/05) seem to have more cumulative change in 37 GHz Tb. Hence, one of the biggest challenges in determining end-of-season SWE is taking into account the nature of the change in Tb throughout the season.

Results using a single frequency approach are encouraging for addressing some of the key challenges in estimating tundra SWE. However, given the relative stability of

19 GHz Tb, and the decrease in 37 GHz Tb during each of the years, using a ΔT_b^{37-19} approach should not be completely discounted (Figure 7.7).

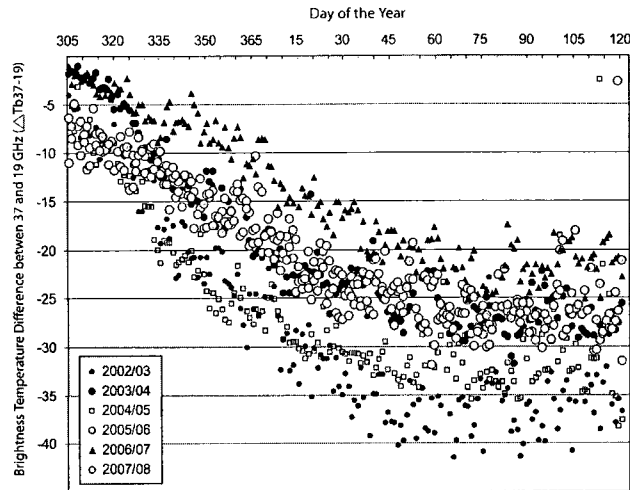


Figure 7.7. The seasonal evolution of the ΔT_b^{37-19} from November 1 to April 30 for 2002/03 to 2007/08 (From Figure 5.3)

Whether using a single frequency or a ΔT_b^{37-19} approach, future algorithm development would benefit from the integration of field observations. A similar approach to Pulliainen (2006), which weights passive microwave data driving a semi-empirical radiative transfer model and prior snow information from ground measurements with their respective statistical uncertainties, could be adopted. In fact, the approach developed by Pulliainen (2006) compares favourably to the 2006, 2007, and 2008 survey data (Solberg et al., 2009). However, an obvious limitation is the proximity of meteorological stations for the assimilation with Tb data.

7.4. Summary

7.4.1. Summary of Contributions

The overall objective of this research is to improve operational capabilities for estimating end of winter, pre-melt tundra SWE using satellite passive microwave data. The first step in improving estimates was to develop a better understanding of the distribution and properties of tundra snow within an EASE grid study area (Chapter 4).

In-situ snow data were then compared to satellite passive microwave data (Chapter 5). Multiple scales of ground based and airborne passive microwave data were then used to help resolve uncertainty in the relationship between satellite Tb and SWE (Chapter 6).

7.4.1.1. Summary of Tundra Snow Cover

The spatial distribution of snow depth, density and SWE is controlled by the interaction of blowing snow with terrain and land cover. The snow cover data collected confirmed that spatially constrained measurements are not sufficient to understand the distribution and properties of tundra snow. Despite the spatial heterogeneity of snow cover, several inter-annual consistencies were identified.

- Tundra snow density is consistent when considered on a site-by-site basis, among different terrain types, and from season to season.

A regional average density of 0.294 g/cm^3 was derived from the six years of measurements. When applied to site snow depths, there is little difference in SWE derived from either the site or the regional average density.

The high variability in SWE demonstrates the need to use a terrain based classification to better understand snow cover distribution.

- Despite potential differences in seasonal weather patterns, there are consistent ratios in the depth of SWE on flat tundra to the depth of SWE on other terrain categories.

As a result, despite differences in snowfall, the inter-annual patterns of terrain based SWE do not change very much. On slopes, the volume of snow in depositional drifts does change as does the aspect upon which the drifts form.

Variability in SWE was observed within and between different terrain types. The variability was described by the coefficient of variation (CV). The variability in SWE was least on lakes and flat tundra, greater on slopes and the highest on plateaus. Despite differences in mean SWE from year to year, the variability (CV) in a given terrain

category is quite similar. The overall weighted mean CV for the study area was shown to be 0.40, which is a useful generalization for studies done using coarse resolution grids at a regional scale.

For application to remote sensing and other grid based modelling, snow cover data need to be generalized and extrapolated over larger areas. Moreover, coarse resolution passive microwave remote sensing data attempt to provide single estimates of SWE over 625 km² EASE grid cells. These estimates are essentially useless unless they can be related to sub-grid snow cover properties.

- A terrain and landscape based classification scheme is used to generalize and extrapolate tundra SWE.

Using this type of classification, sub-grid snow cover properties can be scaled up from point data or down from EASE grid data. Deriving a weighted mean SWE based on the spatial proportion of landscape and terrain features was shown as the best method for generalizing the distribution of tundra SWE.

7.4.1.2. Summary of Satellite Tb Data

Satellite data were summarized for the seasons with in-situ snow cover observations. Within each season and among each season, there was little difference in 19 GHz Tb. However, during each season, there was always a large decrease in 37 GHz Tb from early November through April. The magnitude of the decrease varied from year to year. As a result of the drop in 37 GHz Tb relative to 19 GHz Tb, the ΔT_b^{37-19} decreased from zero in early November to a maximum of -20 to -42 in March or April.

- The change in ΔT_b^{37-19} throughout each season shows a sensitivity in 37 GHz Tb to parameters that evolve over a winter season.

To look for inter-annually consistent spatial patterns of ΔT_b^{37-19} , a principal components analysis (PCA) was applied to a domain of EASE grid cells surrounding the study area. The PCA showed that there are differences in ΔT_b^{37-19} among different EASE grids and

that land cover may have an influence on regional Tb. The PCA was also used for the comparison of the 30 year time series of Tb to EASE grid lake fraction.

- The spatial patterns in end of season ΔT_b^{37-19} were not well correlated to lake fraction in any of the 30 years in the time series.

There was a good relationship between ΔT_b^{37-19} and in-situ SWE. Below 150 mm, the data show a positive linear relationship. As the ΔT_b^{37-19} increases so does the in-situ SWE. Above 150 mm, the relationship is linear but in the opposite direction.

- A quadratic function was fitted to explain 89 percent of the variance in SWE from ΔT_b^{37-19} .

The quadratic relationship provides a good fit between the data; however, the nature of the relationship is opposite to the expected linear relationship between ΔT_b^{37-19} and SWE. Most linear relationships are based on the assumption that as the SWE increases the ΔT_b^{37-19} decreases (a greater difference between 19 and 37 GHz). The quadratic shows that below 150 mm SWE, as the SWE increases, the difference between 19 and 37 GHz decreases. However, beyond 150 mm SWE, a larger ΔT_b^{37-19} corresponds to greater SWE.

7.4.1.3. *Summary of Multi-scale Tb Data*

High resolution Tb data are useful for examining how different snow, land cover and terrain properties influence microwave emission. However, due to the complexity of snow and terrain even in small footprints, it is a challenge to isolate any relationship between SWE and Tb. High resolution Tb data were compared to SWE from both in-situ sites and Magna Probe transects.

- In flat tundra, there was a significant relationship between SWE and ΔT_b^{37-19} .
- On lakes and slopes, no strong relationships were found between SWE and ΔT_b^{37-19} .

Three resolutions of airborne data were available, and the Tb from each were compared along transects through different terrain, land cover and SWE.

- As the airborne footprint size increased, the amplitude of variability in Tb decreased considerably.

As such, it can be assumed that most of the variability seen in the high and mid resolution airborne data is not going to be evident at the EASE grid scale.

- Hence, slopes or other spatially constrained terrain features will not have a major influence on EASE grid scale Tb.

However, as a result, the Tb in large footprints is not sensitive to the local scale variability in SWE.

- In the low resolution airborne data, the only differences in Tb (37 GHz) were between land and lakes.

However, in some years, the SWE on lakes was not significantly different from that on land. Differences in Tb are caused by the difference in snow structure from lakes to terrestrial surfaces.

- The effect of lake fraction on 37 GHz Tb is most pronounced below 20 % and above 80 % lake fraction.

For years in which the SWE were not significantly different from lakes to land, a correction could be applied to compensate for the influence of lake fraction on Tb.

With the exception of lakes and land there is little difference in ΔT_b^{37-19} across the tundra, in the low resolution airborne data. Thus, it is essentially impossible to generate an operational satellite scale algorithm from airborne data. Moreover, satellite scale ΔT_b^{37-19} should not be expected to show much regional variability in a given year. The differences in ΔT_b^{37-19} among years is indicative of relative changes in snow cover properties.

7.4.2. Remaining Challenges

The theoretical challenges to developing an operational algorithm for estimating tundra SWE were outlined in Section 2.4. Essentially the biggest challenge is accounting for influence of sub-grid, snow, terrain and land cover properties on satellite emission (Table 7.1).

Table 7.1. Factors in the tundra that affect passive microwave brightness temperature

Factor	Influences on passive microwave emission
Terrain and Landscape	<ul style="list-style-type: none">- Topography (terrain)- Surface Roughness- Vegetation Cover- Soil Condition- Lake Cover Fraction
Snow Cover	<ul style="list-style-type: none">- SWE- Snow Depth- Snow Density- Grain Size- Stratigraphy (wind slabs/depth hoar)

The airborne, ground based and satellite data all show that Tb responds to differences in snow cover properties. The remaining challenge is relating the change in Tb to changes in SWE. In order to isolate SWE, the influence of all other factors on satellite Tb must be understood.

7.4.2.1. Terrain and Landscape

The most prominent effect of terrain is the influence of topography on the wind-redistribution of snow. Snow accumulation patterns throughout the study area are driven by wind redistribution. This results in uneven snow accumulation patterns with large spatially constrained drifts forming on leeward slopes. Although deep drifts are important components of the hydrologic cycle, they occupy a small spatial percentage of the landscape. Moreover, while these slopes present a challenge to interpreting high resolution airborne and ground based Tb, they have little effect on low resolution

airborne Tb. As such, it is assumed they have even less influence on Tb at the EASE grid scale.

Land surface roughness and vegetation cover have an influence on the accumulation of blowing snow. Deeper snow can be found in the lee of rocks, boulders and shrub vegetation. The variability in the land surface is responsible for local scale variability in snow cover, which limits the ability to link SWE with Tb in the high resolution airborne footprint. Fortunately, much of the variability in high resolution Tb is not evident in the mid and low resolution airborne data.

Soil condition is another factor which has the potential to influence Tb. However, the influence of soil condition would be more prominent in the early part of the season. By late winter, the depth of snow is sufficient that the contribution to 37 GHz Tb would be minimal. Soil condition should have a greater influence on 19 GHz Tb. However, all resolutions of airborne data show little difference in 19 GHz Tb through different terrain and land cover.

Lake fraction is often cited as one of the most prominent challenges in operational algorithm development. The influence of lake fraction, similar to soil conditions, is not temporally static. In early winter, when snow and ice thickness are lowest, there is a greater influence of underlying water on both 19 and 37 GHz Tb. However, as snow and ice accumulate through the winter, the effect on Tb diminishes. By the end of the season, snow depth and ice thickness are sufficient that, even at 19 GHz, there is little influence of lake fraction. The main influence of lakes on 37 GHz Tb is the difference in snow pack properties from lakes to land. However, due to the mixing of lakes and land, there is little evidence of a similar relationship at the satellite scale. As such, the effect of lake fraction on end-of-season satellite scale SWE retrievals should be minimal.

7.4.2.2. *Snow Cover*

Variability in snow cover properties can complicate the understanding of microwave emission and Tb. Snow depth, SWE, grain size and stratigraphy all have a potential influence on Tb which can complicate the isolation of any one parameter. However, most snow cover properties are interrelated, which provides the potential for explaining Tb. For example, lower Tb at 37 GHz is often linked to the presence of large grained basal depth hoar. In the tundra, the presence of depth hoar depends on land surface roughness, vegetation cover and soil moisture. However, the thickness of basal depth hoar is relatively consistent from year to year. What varies from year to year is the thickness of the overlying wind slab. As the slab increases in thickness, the effect of the depth hoar is diminished, and Tb at 37 GHz increases. While linked to grain size, the increase in Tb occurs in conjunction with an increase in both snow depth and SWE.

The low resolution airborne data show that Tb does not vary a great deal across different terrain and snow covered surfaces. Hence, the variability in local scale SWE is not reflected in coarse resolution Tb. As a result, one of the biggest challenges is defining SWE at the EASE grid scale. A terrain weighted mean SWE is presented; however, a single mean value does not account for the variability at any given location. Moreover, spatially constrained features with disproportionate SWE (deep drifts), can skew a weighted mean, despite the fact that they have little influence on coarse resolution Tb.

To resolve uncertainties, a sensitivity analysis approach could be applied. Microwave emission models could be used to simulate Tb under different snow, land and terrain cover conditions. With this approach, it can be determined which snow cover parameters have the greatest influence on coarse resolution Tb.

Algorithm development should be possible as satellite scale ΔT_b^{37-19} changes from year to year in response to changes in snow cover properties. However, the most important contribution to understanding these changes is the in-situ observations of snow cover. In order to develop a better understanding of the relationship between SWE and T_b , collection of in-situ snow cover data should continue into the future.

APPENDIX A: SWE IN HIGH RESOLUTION FOOTPRINTS

One of the main challenges in using passive microwave data to estimate SWE is quantifying footprint SWE. Typically a single SWE value, which is an average of all measurements taken within each footprint, is used for comparison with Tb. However, the variability in SWE within a footprint is not considered. Poor relationships between SWE and Tb could easily stem from an improper quantification of within-footprint SWE.

As outlined in Section 6.2.1, the SWE used for comparison to high resolution Tb were derived either from single sites with 30 random depth and 5 random density measurements in the footprint or from at least 10 Magna Probe depth measurements and 2-4 density measurements on transects through the footprints. Using a mean SWE can be misleading in that there is no indication of within footprint variability. Using a mean assumes that the SWE is relatively homogenous within each footprint and that relative differences in SWE among footprints can be related to corresponding differences in Tb. The variability of SWE within a footprint needs to be examined using the site SWE and Magna Probe SWE data.

Site SWE

Chapter 4 showed that the variability in SWE among sites in different terrain types can be considerable. The site data provide a mean SWE for comparison with Tb; however, the applicability of the mean depends on how much variability is present in 30 depth and 5 density measurements. As such, the variability within a site should be considered when comparing to footprint Tb. To examine variability in SWE to Tb, the 2005 and 2008 flat tundra sites were plotted from low to high SWE including ± 1 STDEV, along with 19 and 37 GHz Tb (Figure A.1).

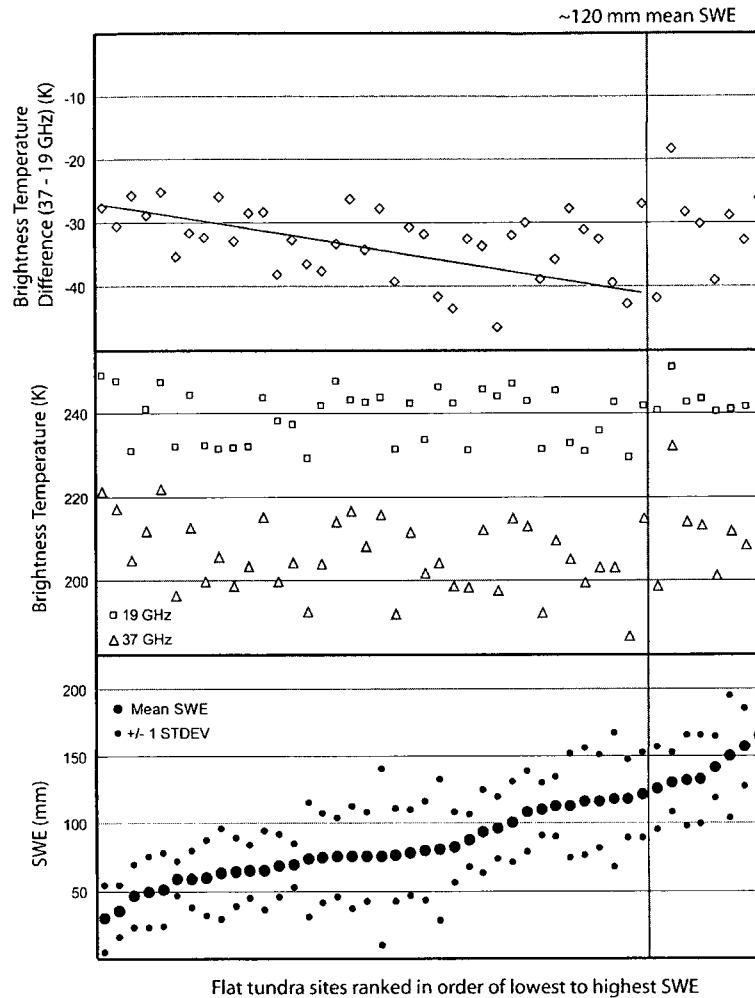


Figure A.1. Plot of SWE \pm 1 STDEV and Tb for flat tundra sites in 2005 and 2008

Figure A.1 shows that at all sites, there is substantial variability in SWE. The highest variability is at sites with a mean SWE of 75 to 100 mm. Above 100 mm and below 75 mm, the STDEV is lower relative to the mean. The 19 GHz remains fairly constant as SWE increases; however, for very similar SWE, the difference in 19 GHz Tb can be up to 20 K. The general pattern in 37 GHz Tb is a decrease with increasing SWE. However, similar to the 19 GHz, there is a high range in Tb for similar SWE. The ΔT_b^{37-19} yields less scatter than the individual Tb, and there is a decreasing trend with increasing SWE. Similar to Section 6.2.1, a relationship is difficult to establish when there is a large range in ΔT_b^{37-19} for a small range in mean SWE. If there should be a relationship

among ΔT_b^{37-19} and SWE, then the mean SWE alone is not properly characterizing the effect snow has on Tb.

Since the variability is high within each footprint, then it is possible that a range of single SWE values could best describe within footprint SWE. For example, using the data from Figure A.1, it is possible to manually modify the SWE, within 1 STDEV of the original mean, and produce a strong relationship with ΔT_b^{37-19} (Figure A.2).

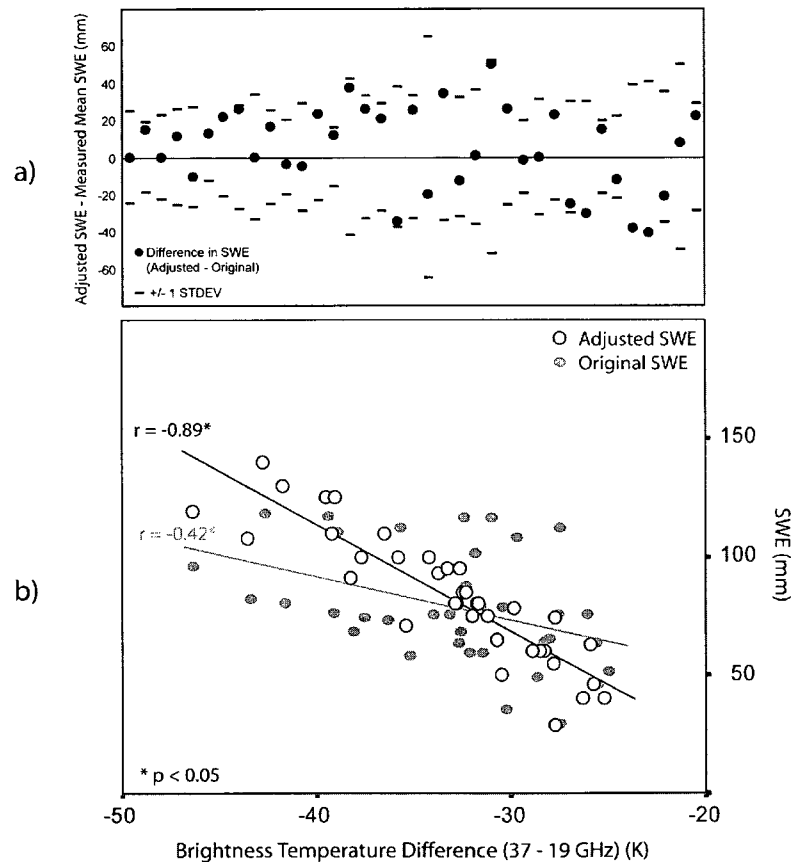


Figure A.2. Adjusted mean SWE and original SWE vs ΔT_b^{37-19}

Figure A.2 b shows that the manual, iterative adjustments made to each original mean SWE drastically improve the relationship. Figure A.2 a shows how the mean SWE were adjusted. A positive adjustment means that the new SWE is higher than the original, while a negative indicates that the new SWE is lower than the original. Both positive and negative adjustments were made, and in some cases, no adjustment was

necessary. In most cases, the adjustments in SWE made were almost a full STDEV away from the original mean. Figure A.2 shows that, by working within 1 STDEV of the mean SWE, it is possible to generate a very strong relationship with ΔT_b^{37-19} .

The variability in SWE at each site and the ability to produce a very strong relationship with ΔT_b^{37-19} bring into question the validity of using a mean site SWE for comparison with footprint T_b . However, without a better perspective of how 30 site measurements compare to the spatial distribution of SWE within the entire footprint, it is difficult to suggest an alternative. Data were collected in Churchill, Manitoba, in February 2010 to better understand how 30 random depth measurements compare to a surface generated from 940 gridded depth measurements in a 50 x 90 m homogenous flat, tundra like fen (Figure A.3).

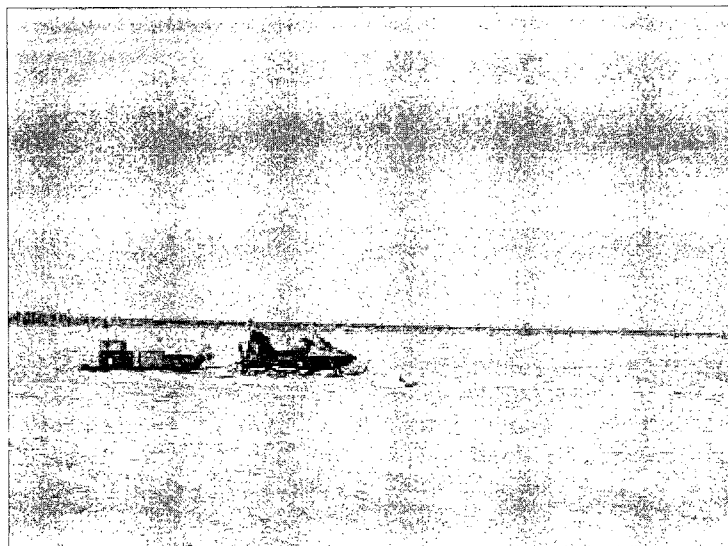


Figure A.3. Open fen site, Churchill, Manitoba

The 940 probe measurements were taken at 1.5 m intervals along 14 transects which were spaced 3.5 m apart. To replicate a typical site, 30 measurements were taken independent of the 940 at random locations through the center of the measurement grid. The descriptive statistics for both data sets were calculated (Table A.1).

Table A.1. Descriptive statistics of the Churchill Magna Probe experiment

	Mean (cm)	STDEV	CV	Min	Max
30 random depth	32.1	7.5	0.23	17.2	48.5
940 gridded depth	32.3	6.7	0.20	12.7	57.5

The mean depth from both methods is essentially the same. However, the 30 measurements show slightly more variability and do not capture as wide a range in depth. Interestingly, despite a small difference in standard deviation, using either technique would yield a very similar mean snow depth.

However, since T_b is an integration of all snow within a footprint, it is necessary to examine if the 30 random measurements can capture the spatial variability within the 50 x 90 m test area. An interpolated surface was generated from the 940 measurements using simple kriging (Figure A.4).

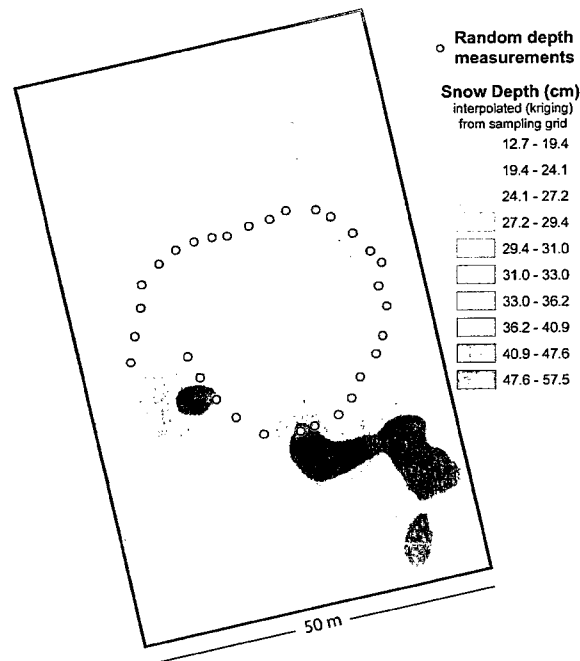


Figure A.4. Interpolated surface from 940 probe measurements and location of 30 random measurements

Using a grid of measurements, it is possible to effectively map the spatial distribution of snow depth. Wind driven re-distribution through the winter produces a

more or less level, dense slab, snow surface (Figure A.3). As a result, the variability in depth on the interpolated map corresponds to the surface roughness, vegetation cover, or micro-topography of the underlying ground. In these types of sites, pockets of deeper SWE are usually associated with water filled depressions while shallower depths are located on hummocky areas between depressions.

To look at the difference between the 30 random points and the interpolated surface, the residual error between the two depths was calculated (residual = depth at random point – depth predicted from interpolated surface). The residuals (un-standardized) were plotted for each of the 30 probe locations (Figure A.5).

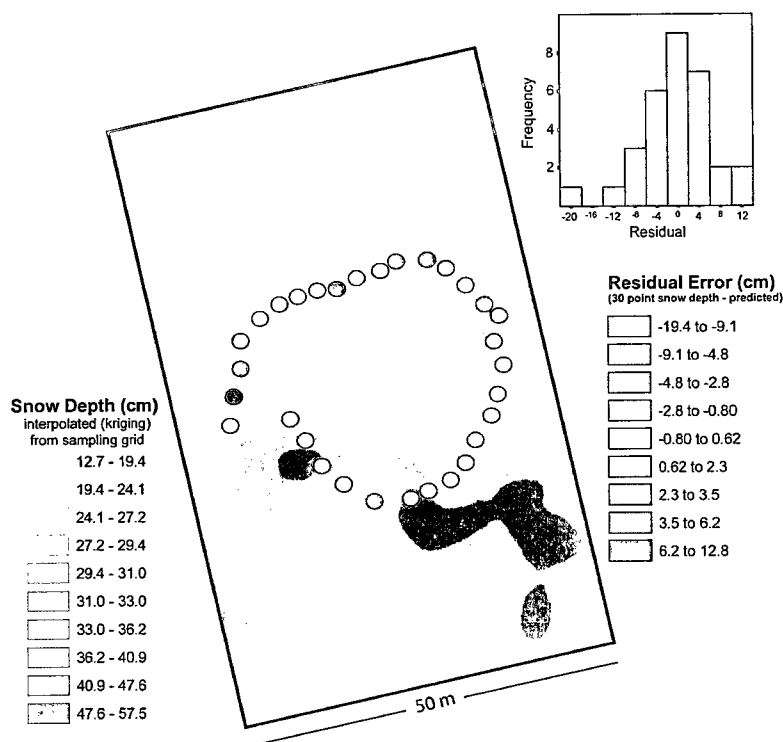


Figure A.5. Residual error between 30 random measurements and predicted surface from interpolation of 940 gridded measurements

Negative residuals show areas where the actual depth is lower than the predicted depth (Red). Positive residuals show areas where actual depth is higher than predicted

(Green). With the exception of one large negative value (-19 cm), the distribution of residuals is fairly normal showing equal points of negative and positive residual error. Moreover, all but six points have an error of equal to or less than one standard deviation of the mean (~ 7 cm).

These data show not only that using either 30 points or 940 points will produce similar mean depth, but also that, in most cases, the depths at the 30 random locations will be ± 1 STDEV of the surface generated by 940 points. However, the inverse is that the interpolated surface cannot accurately predict all of the 30 depth measurements to within 1 STDEV. Hence, the spatial scale of snow depth variability can be less than 2 m at this type of site. It should be noted that some uncertainty in the surface is a product of using GPS. The non-differential GPS on the Magna Probe has an absolute accuracy of ± 10 m and a relative accuracy of ± 2 m on such grid measurements. Nonetheless, this site provides a useful glimpse into the variability of snow depth in an area of similar dimensions to a high resolution airborne footprint. Despite the spatial variability, it presents the most ideal case in that the terrain and land cover (surface roughness) is very uniform compared to the shield tundra of Daring Lake. These sampling techniques should be employed in the future in the tundra to help quantify the spatial variability of depth and SWE in different terrain and land cover. Moreover, these methods would be very useful in establishing a sampling design to accurately reflect the snow cover properties in an efficient manner as possible.

Magna Probe SWE

Magna Probe measurements along transects provide a sense of the spatial distribution of SWE through a footprint. Magna Probe depth measurements were taken at roughly equal intervals along flight lines (5 m). The density data were also taken at roughly equal intervals and applied to the nearest depth measurement. As a result,

transect SWE can be plotted to provide a spatially proportional footprint SWE. Moreover, by plotting successive measurements, the variability in footprint depth can be examined.

The linear relationship among SWE vs. ΔT_b^{37-19} from the flat tundra Magna Probe data was plotted (Figure A.6 a). The Magna Probe SWE from four example footprints was plotted (Figure A.6 b). Two of the footprints were selected which fit well (C and D), and two footprints were selected which do not fit well (A and B) with the linear relationship between SWE vs ΔT_b^{37-19} . The mean footprint SWE calculated from the Magna Probe data was also plotted as well as the mean SWE required to fit well with ΔT_b^{37-19} . The mean Magna Probe SWE is shown as the thick black line in the four footprint areas and the dashed shows where the SWE would need to be in order to be on the line of best fit for ΔT_b^{37-19} SWE (Figure A.6 b).

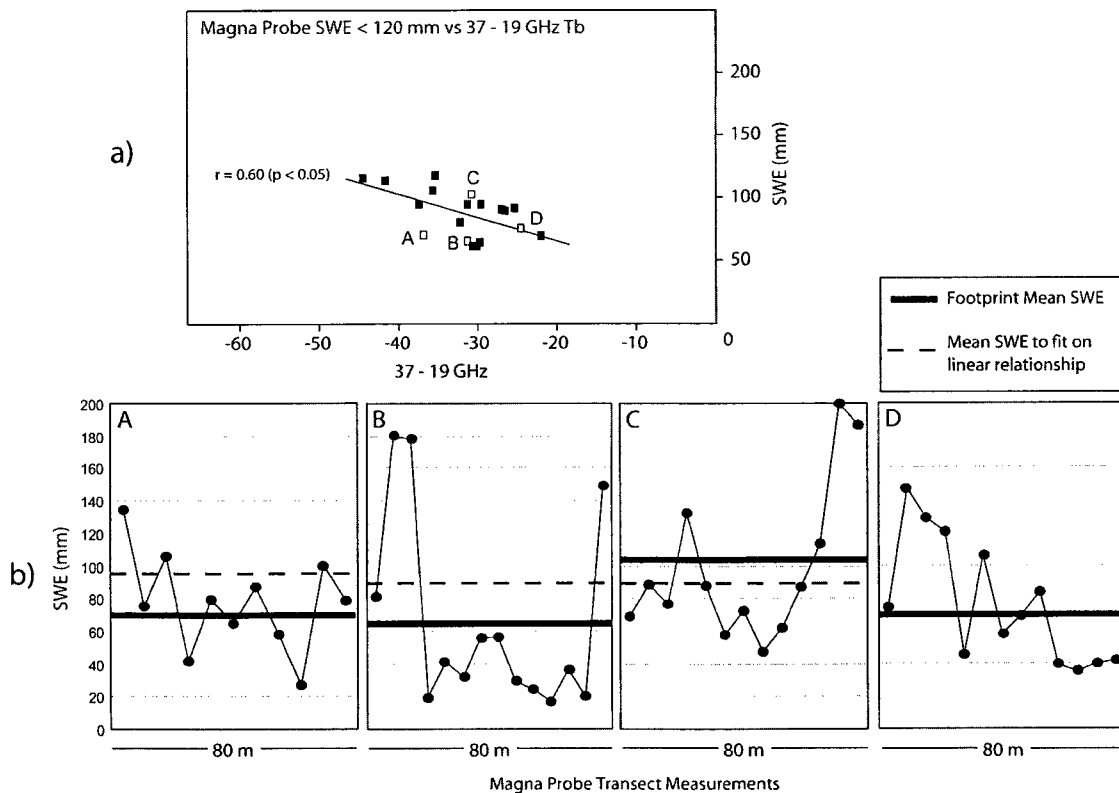


Figure A.6. SWE from four example footprints and SWE vs ΔT_b^{37-19} for Magna Probe SWE < 120 mm on flat tundra

Each footprint (A, B, C, D) shows a high range (~ 100 mm) of SWE across the 80 m distance. In footprints A and B, the mean SWE is too low and would have to be higher in order to be a better fit with the linear relationship in Figure A.6 a. In footprint C, the SWE would need to be lower and essentially the same as footprint B as they both have a very similar ΔT_b^{37-19} . In footprint D, the mean SWE fits perfectly on the linear relationship with ΔT_b^{37-19} .

The variability in SWE in footprints A and D appears to be lower, suggesting that the mean is representative of the spatial distribution of SWE in the footprint. However, in footprints B and C, the mean is skewed to higher SWE by spatially constrained extreme values. In the case of footprint C, ignoring the high SWE at the end of the transect would lower the mean SWE and produce a better fit with ΔT_b^{37-19} . In footprint B, the high SWE could be disregarded; however, this would lower the mean SWE and make the relationship with ΔT_b^{37-19} even worse.

Based on the dashed lines in Figure A.6 b, footprints A, B, and C, all require a similar mean SWE to fit well with ΔT_b^{37-19} . Upon first glance, it seems that each footprint has a dissimilar distribution of SWE. A Games-Howell difference of means test was used to determine if the SWE in each footprint are significantly different. None of the four example footprints has significantly different SWE (Table A.2).

Table A.2. Difference of mean SWE for the four example footprints in Figure A.6

Difference in Footprint SWE		Mean Difference SWE (mm) (GH Post-hoc)	Sig
A	B	-12.82	.900
	C	-19.97	.625
	D	2.65	.998
B	A	-12.82	.900
	C	-32.79	.401
	D	-10.16	.950
C	D	22.63	.552

Some of the footprints have a large mean difference; however, they are not close to being statistically different. Despite the statistical indifference in SWE, the ΔT_b^{37-19} for each footprint ranges from -24 to -37 K. The difference in ΔT_b^{37-19} of 13 K should be related to a change in SWE. Part of the reason for the statistical indifference in SWE is the low sample n in each footprint (10 to 15), as well as the presence of extreme values. The footprints with the highest (-22 K) and lowest (-44 K) ΔT_b^{37-19} from Figure A.6 a) were examined to see if they had dissimilar distributions of SWE (Figure A.7).

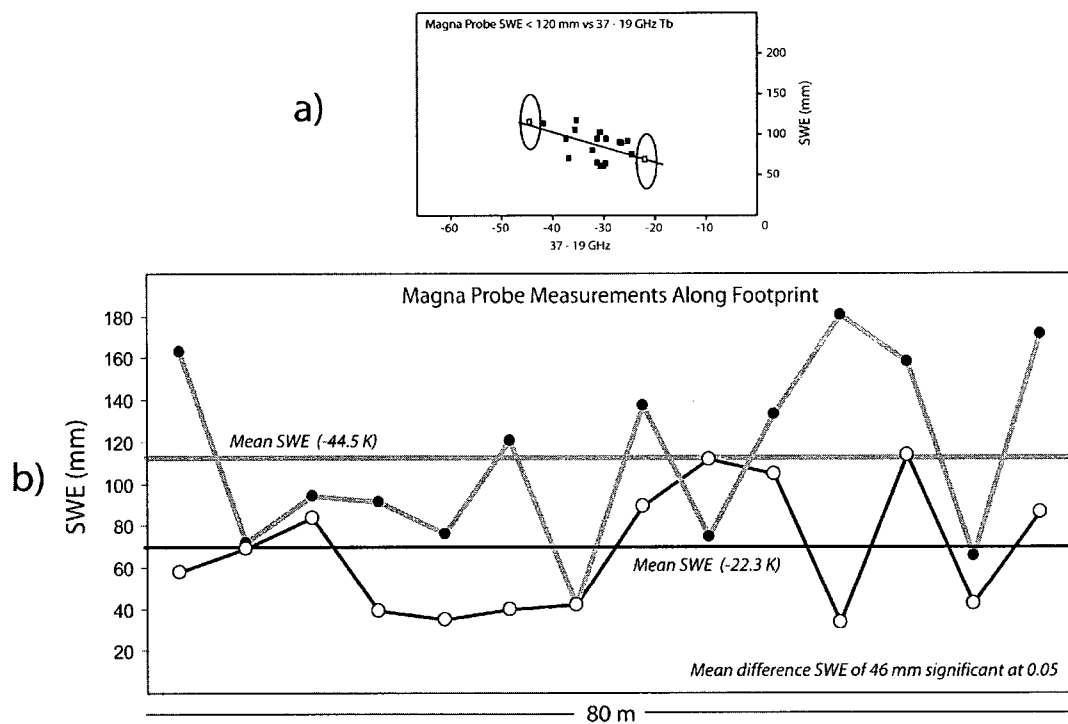


Figure A.7. The distribution of SWE in two footprints with the lowest and highest ΔT_b^{37-19}

The mean difference in SWE of 46 mm between the two footprints in Figure A.7 b) is significant ($p < 0.05$). Despite the means being different, there are similarities in SWE in some locations along each transect. Moreover, both footprints show that on flat tundra the depth of SWE can vary considerably over an 80 m distance. The difference in SWE along the two transects is not as distinct as expected for a 22 K difference in ΔT_b^{37-19} . This illustrates one of the greatest limitations of using high resolution airborne

radiometer data. The benefit of airborne data is that many footprints can be sampled over different terrain along many transects. The hope is to discover a large contrast in ΔT_b^{37-19} or SWE which can then be used to build a predictive model. However, airborne data collected in one season are of limited use to achieve this goal. There is considerable variability within most footprints, and the mean SWE among different footprints is often similar. It is not until the end points of ΔT_b^{37-19} are examined (Figure A.7) that there is a significant difference in SWE.

The Magna Probe data help to show that within small footprints (80 m), there can be a large range of SWE for terrain assumed to be relatively homogenous. The variability in footprint SWE brings into question what can hope to be achieved in terms of relating ΔT_b^{37-19} to a single value of SWE. It is more likely that ΔT_b^{37-19} can be related to relative differences in SWE over large areas which integrate the small scale variability. Moreover, to build a model for estimating SWE from ΔT_b^{37-19} , it is necessary to include other factors to help reduce the uncertainty. Hence, SWE is likely to be predicted with a multivariate approach which includes more than just ΔT_b^{37-19} .

Effect of Land Cover

As discussed in Section 6.2.2.3, a clear relationship between SWE and T_b is hampered by other snow and land cover properties. As discussed in Chapter 4, terrain is clearly not the only factor controlling the distribution of SWE. Land cover and surface roughness should also be considered.

Land cover can influence the distribution of SWE in many ways. The presence of ground vegetation at the base or throughout the snowpack can act as a thermal insulator which helps keep the ground temperature warmer than on bare ground. The vegetation helps increase the snowpack temperature gradient which leads to greater depth hoar development and larger snow grain sizes (Sturm et al., 2000). Furthermore, the height of vegetation also plays a role. Shrubs and dwarf birch trap drifting snow which results in

greater snow depth and limits the development of dense slab layers until the shrubs become completely covered with snow. As a result, the bulk snow density in shrub areas is always lower. Essentially the surface roughness has a dominant influence on snow accumulation and snow grain morphology (Figure A.8).

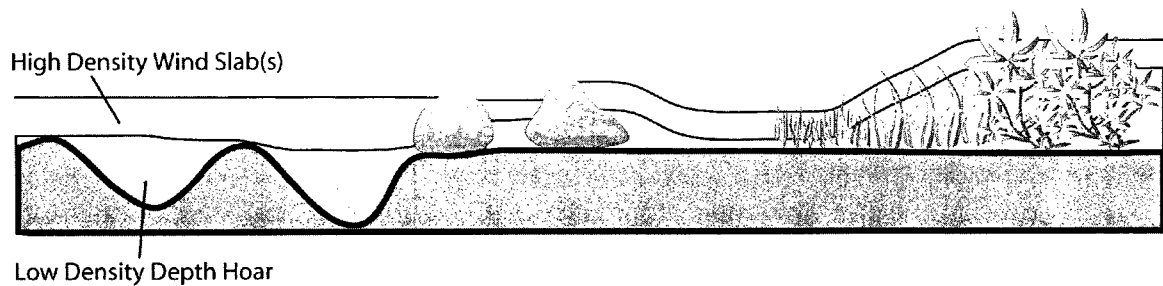


Figure A.8. Idealized relationship between surface roughness and snow pack properties

To assess the effect of land cover, the Magna Probe SWE for flat tundra was compared to the GNWT Landcover Classification discussed in Chapter 3. Figure A.9 shows mean SWE with error bars of ± 1 STDEV for each Flat tundra Landcover Class.

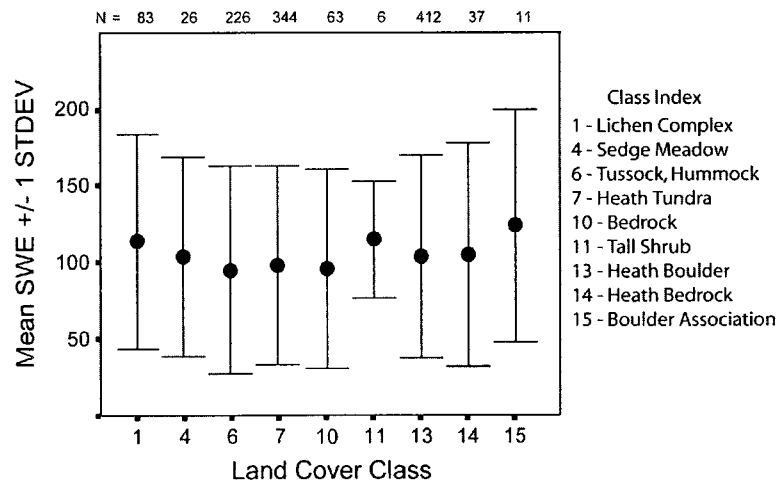


Figure A.9. Mean Magna Probe SWE (± 1 STDEV) for each land cover class

Figure A.9 shows that no land cover class has distinctly higher or lower SWE. The highest mean SWE are in the Tall Shrub and Boulder Classes; however, both

classes have relatively low sample numbers. The Tall Shrub class should have the highest SWE, but such areas are not abundant along the transect lines. The variability (STDEV) for each class is quite high which suggests that there is a high similarity in SWE among the classes and little difference in mean SWE. As a result, there are no dominant patterns between SWE and land cover using the LANDSAT classification data. The variability in SWE shown in Figure A.9 is present at the sub-land cover scale. Hence, as Figure A.8 suggests, local surface roughness may play a greater role in describing SWE than regional terrain and land cover classes. Given the variability in SWE for flat tundra, it is remarkable that there is any discernable relationship between ΔT_b^{37-19} and SWE.

REFERENCES

- ACIA. 2004. *Arctic Climate Impact Assessment*. Cambridge University Press.
<http://www.acia.uaf.edu>. Retrieved September 9, 2008.
- Armstrong, R. L., A. Chang, A. Rango, and E. Josberger. 1993. Snow depths and grain size relationships with relevance for passive microwave studies. *Annals of Glaciology*. 17. 171-176.
- Armstrong, Richard, M. J. Brodzik, A. Varani. 1997. The NSIDC EASE-Grid: Addressing the need for a common, flexible, mapping and gridding scheme. *Earth System Monitor*. 7. 6-7.
- Armstrong, R., L. and M. J. Brodzik. 2002. Hemispheric-scale comparison and evaluation of passive microwave snow algorithms. *Annals of Glaciology*. 34. 38 – 44.
- Asmus, K. W. and C. Grant. 1999. Surface Based Radiometer (SBR) Data Acquisition System. *International Journal of Remote Sensing*. 20. 3125 – 3129.
- Baghdadi, N., J. P. Fortin, and M. Bernier. 1997. Capability of Multitemporal ERS-1 SAR Data for Wet-Snow Mapping. *Remote Sensing of the Environment*. 60. 174-187.
- Baghdadi, N., J. P. Fortin, and M. Bernier. 1999. Accuracy of wet snow mapping using simulated Radarsat backscattering coefficients from observed snow cover characteristics. *International Journal of Remote Sensing*. 20. No. 10. 2049-2068.
- Bamzai, A. 2003. Relationship between snow cover variability and Arctic oscillation index on a hierarchy of time scales. *International Journal of Climatology*, 23. 131–142.
- Barry, R. G. 1997. Cryospheric Data for Model Validations: Requirements and Status. *Annals of Glaciology*. 25.
- Basist, A., D. Garrett, R. Ferraro, N. Grody, and K. Mitchell. 1996. A Comparison Between Snow Cover Products Derived from Visible and Microwave Satellite Observations. *Journal of Applied Meteorology*. 35. 163-177.
- Beringer, J., S. Chapin III, C. C. Thompson, and D. A. McGuire. 2005 . Surface energy exchanges along a tundra-forest transition and feedbacks to climate Jason *Agricultural and Forest Meteorology*. 131. 143–161.
- Berry. M. O. 1981. Snow and Climate. In: *The Handbook of Snow, Principles, Processes, Management and Use*. In D. M. Gray and D. H. Male (eds). Toronto, Canada: Pergamon Press.
- Biancamaria, S., N. M. Mognard, A. Boone, M. Grippa, and E. G. Josberger. 2008. A satellite snow depth multi-year average derived from SSM/I for the high latitude regions. *Remote Sensing of Environment*. 112. 2557-2568.
- Bloschl, G. 1999 Scaling issues in snow hydrology. *Hydrological Processes*. 13. 2149-2175
- Bonan, G. B., E. S. Chapin III, and S. L. Thompson. 1995. Boreal forest and tundra ecosystems as components of the climate system. *Climatic Change*. 29. 145-167.

- Bone, R. M. 1992. *The Geography of the Canadian North. Issues and Challenges*. Toronto ON. Oxford University Press.
- Boone, A., N. Mognard, B. Decharme, H. Douville, M. Grippa, and K. Kerrigan. 2006. The impact of simulated soil temperatures on the estimation of snow depth over Siberia from SSM/I compared to a multi-model climatology. *Remote Sensing of Environment*. 101. 482-494.
- Borner, A. P., K. Kielland, and M. D. Walker. 2008. Effects of simulated climate change on plant phenology and nitrogen mineralization in Alaskan Arctic tundra. *Arctic, Antarctic, and Alpine Research*. 40. 27–38.
- Boudreau, LD, Rouse WR. 1994. Algorithm testing of passive microwave monitoring of snow water equivalent in a tundra environment. Report Contract Number KM040-2-9008, *Atmospheric Environment Service*. Environment Canada, 70 pp.
- Bowling, L. C., J. W. Pomeroy, and D. P. Lettenmaier. 2004. Parameterization of blowing-snow sublimation in a macroscale hydrology model. *Journal of Hydrometeorology – Special Section*. 5. 745-762.
- Brassnet, B. 1999. A global analysis of snow depth for numerical weather prediction. *Journal of Applied Meteorology*. 38. 726–740.
- Brodzik, M. J. and K. W. Knowles. 2002. EASE-Grid: A versatile set of equal-area projections and grids in M. Goodchild (ed.) *Discrete Global Grids*. Santa Barbara, California USA: National Center for Geographic Information & Analysis.
- Brooks, P. D., S. K. Schmidt, and M. W. Williams. 1997. Winter production of CO₂ and N₂O from alpine tundra: environmental controls and relationship to inter-system C and N fluxes. *Oecologia*. 110. 403 – 413.
- Brown, R. D. and B. E. Goodison. 1996. Interannual variability in reconstructed Canadian snow cover, 1915-1992. *Journal of Climate*. 9. 1299-1318.
- Brown, R. D. 1997. Historical variability in northern hemisphere spring snow-covered area. *Annals of Glaciology*. 25: 340-346.
- Brown R. D. and R. O. Braaten, 1998: Spatial and temporal variability of Canadian monthly snow depths, 1946–1995. *Atmos.–Ocean*, 36. 37–45.
- Brown R. D. 2000. Northern hemisphere snow cover variability and change, 1915–1997. *Journal of Climate*. 13. 2339–2355.
- Brown, R. D., B. Brasnett, and D. Robinson. 2003. Gridded North American monthly snow depth and snow water equivalent for GCM evaluation, *Atmosphere Ocean*. 41. 1 – 14.
- Brown, R. D., C. Derksen and L. Wang. 2007. Assessment of spring snow cover duration variability over northern Canada from satellite datasets. *Remote Sensing of Environment*. 111 367–381
- Bruland, O., K. Sand, and A. Killingveit. 2001. Snow distribution at a high Arctic site at Svalbard. *Nordic Hydrology*. 32. 1-12.

- Bruland, O., G. E. Liston, J. Vonk, K. Sand, and A. Killingtveit. 2004. Modelling the snow distribution at two high arctic sites at Svalbard, Norway, and at an alpine site in central Norway. *Nordic Hydrology*. 35. 191 – 208.
- Buss-Hinkler, J., B. U. Hansen, M. P. Tamstorf, and S. B. Pedersen. 2006. Snow-vegetation relations in a high Arctic ecosystem: Inter-annual variability inferred from new monitoring and modeling concepts. *Remote Sensing of Environment*. 105. 237–247.
- Cameron, M.A., R.W. Gorman, M.J. Manore, A.E. Owens, G.M. Shirtliffe, and R.O. Ramsier. 1984. Passive microwave observations of St. Lawrence Seaway ice and snow. In *Proceedings 9th Canadian Symposium on Remote Sensing*. St. John, Nfld. 121-129.
- Caves, R., S. Quegan, T. Nagler. 1999. Geometric and physical constraints on recovering snow covered area from SAR. In *Proceedings CEOS SAR Workshop*, Toulouse. ESA SP-450. 26-29.
- Chang, A. T. C., Richard E. J. Kelly, E. G. Josberger, R. L. Armstrong, J. L. Foster and N. M. Mognard. 2005. Analysis of ground-measured and passive-microwave-derived snow depth variations in midwinter across the Northern Great Plains. *Journal of Hydrometeorology*. 6. 1. 20-33.
- Chang A. T. C., P. Gloersen, T. Schmugge, T. T. Wilheit, and H. J. Zwally. 1976. Microwave emission from snow and glacier ice. *Journal Glaciology*. 16. 23-39.
- Chang A. T. C, J. L. Foster, and D. K. Hall. 1987. Nimbus-7 SMMR derived global snow cover parameters. *Annals of Glaciology*. 9. 39-44.
- Chang, A., J. Foster, and D. Hall. 1990. Satellite sensor estimates of northern hemisphere snow volume. *International Journal of Remote Sensing*. 11. 167-171.
- Chang, A. and J. Foster. 1992. The role of passive microwaves in characterizing snow cover in the Colorado River Basin. *GeoJournal*. 26. 381-388.
- Chapin III, F. S., M. Sturm, M. C. Serreze, J. P. McFadden, J. R. Key, A. H. Lloyd, A. D. McGuire, T. S. Rupp, A. H. Lynch, J. P. Schimel, J. Beringer, W. L. Chapman, H. E. Epstein, E. S. Euskirchen, L. D. Hinzman, G. Jia, C. L. Ping, K. D. Tape, C. D. C. Thompson, D. A. Walker and J. M. Welker. 2005. Role of land-surface changes in Arctic summer warming. *Science*. 310. 657-660.
- Choudhury, B. J. 1989. Monitoring global land surface using Nimbus – 7 37 GHz data: Theory and examples. *International Journal of Remote Sensing*. 16. 1579 – 1605.
- Cohen, J. 1994. Snow cover and climate. *Weather*. 49. 150-156.
- Cohen, J. and D. Rind. 1994. The effect of snow cover on the climate. *Journal of Climate*. 4. 689-706.
- Colbeck, S. C. 1986. Classification of seasonal snow cover crystals. *Water Resources Research*. 22. 59S–70S.
- Derksen, C. and E. LeDrew,. 2000. Variability and change in terrestrial snow cover: data acquisition and links to the atmosphere. *Progress in Physical Geography*. 4. 469-498.

- Derksen, C., E. LeDrew, and B. Goodison. 2000a. Temporal and spatial variability of North American prairie snow cover (1988-1995) inferred from passive microwave-derived snow water equivalent imagery. *Water Resources Research*. 36. 255-266.
- Derksen, C., E. LeDrew, A. Walker, and B. Goodison. 2000b. Influence of sensor overpass time on passive microwave-derived snow cover parameters. *Remote Sensing of the Environment*. 71. 297-308
- Derksen, C., E. LeDrew, and B. Goodison. 2000c. Winter season variability in North American prairie SWE distribution and atmospheric circulation. *Hydrological Processes*. 14. 3273-3290.
- Derksen, C., A. Walker, and B. Goodison. 2003. A comparison of 18 winter seasons of in-situ and passive microwave-derived snow water equivalent estimates in Western Canada. *Remote Sensing of the Environment*. 88. 271-282.
- Derksen, C., R. Brown, and A. Walker. 2004. Merging conventional (1915-92) and passive microwave (1978-2002) estimates of snow extent and water equivalent over central north America. *Journal of Hydrometeorology*. 5. 850-861.
- Derksen, C., A. Walker, and B. Goodison. 2005. Evaluation of passive microwave snow water equivalent retrievals across the boreal forest/tundra transition of Western Canada. *Remote Sensing of Environment*. 96. 315-327.
- Derksen, C. and M. Mackay. 2006. The Canadian boreal snow water equivalent band. *Atmosphere Ocean*. 44. 305-320.
- Derksen, C. 2008. The contribution of AMSR-E 18.7 and 10.7 GHz measurements to improved boreal forest snow water equivalent retrievals. *Remote Sensing of Environment*. 112. 2701-2710.
- Derksen, C., M. Sturm, G. E. Liston, J. Holmgren, H. Huntington, A. Silis, and D. Solie. 2009. Northwest Territories and Nunavut snow characteristics from a subarctic traverse: Implications for passive microwave remote sensing. *Journal of Hydrometeorology*. 10. 448-463.
- Derksen, C., P. Toose, A. Rees, L. Wang, M. English, A. Walker, and M. Sturm. Development of a tundra-specific snow water equivalent retrieval algorithm for satellite passive microwave data. *Remote Sensing of Environment*. In Press, RSE-S-09-01010
- De Sève, D., M. Bernier, J-P. Fortin, and A. Walker. 1997. Preliminary analysis of snow microwave radiometry using the SSM/I passive-microwave data: The case of La Grande River watershed (Quebec). *Annals of Glaciology*. 25. 253-261.
- Dozier, J. and D. Marks. 1987. Snow mapping and classification from LANDSAT thematic mapper data. *Annals of Glaciology*. 9. 97-103.
- Drake, J. J. 1981. The effects of surface dust on snowmelt rates. *Arctic and Alpine Research*. 13. 219-223.
- Duguay, C. R., T. J. Pultz, P. M. Lafleur, and D. Drai. 2002. RADARSAT backscatter characteristics of ice growing on shallow sub-arctic lakes, Churchill, Manitoba, Canada. *Hydrological Processes*. 16. 1631-1644.

- Duguay, C., J. Green, C. Derksen, M. English, A. Rees, M. Sturm, and A. Walker. 2005. Preliminary assessment of the impact of lakes on passive microwave snow retrieval algorithms in the Arctic. *In Proceedings of the 62nd Annual Eastern Snow Conference*. Waterloo, ON, June. 223-228.
- Dunne, T. and L. B. Leopold. 1978. *Water in Environmental Planning*. New York. W.H. Freeman and Company.
- Durand, M., and S. A. Margulis. 2006. Feasibility test of multifrequency radiometric data assimilation to estimate snow water equivalent. *Journal of Hydrometeorology*. 7. 443 – 457.
- Dye, D.G. 2002. Variability and trends in the annual snow-cover cycle in Northern Hemisphere land areas, 1972–2000. *Hydrological Processes*. 16. 3065–3077.
- Dyer, J. L. and T. L. Mote. 2006. Spatial variability and trends in observed snow depth over North America. *Geophysical Research Letters*. 33. 1-6
- Elberling, B. 2007. Annual soil CO₂ effluxes in the High Arctic: The role of snow thickness and vegetation type. *Soil Biology & Biochemistry*. 39. 646–654.
- Essery, R., L. Li, and J. Pomeroy. 1999. A distributed model of blowing snow over complex terrain. *Hydrological Processes*. 13. 2423-2438.
- Essery, R. L. H., 2001. Spatial statistics of windflow and blowing snow fluxes over complex topography. *Bound.-Layer Meteorology*. 100. 131–147
- Essery, R. and J Pomeroy. 2004. Vegetation and topographic control of wind-blown snow distributions in distributed and aggregated simulations for an Arctic tundra basin. *Journal of Hydrometeorology*. 5. 735-744.
- Eugister, W., W. R. Rouse, R. A. Pielke Sr., J. P. McFadden, D. D. Baldocchi, T. G. F. Kittel, S. F. Chapin III, G. E. Liston, L. Pier, E. Vaganov, and S. Chambers. 2000. Land-atmosphere energy exchange in Arctic tundra and boreal forest: Available data and feedbacks to climate. *Global Change Biology*. 6. 1. 84-115.
- Fahnestock, J. T., M. H. Jones, P. D. Brooks, D. A. Walker, and J. M. Welker. 1998. Winter and early spring CO₂ efflux from tundra communities of northern Alaska. *Journal of Geophysical Research*. 103. 29023–29027.
- Field, A. 2005. *Discovering Statistics Using SPSS*. 2nd ed. London: Sage Publications Ltd.
- Fily, M., A. Royer, K. Goita, and C. Prigent. 2003. A simple retrieval method for land surface temperature and fraction of water surface determination from satellite microwave brightness temperatures in sub-Arctic areas. *Remote Sensing of the Environment*. 85. 328-338.
- Foster, J. L., A. Rango, D. K. Hall, A. T. C. Chang, J. L. Allison, and B. C. Diesen, III. 1980. Snowpack monitoring in North America and Eurasia using passive microwave satellite data. *Remote Sensing of Environment*. 10. 285-298.
- Foster, D.J. and R. D. Davy. 1988. Global snow depth climatology. *USAF Environmental Technical Applications Center, USAFETAC/TN-88/006*. 48.

- Foster, J. L., A. T. C. Chang, D. K. Hall, and A. Rango. 1991. Derivation of snow water equivalent in boreal forests using microwave radiometry. *Arctic*. 44. Supp. 1. 147-152.
- Foster, J., G. Liston, R. Koster, R. Essery, H. Behr, L. Dumenil, D. Versegny, S. Thompson, D. Pollard, and J. Cohen. 1996. Snow cover and snow mass intercomparisons of general circulation models and remotely sensed datasets. *Journal of Climate*. 9. 409-425.
- Foster, J. L., A. T. C. Chang, and D. K. Hall. 1997. Comparison of snow mass estimates from a prototype passive microwave snow algorithm, a revised algorithm and a snow depth climatology. *Remote Sensing of the Environment*. 62. 132-142
- Foster, J. L., D. K. Hall, A. T. C. Chang, A. Rango, W. Wergin, and E. Erbe. 1999. Effects of snow crystal shape on the scattering of passive microwave radiation. *IEEE Transactions on Geoscience and Remote Sensing*. 37. 1165 – 1168.
- Foster, J. L., J. S. Barton, A. T. C. Chang, and D. K. Hall. 2000. Snow crystal orientation effects on the scattering of passive microwave radiation. *IEEE Transactions on Geoscience and Remote Sensing*. 38. 2430-2434.
- Foster, J. L., S. Chaojiao, J. P. Walker, R. Kelly, A. Chang, J. Dong, and H. Powell. 2005. Quantifying the uncertainty in passive microwave snow water equivalent observations. *Remote Sensing of Environment*. 94. 187-203.
- Frei, A., D. A. Robinson, M. G. Hughes. 1999. North American snow extent: 1900–1994. *International Journal of Climatology*. 19. 1517-1534.
- Frei, A. and D. Robinson. 1999. Northern hemisphere snow extent: regional variability 1972–1994. *International Journal of Climatology*. 19. 1535–1560.
- Games, P. A., H. J. Keselman, and J. C. Rogan. 1983. A review of simultaneous pairwise multiple comparisons. *Statistica Neerlandica*. 37: 53 – 58.
- Ge, Y. and G. Gong. 2008. Observed inconsistencies between snow extent and snow depth variability at regional/continental scales. *Journal of Climate*. 21. 1066-1082.
- Glass, G. V., P. D. Peckham, and J. R. Sanders. 1972. Consequences of failure to meet assumptions underlying the fixed effects analyses of variance and covariance. *Review of Educational Research*. 42. 237-288.
- Goita K., A. E. Walker, and B. E. Goodison. 2003. Algorithm development for the estimation of snow water equivalent in the boreal forest using passive microwave data. *International Journal of Remote Sensing*. 24. 1097-1102.
- Gong, G., D. Entekhabi, and J. Cohen. 2003. Modeled Northern Hemisphere winter climate response to realistic Siberian snow anomalies. *Journal of Climate*. 16. 3917–3931.
- Goodison, B. E., J. R. Metcalf, R. A. Wilson, and K. Jones. 1988. The Canadian automatic snow depth sensor: A performance update. In *Proceedings of the 56th Annual Western Snow Conference*. 178-181.

- Goodison, B. E., H. I. Ferguson, and G. A. McKay. 1981. Measurement and data analysis. In: *The Handbook of Snow, Principles, Processes, Management and Use*. D. M. Gray and D. H. Male (eds). Toronto: Pergamon Press. 191 -274..
- Goodison, B., and A. Walker. 1994. Canadian development and use of snow cover information from passive microwave satellite data. *Passive Microwave Remote Sensing of Land-Atmosphere Interactions*. 245-262.
- Goodison, B. and Walker, A. 1995. Canadian development and use of snow cover information from passive microwave satellite data. In B. Choudhury, Y. Kerr, E. Njoku, and P. Pampaloni (eds.). *Passive Microwave Remote Sensing of Land-Atmosphere Interactions*. Utrecht: VSP BV. 245-262.
- Grenfell, T., and J. Putkonen. 2008. A method for the detection of the severe rain-on-snow event on Banks Island, October 2003, using passive microwave remote sensing. *Water Resources Research*, 44.
- Grippa, M., N. Mognard, T. Le Toan, and E. G. Josberger. 2004. Siberia snow depth climatology derived from SMM/I data using a combined dynamic and static algorithm. *Remote Sensing of Environment*. 30 – 41.
- Grody, N. C. and A. N. Basist. 1996. Global identification of snowcover using SSM/I measurements, *IEEE Transactions on Geoscience and Remote Sensing*. 34. 1. 237-249.
- Grogan, P. and S. Jonasson. 2006. Ecosystem CO₂ production during winter in a Swedish subarctic region: The relative importance of climate and vegetation type. *Global Change Biology*. 12. 1479–1495
- Groisman, P. Y., T. R. Karl, and R. W. Knight. 1994. Changes of snow cover, temperature, and radiative heat balance over the Northern Hemisphere. *Journal of Climate*. 7. 1633-1656.
- Groisman, P.Y., T. R. Karl, and R. W. Knight. 1994. Observed impact of snow cover on the heat balance and the rise of continental spring temperatures. *Science*. 263. 198–200.
- Gubler, H. 1981. An inexpensive remote snow-depth gauge based on ultrasonic wave reflection from the snow surface. *Journal of Glaciology*. 27. 95. 157-163.
- Guneriussen, T. 1997. Backscattering properties of a wet snow cover derived from DEM corrected ERS-1 SAR data. *International Journal of Remote Sensing*. 18. 375-392.
- Guneriussen, T., H. Johnsen, and I. Lauknes. 2001. Snow cover mapping capabilities using RADARSAT standard mode data. *Canadian Journal of Remote Sensing*. 27. 109-117.
- Gunn, G. E., C. R. Duguay, C. Derksen, and J. Lemmetyinen. Validating the Helsinki University of Technology's modified snow emission model over lake ice using airborne passive microwave measurements. *Remote Sensing of Environment*. In Press.

- Hall, D.K., J.L. Foster and A.T.C. Chang. 1981. Freshwater ice thickness observations using passive microwave sensors. *IEEE Transactions on Geoscience and Remote Sensing*. GE-19 – 4. 189-193.
- Hall, D. K., A. T. C. Chang, and J. L. Foster. 1986. Detection of the depth-hoar layer in the snow pack of the arctic coastal plain of Alaska, U.S.A., using satellite data. *Journal of Glaciology*. 32. 87-94.
- Hall, D. K. 1987. Influence of depth hoar on microwave emission from snow in northern Alaska. *Cold Regions Science and Technology*. 13. 225-231.
- Hall, D. K. 1991. Passive microwave remote and in situ measurements of arctic and subarctic snow covers in Alaska. *Remote Sensing of Environment*. 38. 161-172.
- Hall, D. K., R. E. J. Kelly, G. A. Riggs, A. T. C. Chang, and J. L. Foster. 2002b. Assessment of the relative accuracy of hemispheric-scale snow-cover maps. *Annals of Glaciology*. 34. 24-30.
- Hall, D. K., G. A. Riggs, V. V. Salomonson, N. E. DiGirolamo, and K. J. Bayr. 2002a. MODIS snow cover products. *Remote Sensing of the Environment*. 83. 181-194.
- Helfrich, S. R., D. McNamara, B. H. Ramsay, T. Baldwin, and T. Kasheta. 2007. Enhancements to and forthcoming developments in the interactive multisensor snow and ice mapping system (IMS). *Hydrological Processes*. 21. 1576-1586.
- Henderson, F. M. and A. J. Lewis. 1998. *Principles and Applications of Imaging Radar-Manual of Remote Sensing*. 3rd ed. New York: Wiley and Sons.
- Higgins, P. A. T. and M. Vellinga. 2004. Ecosystem responses to abrupt climate change: teleconnections, scale and the hydrological cycle. *Climatic Change*. 64. 127-142.
- Hinkel, K. M. and J. K. Hurd, Jr. 2006. Permafrost destabilization and thermokarst following snow fence installation, Barrow, Alaska, U.S.A. *Arctic, Antarctic, and Alpine Research*. 38. 530-539.
- Hinzman, L. D., N. D. Bettez, W. R. Bolton, F. S. Chapin, M. B. Dyurgerov, C. L. Fastie, B. Griffith, R. D. Hollister, A. Hope, H. P. Huntington, A. M. Jensen, G. J. Jia, T. Jorgenson, D. L. Kane, D. R. Klein, G. Kofinas, A. H. Lynch, A. H. Lloyd, A. D. McGuire, F. E. Nelson, W. C. Oechel, T. E. Osterkamp, C. H. Racine, V. E. Romanovsky, R. S. Stone, D. A. Stow, M. Sturm, C. E. Tweedie, G. L. Vourlitis, M. D. Walker, D. A. Walker, P. J. Webber, J. M. Welker, K. S. Winker, and K. Yoshikawa. 2005. Evidence and implications of recent climate change in northern Alaska and other arctic regions. *Climatic Change*. 72. 251-298.
- Hirashima, H., O. Tetsuo, Y. Kodama, H. Yabuki, N. Sato, and A. Georgiadi. 2004. Nonuniform distribution in tundra snow cover in Eastern Siberia. *Journal of Hydrometeorology*. 5. 373-389.
- Hollinger, J. P., J. L. Peirce, and G. A. Poe. 1990. SSM/I instrument evaluation. *IEEE Transactions on Geoscience and Remote Sensing*. 28. 781-790
- Holz, R. K. 1985. *The Surveillant Science: Remote Sensing of the Environment*. 2nd ed. New York: Wiley and Sons.

- Horel, J. D. 1981. A rotated principal component analysis of the interannual variability of the Northern Hemisphere 500mb height field. *Monthly Weather Review*. 109. 2080 – 2092.
- IGOS 2007. Integrated Global Observing Strategy Cryosphere – For the Monitoring of Our Environment from Space and from Earth. Geneva: World Meteorological Organization. WMO\TD-No. 1405. 100 pp.
- IPCC, 2007. *Climate Change 2007: Synthesis Report*. <http://www.ipcc.ch>
- Jeffries, M.O., T. Zhang, K. Frey and N. Kozlenko. 1999. Estimating latewinter heat flow to the atmosphere from the lake-dominated Alaskan North Slope. *Journal of Glaciology*, 45. 315-324.
- Josberger, N. M. and E. G. Mognard. 2002. A passive microwave snow depth algorithm with a proxy for snow metamorphism. *Hydrological Processes*. 16. 1557-1568.
- Kelly, R. E., A. T. Chang, L. Tsang, and J. L. Foster. 2003. A prototype AMSR-E global snow area and snow depth algorithm. *IEEE Transactions on Geoscience and Remote Sensing*. 41. 230-242
- Kelly, R. E., 2010. personal communication. February 2010.
- Kidd, C. 2006. Radio frequency interference at passive microwave earth observation frequencies. *International Journal of Remote Sensing*. 27. 18. 3853-3865.
- King, J. C., J. W. Pomeroy, D. M. Gray, C. Fierz, P. M. B. Fohn, R. J. Harding, R. E. Jordan, E. Martin, and C. Pluss. 2008. Snow – Atmosphere, space, energy and mass balance. In *Snow and Climate: Physical Processes, Surface Energy Exchange and Modeling*. R. L. Armstrong, R. L. and E. Brun ed. Cambridge: Cambridge University Press. 70 - 124.
- Klein, A. G., D. K. Hall, and G. A. Riggs. 1998. Improving snow-cover mapping in forests through the use of a canopy reflectance model. *Hydrological Processes*. 12. 1723-1744.
- Koenig, L. and R.R. Forster, 2004. Evaluation of passive microwave snow water equivalent algorithms in the depth hoar dominated snowpack of the Kuparuk River Watershed, Alaska, USA. *Remote Sensing of Environment*. 93. 4. 511-527.
- Kontu, A., S. Kemppainen, J. Lemmetyinen, and J. Pulliainen. 2008. Determination of snow water equivalent on lake ice from passive microwave measurements. In *Proceedings. 2008 IGARSS*, Boston, MA, USA. DVD.
- Krinner, G. 2003. Impact of lakes and wetlands on boreal climate. *Journal of Geophysical Research*. 108. ACL 10. 1 – 18.
- Langlois A., A. Royer, E. Fillol, A. Frigon and R. Laprise. 2004. Evaluation of the snow cover variation in the Canadian regional climate model over eastern Canada using passive microwave satellite data. *Hydrological Processes*. 18. 1127-1138.
- Langham, G. 1981. Physics and properties on snow cover. In: *The Handbook of Snow, Principles, Processes, Management and Use*. D. M. Gray and D. H. Male (eds). Toronto: Pergamon Press. 275 -337.

- Larsen, K. S., P. Grogan, S. Jonasson, and A. Michelsen. 2007. Respiration and Microbial Dynamics in Two Subarctic Ecosystems during Winter and Spring Thaw: Effects of Increased Snow Depth. *Arctic, Antarctic and Alpine Research*. 39. 268–276.
- Leathers, D., and B. I. Luff. 1997. Characteristics of snow cover duration across the northeast United States of America. *International Journal of Climatology*. 17. 1535-1547.
- Lemmetyinen, J., J. Pulliainen, A. Rees, Y. Qiu, and C. Derksen. (in press). Multiple Layer Adaptation of HUT Snow Emission Model: Comparison with Experimental Data. *IEEE Transactions on Geoscience and Remote Sensing*. TGRS-2009-00369
- Lemmetyinen, J., C. Derksen, J. Pulliainen, W. Strapp, P. Toose, A. Walker, S. Tauriainen, J. Pihlflyckt, J-P Kärnä, and Martti Hallikainen. 2009. A comparison of airborne microwave brightness temperatures and snowpack properties across the boreal forests of Finland and western Canada. *IEEE Transactions on Geoscience and Remote Sensing*. 47: 965-978.
- Ling, F. and T. Zhang. 2007. Modeled impacts of changes in tundra snow thickness on ground thermal regime and heat flow to the atmosphere in Northernmost Alaska. *Global and Planetary Change* 57: 235-246.
- Liston, G.E. and M. Sturm. 1998. A snow-transport model for complex terrain. *Journal of Glaciology*. 44: pp 498-516
- Liston, G. 1999. Interrelationships among snow distribution, snowmelt, and snow cover depletion: implications for atmospheric, hydrologic, and ecologic modeling. *Journal of Applied Meteorology*. 38: 1474-1487.
- Liston, G. E. and M. Sturm. 2002. Winter precipitation patterns in arctic Alaska determined from a blowing-snow model and snow-depth observations. *Journal of Hydrometeorology*. 3: 646-659.
- Liston, G. E., J. P. McFadden, M. Sturm, and R. A. Pielke. 2002. Modelled changes in arctic tundra snow, energy and moisture fluxes due to increased shrubs. *Global Change Biology*. 8. 17-32
- Liston, G E. 2004. Representing subgrid snow cover heterogeneities in regional and global models. *Journal of Climate* 17: 1381-1397.
- Liston, G. E. 2005. Global Snow-Water Equivalent Depth Coefficient-of-Variation Classification. *Boulder, CO: National Snow and Ice Data Center. Digital media*.
- Loveland, T. R, B. C. Reed, J. F. Brown, D. O. Ohlen, Z. Zhu, L. Yang, and J. W. Merchant. 2000. Development of a global land cover characteristics database and IGBP DISCover from 1 km AVHRR data. *International Journal of Remote Sensing*. 21. 1303 – 1330.
- Loya, M. W. and P. Grogan. 2004. Carbon conundrum on the tundra. *Nature*. 431. 406 – 408.
- Luce, C. H., D. G. Tarboton, and K. R. Cooley. 1999. Sub-grid parametrization of snow distribution for an energy and mass balance snow cover model. *Hydrological Processes*. 13. 1921 – 1934.

- Lundberg, A., N. Yuichiro, H. Thunehed, and S. Halldin. 2004. Snow accumulation in forests from ground and remote sensing data. *Hydrological Processes*. 18. 1941-1955.
- Lynch, A. H., W. L. Chapman, J. E. Walsh, and G. Weller. 1995. Development of a regional climate model of the western Arctic. *Journal of Climate*. 8. 1555-1570.
- MacKay, J.R. and D. K. MacKay. 1975. Snow cover and ground temperatures, Garry Island, NWT. *Canadian Journal of Earth Sciences* 192, 187–196.
- McKay G. A. and W. P., Adams. 1981. Snow and living things. In: *The Handbook of Snow, Principles, Processes, Management and Use*. D. M. Gray and D. H. Male (eds). Toronto: Pergamon Press. 3 – 31.
- Male, S. K. and E. Nol. 2005. Impacts of roads associated with the Ekati Diamond Mine, Northwest Territories, Canada, on reproductive success and breeding habitat of Lapland longspurs. *Canadian Journal of Zoology*. 83. 1286-1296
- Marshall, S., Roads, J. O., and G. Glatzmaier. 1994. Snow hydrology in a general circulation model. *Journal of Climate*. 7. 1251-1269.
- Mätzler, C., E. Schanda, and W. Good. 1982. Towards the definition of optimum sensor specifications for microwave remote sensing of snow. *IEEE Transactions on Geoscience and Remote Sensing*. GE-20 (1). 57-66.
- Matzler, C. 1994. Passive microwave signatures of landscapes in winter. *Meteorology Atmospheric Physics*. 54. 241-260
- Matzler, C. 1996. Microwave permittivity of dry snow. *IEEE Transactions on Geoscience and Remote Sensing*. 34. 573-581.
- MacPherson, I, D. Marcotte, and J. Jordan. 2001. The NRC atmospheric research aircraft. *Canadian Aeronautical Space Journal*. 47. 1-11.
- McGinnis D. L. and R. G. Crane. 1994. A multivariate analysis of Arctic climate in GCMs. *Journal of Climate*. 7. 1240-1250.
- Meteorological Service of Canada. 2000. Canadian snow data CD-ROM. CRYSYS project, climate processes and Earth observation division Downsview, Ontario: *Meteorological Service of Canada*.
- Mognard, E. G. and N. M. Josberger. 2002. Northern Great Plains 1996/97 seasonal evolution of snowpack parameters from satellite passive-microwave measurements. *Annals of Glaciology*. 34. 145-159
- Morgan, G. A., N. L. Leech, G. W. Gloeckner, and K. Caplovitz Barrett. 2004. *SPSS for Introductory Statistics: Use and Interpretation*. 2nd ed. New Jersey: Lawrence Erlbaum Associates Inc.
- Nagler, T. and H. Rott. 2000. Retrieval of wet snow by means of multitemporal SAR data. *IEEE Transactions on Geoscience and Remote Sensing*. 38. 754-765.
- Neumann, N. N., C. Derksen, C. Smith and B. Goodison. 2006. Characterizing local scale snow cover using point measurements during the winter season. *Atmosphere Ocean*. 44. 257 – 269.

- Nghiem, S. V. and W. Y. Tsai. 2001. Global snow cover monitoring with spaceborne ku-band scatterometer. *IEEE Transactions on Geoscience and Remote Sensing*. 39. 2118 – 2134.
- Nobrega, S. and P. Grogan. 2007. Deeper snow enhances winter respiration from both plant-associated and bulk soil carbon pools in birch hummock tundra. *Ecosystems*. 10. 419-431.
- nsidc.org
- Oelbermann, M., M. English, and S. L. Schiff. 2008. Evaluating carbon dynamics and microbial activity in arctic soils under warmer temperatures. *Canadian Journal of Soil Science*. 31 – 44.
- Oke, T. 1990. *Boundary Layer Climates*. 2nd ed. Oxford: Routledge Press.
- Olsson, P.Q., M. Sturm, C.H. Racine, V. Romanovsky and G.E. Liston. 2003. Five stages of the Alaskan Arctic cold season with ecosystem implications. *Arctic Antarctic Alpine Research*. 35. 74-81.
- Ohmura, A. 2000. Climate on tundra and thoughts on causes of regional climate differences. *Annals of Glaciology*. 31. 10-14.
- Overpeck, J., K. Hughen, D. Hardy, R. Bradley, R. Case, M. Douglas, B. Finney, K. Gajewski, G. Jacoby, A. Jennings, S. Lamoureux, A. Lasca, G. MacDonald, J. Moore, M. Retelle, S. Smith, A. Wolfe, and G. Zielinski. 1997. Arctic environmental change of the last four centuries. *Science*. 278, 1251–1256.
- Qu, X. and A. Hall. 2006. Assessing snow albedo feedback in simulated climate change. *Journal of Climate*. 19. 2617-2630.
- Peramaki, L. and M. Stone. 2007. Fluxes of As, Cu, Hg, Pb in lake sediments in the Coppermine River basin, Canada. *Nordic Hydrology*. 38. 177 – 185.
- Pivot, F. C., C. Kergomard, and C. R. Duguay. 2002. Use of passive-microwave data to monitor spatial and temporal variations of snow cover at tree line near Churchill, Manitoba, Canada. *Annals of Glaciology*. 34. 58-64.
- Poe, G. A. and R. W. Conway. 1990. A study of the geolocation errors of the Special Sensor Microwave/Imager (SSM/I). *IEEE Trans. Geosci. Remote Sensing*. 28. 791-799.
- Pohl, S., B. Davison, P. Marsh, and A. Pietroniro. 2005. Modelling spatially distributed snowmelt and meltwater runoff in a small Arctic catchment with a hydrology land-surface scheme (WATCLASS). *Atmosphere – Ocean*. 43. 193-211
- Pomeroy, J. W. and D. M. Gray. 1995. Snow accumulation, relocation and management. *NHRI Science Report*. No. 7. Supply and Services Canada, Saskatoon.
- Pomeroy, J. W. and B. E. Goodison. 1997. Winter and snow. In *The Surface Climates of Canada*. W.G. Bailey, T. R. Oke, and W. R. Rouse. Eds. Montreal: McGill University Press. 68 – 100.

- Pomeroy, J. W., P. Marsh, and D. M. Gray. 1997. Application of a distributed blowing snow model to the Arctic. *Hydrological Processes*. 11. 1451-1464.
- Pomeroy J.W., D. M. Gray, K. R. Shook, B. Toth, R. L. H. Essery, A. Pietroniro, and N. Hedstrom. 1998. An evaluation of snow accumulation and ablation processes for land surface modelling. *Hydrological Processes*. 12. 2339–2367.
- Pomeroy, J. W., D. S. Bewley, R. L. H. Essery, N. R. Hedstrom, T. Link, R. J. Granger, J. E. Sicart, C. R. Ellis and J. R. Janowicz. 2006. Shrub tundra snowmelt. *Hydrological Processes*. 20. 923–941
- Post, W., M., W. R. Emmanuel, P. J. Zinke, and A. G. Strangenburger. 1982. *Nature*. 298, 156–159.
- Pulliainen, J. T., M. T. Hallikainen, and J. Grandell, 1999: Hut snow emission model and its applicability to snow water equivalent retrieval, *IEEE Trans. Geoscience and Remote Sensing*. 37. 1378–1390.
- Pulliainen, J. and M. Hallikainen. 2001. Retrieval of regional snow water equivalent from space-borne passive microwave observations. *Remote Sensing of the Environment*. 75. 76-85.
- Pulliainen, J. 2006. Mapping of snow water equivalent and snow depth in boreal and sub-arctic zones by assimilating space-borne microwave radiometer data and ground-based observations. *Remote Sensing of Environment*. 101. 257–269
- Ramsay, B. H. 1998. The interactive multisensor snow and ice mapping system. *Hydrological Processes*. 12. 1537 – 1546.
- Ramsay, B. H., 2000. Prospects for the interactive multisensor snow and ice mapping system (IMS). In *Proceedings of 57th Eastern Snow Conference*. May 2000. Syracuse, New York, USA
- Rango, A. 1996. Spaceborne remote sensing for snow hydrology applications. *Hydrological Sciences*. 41. 477-492.
- Rees, A., M. English, C. Derksen and A. Walker. 2005. Assessing snowpack water equivalent distribution in an open tundra environment using various scales of passive microwave data. In *Proceedings of 62nd Eastern Snow Conference*. June 2005. Waterloo ON.
- Rees, A., C. Derksen, M. English, A. Walker and C Duguay. 2006. Uncertainty in snow mass retrievals from passive microwave sensor data in lake-rich high latitude environments. *Hydrological Processes (HP Today)*. 20. 1019-1022
- Rees, A., J. Lemmetyinen, C. Derksen, J. Pulliainen, and M. English. 2010. Observed and modelled effects of ice lens formation on passive microwave brightness temperatures over snow covered tundra. *Remote Sensing of Environment*. RSE-D-09-00172
- Richman M. 1986. Rotation of principal components. *Journal of Climatology* 6: 293-335.

- Riggs, G., D. Hall, and V. Salomonson. 1994. A snow index for the landsat thematic mapper and moderate resolution imaging spectrometer. *In Proceedings of International Geoscience and Remote Sensing Symposium*. Pasadena CA, August. 1942 – 1944.
- Robinson, D. A. 1989. Evaluation of the collection, archiving and publication of daily snow data in the United States. *Physical Geography*. 12. 120–130
- Robinson D. 1993. Hemispheric snow-cover from satellites. *Annals of Glaciology*. 17. 367-371.
- Rott, H. 1987. Remote sensing of snow. Large scale effects of seasonal snow cover. *In Proceedings of the Vancouver Symposium*. August 1987. IAHS Publ. No. 166. 279-290.
- Rosenfeld, S. and N. C. Grody. 2000. Metamorphic signature of snow revealed in SSM/I measurements. *IEEE Transactions on Geoscience and Remote Sensing*. 38. 53 – 63.
- Rouse, W. R., D. W. Carlson, and E. J. Weick, 1992: Impacts of summer warming on the energy and water balance of wetland tundra. *Climate Change*, 22, 305–326.
- Rouse, W. R., R. L. Bello, and P. M. Lafleur. 1997. The low Arctic and Subarctic. In *The Surface Climates of Canada*. W.G. Bailey, T. R. Oke, and W. R. Rouse. Eds. Montreal: McGill University Press. 198 – 221.
- Salomonson, V. V. and I. Appel. 2004. Estimating fractional snow cover from MODIS using the normalized difference snow index. *Remote Sensing of Environment*. 89. 351–360
- Saxena, A. and J. Bentz. 1995. Inventory of existing environmental, traditional and ecological knowledge and socio-economic information in the West Kitikmeot/Slave Geological Province. P. Cizek and J. Burnaby managers. Queen's Printer.
- Schimel J. P., C. Billbrough, and J. A. Welker. 2004. Increased snow depth affects microbial activity and nitrogen mineralization in two Arctic tundra communities. *Soil Biology Biochemistry*. 36. 217–27.
- Serreze, M. C. J. E. Walsh, F. S. Chapin, T. Osterkamp, M. Dyurgerov, V. Romanovsky, W. C. Oechel, J. Morison, T. Zhang and R. G. Barry. 2000. Observational evidence of recent change in the northern high-latitude environment. *Climatic Change*. 46. 159–207.
- Simic, A., R. Fernandes, R. Brown, P. Romanov, and W. Park. 2004. Validation of VEGETATION, MODIS, and GOES + SSM/I snow-cover products over Canada based on surface snow depth observations. *Hydrological Processes*. 18. 1089-1104.
- Shaw, P. J. A. 2003. *Multivariate Statistics for the Environmental Sciences*. Oxford University Press. New York.
- Sokol, J., T.J. Pultz, and A.E. Walker. 1999. Passive and active airborne remote sensing of snow cover. *International Journal of Remote Sensing*. 24. 5327-5344

- Solberg, R., J. Amlien, H. Koren, B. Wangensteen, K. Luojus, J. Pulliainen, M. Takala, J. Lemmetyinen, T. Nagler, H. Rott, F. Muller, C. Derksen, S. Metsamaki, and K. Bottcher. 2009. Global snow monitoring for climate research - design justification file. *European Space Agency Study Contract Report*. 21703/08/I-EC Deliverable 1.7. 246 pages.
- Solheim F. 1993. Use of pointed water vapor radiometer observations to improve vertical GPS surveying accuracy. PhD dissertation, Dept Physics, Univeristy of Colorado, Boulder.
- Stow, D. A., A. Hope, D. McGuire, D. Verbyla, J. Gamon, F. Huemmrich, S. Houston, C. Racine, M. Sturm, K. Tape, L. Hinzman, K. Yoshikawa, C. Tweedie, B. Noyle, C. Silapaswan, D. Douglas, B. Griffith, G. Jia, H. Epstein, D. Walker, S. Daeschner, A. Petersen, L. Zhou, and R. Myneni. 2004. Remote sensing of vegetation and land-cover change in Arctic tundra ecosystems. *Remote Sensing of Environment*. 89. 281-308.
- Stiles, W. H. and Ulaby, F. T. 1980. The active and passive microwave response to snow parameters, I: wetness. *Journal Geophysical Research*. 85 (C2).
- Strack, J. E., G. E. Liston, and R. A. Pielke Sr. 2004. Modeling snow depth for improved simulation of snow-vegetation-atmosphere interactions. *Journal of Hydrometeorology – Special Section*. 5. 723-734.
- Sturm, M. April 2007. *Personal communication*.
- Sturm, M., T.C. Grenfell and D.K. Perovich. 1993. Passive microwave measurements of tundra and taiga snow covers in Alaska, U.S.A. *Annals of Glaciology*. 17. 125-130.
- Sturm, M., J. Holmgren, and G. Liston. 1995. A seasonal snow cover classification system for local to global applications. *Journal of Climate*. 8 (5). 1261-1283.
- Sturm, M. and C. Benson, 1997. Vapor transport, grain growth, and depth-hoar development in the subarctic snow. *Journal of Glaciology*. 43. 42–59.
- Sturm, M., J.P. McFadden, G.E. Liston, F. S. Chapin III, C.H. Racine, and J. Holmgren. 2000. Snow-shrub interactions in arctic tundra: a hypothesis with climatic implications. *Journal of Climate*. 14. 336-344.
- Sturm, M., C. Racine C, and K. Tape. 2001a. Increasing shrub abundance in the Arctic. *Nature*. 411. 547–547.
- Sturm, M., J. P.McFadden, G. Liston, F. S. Chapin III, C. H. Racine, and J. Holmgren. 2001b. Snow-shrub interactions in Arctic tundra: A hypothesis with climatic implications. *Journal of Climate*. 14. 336-344
- Sturm, M. and Liston G. 2003. The snow cover on lakes of the Arctic coastal plain of Alaska, U.S.A. *Journal of Glaciology*. 49. 370-380.
- Tait, A. B. 1998. Estimate of snow water equivalent using passive microwave radiation data. *Remote Sensing of the Environment*. 64. 286-291.
- Tait, A. B., D. K. Hall, J. L. Foster, and R. L. Armstrong. 2000. Utilizing multiple datasets for snow-cover mapping. *Remote Sensing of Environment*. 72. 111-126.

- Toose, P. 2007. The influence of snow cover variability and tundra lakes on passive microwave remote sensing of late winter snow water equivalent in the Hudson Bay Lowlands. Unpublished MSc Thesis. Department of Geography, University of Waterloo.
- Toothaker, L. E. 1999. Multiple comparison procedures. Series in quantitative *Applications in the Social Sciences*. 89. Sage Publications Inc. London.
- Ulaby, F. T., R. K. Moore, and A. K. Fung. 1982. *Microwave Remote Sensing, Active and Passive. Volume II Radar Remote Sensing and Surface Scattering and Emission Theory*. London: Addison-Wesley Publishing Company.
- Ulaby, F. T., R. K. Moore, and A. K. Fung. 1986. *Microwave Remote Sensing, Active and Passive. Volume III From Theory to Application*. London: Addison-Wesley Publishing Company.
- Van der Wall, R., S. Van Lieshout, D. Bos, and R. H. Drent. 2000. Are spring staging brent geese evicted by vegetation succession? *Ecography*. 23. 1. 60-69.
- Walker, A. E. and B.E. Goodison. 1993. Discrimination of a wet snow cover using passive microwave satellite data. *Annals of Glaciology*. 17. 307-311.
- Walker, M. D., D. A. Walker, J. M. Welker, A. M. Arft, T. Bardsley, P. D. Brooks, J. T. Fahnestock, M. H. Jones, M. Losleben, A. N. Parsons, T. R. Seastedt, and P. L. Turner. 1999: Long-term experimental manipulation of winter snow regime and summer temperature in arctic and alpine tundra. *Hydrological Processes*. 13. 2315–2330.
- Walker, A., W. Strapp, and I. Macpherson. A Canadian Twin Otter microwave radiometer installation for airborne remote sensing of snow, ice and soil moisture. *In Proceedings of IGARSS*. 5. 2002. 2678-2680.
- Walker, A., and A. Silis. 2002. Snow cover variations over the Mackenzie River basin from SSM/I passive microwave satellite data. *Annals of Glaciology* 34. 8-14.
- Wang, L., M. Sharp, R. Brown, C. Derksen, and B. Rivard. 2005a. Evaluation of spring snow covered area depletion in the Canadian Arctic from NOAA snow charts. *Remote Sensing of Environment*. 95. 453–463
- Wang, L., M. Sharp, B. Rivard, S. Marshall, and D. Burgess. 2005b. Melt season duration on Canadian Arctic ice caps, 2000–2004. *Geophysical Research Letters*. 32.
- Water Survey of Canada. Available at www.wsc.ec.gc.ca.
- Wiesmann A. and C. Matzler. 1999. Microwave emission model of layered snowpacks. *Remote Sensing of the Environment*. 70. 307-316.
- Woo, M. K. and P. Marsh. 1978. Analysis of error in the determination of snow storage for small high Arctic basins. *Journal of Applied Meteorology*. 7. 1537 – 1541.
- Woo, M. K., A. Walker, D. Yang, and B. Goodison. 1995. Pixel-scale ground snow surveys for passive microwave study of the Arctic snow cover. *In Proceedings of the 52nd Eastern Snow Conference*. Toronto, Ontario, Canada. 1995. 51-57

- Woo, M. K. 1998. Arctic snow cover information for hydrological investigations at various scales. *Nordic Hydrology*. 29. 245-266.
- Woo, M. K., D. Yang, and K. L. Young. 1999. Representativeness of Arctic weather station data for the computation of snowmelt in a small area. *Hydrological Processes*. 13. 1859-1870.
- Woo, M. K. and K. L. Young. 2004. Modeling arctic snow distribution and melt at the 1 km grid scale. *Nordic Hydrology*. 35. 295 – 307.
- Wulder, M. A., T. A. Nelson, C. Derksen, and D. Seemann. 2007. Snow cover variability across central Canada (1978-2002) derived from satellite passive microwave data. *Climatic Change*. 82. 113-130.
- www.ccin.ca
- www.nrcan.gc.ca
- www.nwtwildlife.com
- www.wsc.ec.gc.ca
- Yang, D. and M. K. Woo. 1999. Representativeness of local snow data for large scale hydrologic investigations. *Hydrological Processes*. 13. 1977-1988.
- Zhang, T., 2005. Influence of the seasonal snow cover on the ground thermal regime: an overview. *Review of Geophysics*. 43, RG4002.